To the Graduate Council:

I am submitting herewith a dissertation written by Keith Edwin Holbert entitled "Comprehensive Signal Validation for Nuclear Power Plants." I have examined the final copy of this dissertation for form and content and recommend that it be accepted in partial fulfillment of the requirements for the degree of Doctor of Philosophy, with a major in Nuclear Engineering.

BR Upadhyaya

B.R. Upadhyaya, Major Professor

We have read this dissertation
and recommend its acceptance:

Hall C. Roland

L F Miller

Jack F. Wasserman

Accepted for the Council:

CW Minkel

Vice Provost
and Dean of The Graduate School

COMPREHENSIVE SIGNAL VALIDATION
FOR NUCLEAR POWER PLANTS

A Dissertation
Presented for the
Doctor of Philosophy
Degree
The University of Tennessee, Knoxville

Keith Edwin Holbert

August 1989

ACKNOWLEDGMENTS

In any endeavor as great as this has been, there is inevitably influence from a number of sources. Dr. T.W. Kerlin was the inspiring force which initially led me to graduate school and a M.S. degree. He and Dr. B.R. Upadhyaya were instrumental in my return to U.T. to complete the Ph.D. dissertation. Dr. Upadhyaya has provided many insights as my mentor during this pursuit. This research was sponsored by the U.S. Department of Energy, Division of Technology Supports Program, under grant DE-AC02-86NE37959. The author would like to acknowledge E. Filstein for stimulating the hypercube signal validation methodology based upon work performed at Combustion Engineering using a hypercube for data compression. Lastly, my thanks go to my family, Elizabeth and Kara, who have waited patiently in Texas for the last year for my finish.

ABSTRACT

The optimal control and safe operation of a nuclear power plant requires reliable information concerning the state of the process. Signal validation is the detection, isolation and characterization of faulty signals. Properly validated process signals are beneficial from the standpoint of increased plant availability and reliability of operator actions.

A signal validation technique utilizing a process hypercube comparison (PHC) was originated during the research and other methods were extended. The hypercube is merely a multi-dimensional joint histogram of the process conditions. The hypercube is created off-line during a learning phase. In the event that a newly observed plant state does not match with those in the learned hypercube, the PHC algorithm performs signal validation by progressively hypothesizing that one or more signals is in error. This assumption is then either substantiated or denied. In the case where many signals are found to be in error, a conclusion that the process conditions are abnormal is reached.

A comprehensive signal validation software system has been developed for application to nuclear power plants. This system combines some previously established fault detection methodologies as well as some newly developed ones. The techniques have been implemented in a modular

architecture which allows the addition or removal of signal validation "modules" as deemed necessary. Intra-module confidence factors describing the validity of a given signal are derived using fuzzy membership functions. A final evaluation of signal status is made by the System Executive (SE) based on results from each signal validation module. In order to make reliable decisions in this parallel system a positive decision maker (PDM) was developed.

Both the hypercube signal validation methodology and the comprehensive system were tested using operational data from a commercial pressurized water reactor (PWR) and the Experimental Breeder Reactor II (EBR-II).

TABLE OF CONTENTS

SECTION PAGE

SECTION PAGE

LIST OF TABLES

LIST OF FIGURES

FIGURE | PAGE

FIGURE PAGE

FIGURE PAGE

FIGURE		PAGE

FIGURE PAGE

LIST OF SYMBOLS AND ABBREVIATIONS

APDF	Amplitude Probability Density Function
BND	Bias and Noise Detection
BWR	Boiling Water Reactor
CUSUM	Cumulative Summation
EBR-II	Experimental Breeder Reactor II
ESQ	Expert System for Qualitative
EV	Evaporator
FW	Feedwater
GCC	Generalized Consistency Checking
IHX	Intermediate Heat Exchanger
kpph	Kilo-pounds per hour
MGCC	Multi-variable Generalized Consistency Checking
MISO	Multiple-input Single-Output
MW	Megawatts
Na	Sodium
NR	Narrow-range
NSSS	Nuclear Steam Supply System
PDM	Positive Decision Maker
PEM	Process Empirical Modeling
PHC	Process Hypercube Comparison
PRZR	Pressurizer
PSD	Power Spectral Density
PWR	Pressurized Water Reactor
RCS	Reactor Coolant System
RMS	Root-mean-squared
SE	System Executive
SG	Steam Generator
SGCC	Single Variable Generalized Consistency Checking
SPRT	Sequential Probability Ratio Test
SU	Superheater
SVS	Signal Validation System
UAR	Univariate Autoregression
WR	Wide-range

1. INTRODUCTION

In any process, the system conditions must be measured in order to achieve the desired operating configuration. These measurements include such variables as temperature, pressure, flow, level and others. The question arises, "How reliable are the process measurements?" Basically, the objective of signal validation is to answer the above question. Signal validation may be defined as the detection, isolation and characterization of faulty signals, where these three stages are listed in order of increasing difficulty. Signal validation is also referred to as fault detection. The most difficult task involved in signal validation is the separation of signal changes caused by the process from those due to faults in the measurement system.

The benefits of signal validation are both economic and safety related. Catastrophic signal failure can result in plant shutdown and lost revenue. Pre-catastrophic failure detection would therefore minimize plant downtime and increase plant availability. The control actions taken depend primarily upon the information provided by the plant indicators. Signal validation would thus result in increased reliability of operator actions.

This dissertation first reviews previous work performed in the area of signal validation (Section 2). The current obstacles facing signal validation are presented. This dissertation then reports on advancements made in the area of signal validation during this research.

This doctoral research into the development of signal validation technology has resulted in the following original contributions and innovations:

1. Development of a new technique for performing signal validation. Namely, the process hypercube comparison (PHC) which "learns" the valid operating states of a process to which newly observed data are compared and faulty signals identified.

2. The consolidation of several fault detection techniques into a modular comprehensive signal validation system (SVS). This included the development of a decision maker to assess the final signal status based on the results of the diverse signal processing modules.

3. Application of the signal validation techniques to operational data from a commercial pressurized water reactor (PWR) and the Experimental Breeder Reactor II (EBR-II).

After reviewing prior work in the area of fault detection, the newly-developed signal validation methodology is discussed (Section 3). The development and implementation of the comprehensive signal validation system are presented in Sections 4 and 5, respectively. Lastly, the application of both the hypercube and the signal validation system to PWR and EBR-II data are reported.

2. BACKGROUND

In this section, the current methods of signal validation and decision making are explored as related to the research reported in this dissertation.

2.1 Signal Validation History

There has been extensive research in the area of fault detection. Much of this work originated in the aerospace industry. Initial research centered on the most obvious method of signal validation, that of using redundant signals for a given process variable to check for inter-signal consistency.[1] This method is widely known as the parity-space technique. The simplest method of consistency checking between three signals is to use the median valued signal. This methodology was quickly expanded with the addition of analytical redundancy.[2] Analytical redundancy is the estimation of process variables from physical models using energy, mass and momentum balance equations. There has also been research into the area of redundancy using non-linear empirical models.[3] One of the primary goals behind analytical and empirical redundancy is the detection of common-cause failure.

2.2 Current Industrial Applications

Current applications of signal validation technology are primarily found in the aerospace and nuclear industries.

Signal validation techniques have been applied on a demonstration basis at the Experimental Breeder Reactor-II (EBR-II)[4] and commercially at Northeast Utilities Millstone Units 2 and 3.[5] A System State Analyzer has also been applied to the surveillance of the EBR-II power plant.[6] Fault detection has been implemented in flight control systems[7,8] and the space shuttle.[9] Signal validation has recently been incorporated into a digital feedwater control system that has been retrofitted in several North American nuclear power plants.[10]

2.3 Signal Validation Methodologies

There has been substantial research in the area of signal validation. At present there are several methodologies available for implementation at the University of Tennessee. The following methodologies have been developed for application to nuclear power plants.

1. Generalized consistency checking (GCC) using redundant process signals and empirical redundancy.[11,12]

2. Univariate autoregression modeling (UAR) for wideband frequency analysis.[13,14]

3. Process empirical modeling (PEM) to detect measurement system drift.[15,16]

4. Bias and noise detection (BND) for basic signal changes.[17]

5. A rule-based expert system for qualitative (ESQ) signal validation.[18]

Each of the above methods has been developed as a separate stand-alone signal validation module. Each module uses a unique methodology to detect signal failure. Whereas prior research has concentrated on a single methodology, the above modules are now to be combined into a comprehensive signal validation system. A brief description of each of the above techniques is given below.

2.3.1 Generalized Consistency Checking

Generalized consistency checking (GCC) is a method for systematic cross comparison of the output from redundant signals. A pairwise comparison of the measurements is made based on the individual measurement system tolerances. The GCC effectively includes the parity-space technique as a subset of its computational procedure. In addition to the direct measurements, analytical (or empirical) measurements may be utilized. An inconsistency index is computed for each signal. This index is used to exclude signals from a best estimate of the true signal. In the event the redundant group is only partially consistent or totally inconsistent, the estimate may be computed from a weighted summation using the inconsistency index of each signal. Bias and noise failure detection using the sequential probability ratio test (SPRT) has also been included in this module.

2.3.2 Univariate Autoregressive Modeling

Univariate autoregressive (UAR) modeling is a method for characterizing the dynamic fluctuations (noise) in a signal. These models may be used to compute wideband frequency-domain information such as the power spectral density (PSD) function of a signal. Time-domain quantities, including the autocorrelation function of the signal and the step and ramp response are also estimated. Thus the time constant of a signal may be monitored for possible variations from the normal value.

2.3.3 Process Empirical Modeling

The process empirical modeling (PEM) module establishes nonlinear multiple-input single-output (MISO) models using plant data. The measured sensor output may then be compared against a predicted output based on the previously determined model. This comparison can be used to detect a common-cause failure such as drift in the signal, and as an independent approach for monitoring the changes in process variables.

2.3.4 Bias and Noise Detection

Bias and noise detection (BND) is used to monitor basic changes in the signal characteristics. The observed properties include (1) the signal level, (2) the noise root-mean-squared (RMS) value, (3) the statistical distribution (probability density function [PDF]) and (4) a parameter proportional to the time constant of the signal from its zero-crossing rate. The computed values for the above quantities are compared against specified thresholds in order to identify an anomaly in a given signal.

2.3.5 Expert System

The expert system for qualitative (ESQ) signal validation is a rule-based evaluation of process variables, and it attempts to mimic an operator. Anomalies in a signal are detected using reasoning similar to that used by an operator. The operator compares characteristics such as average output and noise level of redundant measurements, and checks for an output signal which can be considered normal for a particular instrument channel. This module, developed in LISP, performs three tests on each signal for comparison to its redundant measurements:

1. Limit checking on the average output.
2. Limit checking on the noise level.
3. Comparison of sensor response to a change in the operating condition with the expected change.

The ESQ permits learning of the sensor limits over time.

2.4 Decision Making

The combination of several signal validation techniques (modules) into a single comprehensive system requires a systematic evaluation of the individual results in order to reach a final decision regarding the status of a signal. Computer decision making is a subject which has received a great deal of interest. The decision making methods are known by many disciplines --- knowledge engineering, expert systems, pattern recognition, information theory, etc. Each method has been applied to various problems and situations.

The type of decision making of interest in this application is that of dealing with uncertainties. There will be uncertainty in the individual module results as well as in the overall decision. Various theories for dealing with uncertainties have been developed, including:[19]

1. Certainty theory developed for use primarily in expert systems.[20]

2. Dempster/Schafer theory of evidence in which belief functions are specified.[21]

3. Possibility theory for dealing with vagueness based on the use of fuzzy sets.[22]

4. Plausibility theory which provides for reasoning with knowledge obtained from imperfect sources.[23]

Each of the above theories is more or less an extension of probability theory. In each case, confidence measures are developed to indicate the certainty (or uncertainty) of a specific statement. Tests are then performed to determine the most likely conclusions.

The literature contains example applications for each of the above methods. One such application is the selection of a single job applicant from a field of four based upon three selection criteria. This researcher noted that for an application such as this, choices including no hire and multiple hire must also be available but are generally not provided for in the above techniques.

2.5 Fuzzy Set Theory

Fuzzy functions are applied to intra-module decision making and are therefore described below. Fuzzy set theory has been developed to group elements into classes which do not exhibit sharply defined boundaries.[24,25] Two fuzzy membership functions of interest are the S-curve and the π-curve. The S-curve is defined by:

$$S(\mu;\alpha,\beta,\phi) = \begin{cases} 0 & \text{for } \mu \le \alpha \\ 2\left[\dfrac{\mu-\alpha}{\phi-\alpha}\right]^2 & \text{for } \alpha \le \mu \le \beta \\ 1-2\left[\dfrac{\mu-\phi}{\phi-\alpha}\right]^2 & \text{for } \beta \le \mu \le \phi \\ 1 & \text{for } \phi \le \mu \end{cases} \qquad (2.1)$$

where

μ = variable to apply membership function to,

α = lower transition point at which S equals zero,

ϕ = upper transition point at which S equals unity,

β = crossover point at which S equals one-half,

= $(\alpha+\phi)/2$.

The π-curve is defined from:

$$\pi(\mu;\theta,\delta) = \begin{cases} S(\mu;\theta-\delta,\theta-\delta/2,\theta) & \text{for } \mu \leq \theta \\ 1 - S(\mu;\theta,\theta+\delta/2,\theta+\delta) & \text{for } \mu \geq \theta \end{cases} \qquad (2.2)$$

where

δ = bandwidth (separation between crossover points),

θ = central point at which π equals unity.

These two curves are shown in Figure 2.1. Fuzzy functions are somewhat arbitrarily defined and subjectively used. Because fuzzy set theory is an extension of probability theory, in the event that a particular situation is better described by another function (or distribution), this more objectively established relationship should be utilized instead of the fuzzy functions above. The above functions provide a basis for choosing more appropriate decision regions.

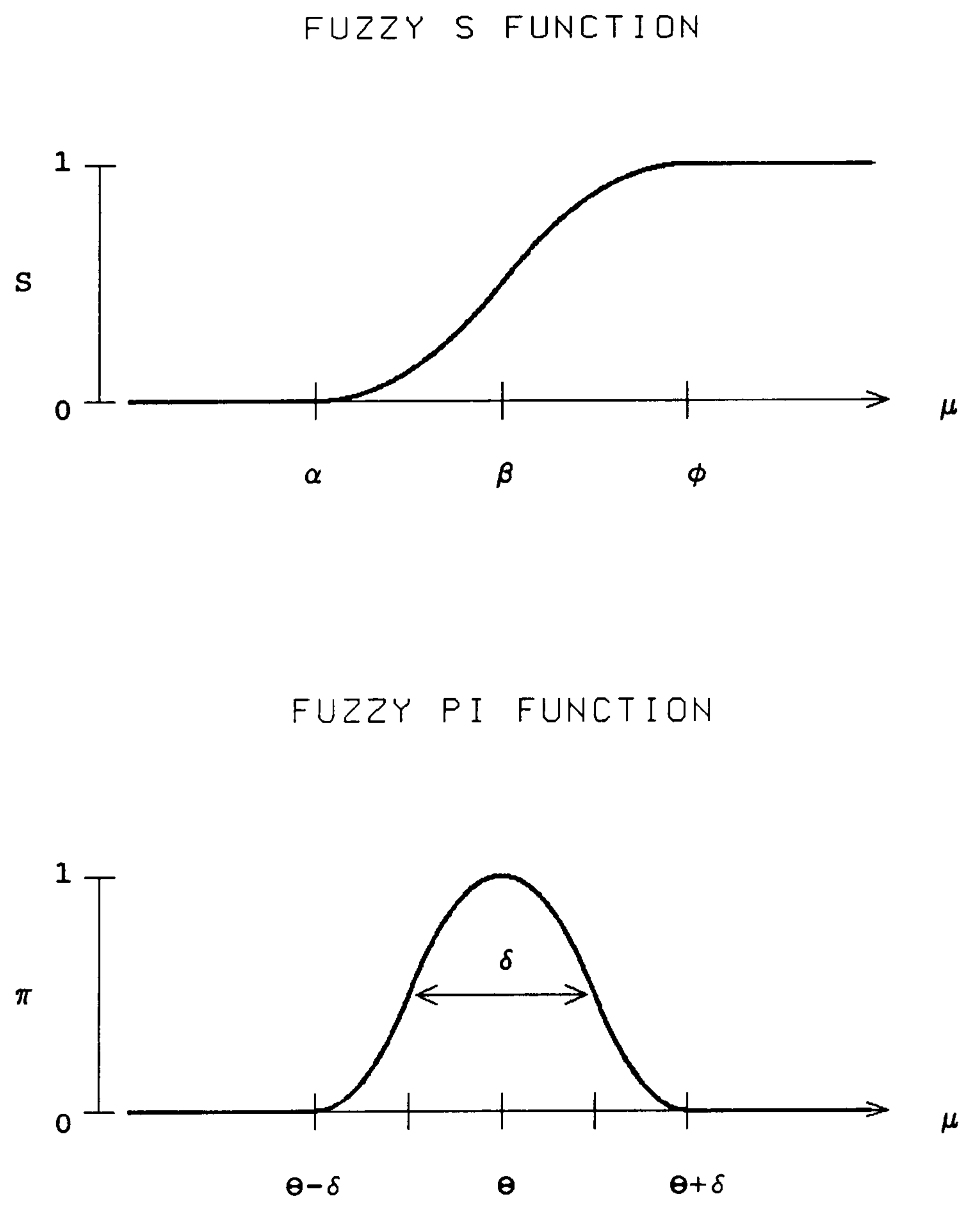

Figure 2.1. Fuzzy Functions for Decision Making.

3. PROCESS HYPERCUBE COMPARISON

A new methodology for signal validation was originated during this research. This new technique basically "learns" the operating states of a system. Once learned, subsequently observed process states are compared against the learned domain. The states having prior existence are declared normal and the signals deemed valid. An evaluation is made on those states which have not been previously observed to identify the abnormal signal(s). This methodology, termed the process hypercube comparison (PHC), derives its name from the fact that the learned process states are stored in a hypercube data structure.

3.1 Basis of Approach

Separation of process changes and signal changes constitutes a significant obstacle to reliable signal validation. That is, process changes can easily "trick" certain methodologies into a determination of signal failure (or non-failure). An ideal method for signal validation would be a detailed model of the process (plant) whereby a determination could be made as to whether the indicated process conditions, as well as the operating path taken, constitute a valid operating regime or not. However, this ideal method is neither feasible nor realistic. An approximation to the ideal process qualifier can, however, be developed. Rather than model the process to determine the valid operating conditions, the process measurements will provide a definition of the valid operating regime.

The concept behind signal validation using the PHC is somewhat similar to the empirical modeling approach. However, rather than model one process variable using a selected group of related process variables, the PHC makes a global (plant-wide) comparison of the process variables. Those conditions judged normal are retained for future reference. A determination can be made as to the normality of future conditions (and the validity of the corresponding signals providing the conditions) based upon this data base of values.

3.2 Hypercube Creation

A hypercube data structure is used to create a history of the valid process conditions. The hypercube is just an efficient method for data storage and compression. In essence the hypercube contains a multi-dimensional histogram of the process conditions. This hypercube data storage is a generic method which could be applied to any type process such as the human body, the financial market or an automobile engine.

The first task is the creation and population of the hypercube. The creation of the hypercube must be a continuously ongoing procedure. The addition of new normal operating conditions must be a continuous process since the plant may be operating at 100% power for some time after which the plant is reduced in power to 90%. This is definitely a valid operating condition but one which has not existed before. A data set which contains data points taken over the entire operating range is most useful for creating the hypercube. Research using plant start-up data has shown good results.

The PHC is first trained off-line using data representing the given operating range. The hypercube is created and each sampled data point is stored. The frequency of occurrence for each data point (process state) is updated. Those process states which appear infrequently may be removed by scanning the entire PHC and noting the frequency of each state. A flow chart of the hypercube creation phase is given in Figure 3.1.

3.2.1 Hypercube Cell Size

During the creation and utilization of the PHC, a prime consideration which must constantly be remembered is that there is a maximum number of potential hypercube cells which may be created. This is limited by the largest unsigned integer number which may be represented by a given computer that is, for a 32-bit machine: 4,294,967,295 cells. The following equation gives the potential number of hypercube memory cells needed given the total number of variables and the number of intervals for each variable.

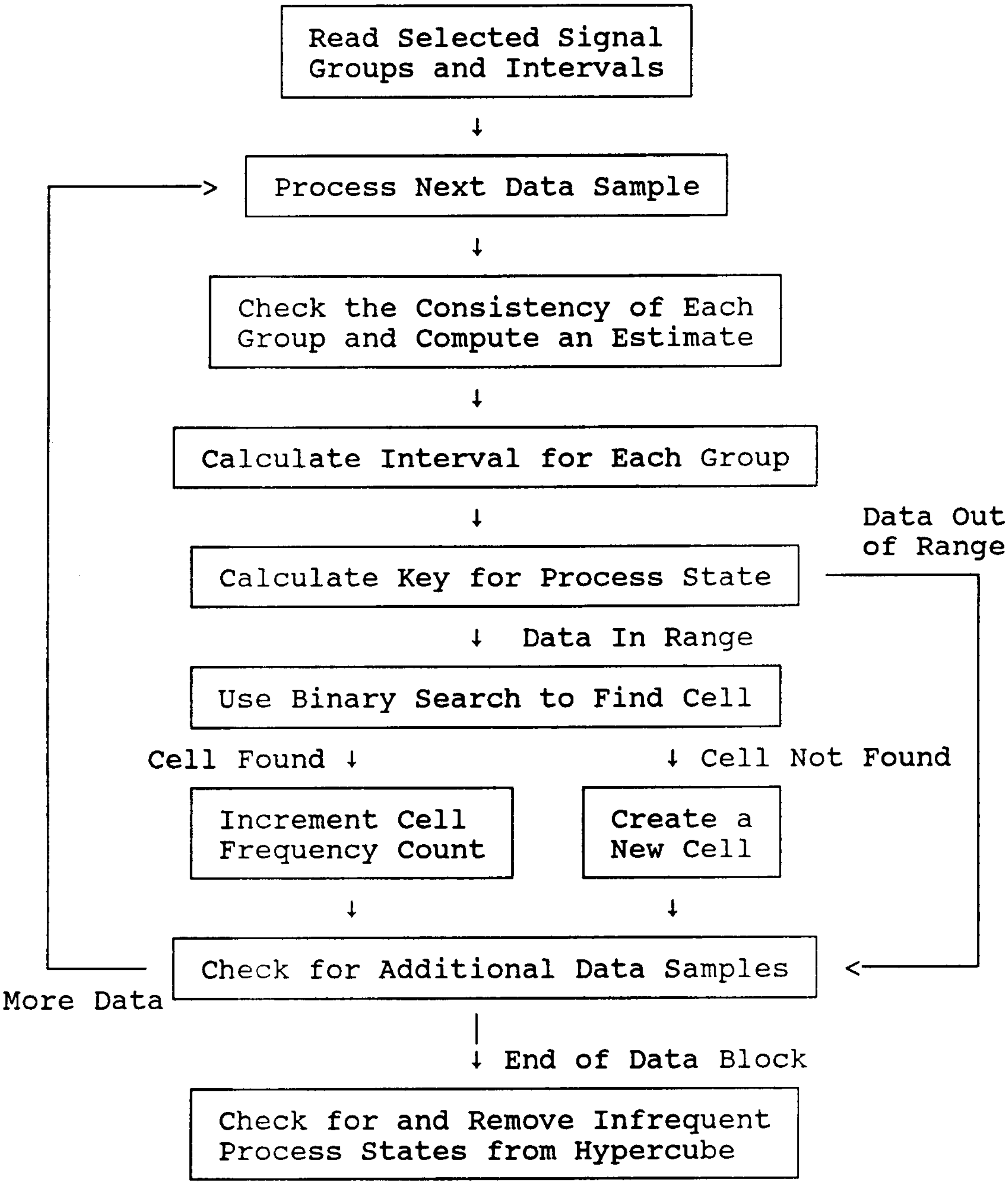

Figure 3.1. Schematic for Creating Hypercube.

$$N_C = \prod_{i=1}^{N_V} N_S(i) \tag{3.1}$$

where

N_C = number of potential hypercube memory cells,

N_V = number of process variables to store,

N_S = number of intervals in each process variable.

Generic Example

Assume that there are three variables to analyze (N_V = 3), and that there are 10, 5 and 8 intervals for the first, second and third variables respectively. The number of potential hypercube cells is

$$N_C = 10 * 5 * 8 = 400 \tag{3.2}$$

The hypercube cell size (or resolution) is a function of the interval widths selected for each variable. One of the primary issues which must be addressed concerning the hypercube memory structure is the optimal width of the hypercube intervals. Small intervals describe the different operating conditions in more detail but require a larger number of potential hypercube cells. Once again, the potential number of cells assumes a limiting role.

Nuclear Plant Example

Now as an example, consider that a hypercube is to be created for a nuclear power plant, specifically a PWR, based on the following process variables:

Hot Leg Temperature	Reactor Power
Cold Leg Temperature	Steam Pressure
Reactor Coolant Flow	Steam Flow
Reactor Coolant Pressure	Feedwater Temperature
Pressurizer Level	Feedwater Flow
Pressurizer Pressure	Steam Generator Level

This gives a total of twelve variables. Assume that each variable is divided into 2 intervals. This results in a total of 4096 cells. Now assume that there are 3 and 4 intervals for each variable; this yields a total of 531,441 and 16,777,216 cells, respectively.

Figure 3.2 is a plot of the number of potential hypercube cells as a function of the number of variables and an equal number of intervals for each variable. One can quickly see that the number of variables and intervals must be minimized as much as possible without losing valuable information. With the large number of monitored process variables in a nuclear power plant, the number of cells in the hypercube can be extremely large as shown in the above example.

The number of variables and the cell resolution (width) must be considered along with the importance placed upon

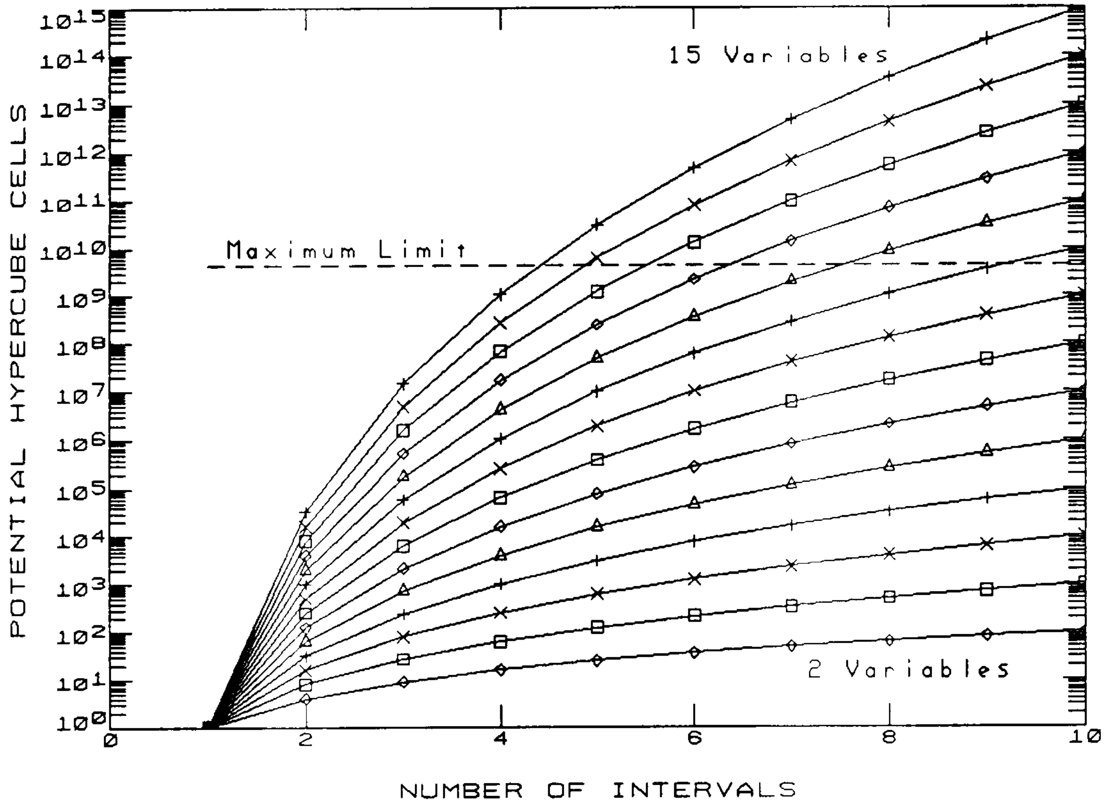

Figure 3.2. Number of Potential Cells as a Function of the Number of Variables.

each of the process variables. The purpose of the signal validation also plays a role in this selection. That is, for detecting shifts in calibration, the interval width must be kept relatively small. For routine plant operation, intervals at infrequently-encountered power levels may be omitted. For signal validation during possible transient conditions, the intervals must cover the entire operating regime. An additional point to consider is that some variables, such as reactor coolant system (RCS) flow, RCS pressure and pressurizer pressure have a nearly constant level from 0% to 100% power. Keeping the above limiting factors in mind, the variables to be validated are selected and the operating range over which a history is to be kept is chosen. Lastly, the resolution (width) of the intervals for each variable is selected.

3.2.2 Redundant Signal Data Compression

In the case where several redundant signals of a given variable exist, it may be infeasible to store each signal individually. Rather, a single estimate for the entire redundant signal group should be used. A check must be performed to ensure that the entire group lies within one interval width of each other. From this fact alone it is easy to see that the smallest interval width ever used need be no smaller than the signal tolerance.

Redundant measurements therefore are reduced to a single value using a compact consistency checking scheme. This scheme is different from the generalized consistency checking (GCC) algorithm. An inconsistency index is calculated using a distance measure based on the signal tolerance. This separation index is computed as

$$S_j = \sum_{k \neq j}^{N} \frac{| m_j - m_k |}{\epsilon} \tag{3.3}$$

where

S_j = inconsistency separation index for signal j,

m_j = measured value for signal j,

ϵ = tolerance ($\leq$ interval width) for the signals,

N = number of redundant signals in the group.

Separation indices are compared and the signal(s) with the largest inconsistency index are declared anomalous. The separation index is recomputed for the remaining signals. The process is repeated until either the separation index is zero or there are no signals.

Those signals with a zero-valued separation index are averaged for an estimated value or the entire group of original signals is used in a weighted average to compute an estimate. The weighting factors are inversely proportional to their most recently computed inconsistency separation index. The weighted average is computed from

$$\theta = \frac{\sum_{j=1}^{N} m_j \, w_j}{\sum_{j=1}^{N} w_j} \qquad (3.4)$$

where

θ = variable estimate for signal group,

m_j = measured value of signal j,

w_j = weighting factor of signal j

= $1.0 - (S_j \;/\; \Sigma\, S_k)$ $\quad [k=1,\ldots,N]$.

The variable estimates from each redundant group are then used to compute the location of the process state in the hypercube. The interval number for each variable is computed first from

$$I_k = \frac{\theta_k - \alpha_k}{\delta_k} \qquad (3.5)$$

where

I_k = interval number for variable k ($I_k=0,1,\ldots,M_k-1$),

θ_k = variable k estimate,

α_k = selected lower limit for variable k,

δ_k = interval width for variable k

= $(\beta_k - \alpha_k) \;/\; M_k$,

β_k = selected upper limit for variable k,

M_k = maximum number of intervals for variable k.

The key used to uniquely identify each process state is computed from

$$\text{Key} = \sum_{k=1}^{N_V} \left[I_k * \prod_{j=0}^{k-1} M_j \right] \tag{3.6}$$

with $M_0=1$. The use of the hypercube requires that only the occupied cells be stored. If the hypercube data compression were not used, storage of the process states could easily require 16 megabytes of memory. This is the motivating factor for using the hypercube rather than a simple multi-dimensional array.

3.3 PHC Signal Validation

The hypercube cannot only determine whether or not a particular process state has existed before, but can also be used to identify abnormal signal(s). Once the hypercube has been created, signal validation may then be performed on future data by comparing the newly observed process states to those previously observed. The PHC is queried at each data sample to make this determination. In order to prevent false alarms, a block of data is used in determining whether or not a given signal is anomalous.

Signal validation is accomplished by alternating which signal(s) are suspected of being in error. By looking at the PHC, the abnormal signal(s) may be identified. The computational effort required for this determination rises as the following increase: (1) the total number of variables stored in the hypercube, (2) the number of potential hypercube cells, and (3) the number of suspected abnormal signals. A flow chart is given in Figure 3.3. Shown in the figure is a new declaration, that of an abnormal process. The process is declared abnormal when several variables are found to be abnormal. The assumption made here is that a catastrophic signal failure is highly unlikely.

PHC Example #1

For example, consider a system in which only three variables (x,y,z) are monitored. (Most examples are restricted to three-dimensional cases for the benefit of the reader.) Suppose that each variable is divided into five intervals. And further suppose that the cells on the diagonal of the cube describing all the possible states are the only ones occupied. These cells would be numbered (1,1,1), (2,2,2), ... , (5,5,5). Now during the observation of this process, a new unobserved state is seen numbered (1,1,5) and labeled (A) on Figure 3.4. It is obvious that both the x and y have been observed together before in this combination but that z was observed in a different state (i.e. z=1 instead of z=5). Thus the true state is probably (1,1,1) and variable z is in error. From this conclusion, it can also be surmised that the correct value of z lies in the range of the first interval.

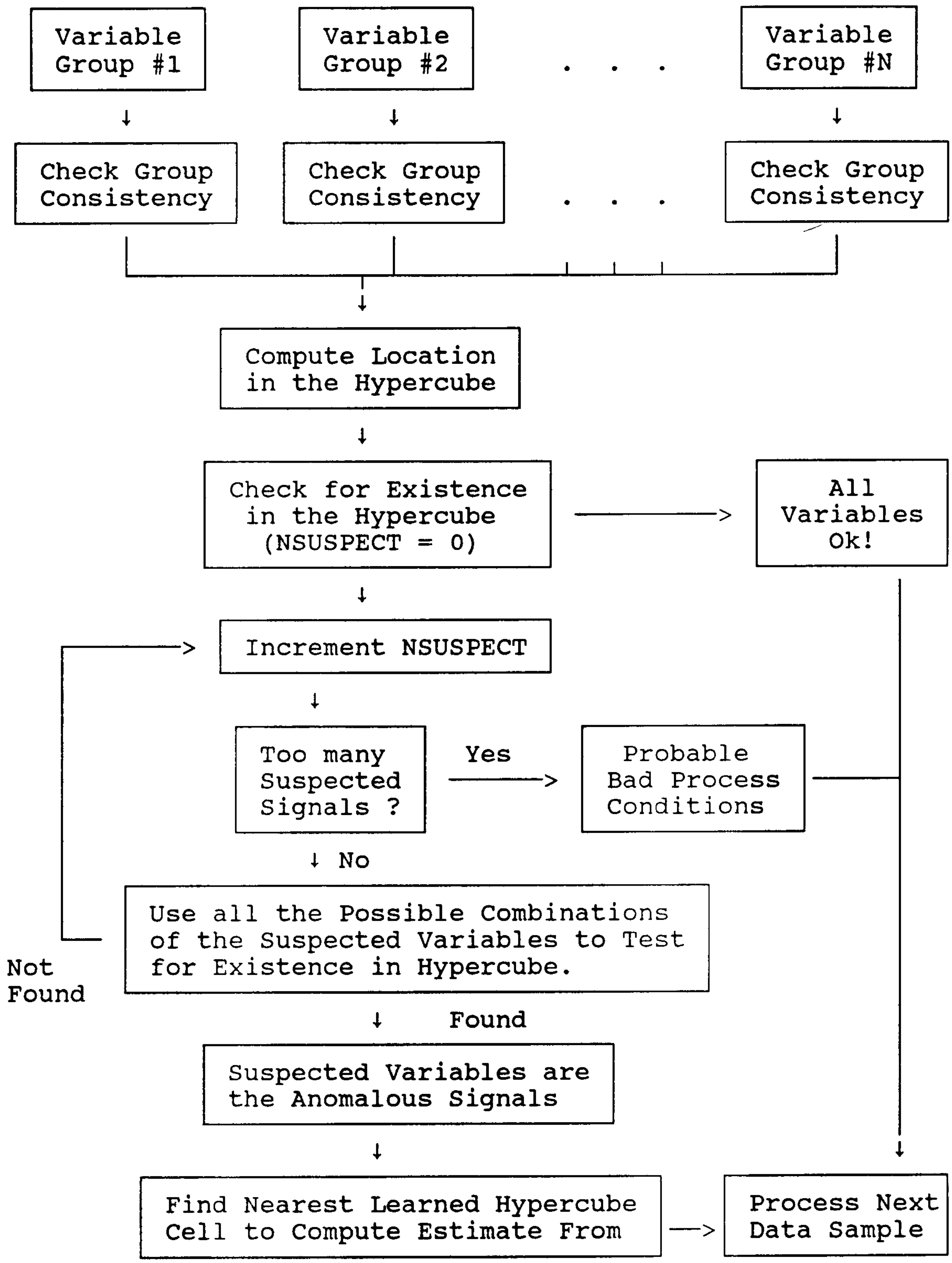

Figure 3.3. Flow Chart of Hypercube Methodology.

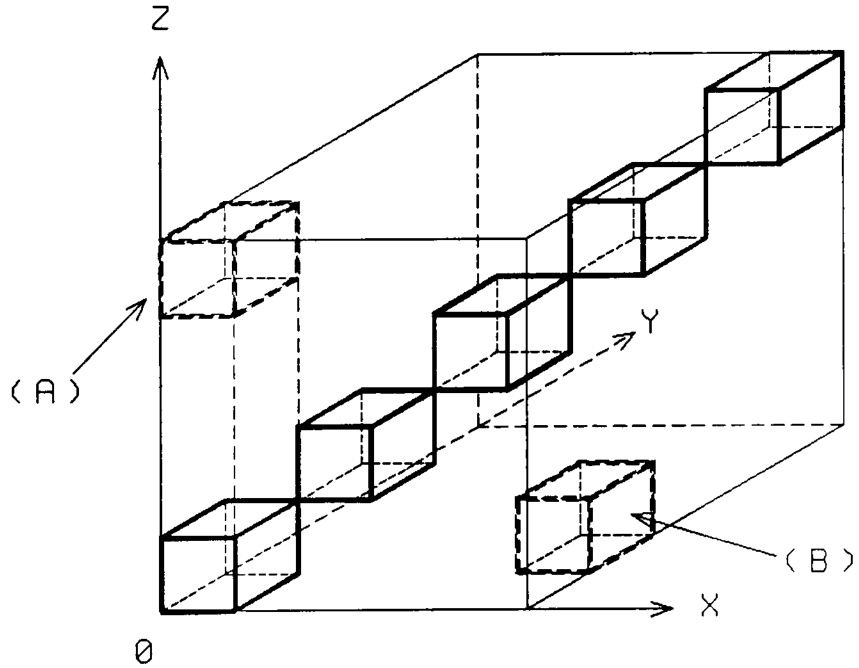

Figure 3.4. Three-dimensional Hypercube Example.

The above example has also demonstrated an additional feature of the PHC, that in the event a signal is identified as incorrect, an estimate of the actual process variable may be provided. This estimate is accurate to within $\pm\ \delta_K/2$ (half the variable interval width).

When the PHC assumes a nearly linear behavior, the hypercube can identify at most N_V - 2 signals as being anomalous, where N_V is the total number of process variables stored in the PHC. Depending on the overall shape of the PHC in the multi-dimensional space, a different number of maximum abnormal signals may be identifiable. The limiting criteria is whether an observed data point is inside or outside of an enclosed region of the hypercube. The following example illustrates this limitation.

PHC Example #2

Note that in Figure 3.5 there are two different two-dimensional hypercubes. Figure 3.5a shows a linearly behaving relationship between the two variables. It is easy to see that an abnormal state is easily identified, however it is impossible to distinguish which variable is in error. In Figure 3.5b the two variables assume a nonlinear relationship and depending on the location of the newly observed state, a specific variable may or may not be noted as abnormal. In location (3) the abnormal variable cannot

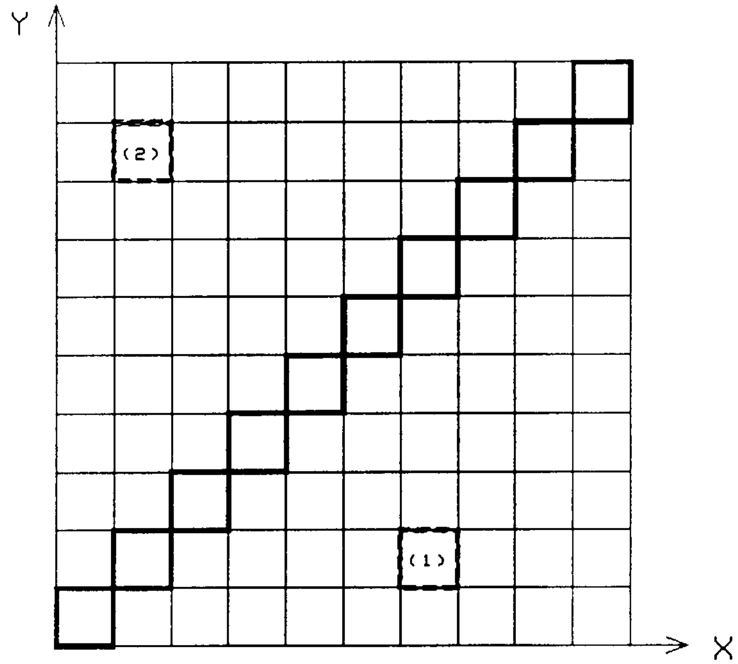

Figure 3.5a

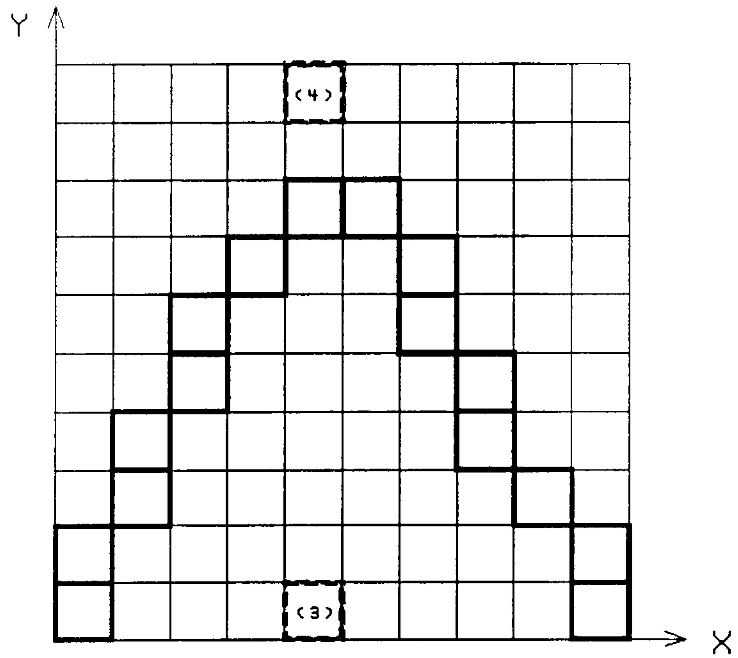

Figure 3.5b

Figure 3.5. Two-dimensional Hypercube Example.

be identified, while at location (4) the abnormal variable may be identified as y.

PHC Example #3

Returning to Figure 3.4, another example in which the abnormal signal cannot be distinguished is given. At location (5,2,1), labeled (B), the combination of x, y and z has not existed before. Further analysis shows that neither can the combination of any two variables be found in the learned hypercube.

The hypercube is a multi-dimensional histogram and is essentially a body in a multi-dimensional space. It is important to recognize that the search for abnormal signal(s) does not always correspond to the shortest distance to the surface of the hypercube.

PHC Example #4

Returning to the first example (Figure 3.4), note that the distance between the learned state (1,1,1) and the newly observed state (A) is 4 units. The nearest cell (3,3,3) however is only $\sqrt{12}$ = 3.46 units away. Thus it is shown that the nearest observed state is not necessarily the true state. This aspect is accounted for in the PHC signal validation algorithm.

Although the hypercube signal validation is somewhat simple in theory, the implementation of the algorithm is not a trivial task, primarily because of the multi-dimensional space which must be searched in determining the anomalous signal(s). The computational effort required to make this analysis is directly proportional to the number of variables stored in the hypercube. There is a geometric increase in computing time needed as the number of postulated signals in error increases.

3.4 Final Signal Status

The PHC methodology provides three basic results from its analysis:

1. An inconsistency separation index.
2. An indication of variable abnormality.
3. An estimate of the process variable.

From the above results, a final determination of the status of individual signals is made. In the simplest case, when a signal is consistent with its redundants and the variable is found in the hypercube, the signal is deemed accurate. A little more thought is required for the other possibilities. Figure 3.6 gives the procedure for determining the final signal status based upon the signal's consistency test results and its variable group results. As previously stated, in order to avoid false alarms a block of data

Decision Criteria for Each Individual Signal	Signal's Variable Group Found in the Hypercube	Process Abnormality Detected by the Hypercube	Signal's Variable Group NOT Found in the Hypercube
Signal Consistent wrt Group	Signal Accurate	Signal Probably Accurate	Signal Possibly Failed
Signal Partially Consistent wrt Group	Signal Marginal	Signal Status Indeterminate	Signal Probably Failed
Signal Inconsistent wrt Group	Signal Failed	Signal Questionable	Signal Possibly Accurate

Figure 3.6. Hypercube Decision Criteria.

samples are analyzed to furnish a final indication of signal validity.

3.5 Experimental Results

The hypercube signal validation methodology has been implemented in a VAX workstation using the C programming language. The program provides several options for data processing and results display.

1. Evaluation of data using the PHC signal validation methodology.
2. Creation and population of a new hypercube.
3. Addition of new data to an existing hypercube.
4. Plotting of the inconsistency separation index.
5. Plotting of the hypercube variable estimate.
6. Plotting of the hypercube variable status.
7. Viewing the final signal status for a data block.
8. Display of the hypercube features (ranges and interval widths of the variables).
9. Listing of the hypercube cells and frequencies.
10. Removal of hypercube cells appearing infrequently.

A sampling of the results provided by the PHC is presented at this point to familiarize the reader with the PHC output. More complete results from the application of the PHC are presented in Sections 6 and 7. Figure 3.7 gives a printout from the PHC after finding 3 of 11 signals to be

Process state absent from learned hypercube domain!

The anomalous process variables are 3, 6 and 8.

```
Variable #  1, Measurement:    1.89
Variable #  2, Measurement:   25.99
Variable #  3, Measurement: 2250.00      Estimated: 2237.50
Variable #  4, Measurement:  554.80
Variable #  5, Measurement:  559.30
Variable #  6, Measurement: 2251.50      Estimated: 2225.00
Variable #  7, Measurement:   27.95
Variable #  8, Measurement:   55.42      Estimated:   50.00
Variable #  9, Measurement: 1069.67
Variable # 10, Measurement:  108.93
Variable # 11, Measurement:  110.00
```

Figure 3.7. Printout from Hypercube Signal Validation.

abnormal. The anomalous signals are identified along with an estimate of the true process conditions.

An example plot of each of the primary hypercube results is given in Figures 3.8, 3.9 and 3.10. The PHC inconsistency index shows that only one signal (RCS-P458) was consistent with respect to the rest of its redundant group at all time instances. The other signals were excluded from the variable estimate at those places marked with an asterisk. A validated variable estimate from the PHC evaluation is given in Figure 3.9. Lastly, the variable status is presented in Figure 3.10. The variable status shows the PHC results for a particular variable. The y-axis can indicate that the variable was found or normal (zero), the process was abnormal (one) or the variable was not found in the hypercube (two). If the signal is beyond the selected range for the hypercube, an asterisk is plotted along with the fact that the variable was not found.

The hypercube range (upper and lower limit) is selected along with the number of intervals. The selected values for the PWR and EBR-II data are given in Tables 3.1 and 3.2, respectively. The experimental results from the creation of the two hypercubes is shown in Table 3.3. The important result to note in this table is that the number of potential cells is tremendous while the actual number of occupied cells is relatively small. Also a comparison of the hypercube before and after the removal (clean-up) of

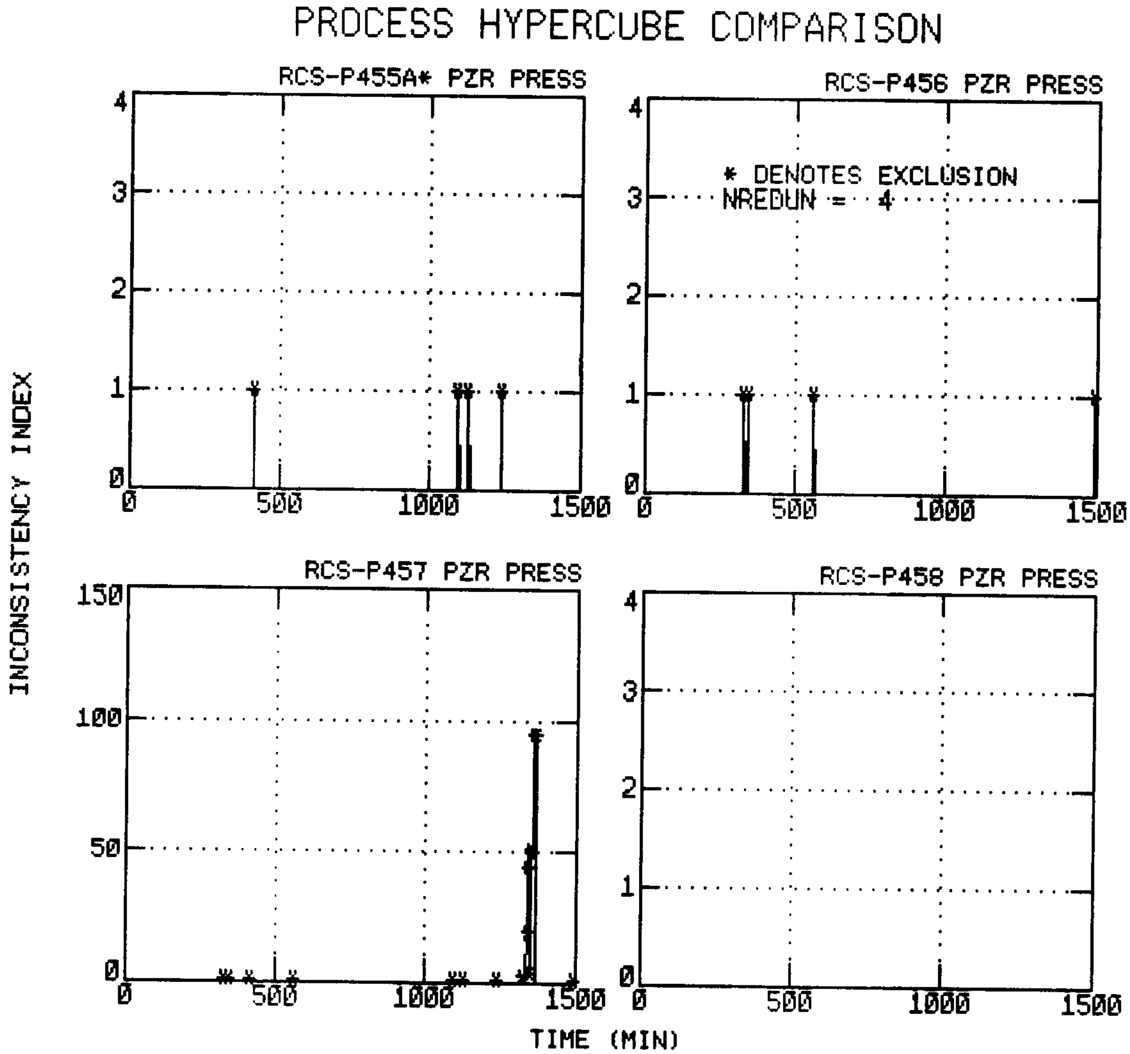

Figure 3.8. PHC Inconsistency Separation Index.

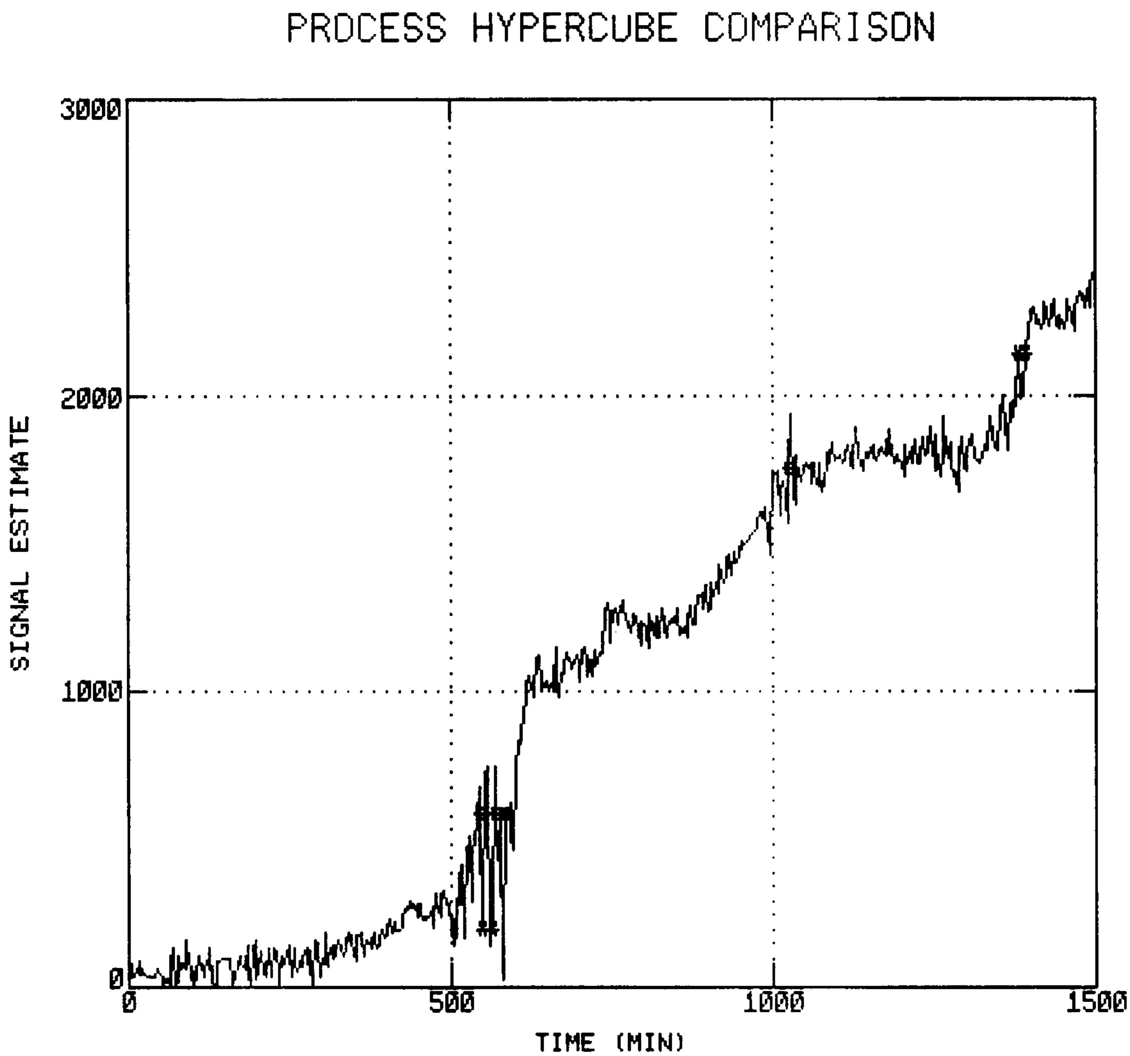

Figure 3.9. **PHC Variable Estimate.**

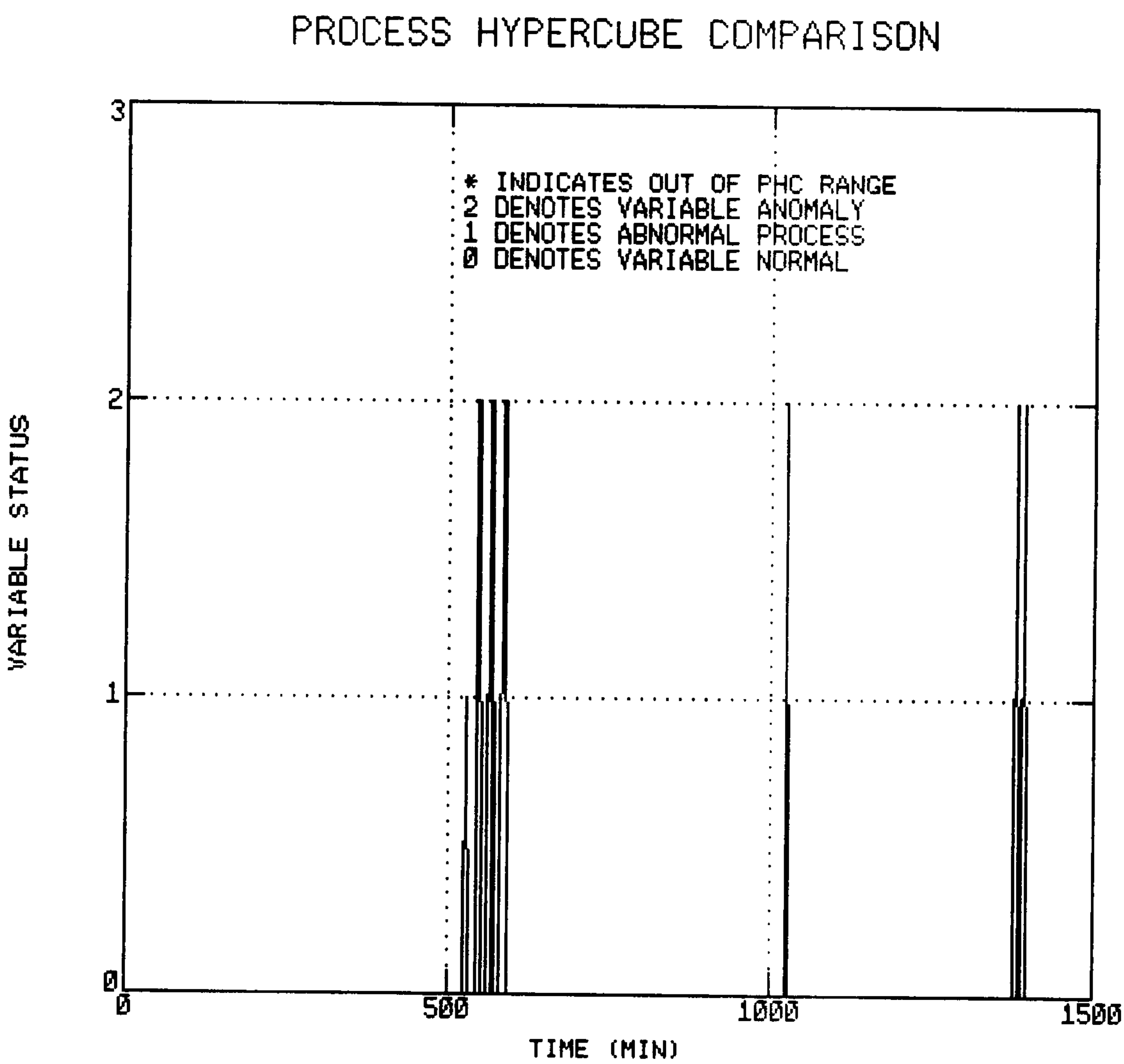

Figure 3.10. PHC Variable Status.

TABLE 3.1

PWR Hypercube Specifications

Variable	Lower Limit	Upper Limit	Number of Intervals	Width of Interval
Power (%)	0	100	20	5
PRZR Level (%)	25	75	5	10
PRZR Pressure (psia)	2200	2300	4	25
Cold Leg Temp. (°F)	530	580	5	10
Hot Leg Temp. (°F)	530	630	10	10
RCS Flow Rate (%)	70	120	5	10
RCS Pressure (psia)	2150	2350	4	50
Feedwater Flow (kpph)	0	3900	10	390
SG Level (%)	25	75	5	10
Steam Pressure (psig)	900	1150	5	50
SG Steam Flow ()	70	120	5	10

Number of Potential Cells: 500,000,000

TABLE 3.2

EBR-II Hypercube Specifications

Variable	Lower Limit	Upper Limit	Number of Intervals	Width of Interval
Power (%)	0	100	10	10
Inlet Plenum Temp (°F)	690	710	2	10
Upper Plenum Temp (°F)	700	875	5	35
IHX Primary Outlet (°F)	700	720	2	10
IHX Secondary Outlet (°F)	690	865	5	35
SU Na Inlet Temp (°F)	620	860	4	60
SU Na Outlet Temp (°F)	600	780	4	45
EV Na Outlet Temp (°F)	540	600	3	20
IHX Secondary Inlet (°F)	540	600	3	20
Secondary Na Flow (%)	0	100	5	20
Drum FW Flow (lbm/hr)	0	$3x10^5$	5	60,000
Drum Feedwater Temp (°F)	355	555	4	50
EV Feedwater Temp (°F)	530	590	3	20
EV Steam Outlet Temp (°F)	535	595	3	20
SU Steam Inlet Temp (°F)	560	650	3	30
SU Steam Outlet Temp (°F)	600	825	5	45
		Number of Potential Cells:	1,944,000,000	

TABLE 3.3

Hypercube Experimental Results

Result	Data Set	
	PWR	EBR-II
Number of Signals	77	72
Number of Signal Groups	26	16
Number of Loops	4	1
Number of Variables	11	16
Number of Potential Cells	$5x10^8$	$1.944x10^9$
Number of Occupied Cells Before Clean-up Operation	363	73
Frequency Range of Cells Before Clean-up Operation	1 - 367	1 - 667
Total Number of Samples Before Clean-up Operation	3117	3440
Number of Occupied Cells After Clean-up Operation	155	61
Frequency Range of Cells After Clean-up Operation	3 - 367	3 - 667
Total Number of Samples After Clean-up Operation	2848	3424

infrequently appearing states shows a considerable difference in samples. The number of cells drops by more than half while the number of samples is decreased by only ten percent in the PWR case. This outcome provides definitive proof of the efficiency of the hypercube.

3.6 Summary

A process hypercube comparison (PHC) has been implemented for the purpose of signal validation. A hypercube is created during a learning period, after which the hypercube may be used to detect abnormal signal(s). An estimate of a variable may be provided in the event an abnormality is detected. A simple consistency checking scheme is used to reduce a group of redundant measurements to a single estimate.

The PHC methodology might well be applied to noise level failure detection also. The PHC noise level validator could be implemented on a sample-by-sample basis in which the data processing would be identical to that used for the signal level processing above except that the signal noise is compared and stored rather than the d.c. signal level. A PHC noise validator could also be based on block-by-block data processing in which the root-mean-square (RMS) noise level for the block is utilized for comparison and storage.

4. DEVELOPMENT OF COMPREHENSIVE SIGNAL VALIDATION SYSTEM

As previously stated much work has gone into developing distinct signal validation modules, but none has been devoted to a comprehensive signal validation system. The realization of such a system entails both a developmental and testing effort.

4.1 Comprehensive Signal Validation System Objectives

The primary objectives of the comprehensive signal validation system development must first be examined.

1. The system is to be constructed with a modular architecture such that the new signal validation modules can be added or old modules removed without altering the system.

2. A final determination of the signal status must be provided by the system based on the results of the individual modules.

3. The system should be created in such a manner as to be generic with regard to its application, that is, it should not be system specific.

A schematic of the comprehensive signal validation system is shown in Figure 4.1. The integration of these modules is not a trivial task. A systematic method for combining the information from the various modules has to be developed.

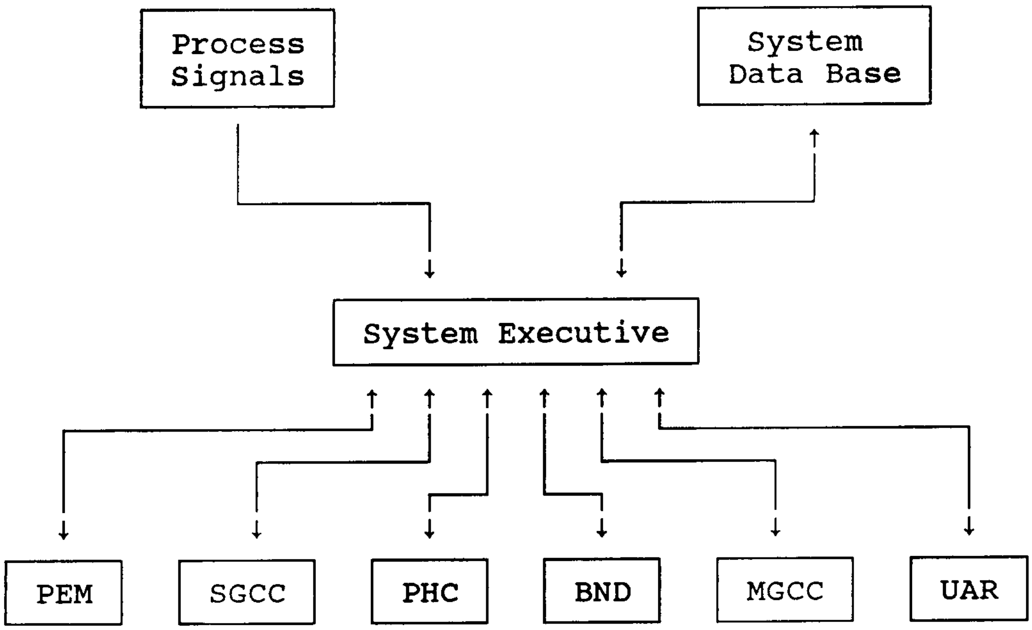

Figure 4.1. Schematic of the Comprehensive Signal Validation System.

This section focuses on this decision making, and the problems and limitations associated with it.

4.2 System Executive

The System Executive (SE) is the control module (or program) which handles the following basic tasks:

1. Reads data from some source --- a data file, the plant computer or an analog-to-digital converter.
2. Selects the signals to be validated.
3. Validates each signal using the individual signal validation modules.
4. Makes the final overall determination of the signal status.
5. Displays the results obtained in the form of graphs, tables, charts,... as appropriate.

Thus, the primary tasks delegated to the System Executive are controlling the modules and that of making the final signal status determination in a modular environment.

4.3 Problem Definition

4.3.1 Modularity Considerations

One of the primary objectives of the SVS is to maintain a modular (parallel processing) architecture. The modular design provides both the facility to incorporate newly developed signal validation techniques and the ability to remove signal validation modules which prove to be either unsatisfactory or unsuited for certain applications. To maintain the modularity, the module outputs must be kept uniform, however the input requirements need not be as restrictive.

4.3.2 Process Considerations

An analysis of the present problem and situation is appropriate at this point. The following is a list of facts associated with the process under consideration (a nuclear power plant).

1. Nuclear power plants are generally base-loaded and therefore run at a steady full power.
2. Nuclear power plants have three or four redundant signals for each of the major process variables.
3. Catastrophic failure of a signal will probably lead to a rapid process shutdown (plant trip).
4. Design criteria are engineered to minimize the possibility of common-cause failure.
5. Nuclear quality standards attempt to ensure that failure occurs on an infrequent basis.

4.3.3 Module Considerations

A number of facts associated with the individual signal validation modules should also be noted at this point.

1. Most of the modules are designed for use at steady-state process conditions, therefore erroneous results can be expected during changing process conditions.
2. Because the modules employ unique methodologies which look at different failure modes, it is entirely feasible for one module to indicate signal malfunction while the remaining modules will not.

3. Each module has three zones of knowledge -- signal failure, signal correct and status indeterminate.

The three knowledge zones (failed, correct and unknown) for each module must be determined from a systematic evaluation of real process data. Initially, the widest zone will be the unknown (grey) zone. As experience with a given module increases, the width of the grey zone should be narrowed and the positive conclusion zones (failed and correct) widened (see Figure 4.2). These three zones can be thought of much like a traffic light where the failed zone is red (stop, danger), the correct zone is green (proceed) and the unknown zone is yellow (caution, look closely). These three zones are more simply "yes," "no" and "I don't know." These same zones can be found in any discipline, for instance the medical profession. A visit to the doctor may result in a healthy checkup, specific illness diagnosed or the need to see a specialist.

4.4 Decision Making

A comprehensive signal validation system has been developed. The fully integrated system required the development of an inter-module decision maker and a process qualifier. These two elements were configured into a unit known as the System Executive (SE). The purpose of the System Executive is to combine results of different signal validation modules (techniques) into a final determination

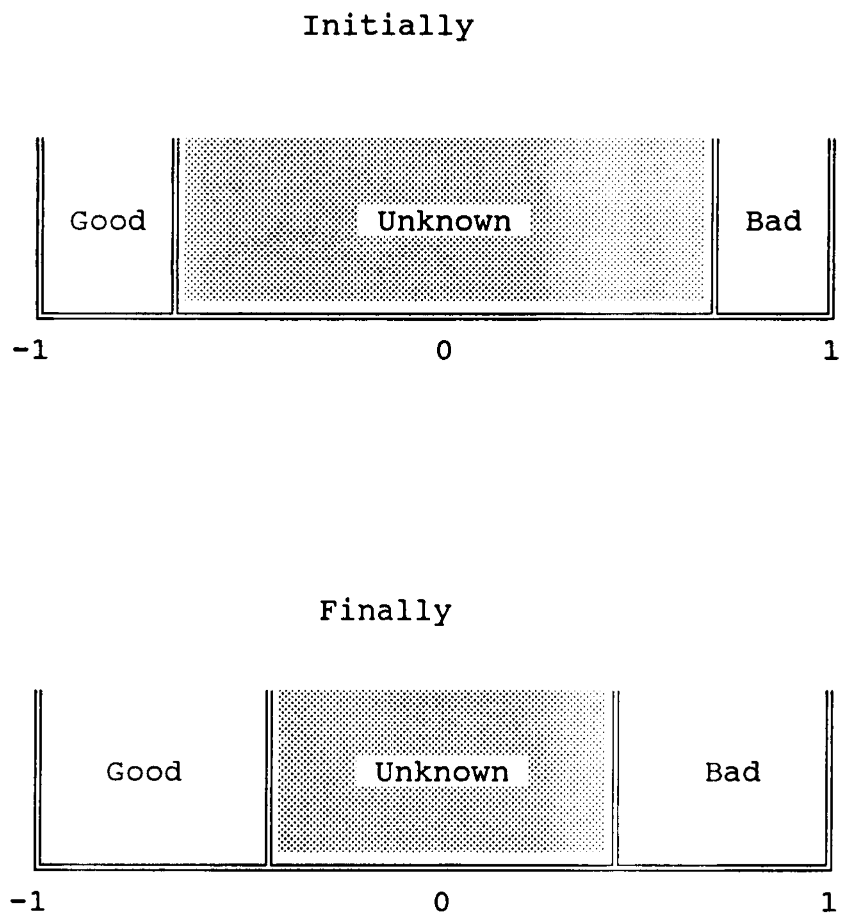

Figure 4.2. Module Knowledge Zones.

of the signal status. One primary objective is that the signal validation methodologies (modules) are to be implemented in such a manner that modules can either be added or removed easily (rack mountable). Also, rather than creating a system specific signal validation system, another important objective is to keep the approach as generic as possible with respect to the applicable processes. As with any decision methodology the primary objective is to minimize the probability of both missed alarms and false alarms (performed qualitatively in this research).

4.4.1 Decision Maker Development

Two different types of decision makers were considered. The first (designated type I) is simpler in design and requires no knowledge of the inter-workings of the individual modules and enables a completely modular signal validation system. The second (type II) maintains a data base which describes each module's scope of failure detection but defeats the modularity of the signal validation system. The characteristics of both decision makers are presented below.

In order to achieve uniformity in the result reported by each module and thereby construct a decision maker in which no knowledge of the individual modules is required, it has been established that each module will compute a confidence factor identifying whether a given signal is anomalous (or is accurate). This confidence factor ranges from -1.0 to +1.0, where -1.0 indicates that the signal is reliable and +1.0 indicates that the signal is faulty. The System Executive will use these confidences in its overall determination of the signal status.

4.4.1.1 Type I Decision Maker

With a single module a final decision is simple, but an overall conclusion is more difficult to reach when there are two or more modules. It was previously noted that the modules can detect independent failure modes. Thus it stands to reason (assuming the knowledge zones have been properly established) if any one module indicates that a failure has occurred, then the overall conclusion by the System Executive should be one of failure (even if all the other modules indicate normal functioning). Figure 4.3 illustrates this with two hypothetical modules which detect failure based on noise level and actual signal level, respectively. As shown, if either module indicates failure then the overall conclusion should be failure. This is a somewhat simple yet bold statement, hence consider the alternatives.

1. <u>False Alarm</u> A single module indicates failure while the remaining modules state either indeterminate or correct, but the truth of the matter is that the signal is good. In this case

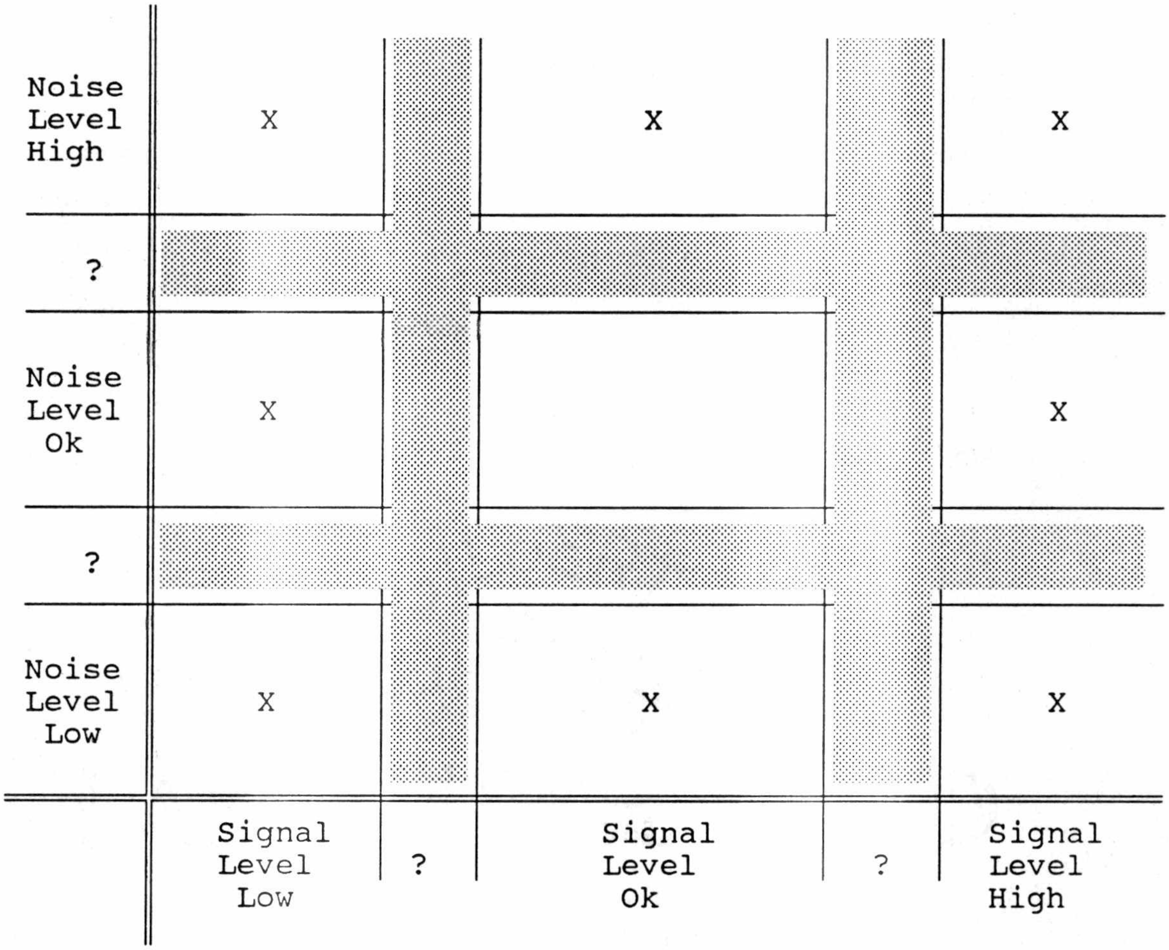

Letter "X" indicates failure region.

Figure 4.3. Independence of Module Analyses.

the failure zone has been incorrectly identified and must be re-established.

2. Missed Alarm A failure occurs while the modules indicate an acceptable signal. The first question which must be asked is "was this failure mode detectable by any module(s)." If so, then once again the module knowledge zones are incorrect; if not, the system has performed as expected and a new module should be constructed to detect this type of failure.

If any module is chronically in error, an evaluation should be conducted as to whether or not the module should be removed from the system.

The overall conclusion is based upon the following criteria.

1. Signal Anomaly: A signal will be declared to be invalid when one or more modules indicate anomaly.

2. Status Indeterminate: The status of a signal will be declared indeterminate when a failure has not occurred and at least one module indicates status unknown.

3. Signal Accurate: A signal will be declared correct when all modules indicate correct.

The overall conclusion of failed or indeterminate state when any one module indicates failure or unknown stems from three reasons:

1. The train of thought presented above which shows that given failure modes may be detectable only by a single module.

2. The unknown (caution) will warn the plant personnel that further examination may be warranted.

3. Most importantly, this is the most conservative approach.

This decision maker, though simple in design, could provide a method by which correct conclusions are reached and false alarms are greatly minimized. Using the decision making methodology presented above, the System Executive would also be able to combine information from modules performing independent analyses without knowledge of the modules themselves.

4.4.1.2 Type II Decision Maker

Next signal failure is examined beginning from a global viewpoint down to the microscopic elements (see Figure 4.4). At the global level, there are numerous possible signal failure modes. A failure mode is a particular type of anomaly such as drift or abnormal response time. Each signal failure mode is composed of one or more signal failure characteristics (some of which are more important than others). Failure characteristics are the distinguishing qualities or properties of the various failure modes such as RMS noise. Some failure characteristics are present in more than one failure mode. It is noted that failure can occur at normal or abnormal process conditions (the two are independent).

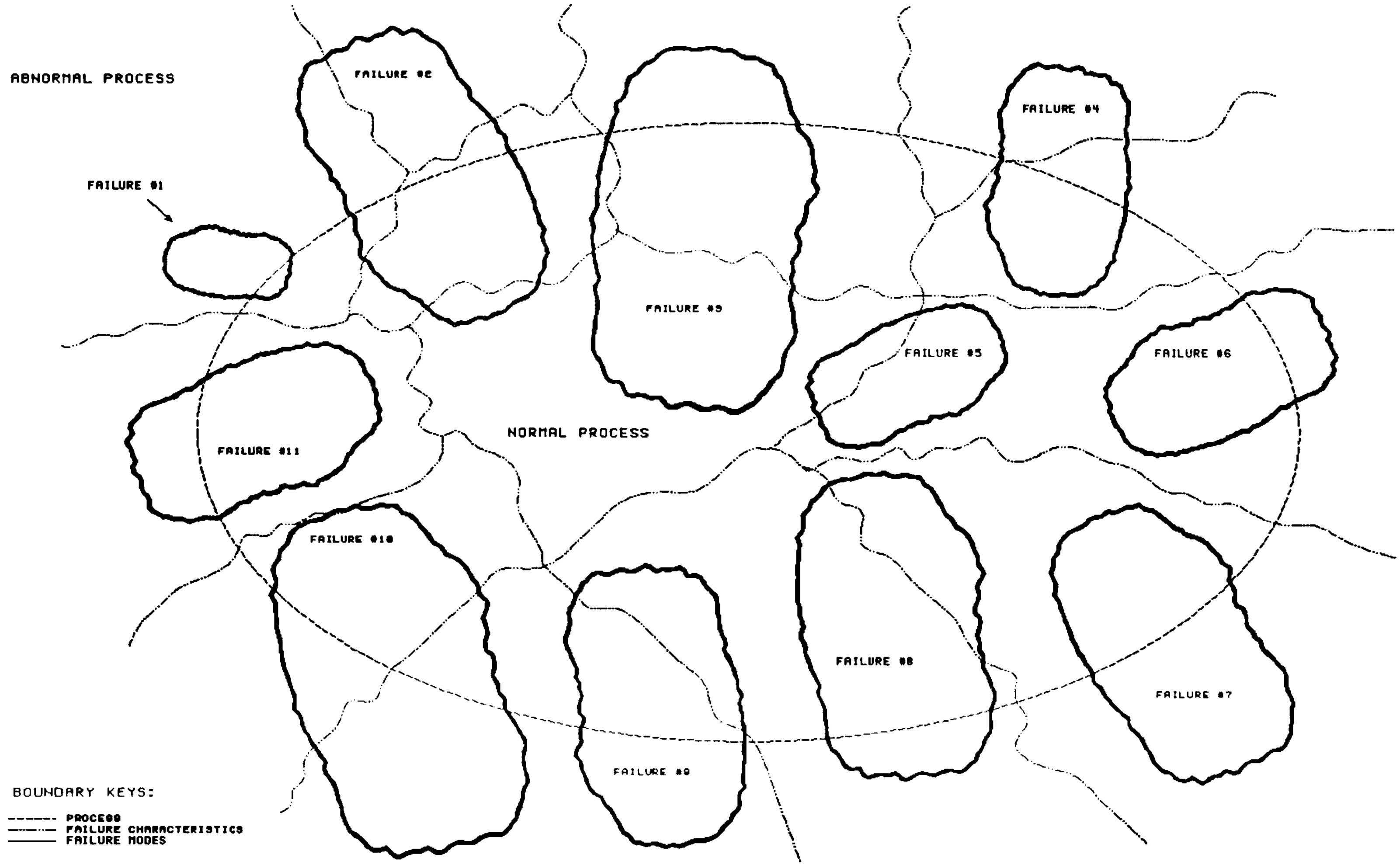

Figure 4.4. Global Representation of the Signal Failure Identification Problem.

Now superimposing the signal validation modules onto the above failure modes (see Figure 4.5), the important facts associated with the decision making may be seen.

1. Each module can detect one or more fault characteristics.

2. There is overlap between the various module detection methods and the detectable fault characteristics.

3. Not all fault modes are detectable.

4. Some modules do not perform correctly under abnormal process conditions.

5. Some modules are inherently more reliable (important) than others (not shown in the figure).

Based upon the above observations the most obvious decision maker (rule-based) would require the following.

1. A list of all detectable fault modes and their respective characteristics with the characteristics rated as to the importance within each fault mode.

2. A list of fault characteristics and the module(s) which can recognize each including a comparative inter-module rating of its ability to detect the specific characteristic.

3. A rating of each module's ability to function under abnormal (transient) process conditions.

Each module would then return a confidence level of failure for each of its detectable characteristics. The decision maker would then evaluate the results by looking at the extent to which each fault mode has been detected. The primary disadvantage to this decision maker is its removal

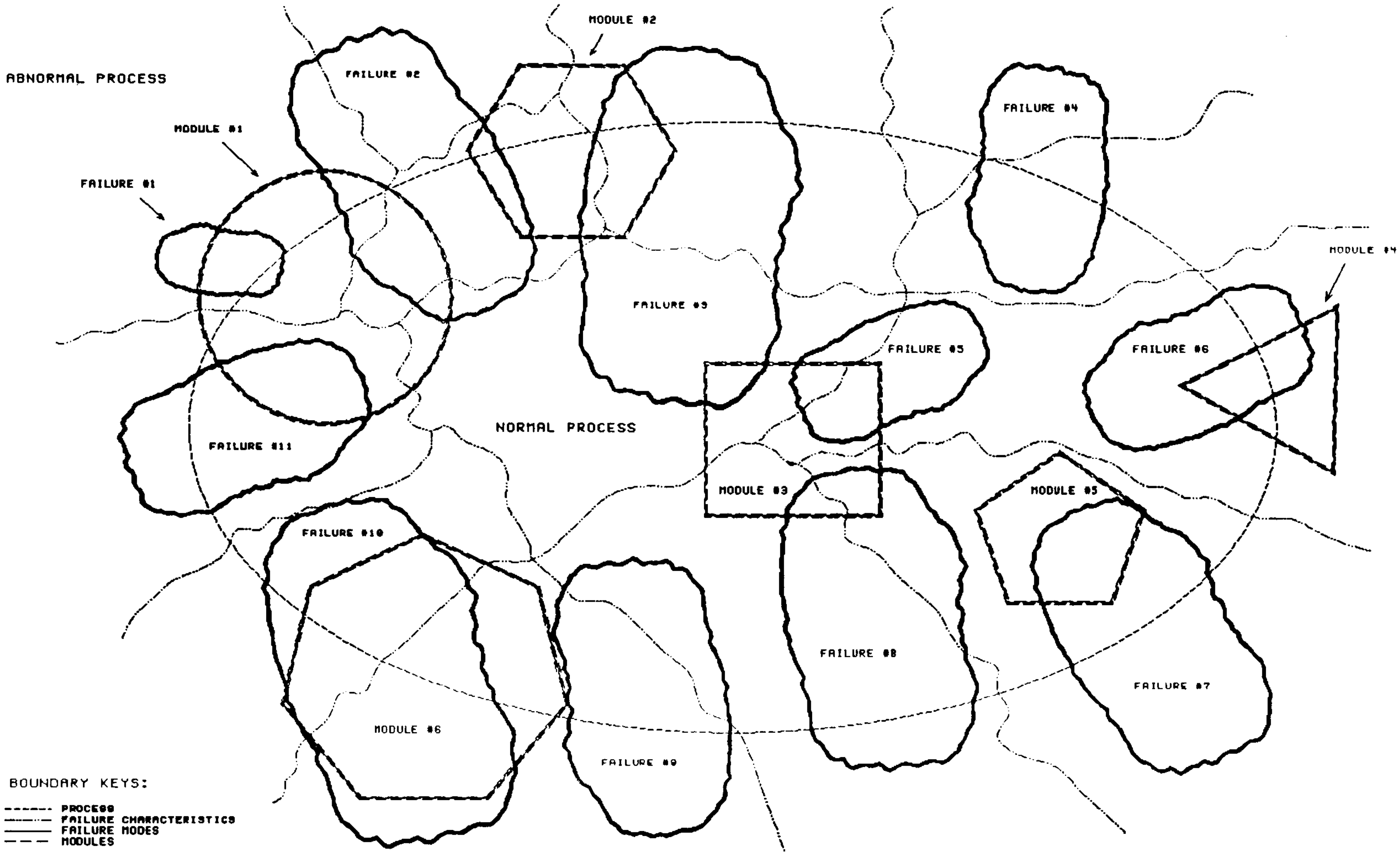

Figure 4.5. Global Viewpoint of Failure Detection by the Signal Validation Modules.

of the modular signal validation system concept. And worse yet, in the event a module is added or removed, these ratings must be totally re-determined. The key to accurate signal validation would lie in the correct determination of the ratings and confidences listed above, a difficult task to accomplish.

4.4.2 Positive Decision Maker

Each of the above two decision makers has its advantages and disadvantages. Selection of the best decision maker should be made on the basis of the one with the lowest missed-alarm and false-alarm probabilities. The two decision makers are compared in Table 4.1. A complete analysis of the two methods shows that neither is perfect. The major disadvantage of the type I decision maker is its disregard of individual module ability and the overlap between modules. The primary drawback of the type II decision maker is the establishment of the different ratings and the overall complexity. What is needed is a combination of the two methods --- a "positive" decision maker.

The Positive Decision Maker (PDM) utilizes the best elements of the type I and type II decision makers. First, the failure mode(s) detectable by each module must be identified. Second, the module returns a confidence factor (CF) for each of its detectable failure modes rather than the failure confidences as in the type II decision maker.

TABLE 4.1

Decision Maker Comparison

Comparison Criterion	Decision Maker: Type I	Decision Maker: Type II
Failure Detection	Good if knowledge zones properly fixed.	Good if ratings properly established.
False Alarm Probability	Moderate since if failure zone is not reached, no conclusion is made.	Low since agreement between modules is required for a conclusion.
Missed Alarm Probability	Higher since failure zones are established with a high degree of confidence.	Lower since more information from independent sources is available for cross analysis.
Failure Classification	Lower without inter-module knowledge.	Better with the cross information.
Modularity	Totally preserved.	Lost to most extent.
Implementation	Relatively simple.	Complex; not straightforward.

These confidences shall be in the range from -1.0 to +1.0 where the following relationships hold:

CF = -1.0 when the signal is good.
CF = 0.0 when the signal status is indeterminate.
CF = +1.0 when the signal has failed.

Intermediate confidence values shall indicate a relative measure of goodness or failure. These confidences are directly reduced by the process abnormality fraction computed from the process qualification (see Section 4.5). The reduced confidence is computed from:

$$CF' = CF * Ag \tag{4.1}$$

where

CF' = reduced confidence factor from a module,

CF = original confidence factor from a module,

Ag = process abnormality fraction.

Note that the selected confidence range (-1.0 to +1.0) allows the direct reduction of the confidence value. That is, no matter what the original value of confidence factor, the reduction causes the value to move towards zero (status indeterminate) which correctly describes the situation.

The final conclusion is then based on using the following selection criteria:

1. Signal Anomaly (Red Zone): A signal will be declared invalid by a specific failure mode if and

only if at least one module detecting this failure mode indicates failure and all other modules detecting this type of failure indicate failure or status indeterminate. That is to say, no other module which can detect this type of failure may indicate the signal to be accurate.

2. <u>Signal Correct</u> (Green Zone): A signal will be declared accurate if and only if no module indicates a failure of any kind.

3. <u>Status Indeterminate</u> (Yellow Zone): The status of a signal is declared indeterminate in those cases where a signal is not found valid or anomalous.

4. <u>Impending Failure</u> (Orange Zone): Consistent prolonged indication of indeterminate for a given failure mode will be tagged as a likely impending failure warranting additional attention.

Four example PDM conclusions are given in Figure 4.6 from the results of three hypothetical modules. In the event more than one failure is indicated the relative confidences and agreement between modules are used to determine the most likely (primary) failure. The remaining failures may be listed as secondary failures. The flow chart shown in Figure 4.7 illustrates the PDM in detail. Table 4.2 lists the individual failure modes detectable by each module.

The Positive Decision Maker strategy has the following advantages:

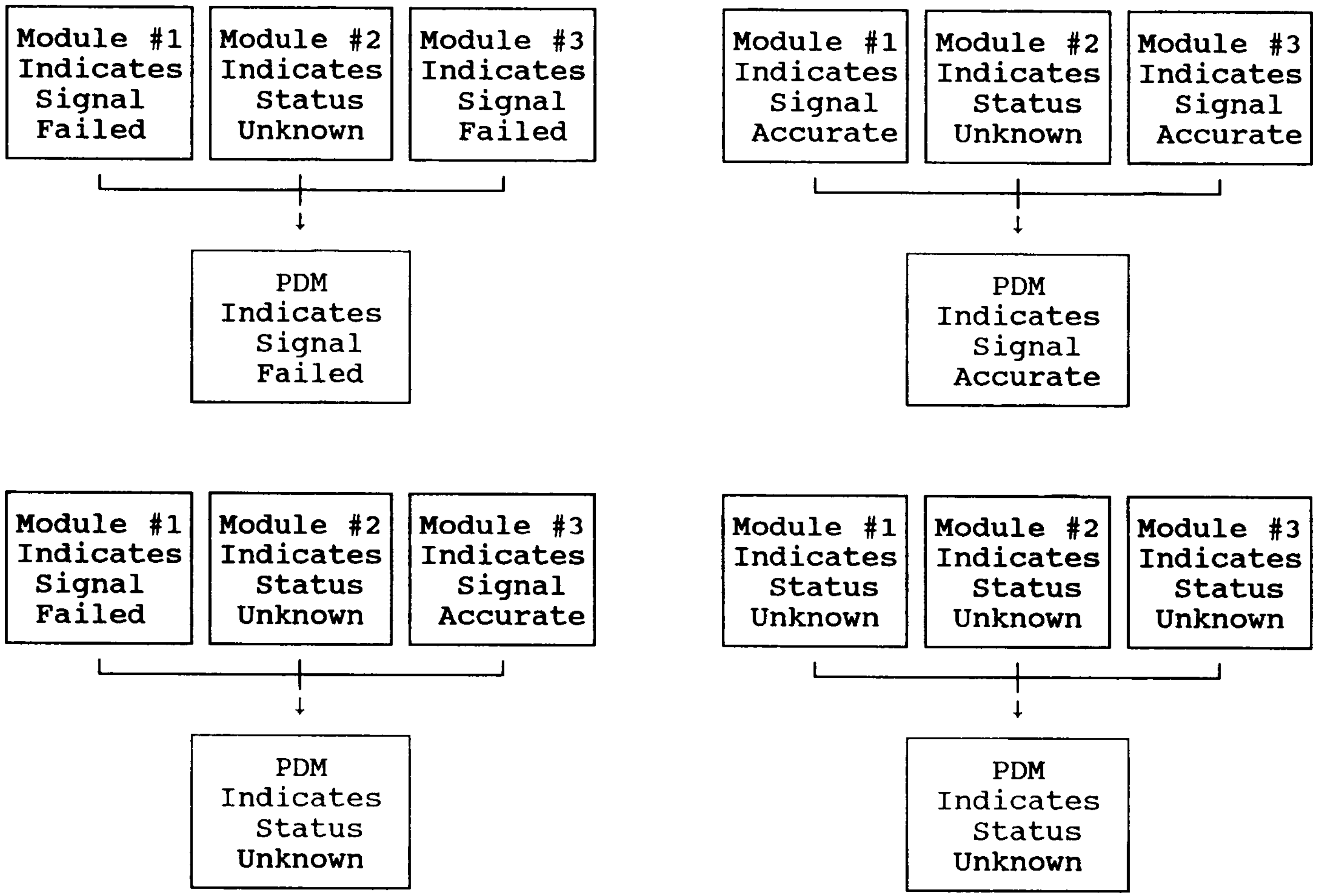

Figure 4.6. Example Conclusions From Positive Decision Maker.

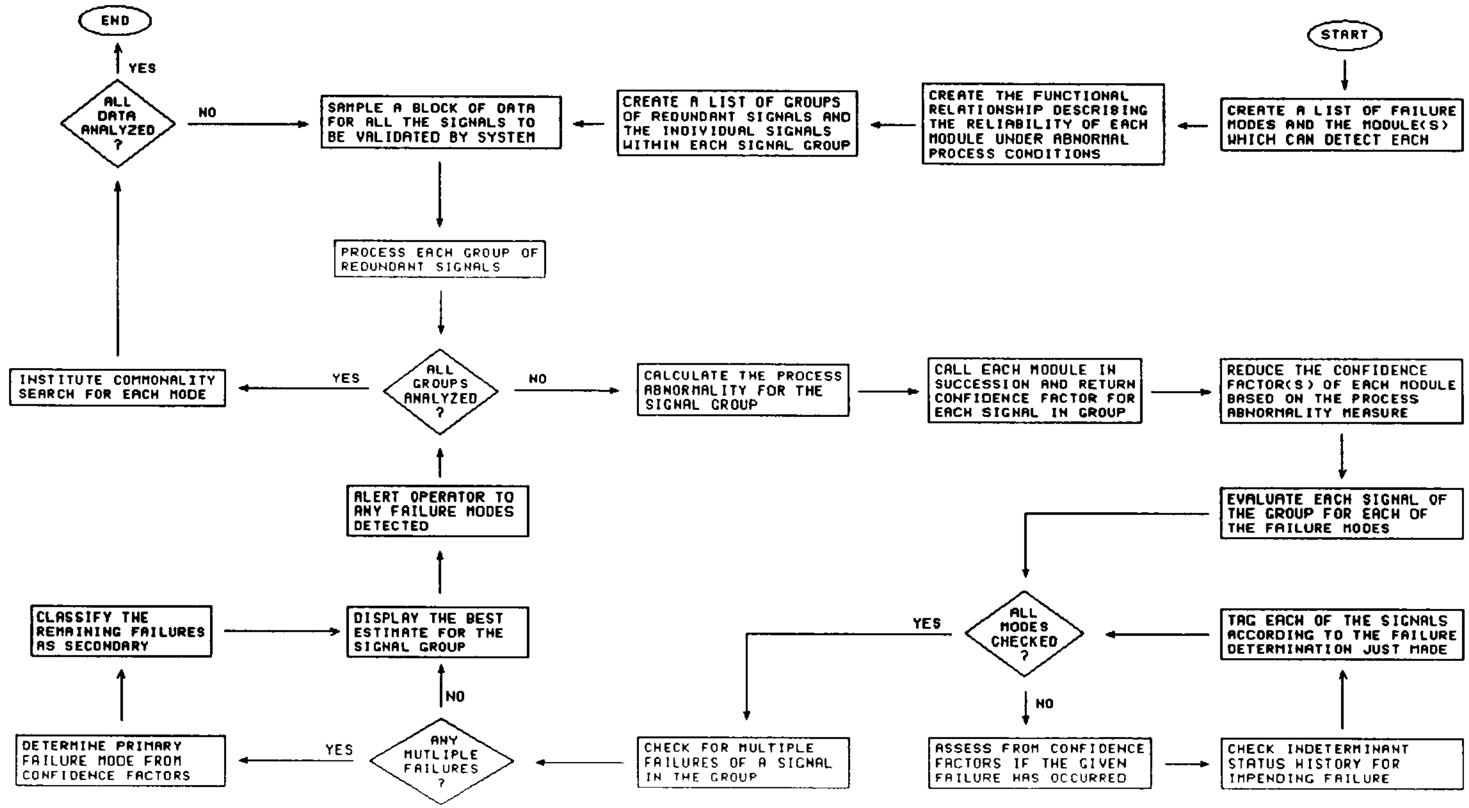

Figure 4.7. Positive Decision Maker Methodology Flow Chart.

TABLE 4.2

Detectable Failures for the Modules

	Detectable Failure			
Module	Level	Noise	Bias/Drift	Response Time
BND	X	X	X	X
MGCC	X		X	
PEM			X	
PHC	X			
SGCC	X	X	X	
UAR				X

1. The rack-mountable concept is totally preserved to allow flexibility.

2. Decisions are made more succinctly from inter-module comparisons versus blind decision making.

3. Decision maker is less difficult to implement than the type II decision maker.

4. The inter-module ratings which would have been subjective to a certain degree and difficult to properly determine will be unnecessary.

The simple ±1 scheme allows the user to quickly survey and ascertain the status of any or all of the signals. The user need not rely on mental retention of numerous fault modes and error conditions, one less fact to recall in a busy environment or even a plant emergency.

4.5 Process Qualification

Process changes can easily "trick" certain methodologies (modules) into a determination of signal failure (or non-failure). There are several statistical measures which may be employed to determine whether or not the process is at steady-state. These statistical quantities include the mean, variance, skewness and flatness of the signal. However, these quantities are used in the signal validation modules themselves. Thus a simpler quantity, the ramp rate, is selected on which to base the computation of the process abnormality fraction.

$$A_g = f(\text{Process Variable Ramp Rate}) \tag{4.2}$$

Each module's ability to perform under abnormal conditions must be assessed. A functional relationship is established to reduce the confidence of a given module's results based upon the degree of process abnormality. The confidence would range from zero to one with one indicating 100% reliability of module results under the given process conditions and zero indicating 0% reliability. Possible functional relationships are shown in Figure 4.8 in addition to those of the fuzzy set theory presented earlier.

4.6 Commonality Search

In order to lower the probability of false alarms, a "commonality search" has been implemented. The purpose behind the commonality search is to identify a possible cause of multiple instrument failures within the plant. A catastrophic failure of the plant instrumentation is highly unlikely. What is more likely is that the process has changed in such a manner as to indicate a high degree of signal anomaly.

Thus far several steps have been taken to alleviate possible false alarms -- the positive decision maker and the process qualification. An example in which both of the above techniques may fail is the time during which a nuclear power plant is at hot standby. At hot standby, certainly all the process parameters may be at steady-state, however, the noise level of the signals during this time is

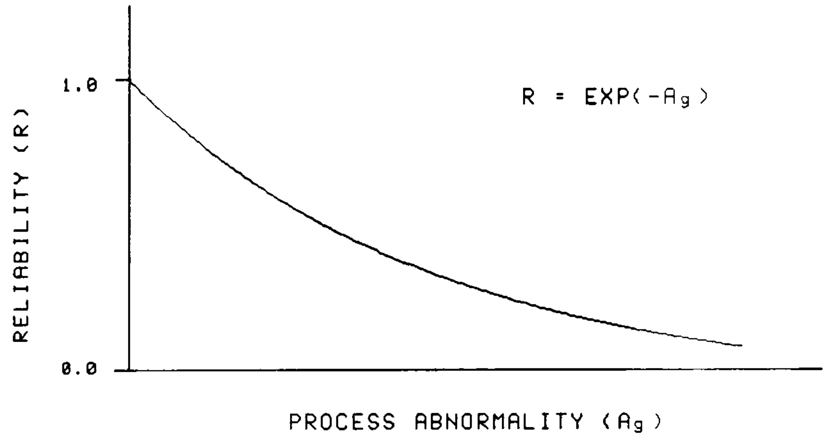

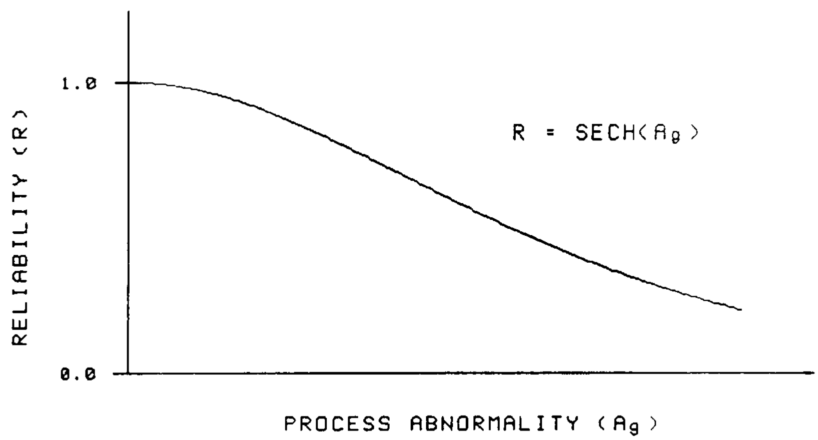

Figure 4.8. **Functional Relationships for Describing Module Reliability Under Abnormal Process Conditions.**

practically nil. The signal validation methods utilizing the noise level will be "tricked" into an indication of signal anomaly.

The commonality search may be used to survey the entire plant to determine whether possible situations as above occur. The commonality search may be based on any number of aspects which the signals have in common.

1. Signals in the entire plant.
2. Signals at a particular location.
3. Signals measuring the same process variable.
4. Signals in the same redundant group.
5. Signals in the same protection channel.

Thus each failure mode may be checked against the above common denominators. In the event that a preset percentage of the signals in each case have failed by a particular failure mode, a flag is set which elects to call the failure as indeterminate by reason of "commonality."

The protection channel of a nuclear power plant is the collection of one redundant signal from each group (process variable) for input to a process monitoring (or safety) system. There are generally three or four of these protection channels for each commercial nuclear power plant. The plant is tripped (shutdown) based on abnormal process conditions being observed in either 2 of 3 or 2 of 4 protection channels (this is referred to as 2/3 or 2/4 logic). Thus there are electrical system type common-cause failures which may occur across a protection channel.

4.7 Summary

A comprehensive signal validation system (SVS) has been developed. Diverse fault detection methodologies are implemented in a modular signal processing architecture. A System Executive controls the individual modules and makes the final assessment of the signal status. A Positive Decision Maker (PDM) has been formulated to make this determination. A commonality search is used to identify possible causes of multiple instrument failures.

5. IMPLEMENTATION OF COMPREHENSIVE SIGNAL VALIDATION SYSTEM

A comprehensive signal validation system (SVS) has been developed incorporating six signal validation modules. The six modules currently installed are

1. Process Empirical Modeling.
2. Single Variable Generalized Consistency Checking.
3. Multivariate Generalized Consistency Checking.
4. Univariate Autoregressive Modeling.
5. Process Hypercube Comparison.
6. Bias and Noise Detection.

A schematic of the signal validation system is shown in Figure 4.1. The system presently has space allocated for a total of ten modules (this number can be increased). The SVS has been implemented in a VAX workstation. Analysis of 150 signals over 100 data samples requires approximately two hours of computer time.

5.1 <u>System Executive Implementation</u>

5.1.1 <u>Data Collection</u>

At this point in time no effort is being directed towards data collection by the System Executive (SE). It is assumed that the data already exists in a disk file and is readily available. Data includes both the actual process measurements and the corresponding noise data. See Appendix

C entitled "Data File Structure." The programming effort has, however, been directed in such a manner as to facilitate direct data collection from either a plant computer or an analog-to-digital (A/D) converter. The individual modules must not alter the data in any manner.

If there is no real noise data file present, the SE creates one by removing the mean value. The mean value is computed using a moving average approach (essentially a digital high pass filter).

5.1.2 Pseudo Noise Data Generation

Optimal noise data collection requires proper signal conditioning of the process signal. First, the d.c. component of the signal is removed using a high-pass filter. The noise fluctuations are then amplified and the high frequency components removed using a low-pass filter.

D.C. Signal	—>	High-Pass Filter	—>	Amplifier	—>	Low-Pass Filter	—>	Noise Data

Unfortunately, noise data are not routinely available from nuclear power plants for analysis. For this reason, noise data are artificially created using a moving-average. The noise data for each signal are created from:

$$v_k = x_k - \mu_k \tag{5.1}$$

where

v_k = noise data at sample k,

μ_k = moving-average at data sample k,

x_k = measured data at sample k.

The moving average of the data is computed from:

$$\mu_k = \alpha \, \mu_{k-1} + (1-\alpha) \, x_k \tag{5.2}$$

where

α = parameter related to cut-off frequency.

The pseudo noise created from the moving average is essentially trend removal using a first-order differencing equation. The moving average being the result of a digital, first-order low-pass filter. The noise data resulting from subtracting the moving average from the raw data in turn is equivalent to a form of digital high-pass filtering.[26]

The correct method of noise data acquisition has four fundamental advantages over the pseudo noise data:

1. Removal of d.c. and low frequency components.
2. Amplification of the noise to a level which provides an adequate resolution of the noise data.
3. Removal of high frequency sources to avoid aliasing about the Nyquist frequency.
4. Independent of plant data acquisition system (slow sampling).

Without proper signal conditioning, even the pseudo noise data may be unattainable. An example of this is seen in the pseudo noise data created from the PWR core-exit thermocouple (TC) data shown in Figure 5.1. Note that the range of the core-exit TC is so large (200 - 2300 °F from Table A.2) that the A/D resolution is such that no change in output is seen over a 0.5 °F span. Since the core-exit temperature is generally holding steady within this range, there is no observable noise on the signal because of the large sampling interval and poor resolution, and thus no pseudo noise data can be constructed. Acceptable pseudo noise data from the PWR feedwater flow and cold leg temperature are shown in Figures 5.2 and 5.3, respectively.

A rule of thumb to use in determining whether or not the pseudo noise data are acceptable is to use the fractional noise level. The fractional noise level of the pseudo noise is compared to that of the digitizing process. The quantization error associated with the digitization is no more than ±0.5 units with an rms error of [27]

$$\frac{\pm\ 0.5}{\sqrt{3}} = \pm\ 0.29 \text{ units} \tag{5.3}$$

The fractional noise is computed from:

$$f_n = \frac{\sigma}{\mu} \tag{5.4}$$

where

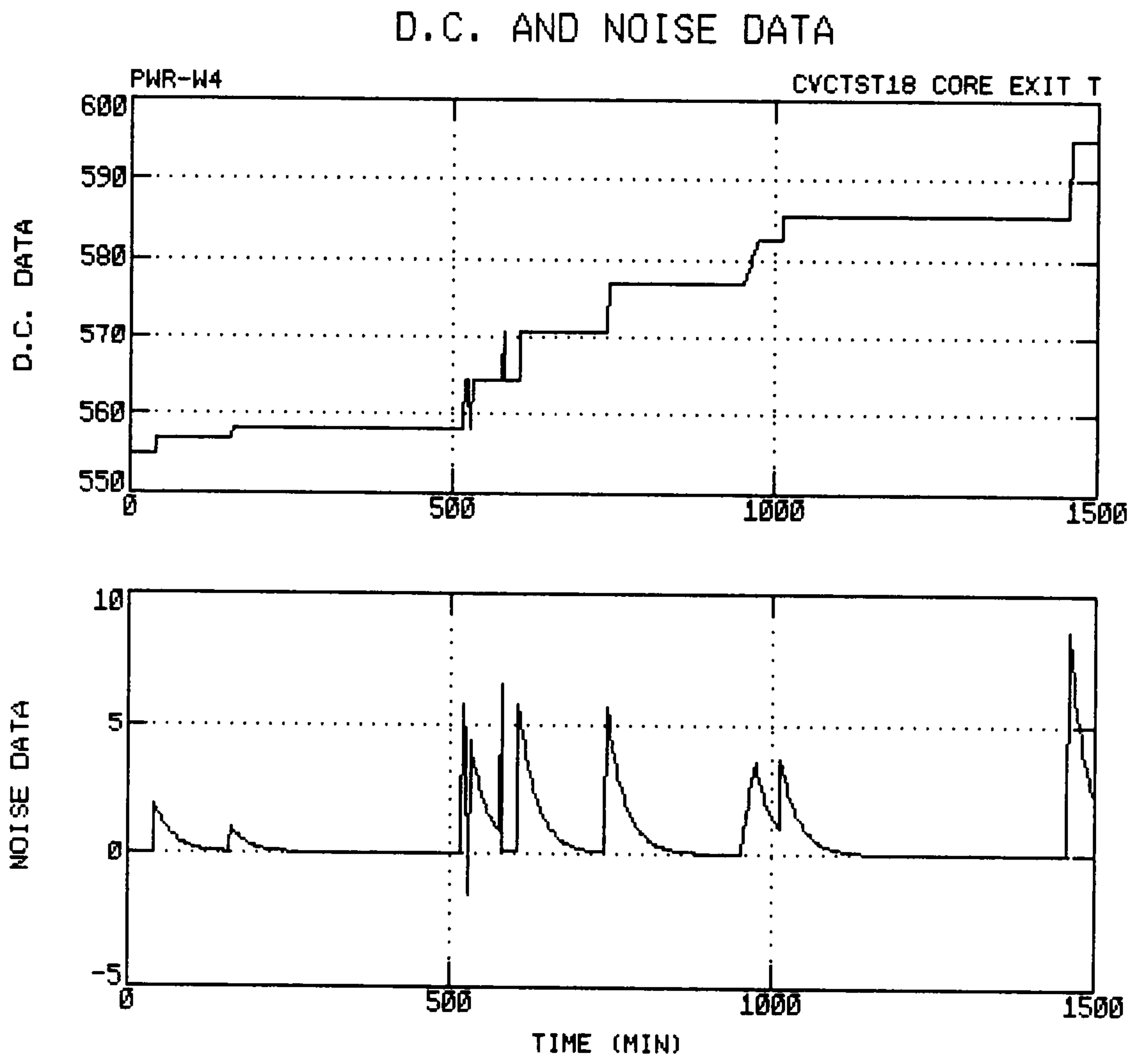

Figure 5.1. Unacceptable Pseudo Noise Data From Core-Exit Thermocouple.

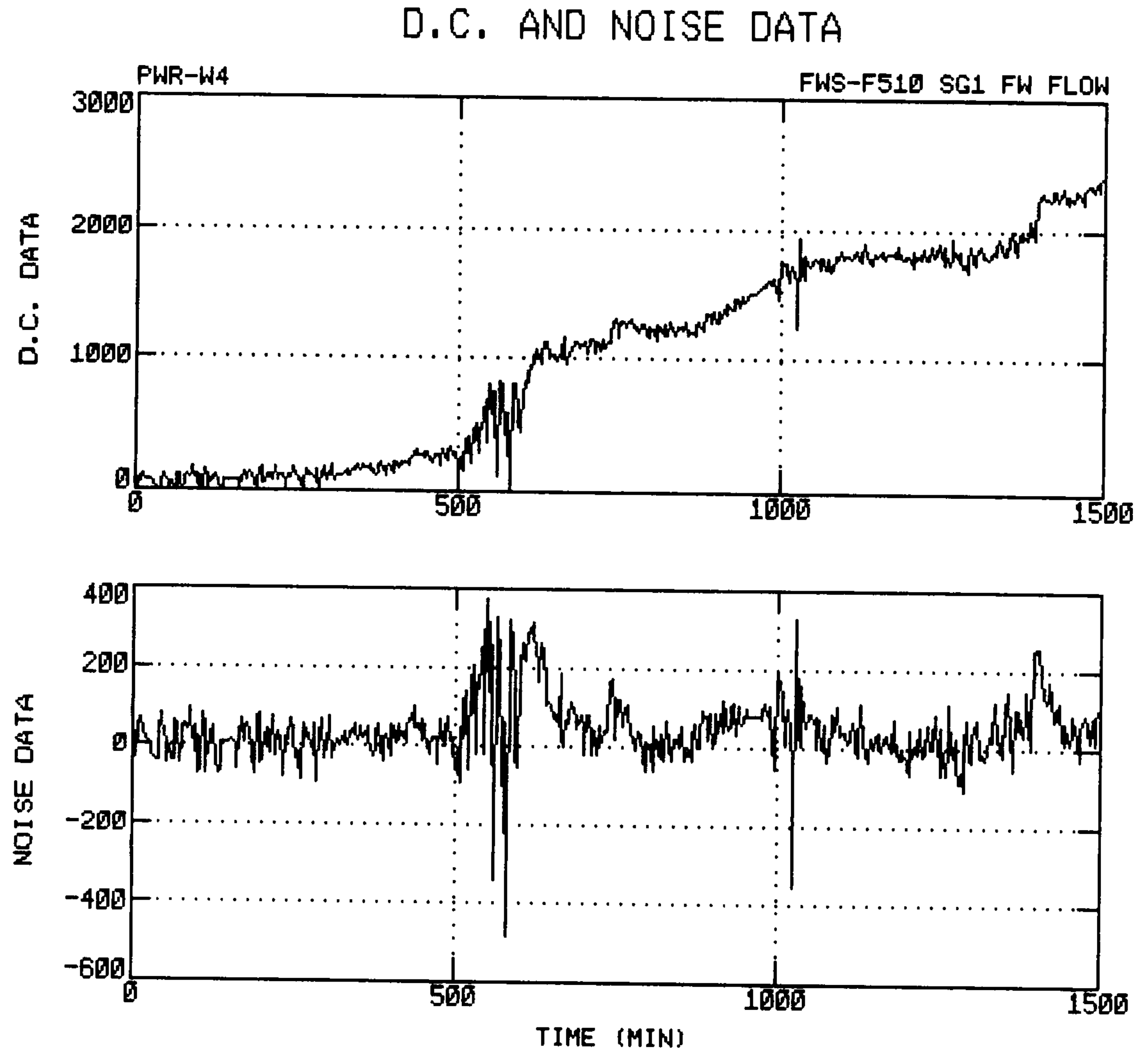

Figure 5.2. Acceptable Pseudo Noise Data From Feedwater Flow Signal.

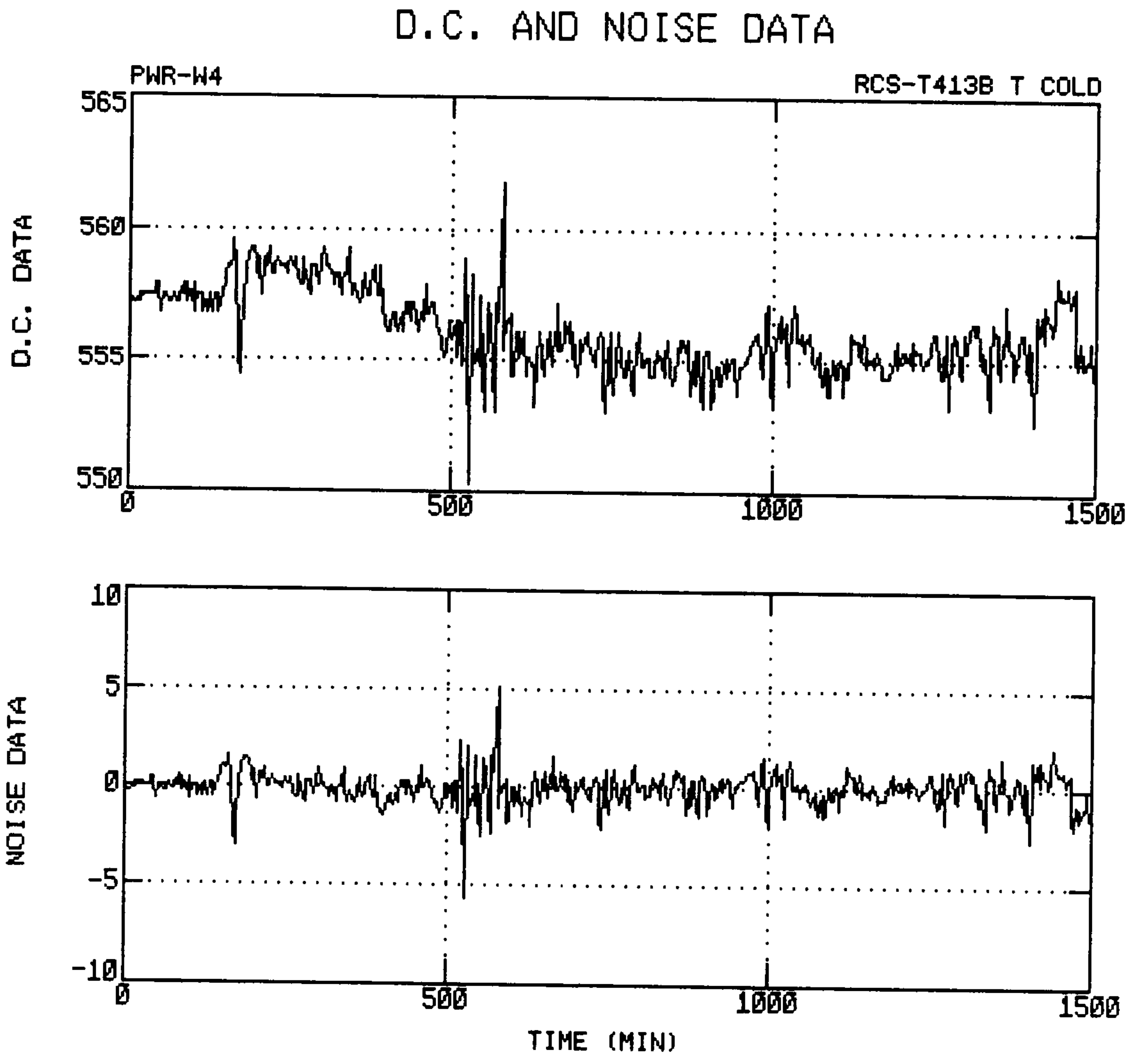

Figure 5.3. Acceptable Pseudo Noise Data From Cold Leg Temperature Signal.

f_n = fractional noise,

σ = noise standard deviation (rms noise),

μ = average d.c. signal level.

The rms quantization noise (from digitizing) must be small as compared to the fractional noise so as to achieve the desired dynamic range.

5.1.3 Data Processing

It must be noted that some modules can operate on a sample-by-sample basis. However, other modules must operate on a block of samples. It has been concluded that operation on a block basis is most desirable. This lies primarily in the fact that a block basis will allow the reduction of spurious false alarms concerning the signal status. The drawback is that sample-by-sample processing by the modules would provide real-time estimates of the process variables to the operators. A set block size for all the modules is imposed so that the final results of a given block of data may be determined by the SE at a single time. This block size is determined experimentally during the testing of the completed system, but is expected to range from 100 to 1000 data samples.

The process signals are grouped with like (redundant) signals together. With the grouping of like signals, the modules requiring unlike signal groups are forced to keep track of which signals are in each model; however, this is a relatively easy task. These modules will have a data base on each group of signals to make the identification.

5.1.4 Modularity

The comprehensive signal validation system maintains a modular (parallel processing) architecture. The modular design provides both the facility to incorporate newly developed signal validation techniques and the ability to remove signal validation modules which prove to be either unsatisfactory or unsuited for certain processes. In fact, system specific modules can be inserted and withdrawn as desired using this approach.

The SE handles all input and output (I/O). It is assumed that the SE reads the required data for input into the various modules. The data may either be read from a data file, the plant computer or sampled directly using an analog-to-digital (A/D) converter.

To maintain the modularity, the module outputs must be kept uniform; however, the inputs need not be as restrictive. The input information is made available to each of the modules which may or may not have need for all of the information. The data are provided to the modules by the SE.

Each module has the following available input parameters:

NSAMPLE	- number of data samples in a block of data.
NBLOCK	- the current block number.
DELTAT	- the data sampling interval (in seconds).
NCHANNEL	- the total number of signals being analyzed.
NGROUP	- signal group identification number.
NREDUN	- number of redundant signals to be processed.
MCHAN(I)	- the signal numbers to process (I=1,..,NREDUN).
YDATA(K,L)	- sampled data for K-th signal and L-th sample (K=1,...,NCHANNEL; L=1,...,NSAMPLE).
YNOISE(K,L)	- noise data for K-th signal and L-th sample.
IVIEW	- detail of results to display in background.

Each module must supply the following outputs:

CONFID(I,J)	- confidence factor for signal I and failure J.
ESTIMATE	- a best estimate for the group of signals.
IERROR	- general internal module error.

The last input and output parameter (IVIEW and IERROR) are discussed in Sections 5.1.5 and 5.1.7, respectively.

5.1.5 Results Display

One of the more important objectives of signal validation is to provide a best estimate of the true process state. For this reason, whenever possible a signal estimate is returned by the individual modules. The combined resultant estimate for all the modules is displayed by the System Executive on the process (plant) schematic.

Normally the validated signals are displayed on the screen using a schematic of the process (plant). A validated value for each process signal is displayed. In the case of a plant with four steam generators, four levels are displayed. The current time is indicated in order to quickly determine if the signal values are current or if the data processing is lagging.

A faulty signal is indicated by sounding a bell and altering the signal estimate display. For instance the predicted value can be blinked, reverse colored, or color changed. Colors (red, yellow, green) are appropriate for indicating the status of various signals. The color of the estimates can be shaded according to the last confidence value returned by the SE.

The results from the system executive decision making are examined at five levels:

1. The top level contains the estimates displayed on the process (plant) schematic.

2. The next level displays the final status results for each sensor in a selected redundant group.

3. The detailed results status for a sensor group may also be shown which includes results for each failure mode.

4. The brief results for a single sensor includes an output similar to #3 above.

5. The last level is detailed results for a selected signal including results from each failure mode as well as the final results from each module.

Windows are used to access the results of the individual modules. Deeper level menus are used to select the specific results of the individual modules. In the view results mode, each module has its own format to show the results since each has varying information available. The view results display allows each module the opportunity to show its validation reasoning methodology.

During data processing, intermediate computational results from the individual modules are displayed in a separate window. The IVIEW input parameter introduced in the last section is used to control the amount of intermediate results provided by each module. One of four levels may be selected.

1. No results.
2. Minimal results - which displays only the resultant confidence factors for each signal.
3. Detailed results - which provides intermediate computational results. The exact results shown depend on the specific module.
4. Debug level - which is basically used in debugging when new modules are added for viewing all the steps of the data processing.

The results view level can be altered any time during data processing.

Certain utility functions are provided by the system executive. These include:

1. Signal d.c. data plotting.
2. Signal noise data plotting.

3. Alteration of the results view level.
4. Display of the entire plant data base.
5. List redundant sensors in a group.
6. List sensors at a given location.
7. List all locations in the plant.
8. List locations upstream and downstream.
9. Stop the data processing.

5.1.6 System Data Base

The entire System Executive was written using the C programming language. The C language allows programming constructs not normally available in languages such as FORTRAN. One such construct is the use of pointers which has been used in the creation of a large tree structured data base for the SE. A schematic of this tree structure is shown in Figure 5.4. This data base contains most of the information about the process instrumentation.

There are five levels of information kept in this tree structured data base. These levels are

1. Plant Level - Facts that are pertinent to the plant and data analysis are located here. The plant specific information includes the number and list of process variables, the number and list of different sensor locations, and the total number of redundant sensor groups. Data analysis parameters such as the data filename, data sampling interval, number of data samples and number of data blocks are kept here.

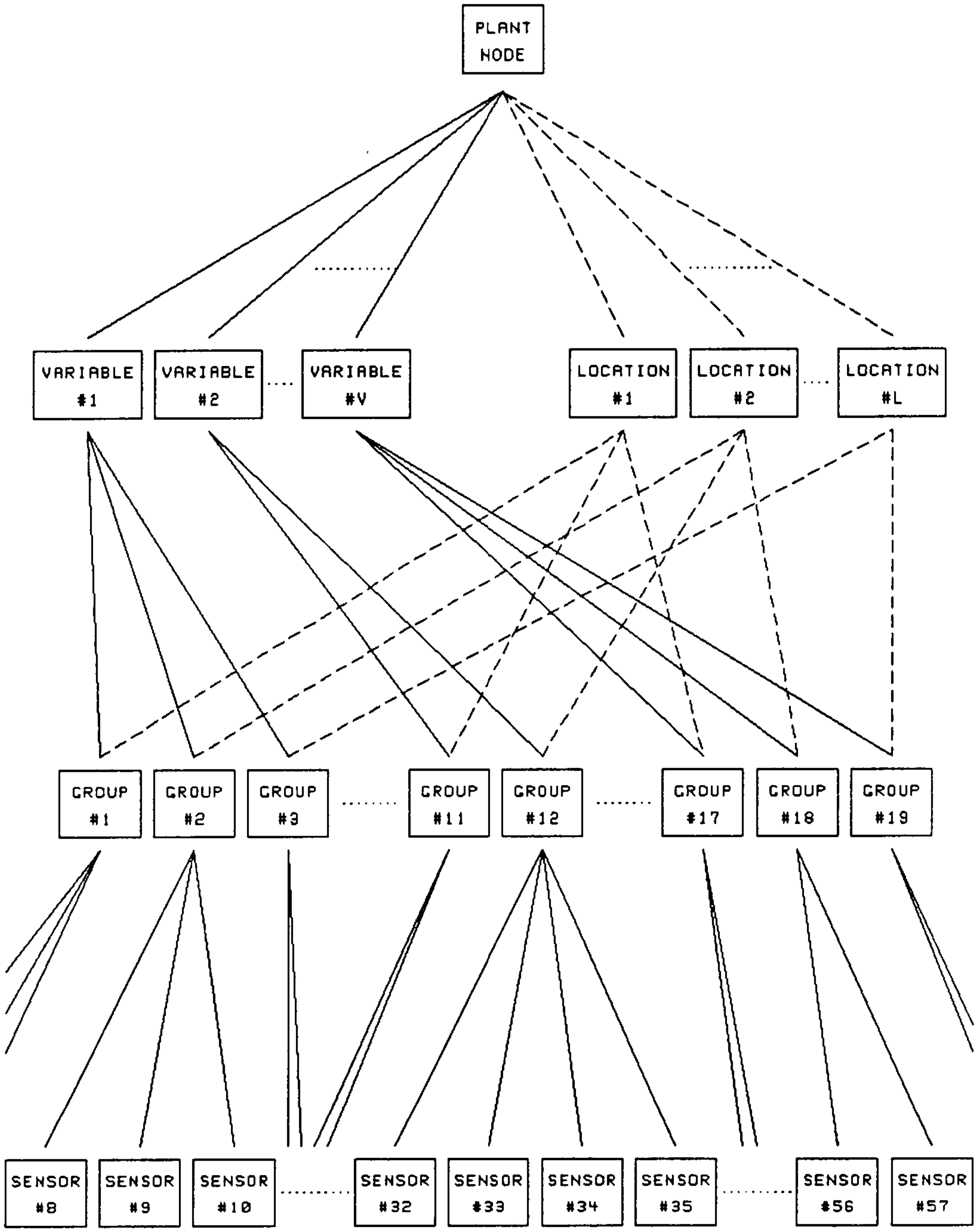

Figure 5.4. System Executive Data Base Structure.

2. Variable Level - Each process variable maintains a listing of its name, its variable identification number, and the number and list of redundant sensor groups this variable includes.

3. Location Level - The location is on a parallel level to the variable level above. This level also holds its name, a locational reference number, and the number and list of redundant groups at this location. A list is kept of those locations upstream and downstream from this one.

4. Redundant Group Level - Each redundant group retains a unique reference number, the group name, and the number and list of sensors in this particular redundant sensor group.

5. Sensor Level - The lowest level is the sensor level. The sensor information includes its data channel number, tag number, the results from the individual module analyses and the final results from the positive decision maker (PDM).

The System Executive maintains two files in its data base:

1. SYSEXE.DRAWRX - the information necessary to create the schematic of the process (plant) is placed in this file.

2. SYSEXE.PLANT - all the information about the signals in the plant data base is kept here. This information includes the redundant signal groups, sensor location and signal channel numbers.

5.1.7 Module Error Codes

A facility has been provided by the SE decision maker to allow modules to return an error code which indicates that a module was unable to provide a confidence result. This is the IERROR output parameter introduced in Section 5.1.5. This error code can be either of a fatal or non-fatal (warning) nature. The error codes are listed in Table 5.1. In the event the error is fatal, data processing is halted and the problem is reported.

Some error codes are of a non-fatal nature. For example, absence of any (PEM) models. In the event a non-fatal error is returned, the occurrence is reported to the user and the PDM treats the module as non-existent in its decision making and the data processing is continued. This non-fatal error code is a powerful feature allowing modules the opportunity to remove themselves from the decision making process when necessary.

Some modules (e.g. UAR and BND) compute statistical quantities which require a large number of data samples to achieve an acceptable degree of certainty. The correlation function computed by the UAR module and the quantities calculated by the BND module, each have this large input data requirement. If the models lacked statistical significance, the non-fatal error code may be returned. Another example is a case in which the sampling interval is too large to adequately resolve a smaller time constant.

TABLE 5.1

Module Error Codes

Error	Module Internal Error Codes
<0	Non-Fatal error detected by module (Unable to analyze this group of signals)
0	No error detected by module
>0	Fatal error detected by module
1	Too many redundant signals in group
2	Too many signals in data matrix
4	Too many data samples in the block
8	Too many redundant signal groups
16	Too many different variable types

5.1.8 Final Signal Status

Finally after the data have been completely analyzed by all the modules, the positive decision maker (PDM) and commonality search described in Section 4 are instituted. The indicated signal status can be any one of the following:

1. Valid.
2. Indeterminate.
3. Anomalous.
4. Valid under abnormal process conditions.
5. Commonality indeterminate.
6. Possibly anomalous under abnormal process conditions.
7. Possible impending anomaly.
8. Possible impending anomaly with commonality present.

The failure commonality can be found with respect to several factors.

1. The entire plant (indicative of process).
2. The sensor's location.
3. The sensor's variable type.
4. The sensor's redundant group.
5. The sensor's protection channel.

The above commonality factors are listed in order of broadest to narrowest extent.

5.2 Module Implementation

5.2.1 Intra-Module Decision Making

The fuzzy set functions described in Section 2.5 are used for intra-module decision making to produce the confidence factor required by the SE. The two basic curves (S and π) are used for this purpose and can be selected in a straightforward manner based on the following cases.

1. In the event that the module result is such that there is both a low and high threshold of failure, the π-curve is best utilized. Noise level failure can be either in a high or low direction and is an example of such a failure requiring the π-curve.
2. In those cases where the module result has only an upper or lower threshold, the S-curve should be selected. An example of this is the fractional amount that a particular signal is excluded by a consistency checking algorithm.

The remaining task is to identify the functional coefficients of the fuzzy functions. This selection is based on two primary factors:

1. Cost of failure, that is the severity of consequences resulting from a particular failure type.
2. The plant technical (or operating) specifications which may limit the acceptable signal error.

Later alterations in these coefficients can be made on the basis of experience. Generally the cross-over point (where the confidence value equals zero) is set to the tolerance given in the plant technical specifications. In those instances where no such specification is given or available, utilization of the cost of failure criteria proves to be more useful (along with a little common sense). The fuzzy function threshold limits are refined as additional data are analyzed.

5.2.2 Module Data Base

Each module is responsible for keeping its own data base. Each module has a system parameter file to store various constants which can be changed later (rather than putting these constants in the text of the program itself). Such parameters would be tailored towards a specific process or plant. Most of these parameters are the thresholds of each signal for the various failure modes detectable by the given module.

5.3 Single Variable Generalized Consistency Checking[11,12]

Single variable generalized consistency checking (SGCC) is a method for systematic cross comparison of the redundant measurements of a variable. A pairwise comparison of the measurements is made based on the individual measurement system tolerances. An inconsistency index is computed for each signal. This index is used to exclude signals from a best estimate of the true signal. In the event the redundant group is only partially consistent or totally inconsistent, the estimate is computed from a weighted summation using the inconsistency index of each signal. Bias and noise failure detection using the sequential probability ratio test (SPRT) has also been included in this module.

5.3.1 Consistency Checking

The single variable generalized consistency checking (SGCC) algorithm is a systematic method of checking for inconsistencies among redundant measurements of a single process variable. Two measurements are said to be consistent with respect to each other if

$$| m_i - m_j | \leq \epsilon_i + \epsilon_j \qquad (5.5)$$

where

m_k = measurement of signal k,

ϵ_k = tolerance of signal k.

The error indices of both signals are increased by one each time the given signal pair is inconsistent. This comparison is performed for all possible signal pairings. This error index thus ranges between zero and n-1, where n is the number of redundant signals. The complex logic used to separate the correct and incorrect signals is given in Figure 5.5. A best estimate for this process variable is computed from the SGCC algorithm.

5.3.2 Sequential Probability Ratio Test

The sequential probability ratio test (SPRT) is utilized to detect bias in both the d.c. and the noise level of a signal. The SPRT has the ability to check for sensor degradation and to record the sensor degradation history.

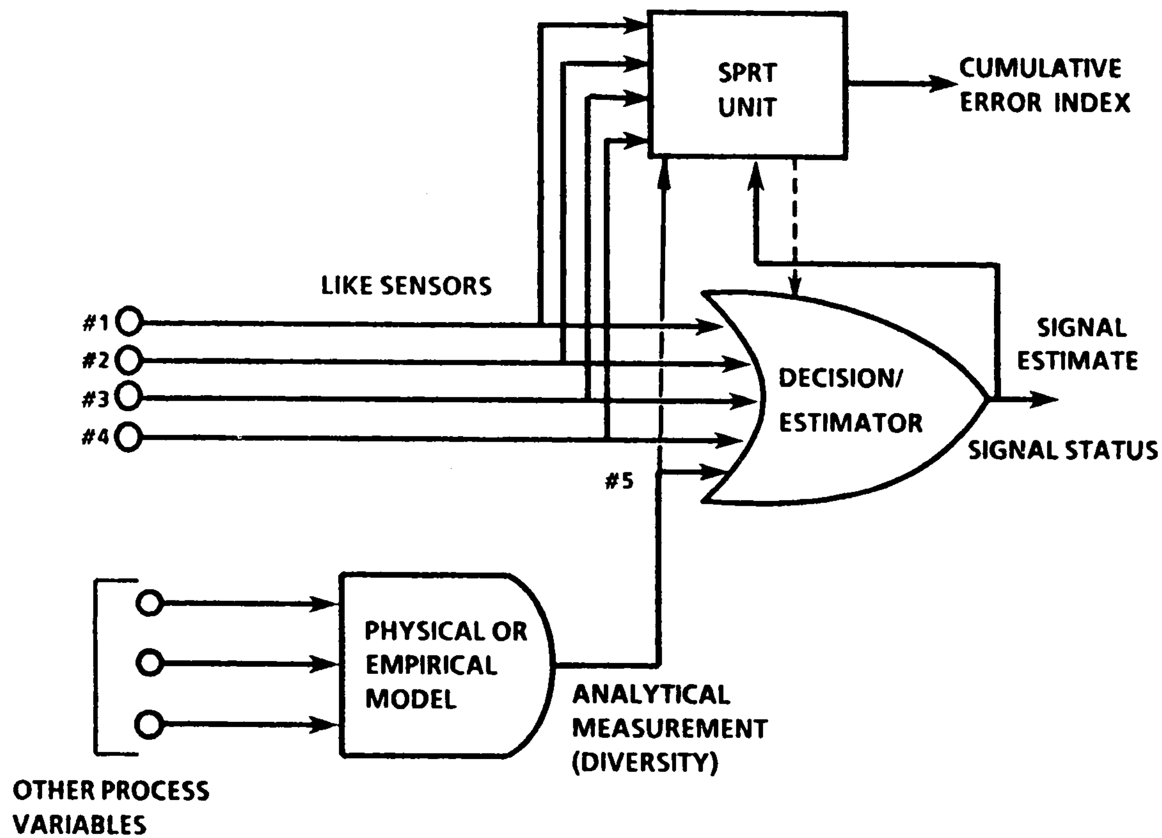

Figure 5.5. SGCC Module Logic Schematic.

The SPRT is applied to the difference between measured sensor output and the SGCC estimated value --- the measurement residual. The basis of the SPRT lies in the recursive calculation of the logarithm of the likelihood ratio (LLR) function, ϕ. The expression for detecting bias degradation is

$$\phi_n = \phi_{n-1} + \frac{\mu}{\sigma^2} \left[s_n - \frac{\mu}{2} \right] \tag{5.6}$$

where

ϕ_n = LLR function at the n-th sample,

s_n = residual at the n-th sample,

μ = mean value of the residual,

σ^2 = variance of the residual.

The expression for noise degradation is given by:

$$\phi_n = \phi_{n-1} + \frac{1}{2} \left[\frac{1}{\sigma_0^2} - \frac{1}{\sigma_1^2} \right] s_n^2 + \ln \frac{\sigma_0}{\sigma_1} \tag{5.7}$$

In this case the subscript zero refers to the measured value and subscript one to the failure threshold value. An upper (LLR_u) and lower (LLR_l) degradation threshold is computed as

$$\begin{aligned} LLR_u &= \ln[(1-\beta)/\alpha] \\ LLR_l &= \ln[\beta/(1-\alpha)] \end{aligned} \tag{5.8}$$

where

α = false alarm probability,

β = missed alarm probability.

The SGCC module thus detects three types of failure:

1. Level failure with consistency checking.
2. Bias failure from the bias SPRT.
3. Noise failure from the noise SPRT.

In each of the above cases, the fuzzy S-curve is utilized. The level confidence factor is a function of the fractional number of times that a signal is excluded (inconsistent) with respect to its redundant group. The lower level is set at zero and the upper at one-half since failure is identifiable long before a signal is excluded 100% of the time. The bias and noise failure thresholds also use the S-curve. Failure is determined based on the number of times the SPRT threshold is exceeded over a block of data samples.

5.3.3 SGCC Data Base

The SGCC parameter file contains four parameters for each process signal:

1. The tolerance (error bounds).
2. The bias threshold.
3. The upper and lower noise variance limits.

The SGCC module creates four files to hold the results over the last block of data:

1. ESTIMATE.SGCC - contains the best estimates for each redundant group of signals. The tolerance for the signal group is saved here for reference.

2. BIASSPRT.SGCC - the results of the bias sequential probability ratio test (SPRT) are kept here for each signal. The bias threshold is saved for reference also.
3. NOISESPRT.SGCC - the results of the noise bias sequential probability ratio test (SPRT) are saved in this file for each signal. The upper and lower bounds for noise bias degradation are also stored for reference.
4. INDICES.SGCC - the inconsistency indices for each signal as computed are maintained here. The total number of redundant signals is kept here for comparison with the inconsistency index.

Thus the SGCC module provides the user with four separate results to plot: for the signal group (1) a variable estimate, and for each signal (2) an inconsistency index, (3) the bias SPRT and (4) the noise SPRT.

5.4 Bias and Noise Detection[17]

The bias and noise detection (BND) module is used to monitor basic changes in the signal characteristics. The observed properties include (1) the signal level, (2) the noise root-mean-squared (RMS) value, (3) the statistical distribution (probability density function [PDF]) and (4) a parameter proportional to the time constant of the signal from its zero-crossing rate. The computed values for the above quantities are compared against specified thresholds in order to identify an anomaly in a given signal.

5.4.1 Signal Level

The mean value μ of each signal is computed and compared to an expected value. The mean value is computed from:

$$\mu = \frac{1}{N} \sum_{k=1}^{N} y(k) \qquad (5.9)$$

where

N = number of data samples,

y(k) = the k-th data sample.

5.4.2 RMS Noise Level

The standard deviation of the signal noise is calculated from:

$$\sigma = \left[\frac{1}{N} \sum_{k=1}^{N} [y(k) - \mu]^2 \right]^{\frac{1}{2}} \qquad (5.10)$$

The standard deviation of noise is compared to a nominal value. An anomalous signal is detected with either a higher or lower than normal reading.

5.4.3 Signal Symmetry

The amplitude probability density function (APDF) is computed to determine the statistical distribution of a signal. The symmetry of this distribution may be assessed using the skewness of the signal. The skewness is computed as:

$$G_3 = \frac{1}{N\sigma^3} \sum_{k=1}^{N} [y(k) - \mu]^3 \qquad (5.11)$$

The skewness is also compared against a nominal value. For a Gaussian distribution (or a symmetric APDF) the skewness is zero.

5.4.4 Zero-Crossing Rate

One of the simplest methods of observing relative changes in response time is to count the number of times a signal crosses its mean value over a given time period. The level crossing rate (zero-crossing rate) can be related to the signal time constant. For a second order system in which the two time constants are proportional to one another, it has been shown that:[28]

$$\tau = \frac{C}{Z_C} \qquad (5.12)$$

where

τ = time constant,

C = proportionality constant unique to a sensor,

Z_C = number of zero crossing per unit time.

The drawback to this method is that the proportionality constant, C, must somehow be determined. However, the zero crossing rate may be compared against a preset threshold.

Once a sensor has been isolated as suspicious, the anomaly characterization and classification as to the type of anomaly is performed. The characterization is made using a modified cumulative sum (CUSUM) algorithm. The classification takes into consideration time duration, and relations among mean, peak and rms values of the signal. The failure classification results in the identification of (1) jump or persistent change in mean value, (2) pulse or spurious changes in the signal level and (3) sinusoidal noise.

Each of the four failure modes, except for noise failure, uses the fuzzy S-curve to compute a confidence factor from the stored thresholds. The noise failure mode uses a non-symmetric π (bell-shaped) function to arrive at a confidence factor.

5.4.5 BND Data Base

The BND parameter file contains the following parameters for each process signal:

1. The signal level (d.c.) tolerance.
2. The nominal standard deviation of the noise.
3. A maximum and minimum noise standard deviation.
4. A nominal time constant value.

The results from the BND analysis are kept in two files:

1. SAPDF.BND - the amplitude probability density function is kept for each data signal. The values represent the cumulative results over all prior data blocks. The cumulative variance, skewness and flatness of the signal are also retained here.

2. CUSUM.BND - the cumulative summation (CUSUM) results for the data block are stored along with the type of anomaly (if any) that was detected.

The APDF may be plotted by the user with results from the variance and skewness computations. The CUSUM results from the BND analysis may also be displayed.

5.5 Process Empirical Modeling[15,16]

The process empirical modeling (PEM) module establishes nonlinear multiple-input single-output (MISO) models. The measured sensor output may then be compared against a predicted output based on the previously determined model. The PEM module provides an independent estimation of the process state. The PEM module utilizes the estimates for monitoring sensor degradation or drift by on-line monitoring of the sensor output. These estimates are also used for the MGCC module for the consistency checking of instrument outputs and for isolating common-mode failures.

The analytical measurement or prediction of a critical signal y as a function of related variables in a subsystem, during steady-state or quasi steady-state operations is given by:

$$y = f(\underline{x}) = f(x_1, x_2, \ldots, x_m) \qquad (5.13)$$

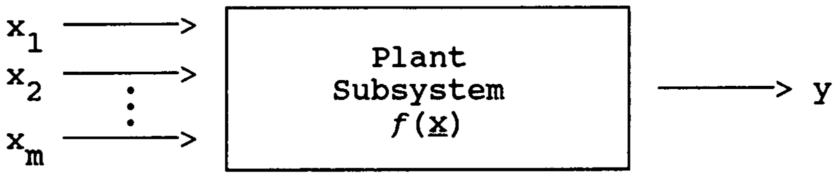

No assumption is made that the input variables are independent of the output variable.

5.5.1 Empirical Modeling Algorithm

The empirical modeling method creates an optimal nonlinear multiple-input single-output (MISO) model from the given data. The form of the data-driven predictive model is

$$y = C_0 + \sum_{i=1}^{n} C_i \, \Phi_i(\underline{x}) \tag{5.14}$$

where

y = output signal of interest,

$\underline{x}$ = vector of input signals,

n = number of terms in the model,

Φ_i = nonlinear combination of input signals,

C_i = constant coefficient.

A geometrical description of the nonlinear modeling algorithm follows. The closest nonlinear cross-product vector relative to the output vector is determined. New nonlinear vectors (terms) are subsequently selected by projecting the remaining unselected vectors onto a subspace of the original vector space orthogonal to the selected vector(s). This procedure continues until n terms (vectors) are chosen. The final step is to fit a linear type model using the selected terms to compute the coefficients. A more mathematical description is given in Figure 5.6.

The modeling program varies both the polynomial order and the number of terms. The optimal model is selected from the model with the minimum error between the predicted output and the measured output. The overall fractional prediction error, ϵ_p, is defined by

$$\epsilon_p^2 = \frac{1}{N} \sum_{k=1}^{N} \left[\frac{y_m(k) - y_p(k)}{y_p(k)} \right]^2 \tag{5.15}$$

where

N = number of fitted measurements,

$y_m(k)$ = measurement at time instant k,

$y_p(k)$ = prediction at time instant k.

The actual standard deviation of the prediction error of the signal at any time instant is estimated from:

$$\sigma_p(k) = \epsilon_p \, y_p(k) \tag{5.16}$$

This error analysis does not include the measurement errors.

The PEM module is used to detect bias/drift failure. An average deviation between the measured and predicted signal output is computed over a block of data samples. The

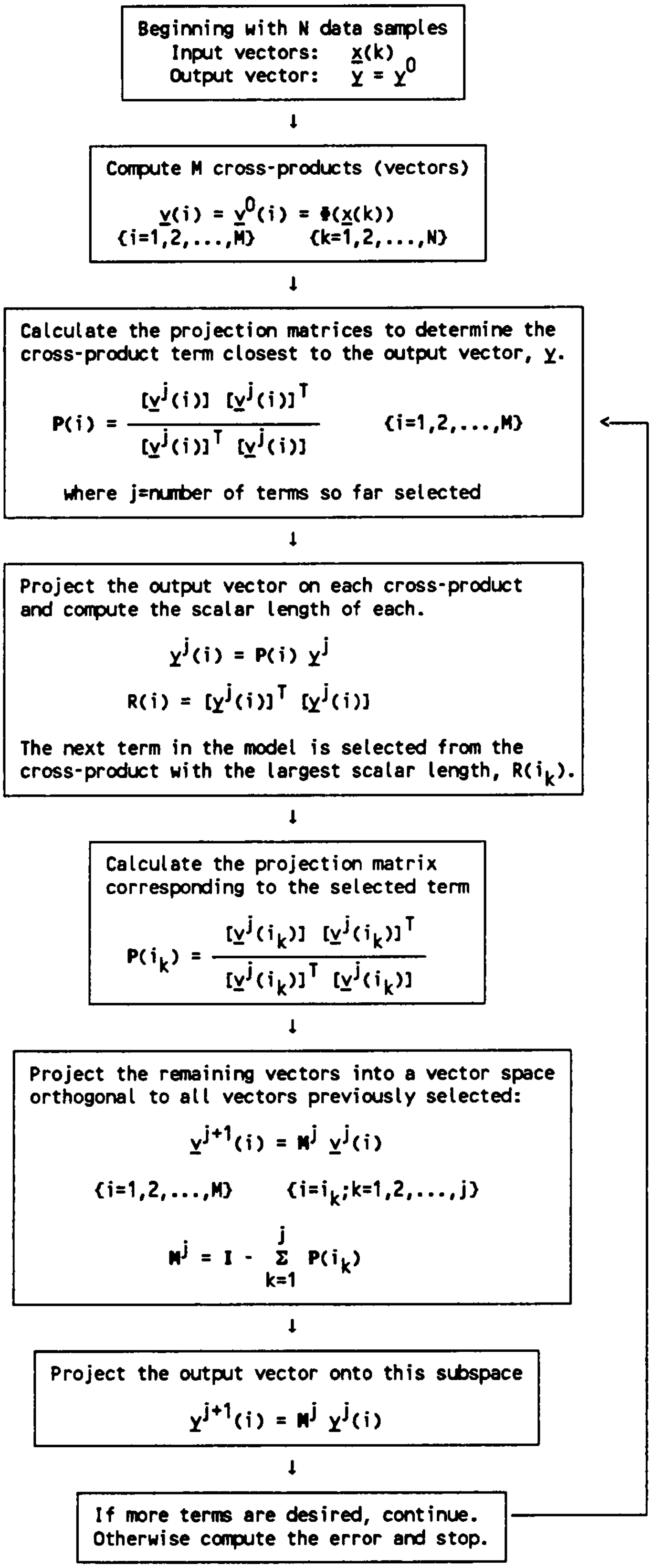

Figure 5.6. Empirical Modeling Schematic.

fuzzy S-curve is then used to compare this deviation to the signal tolerance to identify the presence of drift.

5.5.2 PEM Data Base

The PEM module's parameter file requires only the tolerance of each signal, but of course the PEM models must also exist. There is a single results file (ESTIMATE.PEM) containing the PEM estimates for each process signal. The PEM estimates may be plotted against the SGCC estimates for comparison using the SVS.

5.6 Univariate Autoregressive Modeling[29]

The univariate autoregressive modeling (UAR) module is a method for characterizing the dynamic fluctuations (noise) in a signal. These models may be used to compute wideband frequency-domain information such as the power spectral density (PSD) function of a signal. Time-domain quantities, including the autocorrelation function of the signal, and the step and ramp response are also estimated. Thus the time constant of a signal may be monitored for possible variations from the normal value.

5.6.1 Definition of Response Time

The speed of response of an instrument can be characterized by several different quantities including time constant, ramp delay and settling time. The response of the first order system to a step input is

$$S(t) = K\ (1 - e^{-t/\tau}) \tag{5.17}$$

Note the system output at time, $t=\tau$:

$$S(t=\tau) = K\ (1 - 0.378) = 0.632\ K \tag{5.18}$$

Thus, the definition of time constant, τ, is the time required to reach 63.2% of the final value after a step change in the input.

5.6.2 Response Time Determination

The determination of sensor response time by noise analysis requires that proper noise data collection be performed. The digitizing of the noise data requires some a priori information about the system of interest. The frequency range of interest must be known as there are several competing factors:

$$f_{min} < f_b < f_{Ny} \tag{5.19}$$

where

f_b = sensor break frequency (Hz),
= $1/2\pi\tau$ (for first order system only)

f_{min} = minimum frequency of interest (Hz),
= f_s / N

f_{Ny} = Nyquist frequency (Hz),
= f_s / 2

f_s = sampling frequency (Hz),

N = data samples per block.

The response time of a sensor can be determined from the signal fluctuations caused by process noise. Several techniques exist for making the determination. The noise techniques can be classified as those in the time-domain and those in the frequency-domain. In all noise analysis methods, the governing assumption is that the driving noise is a wideband random process and that the bandwidth of the driving noise is greater than the sensor bandwidth. A reduction in noise bandwidth results in an over estimation of the time constant. The random noise of the process fluctuations must be distinguished from noise due to electronics or recording instrumentation.

5.6.3 Autoregressive Modeling

A time-domain method of characterizing the dynamics of a signal is autoregressive (AR) modeling of the stationary signal. The AR model is one of several empirical time-series modeling techniques. An autoregressive process is described by:

$$y_k = \sum_{i=1}^{n} a_i \, y_{k-i} + v_k \tag{5.20}$$

where

n = the AR model order,

y_k = random stationary process output,

a_i = the i-th AR coefficient,

v_k = a white noise sequence.

The AR coefficients are computed from the auto-correlation function using the Yule-Walker equations:

$$C_k = \sum_{i=1}^{n} a_i C_{k-i} \tag{5.21}$$

The auto-correlation is a time-domain statistic comparing the similarity of a signal to itself. Oscillations in the auto-correlation indicate the presence of sinusoidal components in the signal. If the signal is periodic, the correlation function will also be periodic with an equal period. If the signal is truly random noise, the correlation begins at a value of one, and quickly drop and remain at a value of zero. The auto-correlation, a symmetric function, is computed from:

$$C_k = \frac{1}{N} \sum_{i=1}^{N-k} y_k \, y_{i+k} \qquad \{k=0,1,2,\ldots N-1\} \tag{5.22}$$

where

N = number of data samples.

The optimal AR model order may be selected by computing one of several decision criteria. The Akaike Information Criterion (AIC) is computed from:

$$AIC = N \ln(\sigma_V^2) + 2\,n \tag{5.23}$$

where

σ_V^2 = noise variance.

The optimal model order, n, is selected such that the AIC is a minimum.

The auto power spectrum, S_{yy}, is estimated from the AR model as:

$$S_{yy}(f) = \frac{\sigma_v^2 \ \Delta t}{\left| 1 - \sum_{k=1}^{n} a_k \ e^{-j2\pi f k \Delta t} \right|^2} \tag{5.24}$$

where

Δt = sampling interval (seconds),

f = frequency (Hz).

Given a correctly identified AR model, this power spectrum is equivalent to that computed directly by the Fast Fourier Transform (FFT). The AR PSD is not fit to a model, rather the already determined AR model is used to estimate the system response to a selected input function. The impulse response is computed from:

$$y_I(k) = \sum_{i=1}^{n} a_i \ y_I(k-i) \tag{5.25}$$

with

$y_I(-k) = 0,$

$y_I(0) = \text{constant}.$

The step response is readily computed from an integration of the impulse response:

$$x_S(k) = \int_0^t x_I(\tau)\, d\tau \tag{5.26}$$

The ramp response is likewise computed by integrating the step response:

$$x_R(k) = \int_0^t x_S(\tau)\, d\tau \tag{5.27}$$

The step response and ramp response functions may be used to compute the signal time constant and ramp time delay, respectively. The estimated time constant is compared to a nominal value using a fuzzy S-curve.

5.6.4 UAR Data Base

The UAR parameter file requires only the nominal time constant value of each signal. The result file (CORREL.UAR) produced by the UAR model contains the auto-correlation of each signal from which the AR model (and subsequently the AR PSD or AR step response) may be reproduced. The optimal model order from the AIC is retained for reference. The auto-correlation is updated after each data block. The SVS provides a facility for plotting the auto-correlation, PSD and AR step response of each signal.

5.7 Multivariate Generalized Consistency Checking[30]

The multivariate generalized consistency checking (MGCC) algorithm is similar to that of the SGCC except for the addition of empirical estimates with which to compare the measured outputs. The purpose of the MGCC module is to separate sensor fault (bias, decalibration) from normal changes in the system, and to detect and isolate common-mode sensor failures.

5.7.1 Consistency Checking

The MISO model is used to compute a prediction from all available combinations of the redundant signals from each process input signal. The number of combinations is equal to the product of the number of redundant signals for each input variable. Two different inconsistency error indices are computed for each signal. The first error index is called the output inconsistency index, IO, is computed from the inconsistencies observed between the measurements themselves and the model predictions. The maximum output inconsistency index is therefore:

$$IO_{max}(k) = \prod_{i=1}^{n_i} N_r(i) \tag{5.28}$$

where

IO_{max} = maximum output inconsistency index for variable k,

n_i = number of input signals to model for variable k,

$N_r(i)$ = number of redundant signals of variable i.

The input inconsistency index represents the number of times a signal is involved as an input to a MISO prediction which was inconsistent with the measurement. The maximum input inconsistency index is computed from

$$II_{max}(k) = \sum_{i=1}^{m} IO_{max}(i) \; N_r(i) \; / \; N_r(k) \qquad (5.29)$$

where

m = number of models the signal is an input to,

II_{max} = maximum input inconsistency index for variable k.

As in the SGCC algorithm, the inconsistency error index is incremented when the following does not hold

$$| \; m_k - m_p \; | \;\; \leq \epsilon_k + \epsilon_p \qquad (5.30)$$

where

m_k = measurement of signal k,

m_p = measurement prediction,

ϵ_k = tolerance of signal k,

ϵ_p = prediction error.

The difference is that in the event an inconsistency is observed, both the output inconsistency index of the output signal and the input inconsistency index of each input signal is incremented by one.

After computing the above inconsistency indices, the MGCC algorithm excludes those signals with indices equaling the maximum possible values. The inconsistency indices of those accurate signals affected by the failed signal(s) are adjusted to account for this occurrence. The logic of the MGCC algorithm is shown in Figure 5.7. The MGCC module detects two types of failure (1) signal level failure and (2) drift failure. The MGCC utilizes the fuzzy S-curve to compute a confidence factor for these failures based on the fractional number of times a signal is excluded over a block of data samples.

5.7.2 <u>MGCC Data Base</u>

The MGCC parameter file contains the empirical models (input signals, output signals, tolerances, coefficients, powers, model accuracy...) for each variable group. Two results files are created by the MGCC module.

1. ESTIMATES.MGCC - the best estimates for each variable group along with the signal error and model error.

2. INDICES.MGCC - the input and output inconsistency indices are kept separately in this file for each process signal. The maximum possible input and output inconsistency index values are stored here for reference. The number of redundant signals for each variable is also saved.

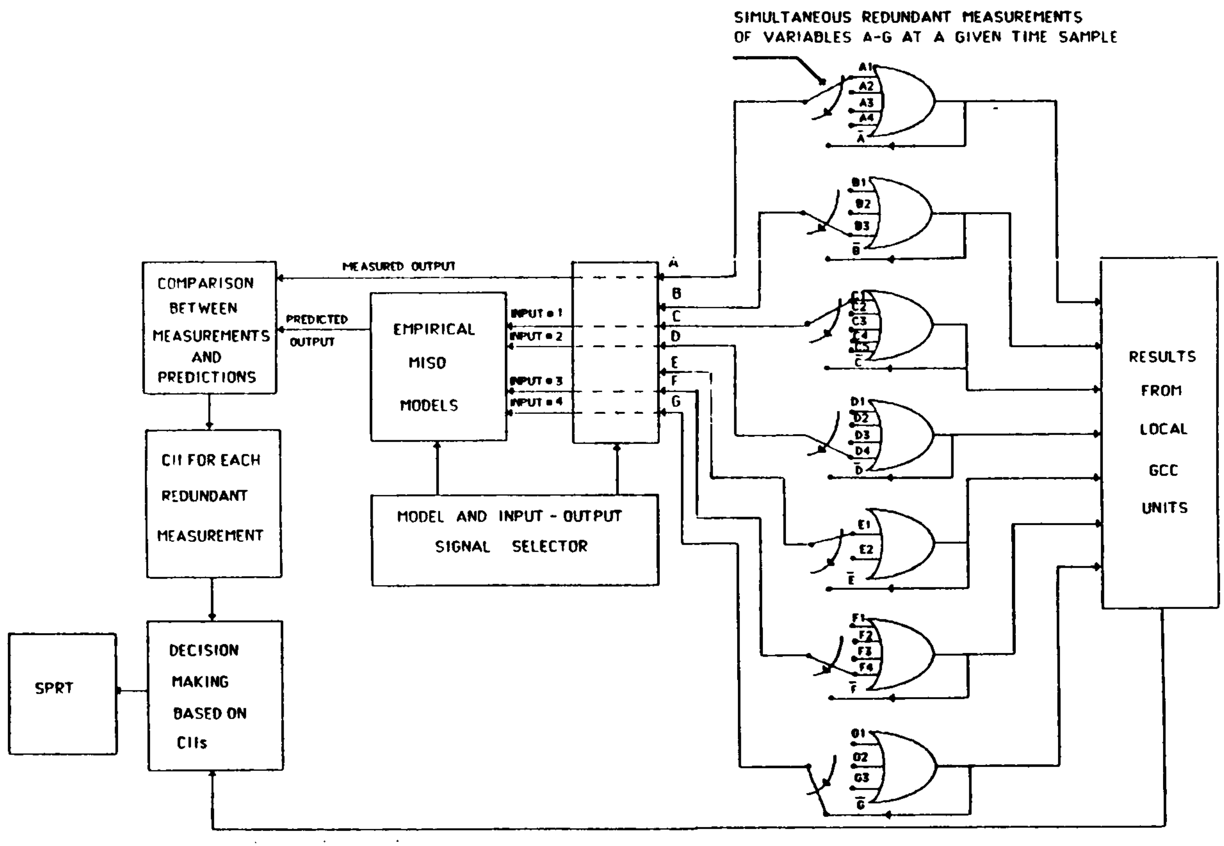

Figure 5.7. MGCC Module Logic Schematic.

These two results, the variable estimates and inconsistency indices (input and output), may be plotted from the SVS.

5.8 Process Hypercube Comparison

5.8.1 Hypercube Methodology

The process hypercube comparison (PHC) module algorithm and module development were discussed in Section 3. The PHC module detects consistency failure using a combination of the inconsistency separation index and variable exclusion status results as described in Section 3.4.

5.8.2 PHC Data Base

The PHC module retains several parameter files for reference:

1. KEYINDEX.PHC - the process state keys are kept here to indicate the process states that were observed during the learning period.

2. FREQUENCY.PHC - the number of times that a particular process state occurred is saved here.

3. SIGNALS.PHC - the information describing signal relationships is stored here. This information includes signals in the redundant groups, variable and group identifications.

4. INTERVALS.PHC - the upper and lower limits and the number of intervals for each variable as specified by the user are retained here.

The PHC outputs three different results files:

1. INDICES.PHC - the inconsistency separation indices found by the PHC algorithm are stored here with the number of signals in each redundant group.

2. ESTIMATE.PHC - the best estimate from either the consistency checking or the hypercube algorithm, as appropriate, is saved here along with the source of the estimate (the specific algorithm).

3. VARIABLE.PHC - the results of the hypercube analysis for each signal group is kept here.

Each of these three results can be plotted by the SVS for the user to view.

5.9 SVS Implementation Summary

The implementation and integration of six signal validation modules into a comprehensive signal validation system (SVS) has been described in this section. A system executive (SE) oversees the input of data, maintains a signal data base, activates the modules and displays the results. The modular architecture of the SVS contains modules using diverse techniques to detect various signal failure modes. Fuzzy functions convert these results to a confidence factor which is returned to the system executive. A final decision regarding the signal status is made by a unit called the positive decision maker (PDM) within the system executive.

6. PWR DATA ANALYSIS

6.1 Introduction

This section presents results of the comprehensive signal validation system (SVS) applied to operational data from a Westinghouse pressurized water reactor (PWR) plant. The PWR process data were taken during a plant start-up procedure. A short description and schematic of the plant, and a list of the available signals and their tolerances can be found in Appendix A. Results from each module showing examples of both valid and anomalous signals are presented along with the System Executive's (SE) final indication of signal status. It must be remembered that data with signal failure are not routinely available and thus some modules may not detect failure of any type. Also, most of the noise analysis methodologies have suboptimal results since the "noise" data were artificially generated by digitally filtering the d.c. data. This data is transient in nature (taken during plant start-up) and not entirely suitable for systematic evaluation of the signal validation system.

Testing of the modules has revealed some methodology limitations and minor errors. For instance, the generalized consistency checking (GCC) and process empirical modeling (PEM) modules have shown good results during transient conditions while the bias and noise detection (BND) module has not. Preliminary results with the BND have shown anomaly detection even with the less optimal digital (versus analog) implementation.

The process (plant) schematic used as the top level display by the System Executive is shown in Figure 6.1. The validated process conditions are displayed on the schematic along with an indication as to the validity of the signal group.

6.2 Consistency Failure Detection

The modules capable of reporting consistency (signal level) failure results include SGCC, MGCC and PHC. The consistency checking algorithms found several cases of signal anomaly. The techniques were shown to work well even in changing process (transient) situations. Only differences in sensor response time (or relative location) should cause erroneous results between steady-state and transient process conditions.

6.2.1 Consistent Power Signals

The first results from the consistency checking modules is for a case of consistent signals. The consistent signals are the four power signals shown in Figure 6.2. Figures 6.3 and 6.4 show an example of the inconsistency indices computed for the four redundant power signals by the SGCC and PHC modules, respectively. The graphs are blank (that is the inconsistency index is zero) which indicates that the

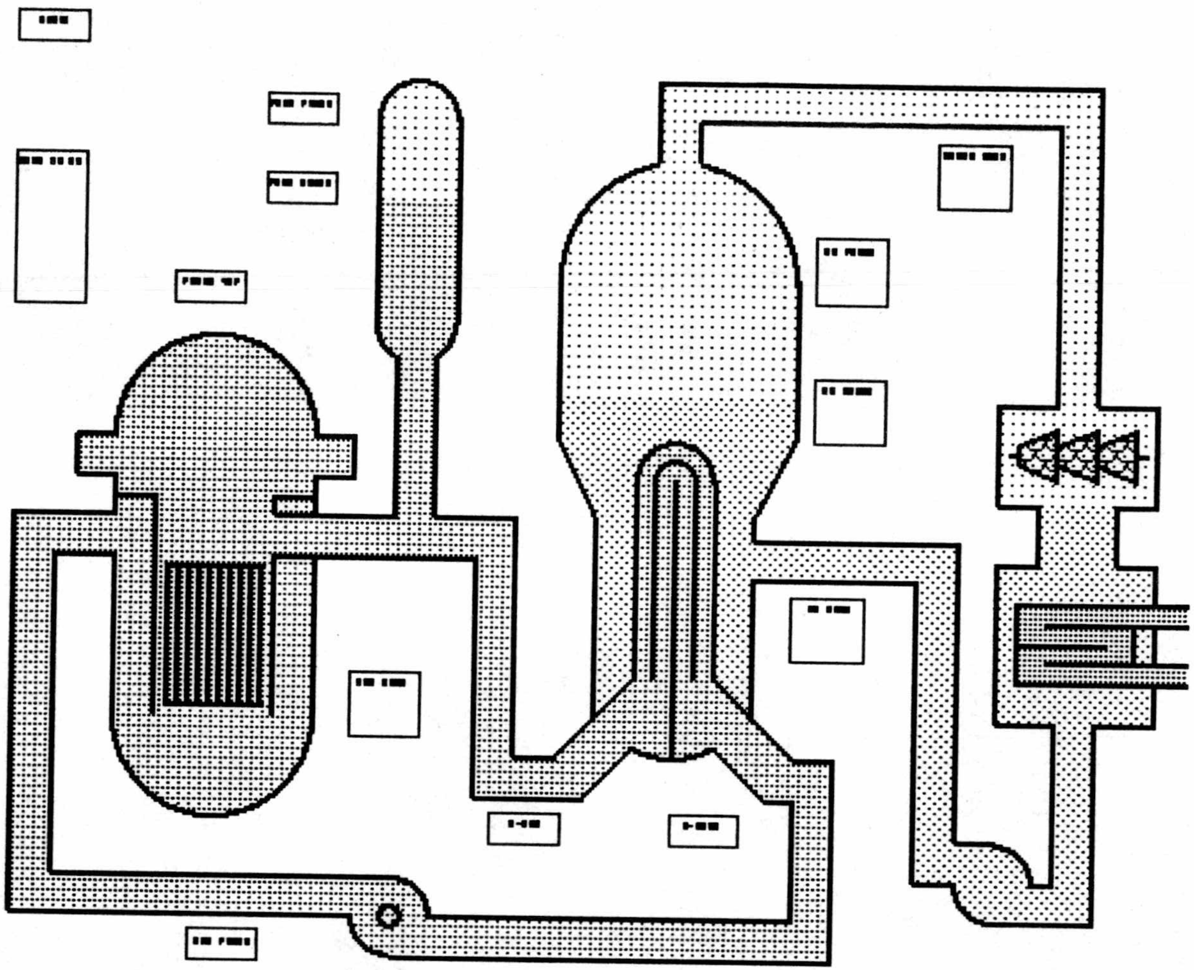

Figure 6.1. Comprehensive Signal Validation System Process Schematic for PWR.

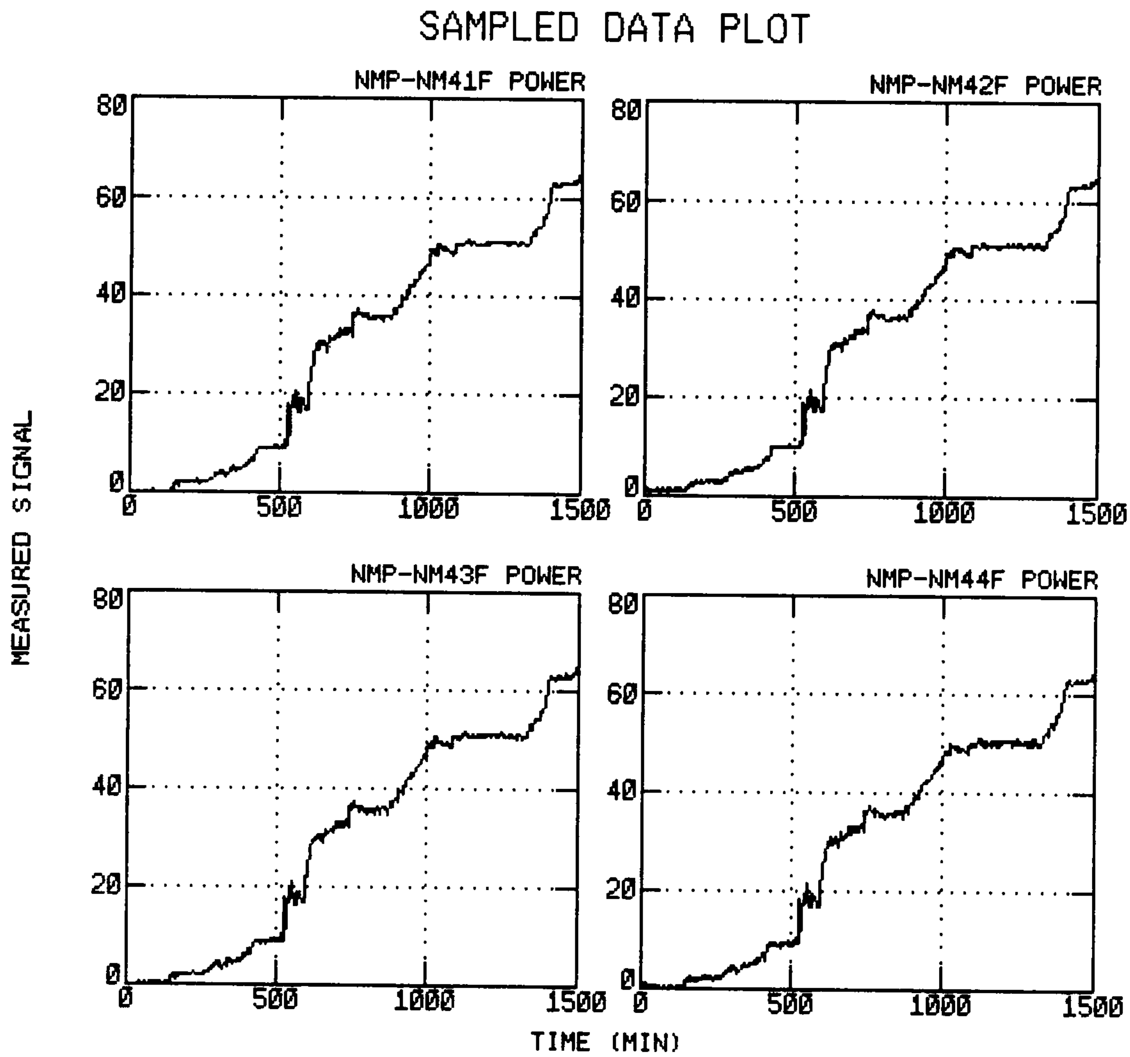

Figure 6.2. Measured Data for the PWR Power Signals.

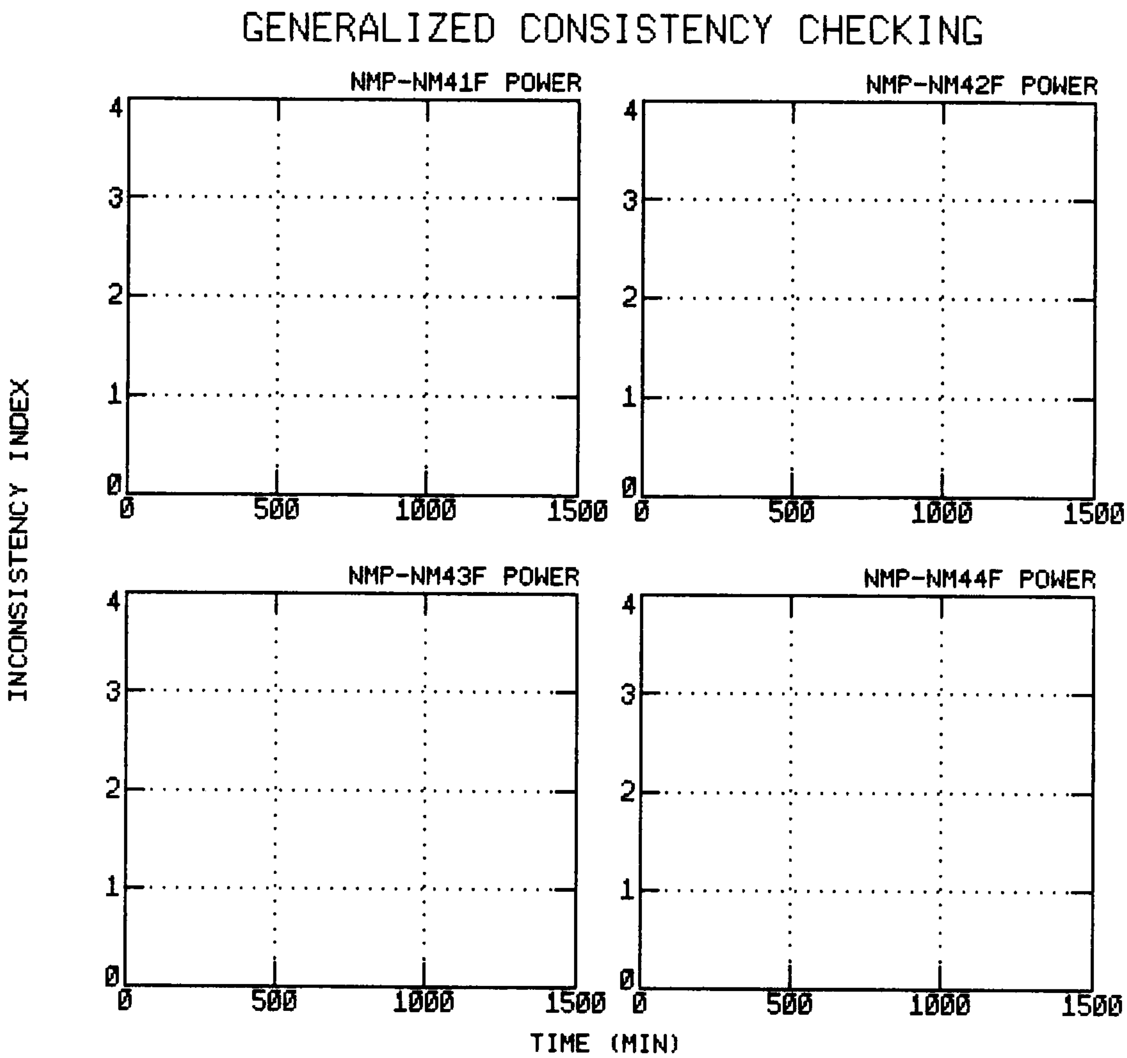

Figure 6.3. SGCC Inconsistency Indices for the PWR Power Signals.

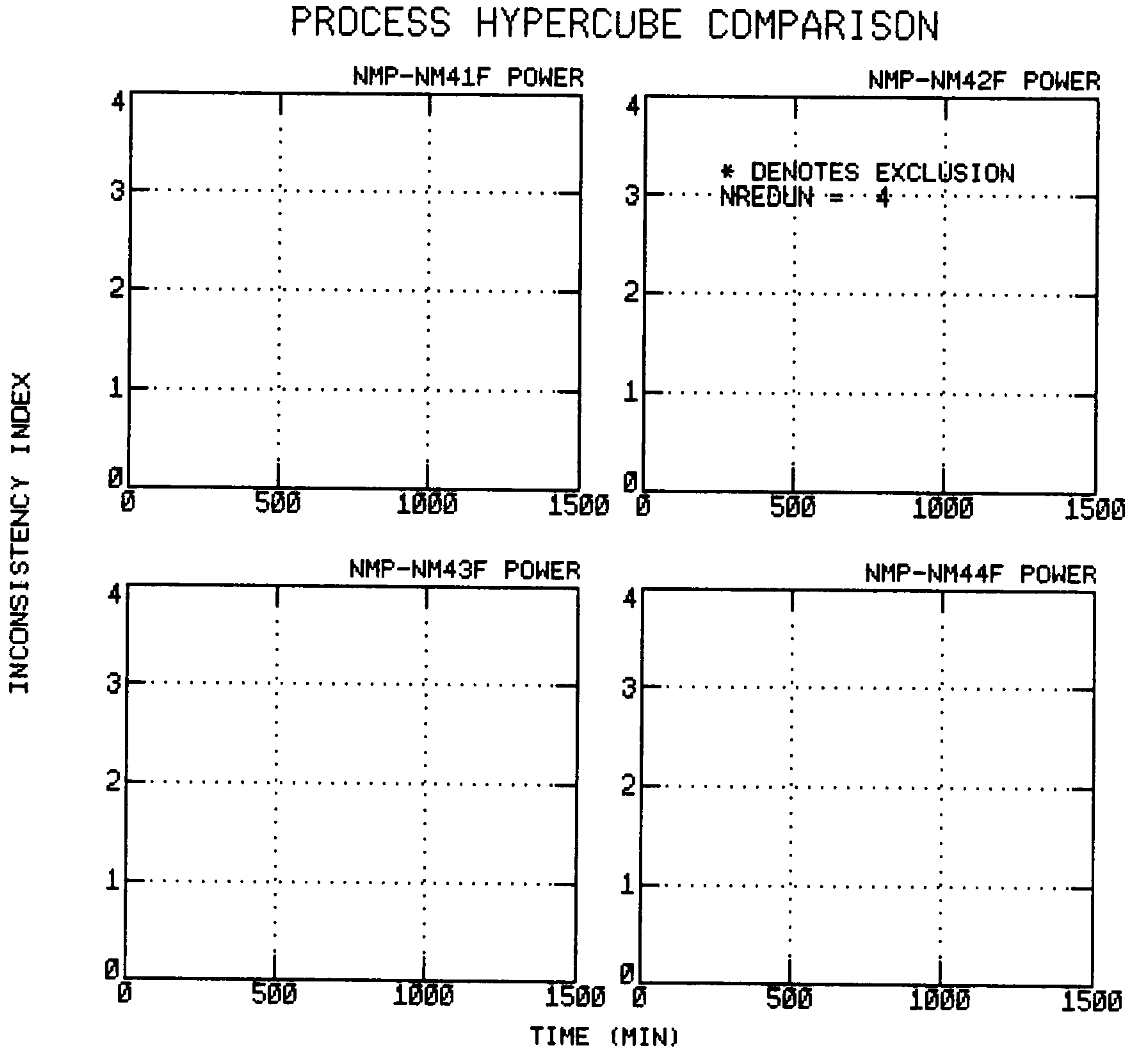

Figure 6.4. PHC Inconsistency Indices for the PWR Power Signals.

signals are consistent with respect to one another. The MGCC inconsistency indices given in Figure 6.5 are not exclusively zero valued as in the SGCC and PHC results, but are well below the maximum value. Note that the maximum possible MGCC inconsistency index is the sum of the maximum output cumulative inconsistency index (CII) and the maximum input CII, which in this case is 16+456=472 (from the graph). These non-zero values are a result of the power signals being an input to empirical models of other variables which were inconsistent. This non-zero level should be expected and should not give rise to a false indication of signal failure. MGCC power models are given in Section E.2.1. The final signal status from the SE is given in Figure 6.6 for one representative power signal.

During changing process conditions it is not unusual for some limited number of inconsistencies to be detected. Other signals have shown cases in which the signal was found to be inconsistent a few times, but this should not result in a premature decision of signal failure. This illustrates the importance of analysis on a block-by-block basis to prevent false alarms.

6.2.2 Loss of Signal Example

The second example of consistency failure detection involves a group of redundant signals in which one signal is lost for a short time period. Data from three redundant

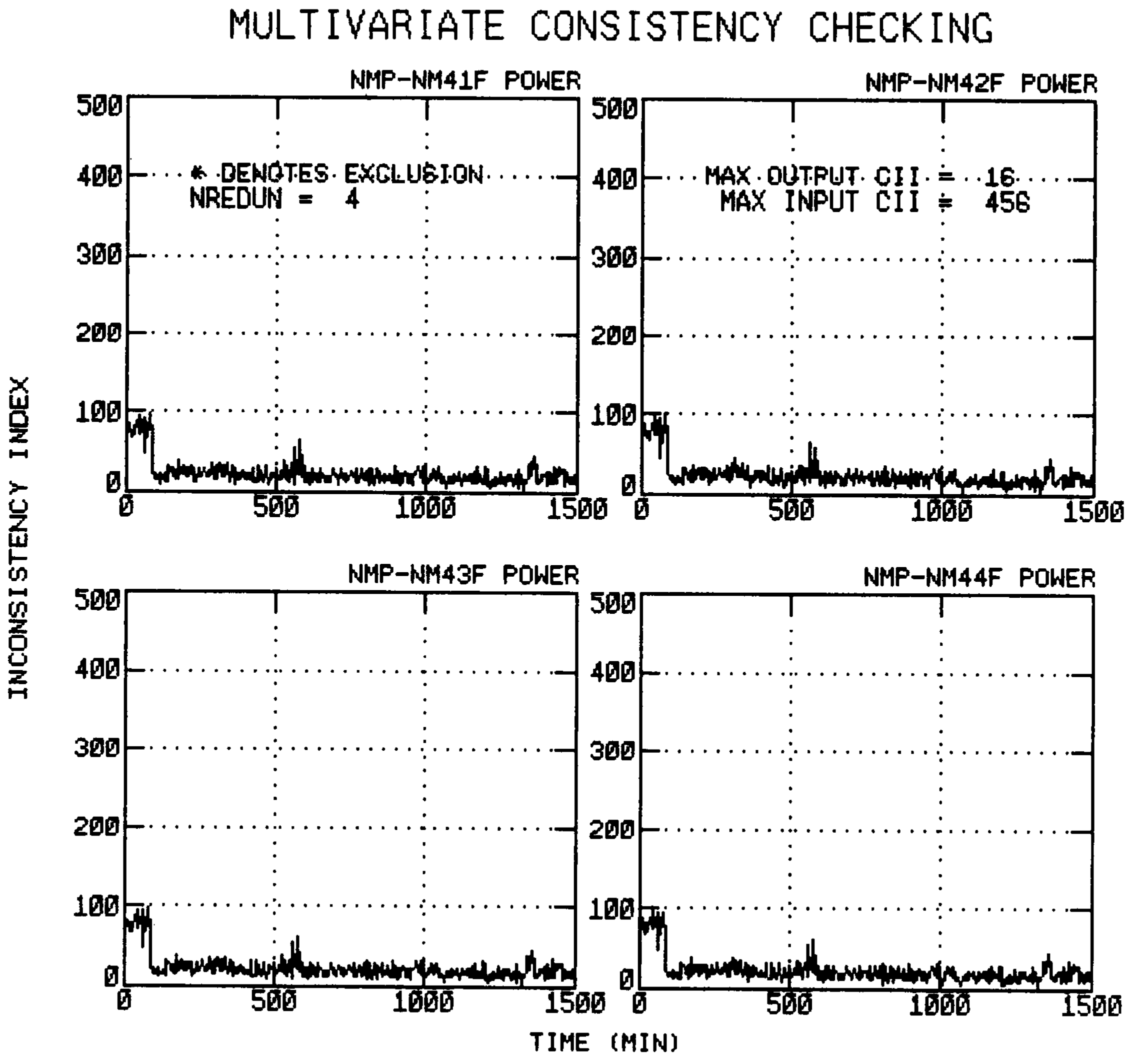

Figure 6.5. MGCC Inconsistency Indices for the PWR Power Signals.

```
Results for Sensor NMP-NM41F POWER, channel # 1.
   Final result indicates signal status is indeterminate.

  Consistency Failure Test indicates signal is valid.
    SE indicates signal is valid.
    SGCC indicates signal is valid.
    MGCC indicates signal is valid.
    BND indicates signal status is indeterminate.
    PHC indicates signal is valid.

  Bias/Drift Failure Test indicates signal status is indeterminate.
    SE indicates signal status is indeterminate.
    SGCC indicates signal is valid.
    BND indicates signal is ANOMALOUS.
    PEM indicates signal status is indeterminate.

  Response Time Failure Test indicates signal status is COMMONALITY indeterminate.
      Failure commonality has been found in the entire plant (process?).
    SE indicates signal is ANOMALOUS.
    BND indicates signal is ANOMALOUS.
    UAR indicates signal is ANOMALOUS.

  Basic Noise Failure Test indicates signal is valid.
    SE indicates signal is valid.
    SGCC indicates signal is valid.
    BND indicates signal status is indeterminate.
```

Figure 6.6. SE Final Signal Status for a Power Signal.

steam generator pressure signals are given in Figure 6.7. It is obvious at first glance that the signal MSS-P516 was lost around t=1000 minutes. The SGCC inconsistency index plot of Figure 6.8 shows an inconsistency index of two during the duration of the signal loss. This value of two is interpreted as meaning the signal is inconsistent with respect to two other signals (in this case both of the remaining redundant signals). The closely grouped asterisks on the plot of the inconsistency indices indicate that this signal was excluded from the variable estimate for the redundant group during the loss of signal event. The PHC inconsistency indices (Figure 6.9) for this signal also show the omission of the signal. Note the values of the inconsistency indices. The PHC indices indicate a relative measure of the degree of error in the signal. At the worst point, the signal is one-hundred tolerance bands from the other two signals. This PHC inconsistency separation index provides not only an indication of anomaly, but also the degree of error in a signal. Lastly, the MGCC inconsistency indices displayed in Figure 6.10 detect the anomaly in the signal.

One of the touted benefits of signal validation is the computation of a best estimate of the process variable. Figure 6.11 shows the best estimate for the steam generator pressure from each of the three modules plus the PEM prediction. Comparison of the estimate and the raw data of

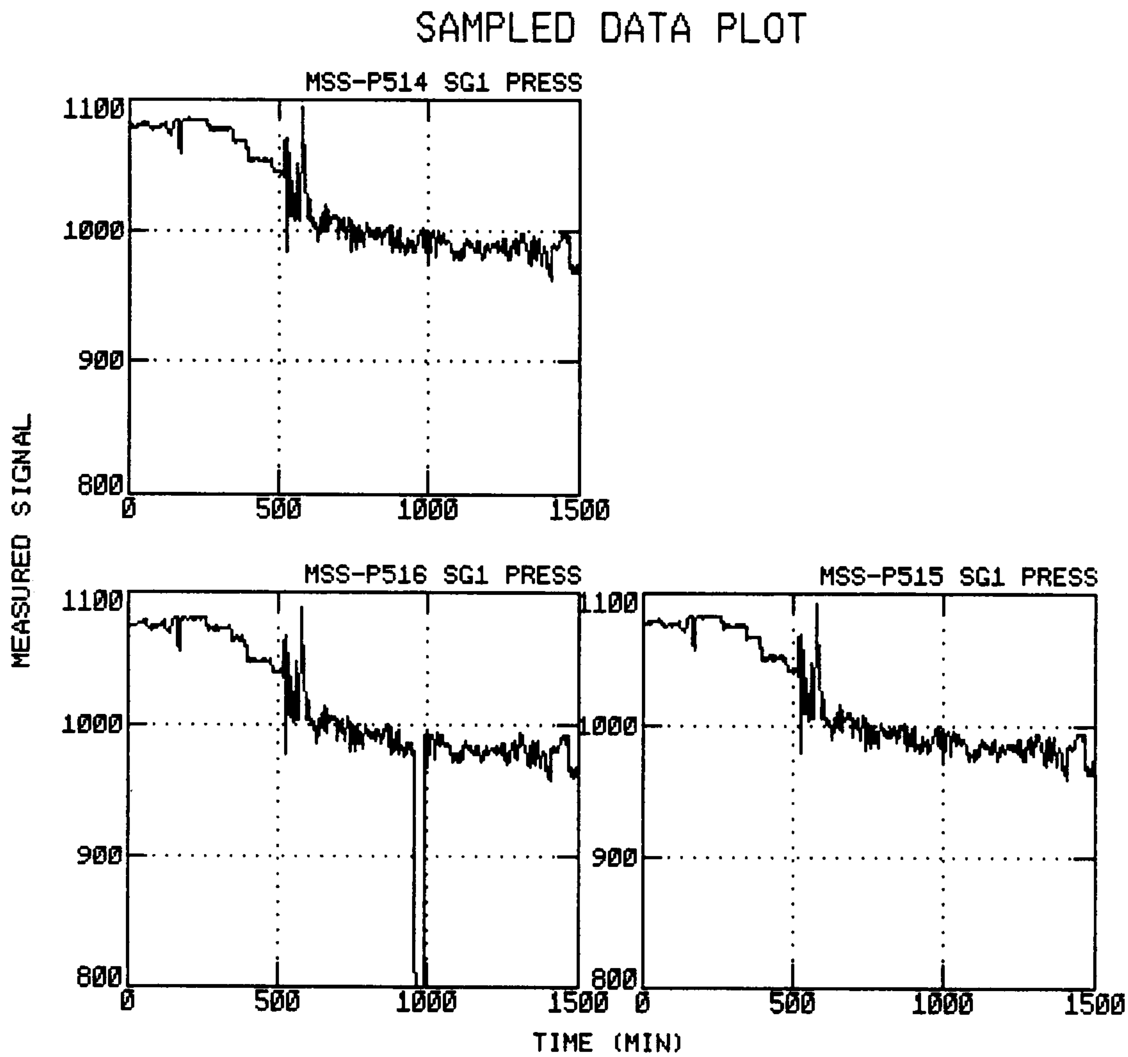

Figure 6.7. Measured Data for Three Redundant PWR Steam Generator Steam Pressure Signals.

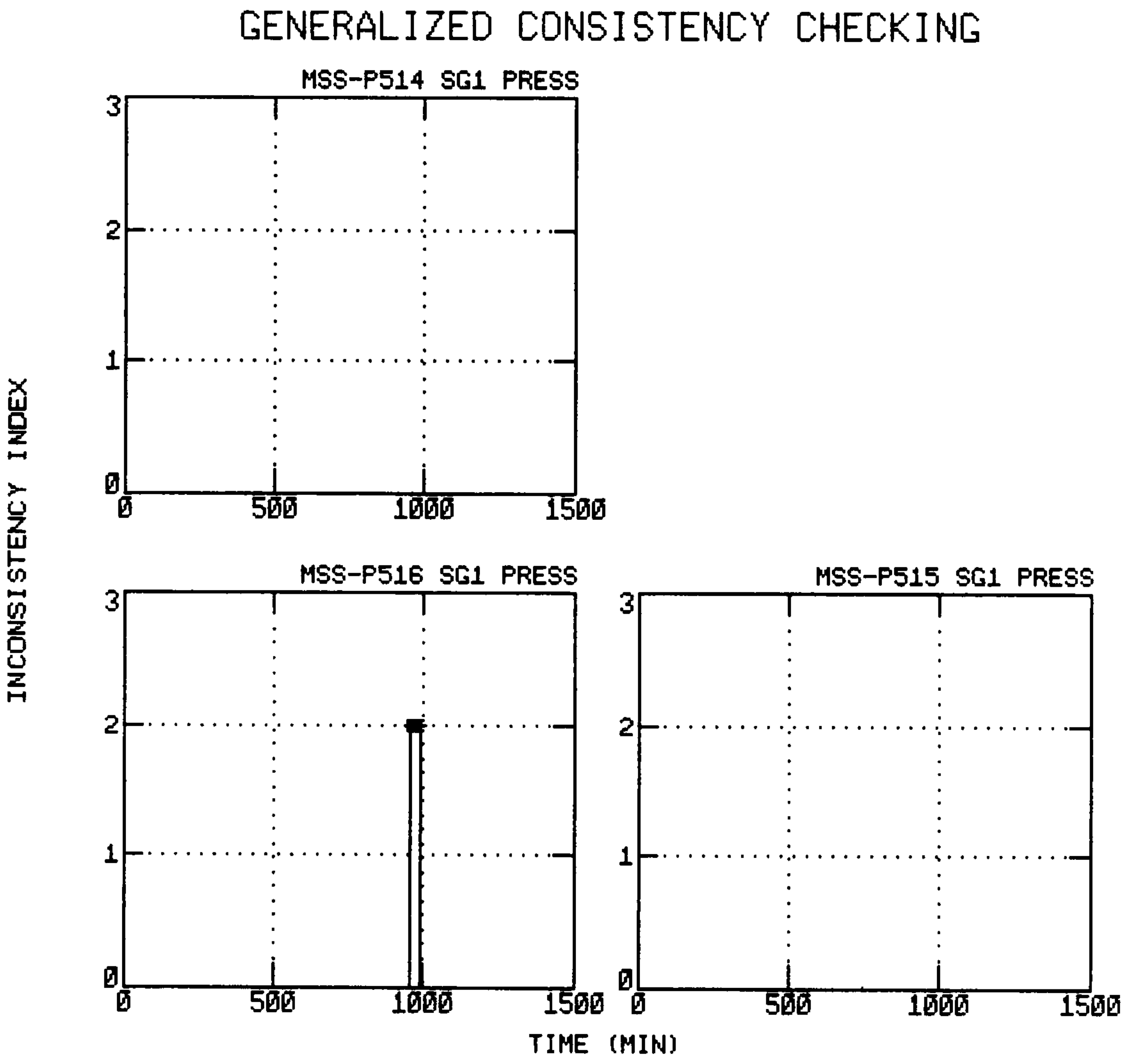

Figure 6.8. SGCC Inconsistency Indices for the PWR Steam Generator Steam Pressure Signals.

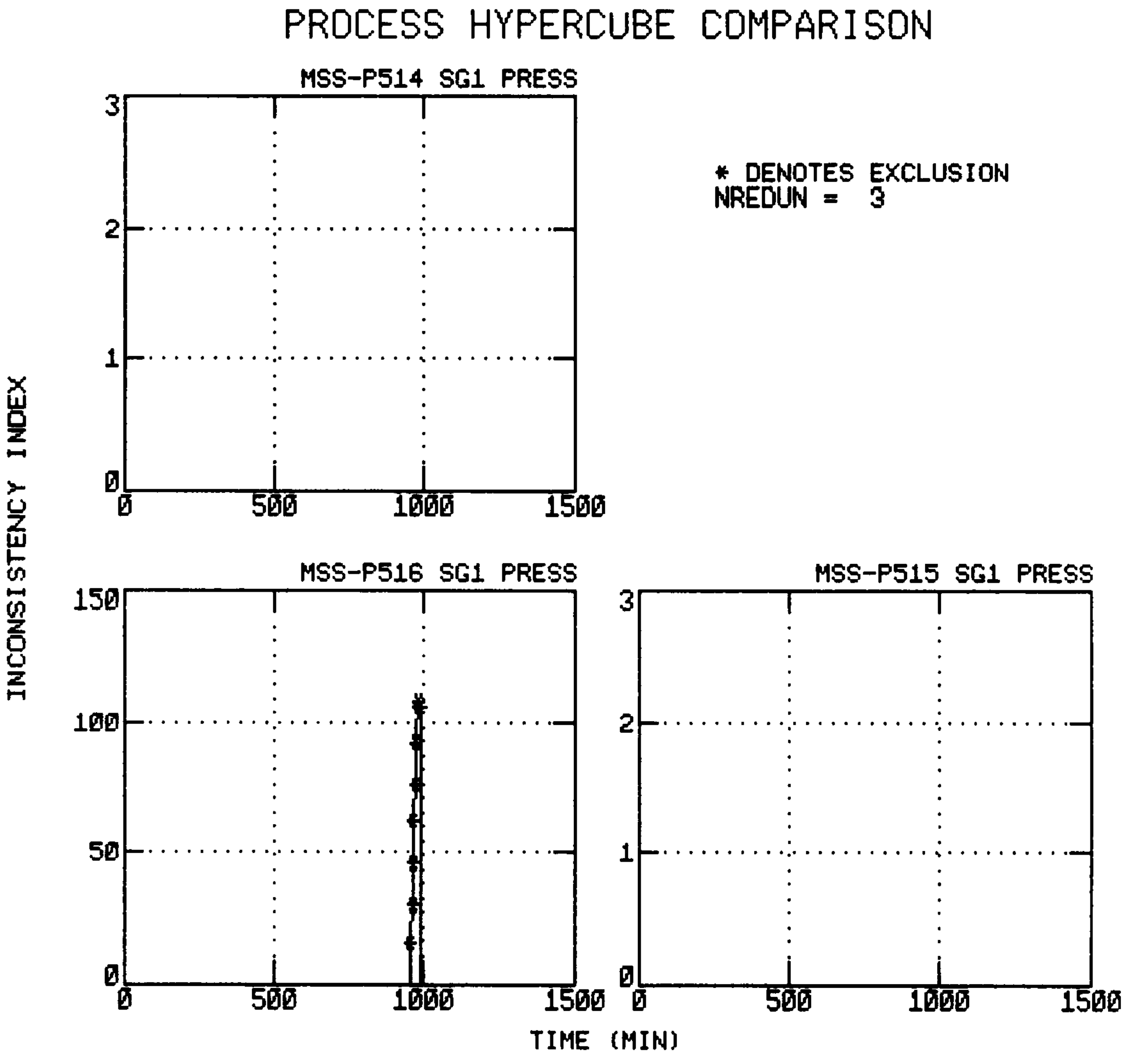

Figure 6.9. PHC Inconsistency Indices for the PWR Steam Generator Steam Pressure Signals.

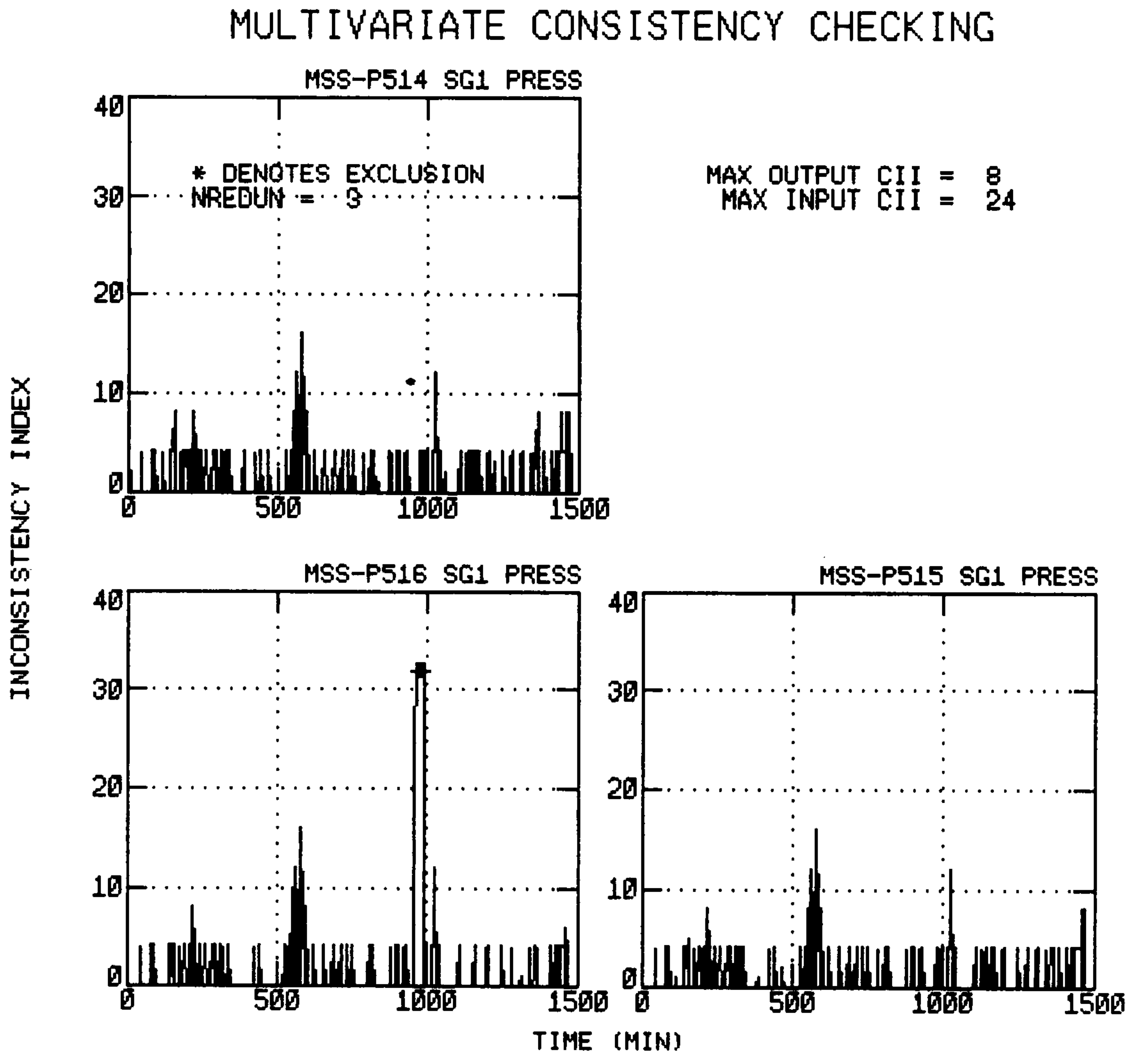

Figure 6.10. MGCC Inconsistency Indices for the PWR Steam Generator Steam Pressure Signals.

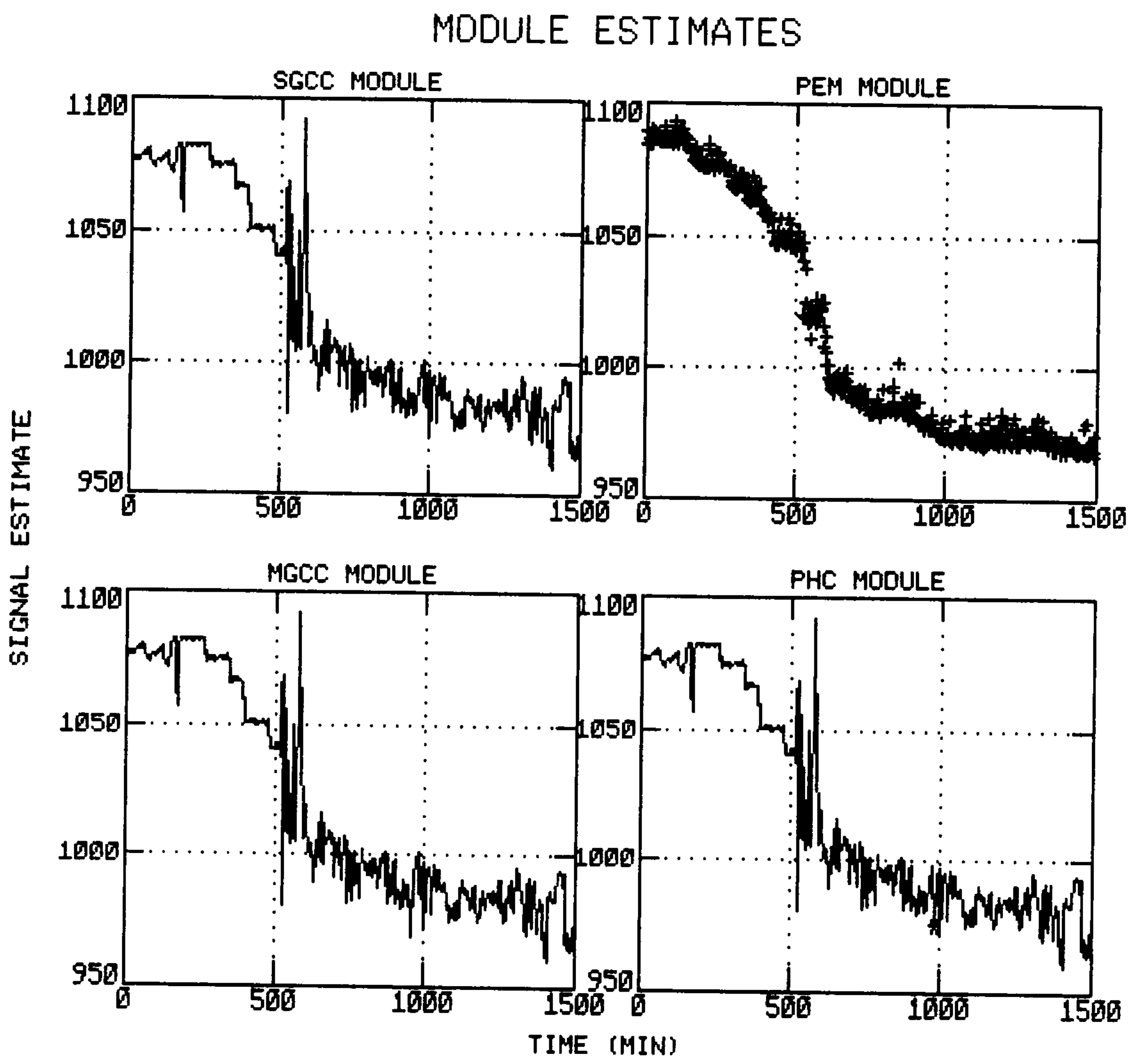

Figure 6.11. PWR Steam Generator Steam Pressure Estimates.

Figure 6.7 shows the omission of the faulty signal from the estimate during the loss of the signal. This validated estimate of the process conditions is the signal of choice for display to an operator and as input to a control or safety system. Also, the PEM module provides a smoother estimate of the variable.

6.2.3 Biased RCS Flow Signal

Next an example of bias in a reactor coolant system (RCS) flow signal is presented as related to consistency testing. The actual detection and characterization of bias failure is explored in Section 6.3. Figure 6.12 indicates that one signal (RCS-F435) is biased about 15% (real units) from the other two flow signals. The resultant consistency indices from the SGCC, PHC and MGCC modules are shown in Figures 6.13, 6.14 and 6.15, respectively. Important to note here is the rejection of the faulty measurement from the variable estimate. The SE results from the faulty and a normal flow signal are given in Figure 6.16.

6.2.4 Difference in Module Estimates

This is a rare example showing a noticeable difference in the manner in which the different modules conduct their consistency checking as well as the computation of the variable estimates. Recorded measurements from three redundant pressurizer level signals are shown in Figure

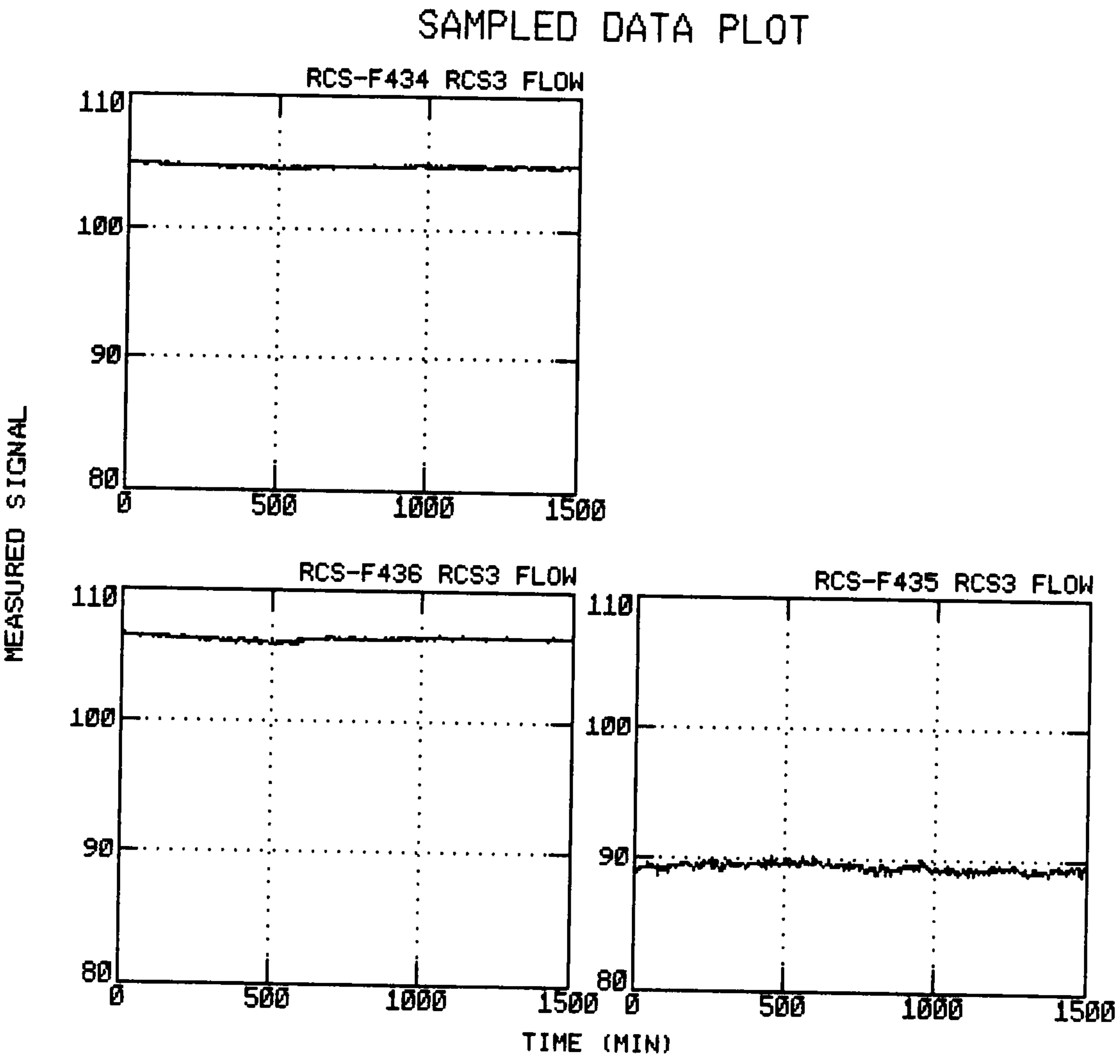

Figure 6.12. Measured Data for Three Redundant PWR RCS Flow Signals.

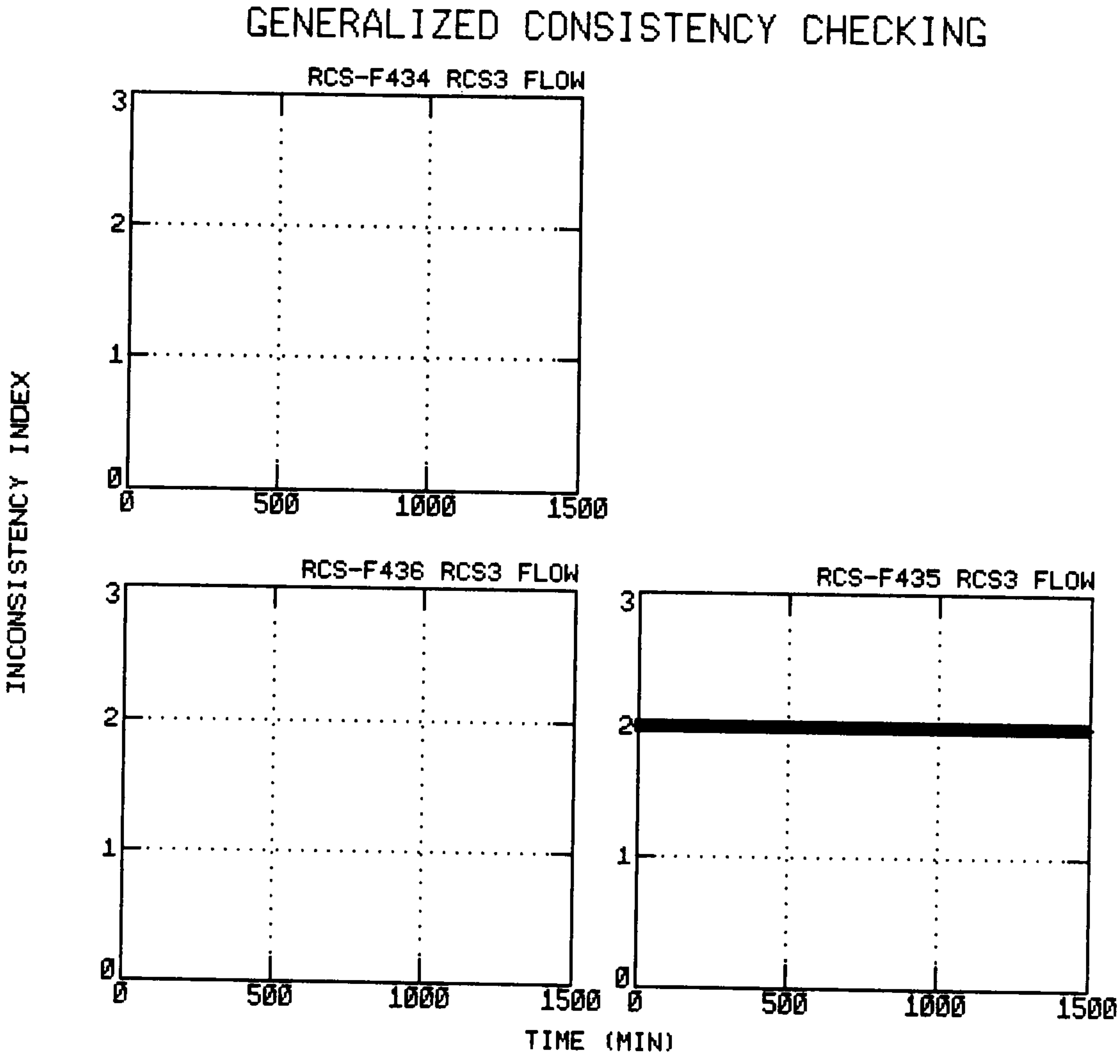

Figure 6.13. SGCC Inconsistency Indices for the PWR RCS Flow Signals.

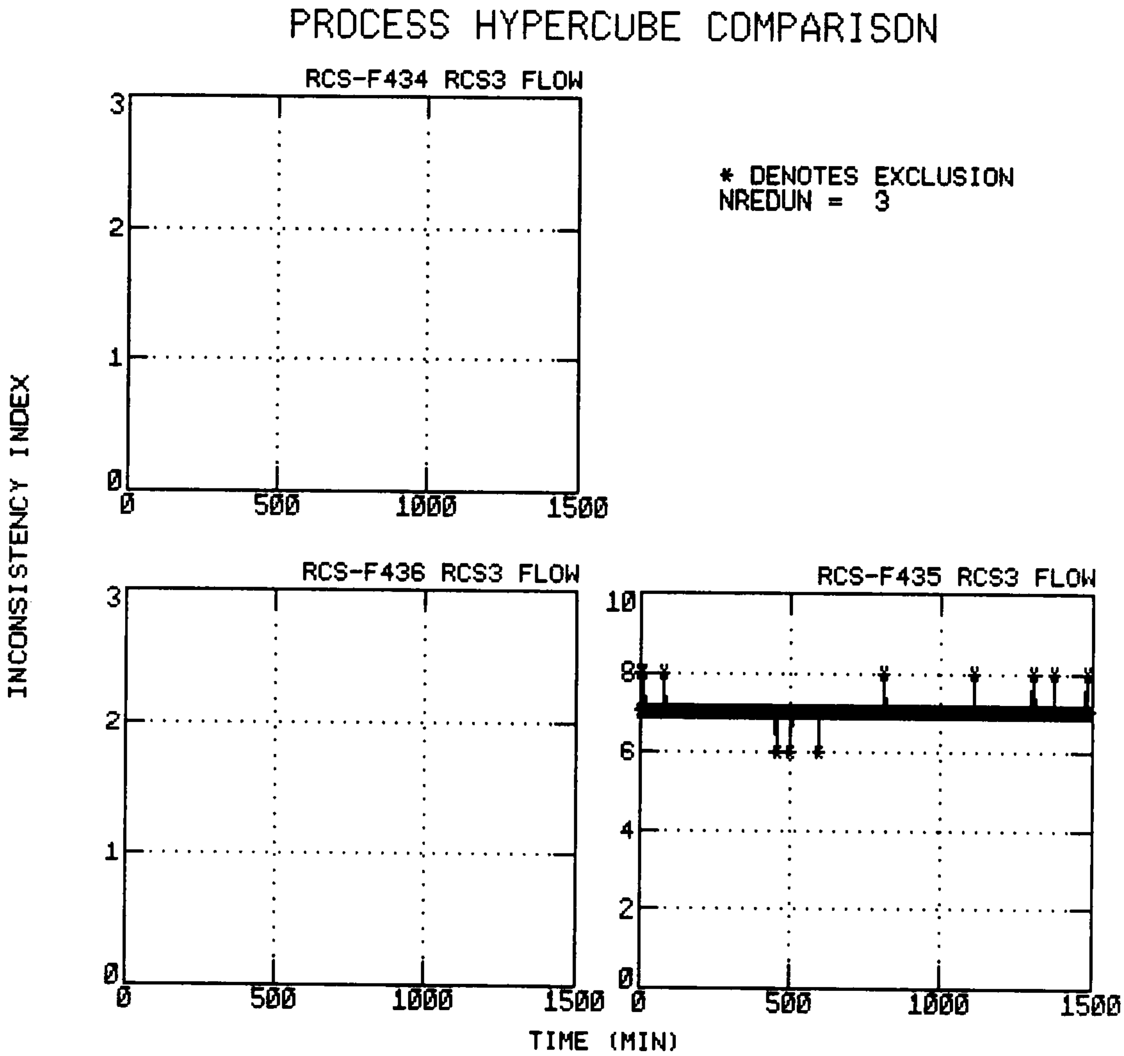

Figure 6.14. PHC Inconsistency Indices for the PWR RCS Flow Signals.

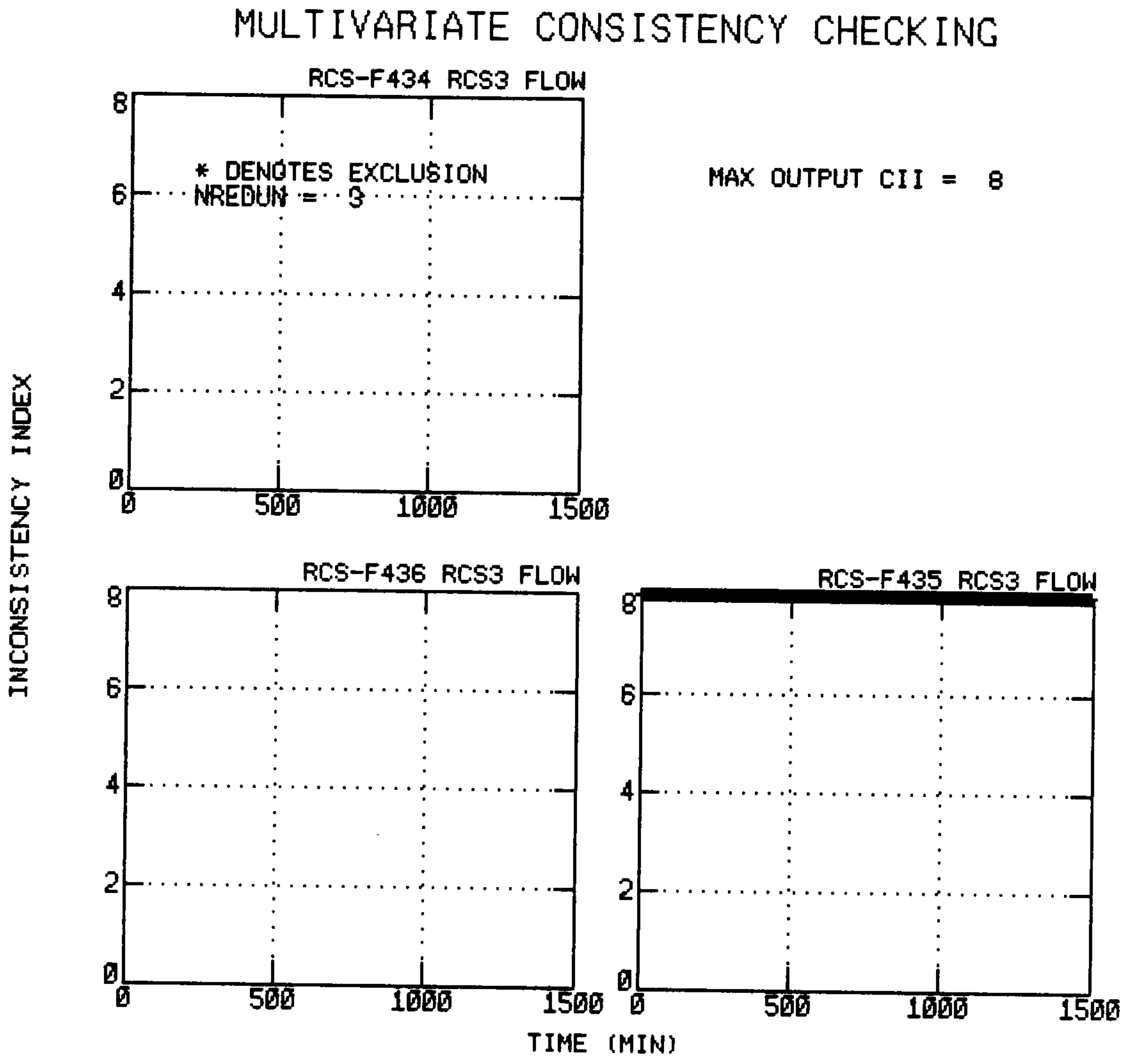

Figure 6.15. MGCC Inconsistency Indices for the PWR RCS Flow Signals.

```
Results for Sensor RCS-F434 RCS3 FLOW, channel # 65.
    Final result indicates signal status is indeterminate.
  Consistency Failure Test indicates signal is valid.
    SE indicates signal is valid.
    SGCC indicates signal is valid.
    MGCC indicates signal is valid.
    BND indicates signal status is indeterminate.
    PHC indicates signal is valid.
  Bias/Drift Failure Test indicates signal is valid.
    SE indicates signal is valid.
    SGCC indicates signal is valid.
    BND indicates signal is valid.
    PEM indicates signal is valid.
  Response Time Failure Test indicates signal status is COMMONALITY indeterminate.
      Failure commonality has been found in the entire plant (process?).
    SE indicates signal is ANOMALOUS.
    BND indicates signal is ANOMALOUS.
    UAR indicates signal status is indeterminate.
  Basic Noise Failure Test indicates signal is valid.
    SE indicates signal is valid.
    SGCC indicates signal is valid.
    BND indicates signal status is indeterminate.
```

Figure 6.16a. Valid Flow Signal.

```
Results for Sensor RCS-F435 RCS3 FLOW, channel # 66.
    Final result indicates signal is ANOMALOUS.
  Consistency Failure Test indicates signal is ANOMALOUS.
    SE indicates signal is ANOMALOUS.
    SGCC indicates signal is ANOMALOUS.
    MGCC indicates signal is ANOMALOUS.
    BND indicates signal is ANOMALOUS.
    PHC indicates signal is ANOMALOUS.
  Bias/Drift Failure Test indicates signal status is indeterminate.
    SE indicates signal status is indeterminate.
    SGCC indicates signal is ANOMALOUS.
    BND indicates signal status is indeterminate.
    PEM indicates signal is valid.
  Response Time Failure Test indicates signal status is COMMONALITY indeterminate.
      Failure commonality has been found in the entire plant (process?).
    SE indicates signal is ANOMALOUS.
    BND indicates signal is ANOMALOUS.
    UAR indicates signal status is indeterminate.
  Basic Noise Failure Test indicates signal is valid.
    SE indicates signal is valid.
    SGCC indicates signal is valid.
    BND indicates signal status is indeterminate.
```

Figure 6.16b. Anomalous Flow Signal.

Figure 6.16. SE Final Signal Status for RCS Flow Signals.

6.17. The data portion of interest is t<100 minutes. The signals assume nearly constant values of 27%, 24% and 13% with a tolerance of 10%. Note that percent (%) is the measured units for this signal. The SGCC requires that the signals be within 20% (twice the tolerance) while the PHC and MGCC require a stricter 10% difference. This is evidenced in the SGCC, PHC and MGCC inconsistency indices shown in Figures 6.18, 6.19 and 6.20, respectively. The SGCC with its looser restriction finds no inconsistency while the PHC and MGCC algorithms indicate inconsistency.

Especially interesting are the estimates from the modules given in Figure 6.21 (empirical models are found in Section E.2.7). As compared to the measured data of Figure 6.17, the following comparisons are noted for t<100 minutes.

1. The PHC and PEM estimates seem to be very good.
2. The MGCC estimate appears to be slightly low.
3. The SGCC is definitely low from including the data from signal RCS-L461.

While it is recognized that the SGCC estimate could, in fact, be the more accurate result, experience indicates otherwise from a mere visual analysis of the raw data.

6.2.5 Multiple Consistency Anomaly Detection

This consistency failure detection example explores a case in which multiple anomalies occur simultaneously (a more difficult problem to resolve). The measured data for a

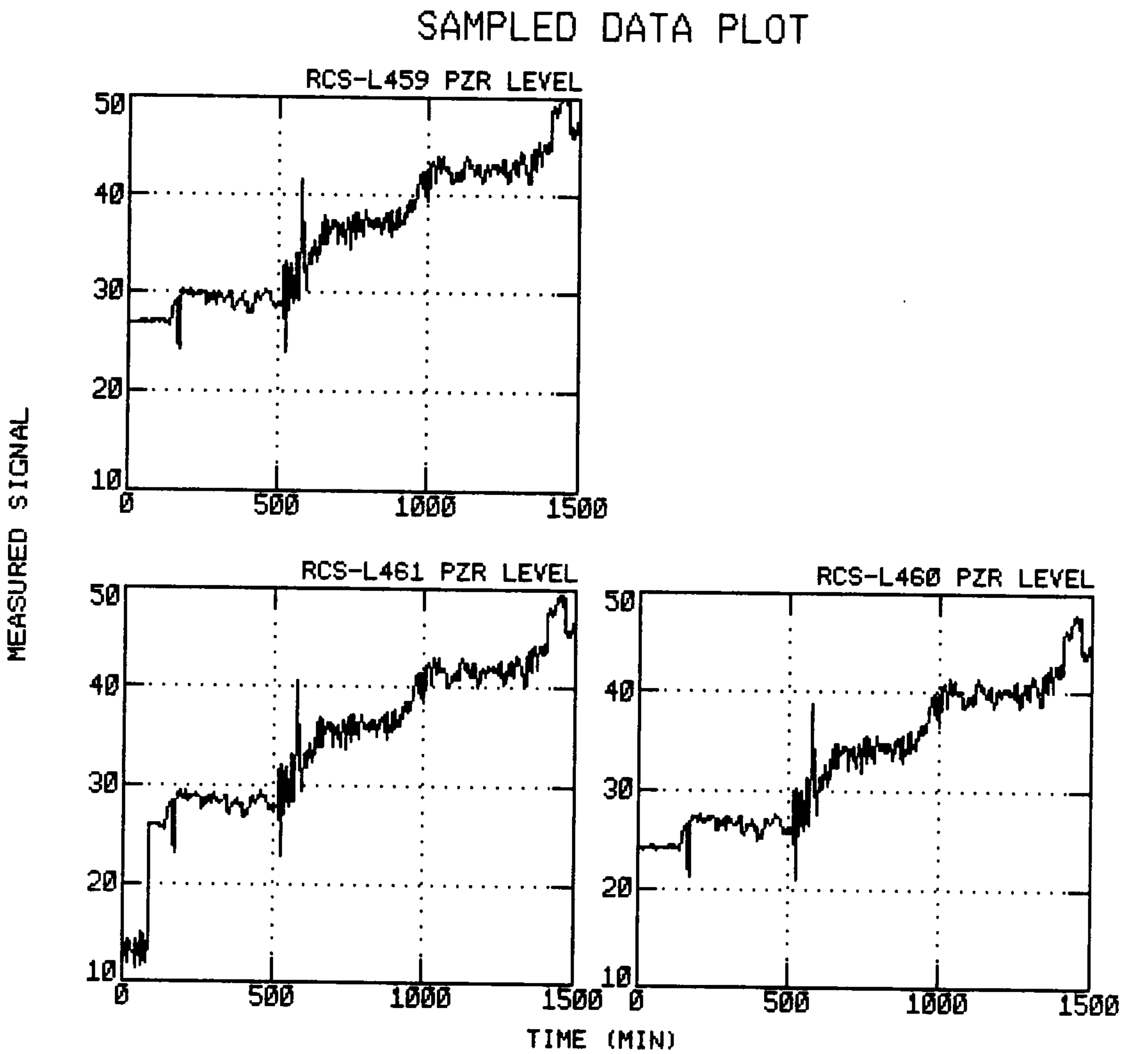

Figure 6.17. Measured Data for the Redundant PWR Pressurizer Level Signals.

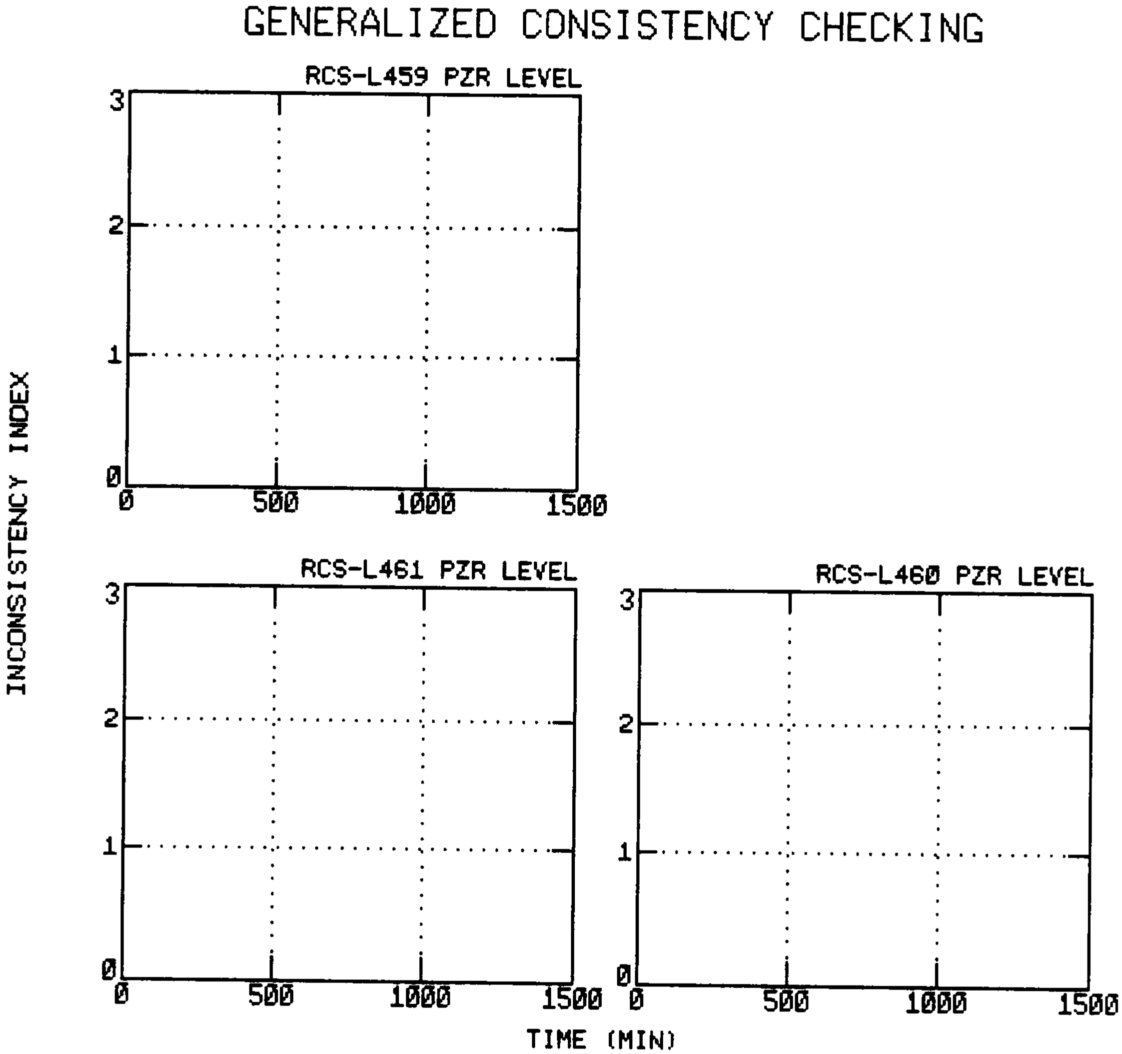

Figure 6.18. SGCC Inconsistency Indices for the PWR Pressurizer Level Signals.

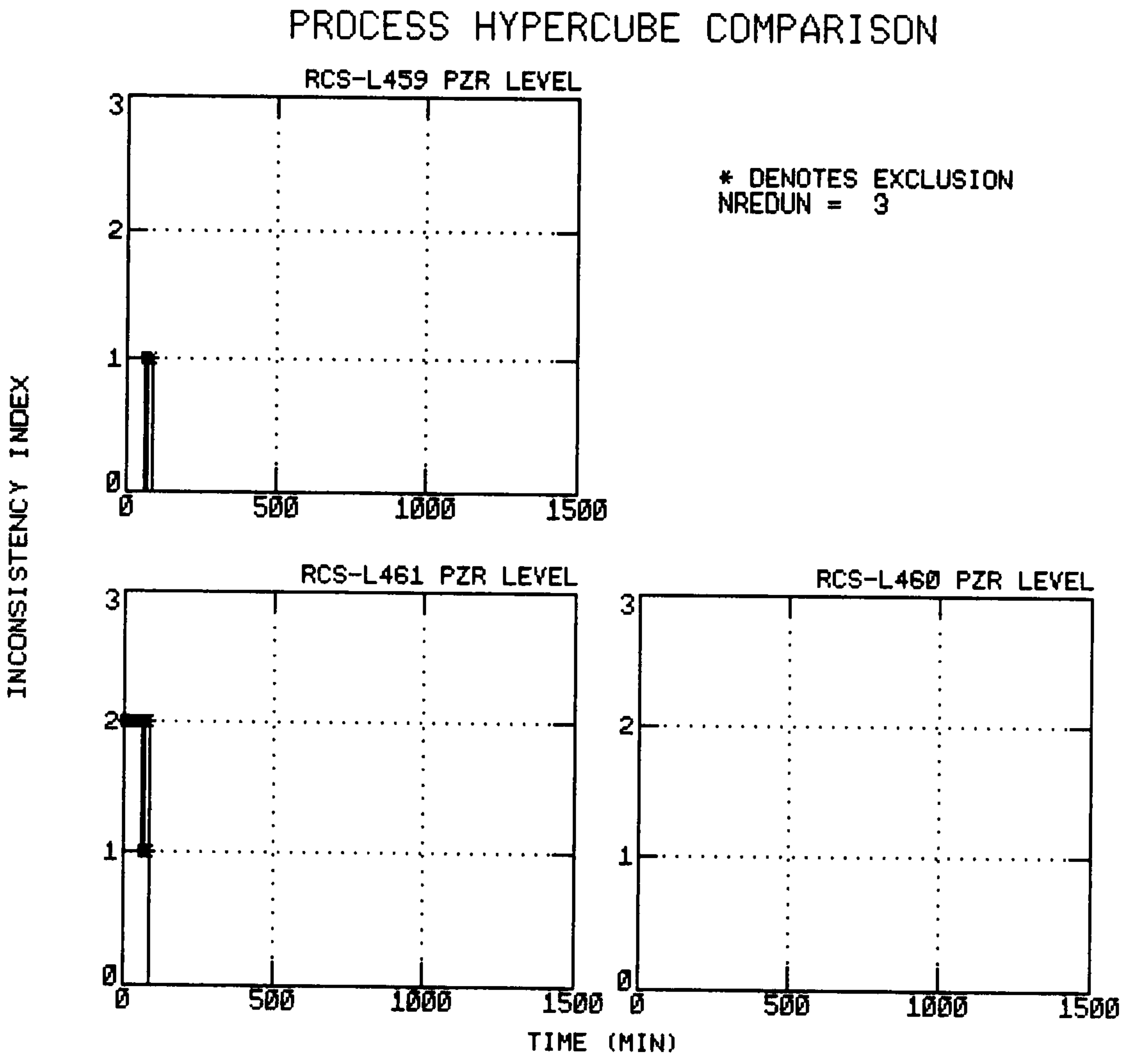

Figure 6.19. PHC Inconsistency Indices for the PWR Pressurizer Level Signals.

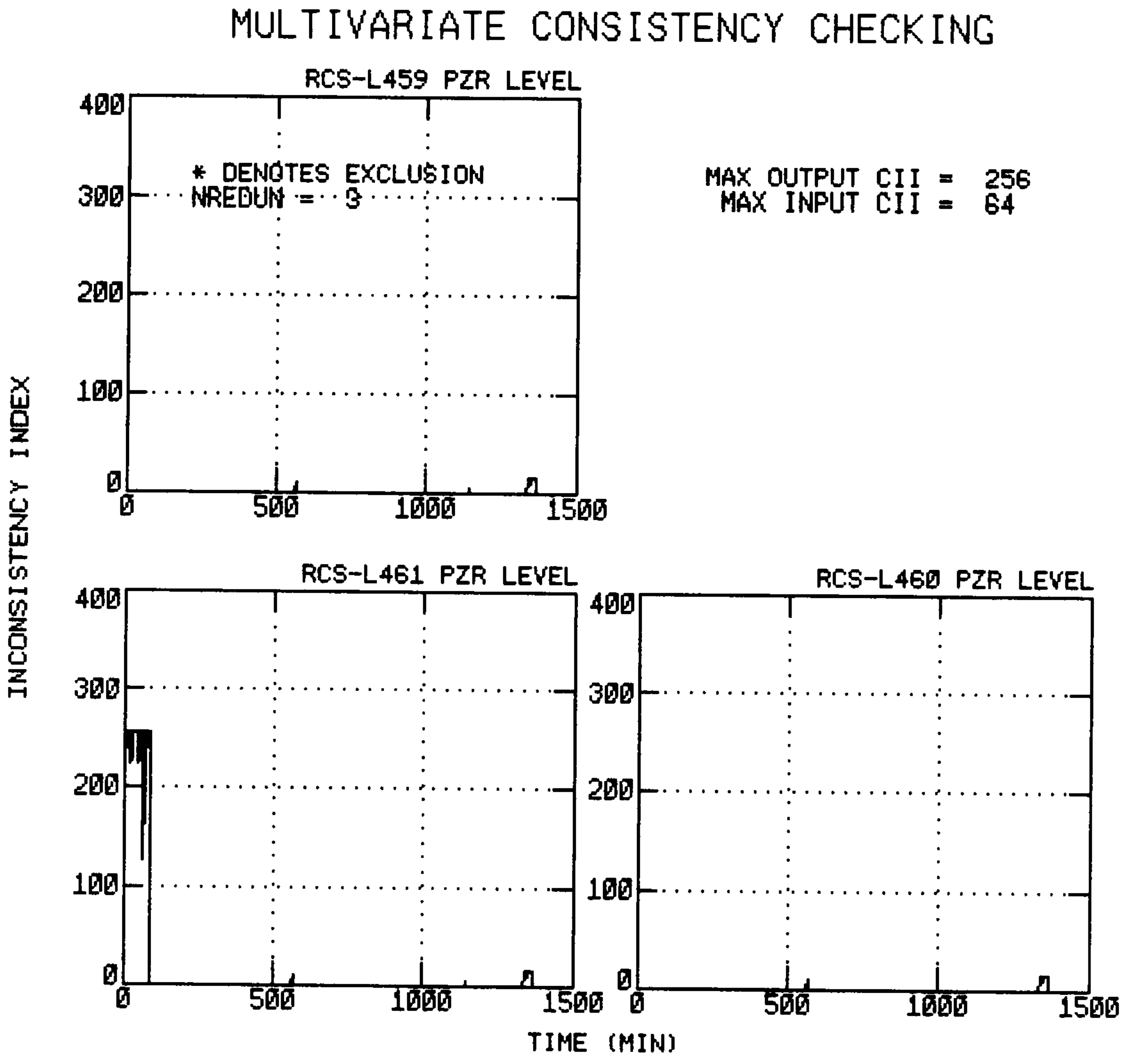

Figure 6.20. MGCC Inconsistency Indices for the PWR Pressurizer Level Signals.

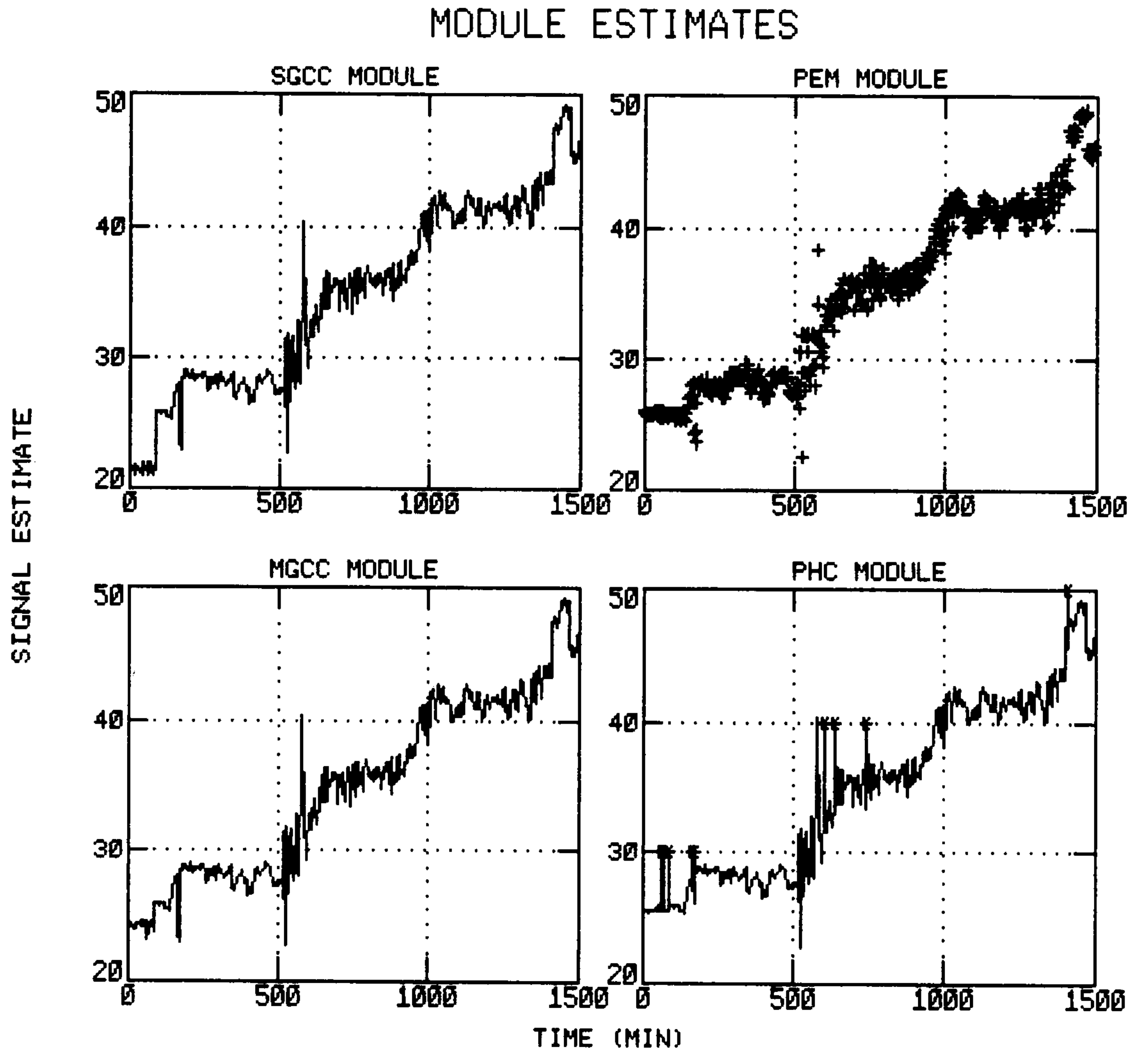

Figure 6.21. PWR Pressurizer Level Estimates.

group of four core-exit thermocouples at nearly the same location are given in Figure 6.22. One signal (CVCTST2) shows a nonchanging behavior before t=1000 minutes after which the signal abruptly drops to zero. Two other signals (CVCTST1 and CVCTST26) demonstrate some type of "spike" in the signal. The SGCC inconsistency indices are shown in Figure 6.23. Note that the SGCC methodology was able to resolve and omit the multiple signal failure case of this example. The MGCC and PHC modules were not used in the analysis of the core-exit thermocouple signals due to the large number of redundant thermocouple groups and realistic computer implementation restrictions. The final SE results for the four signals are given in Figure 6.24. Only signal CVCTST2 is indicated to be anomalous (consistency test) as is expected since the two signals with spikes did not exceed the time duration required to be considered an anomaly.

6.2.6 Effect of Tolerance

Finally, an example where a signal was not identified as inconsistent due to a difference in the signal tolerance is presented. There are four steam generator level signals for each steam generator. It was observed that each signal follows the same trend, but upon closer examination the indicated signal level is different for the last level signal for each of the steam generators. The difference is that the first three level signals are narrow-range

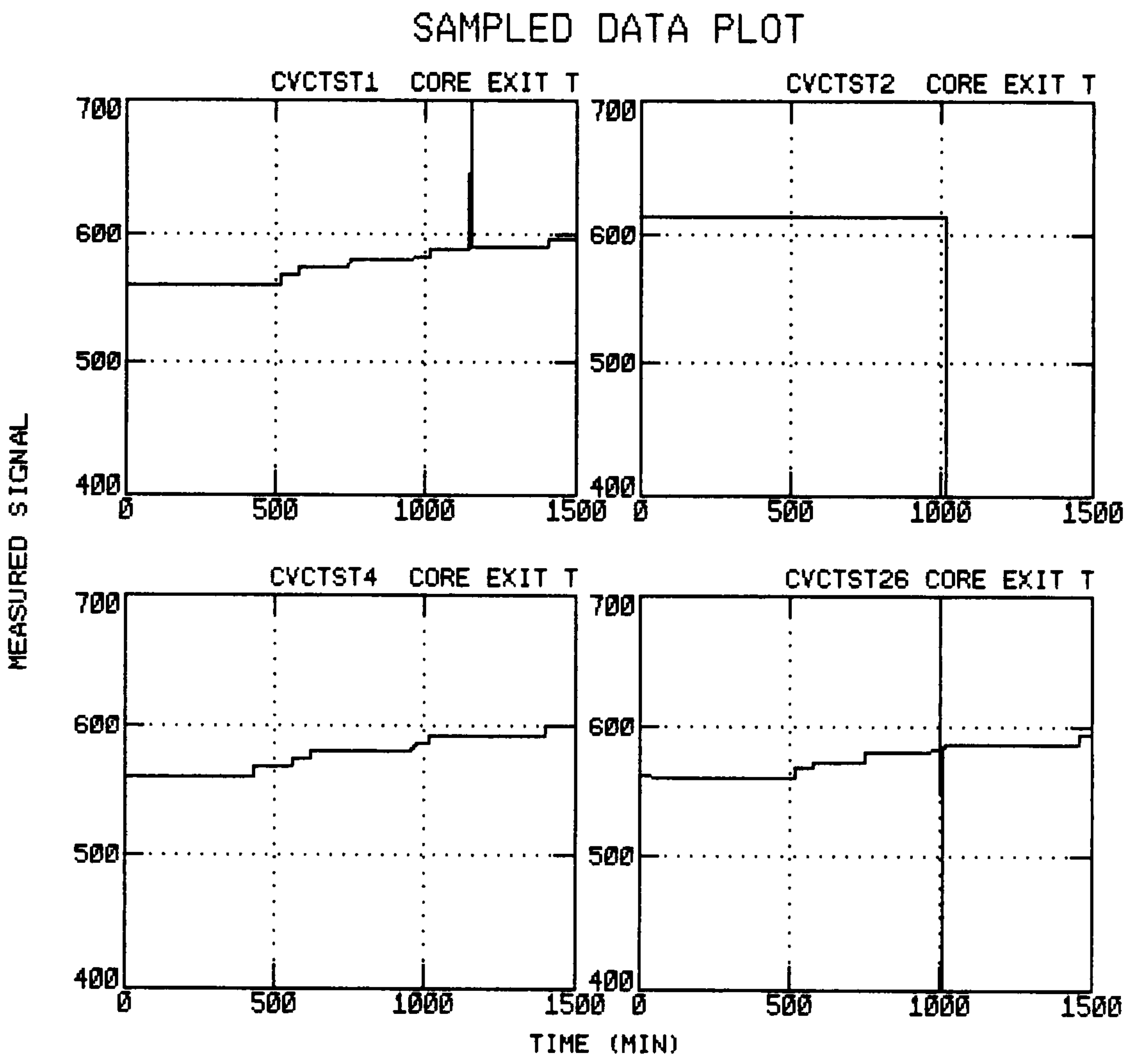

Figure 6.22. Measured Data for Four Redundant PWR Core-Exit Thermocouples.

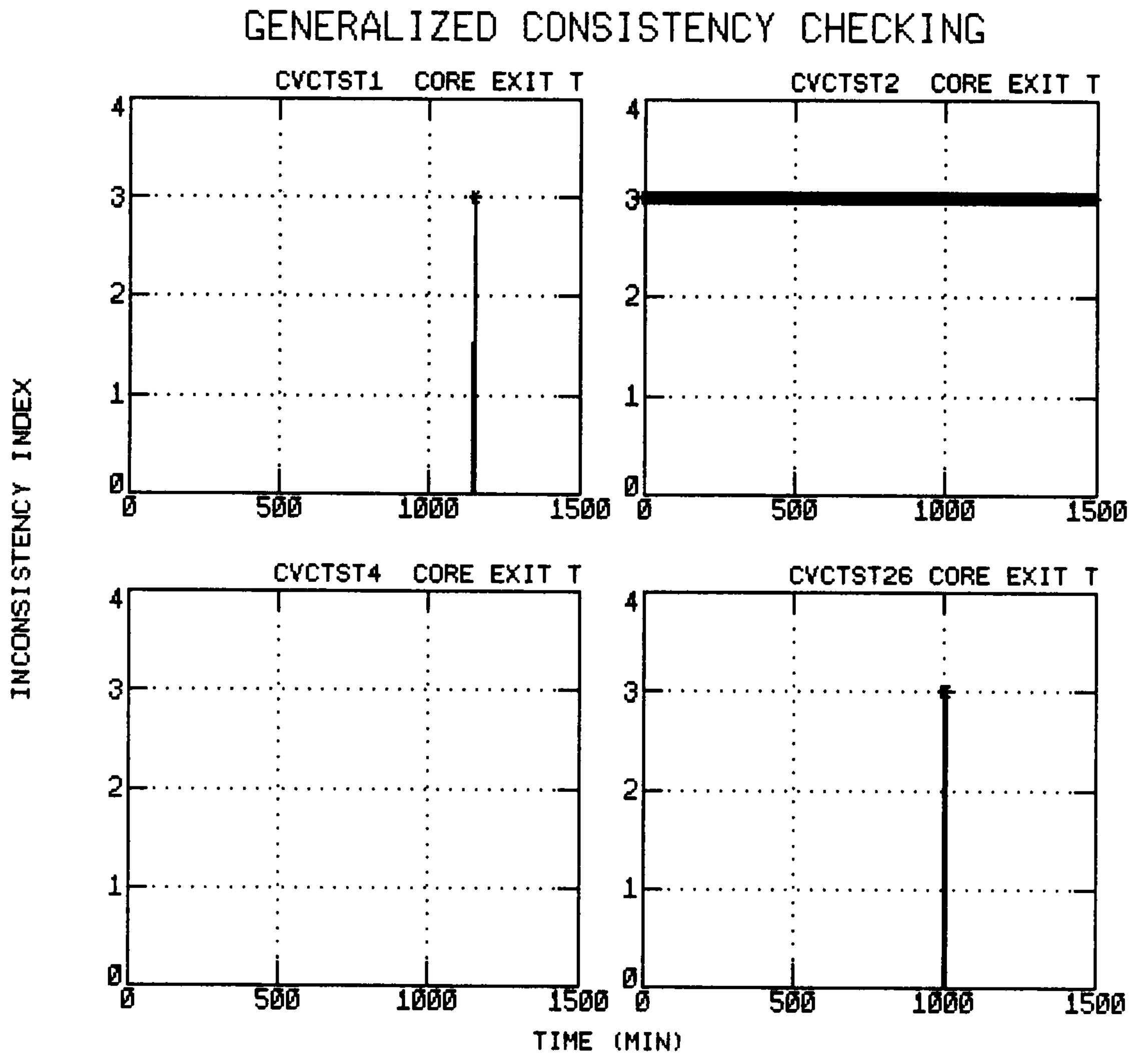

Figure 6.23. SGCC Inconsistency Indices for the PWR Core-Exit Thermocouples.

```
Results for CORE EXIT TEMP #10.

 Results for Sensor CVCTST1 CORE EXIT T, channel # 83.
   Final result indicates signal is ANOMALOUS.
     Consistency Failure Test indicates signal is valid.
     Bias/Drift Failure Test indicates signal status is indeterminate.
     Response Time Failure Test indicates signal status is COMMONALITY indeterminate.
     Basic Noise Failure Test indicates signal is ANOMALOUS.

 Results for Sensor CVCTST2 CORE EXIT T, channel # 84.
   Final result indicates signal is ANOMALOUS.
     Consistency Failure Test indicates signal is ANOMALOUS.
     Bias/Drift Failure Test indicates signal is ANOMALOUS.
     Response Time Failure Test indicates signal status is COMMONALITY indeterminate.
     Basic Noise Failure Test indicates signal is ANOMALOUS.

 Results for Sensor CVCTST4 CORE EXIT T, channel # 86.
   Final result indicates signal status is indeterminate.
     Consistency Failure Test indicates signal is valid.
     Bias/Drift Failure Test indicates signal status is indeterminate.
     Response Time Failure Test indicates signal status is COMMONALITY indeterminate.
     Basic Noise Failure Test indicates signal is valid.

 Results for Sensor CVCTST26 CORE EXIT T, channel # 108.
   Final result indicates signal is ANOMALOUS.
     Consistency Failure Test indicates signal is valid.
     Bias/Drift Failure Test indicates signal status is indeterminate.
     Response Time Failure Test indicates signal status is COMMONALITY indeterminate.
     Basic Noise Failure Test indicates signal is ANOMALOUS.
```

Figure 6.24. SE Final Signal Status for Core-Exit Thermocouple Group.

indicators with a tolerance of 5% while the fourth signal is a wide-range indicator with a tolerance of 22%. This difference in tolerances is taken into account by the consistency checking algorithms. The difference in signal range is part of the cause, but the signal was also obviously calibrated very close to its tolerance. This peculiarity was noted in each of the four steam generator wide-range level indicators. What is undesirable is the use of the wide-range value (along with the three narrow-range values) in computing the variable estimate.

6.3 Bias/Drift Failure Detection

Bias and drift failure is detectable by the PEM, SGCC, MGCC and BND modules. The SGCC module monitors drift using the sequential probability ratio test (SPRT). The BND module monitors bias using the symmetry of the amplitude probability density function (APDF) as compared to an expected value. There was only one actual bias/drift anomaly detected by the modules.

6.3.1 Empirical Modeling

In order to monitor bias or drift failure in the signals with the PEM and MGCC modules, it was first necessary to create empirical models off-line for input to these modules. The modeling effort was a research project in itself. The empirical modeling results for the PWR data are given in Appendix E.

The objectives of the modeling effort were

1. to determine whether a single model can be developed which will properly describe a signal over the complete normal operating range of the signal,

2. to assess whether or not a single generalized functional form can be used to fit the given data,

3. to develop models for input into both the Process Empirical Modeling (PEM) module and the Multivariate Generalized Consistency Checking (MGCC) module of the Signal Validation System (SVS).

The modeling for the MGCC module was performed in a slightly different manner than that for the PEM module. For the MGCC models a data set of best estimates was used as input to the empirical modeling program after which a single empirical model was created for each process variable (redundant group) for entry into the MGCC module. Multiple models for each signal were computed for the PEM module using different combinations of individual signals from a given redundant signal group.

The PWR empirical modeling did show that a single model can be constructed which accurately describes a given signal over its normal operating range. The start-up type data used is somewhat desirable since many valid operating states are represented by such data; however, there may be transient lags present affecting the results.

With redundant signals available in a nuclear power plant, more than one model may easily be generated for each process signal. It should be pointed out that signal substitutions may also be made. For example, instead of using power as an input for modeling certain parameters on the secondary side, the combination of cold leg and hot leg temperature could just as easily have been used. This is important in situations when certain measurements are not available. Some questions still remain unanswered. For instance, will the models change over time (e.g. a core-exit temperature model over a given fuel cycle).

6.3.2 Ramping Signal

The previously explored power signals of Section 6.2.1 are an example of ramping signals and show the effect on bias detection by the various modules. Figure 6.25 shows a comparison between the SGCC, MGCC and PEM estimates of the power signal. The empirical model estimates from the MGCC and PEM modules track the power signal well indicating the ability of these two modules to detect drift during changing process conditions. The ability of the SGCC in correctly identifying the lack of bias from its SPRT is shown in Figure 6.26. The bias SPRT does not exceed the threshold at

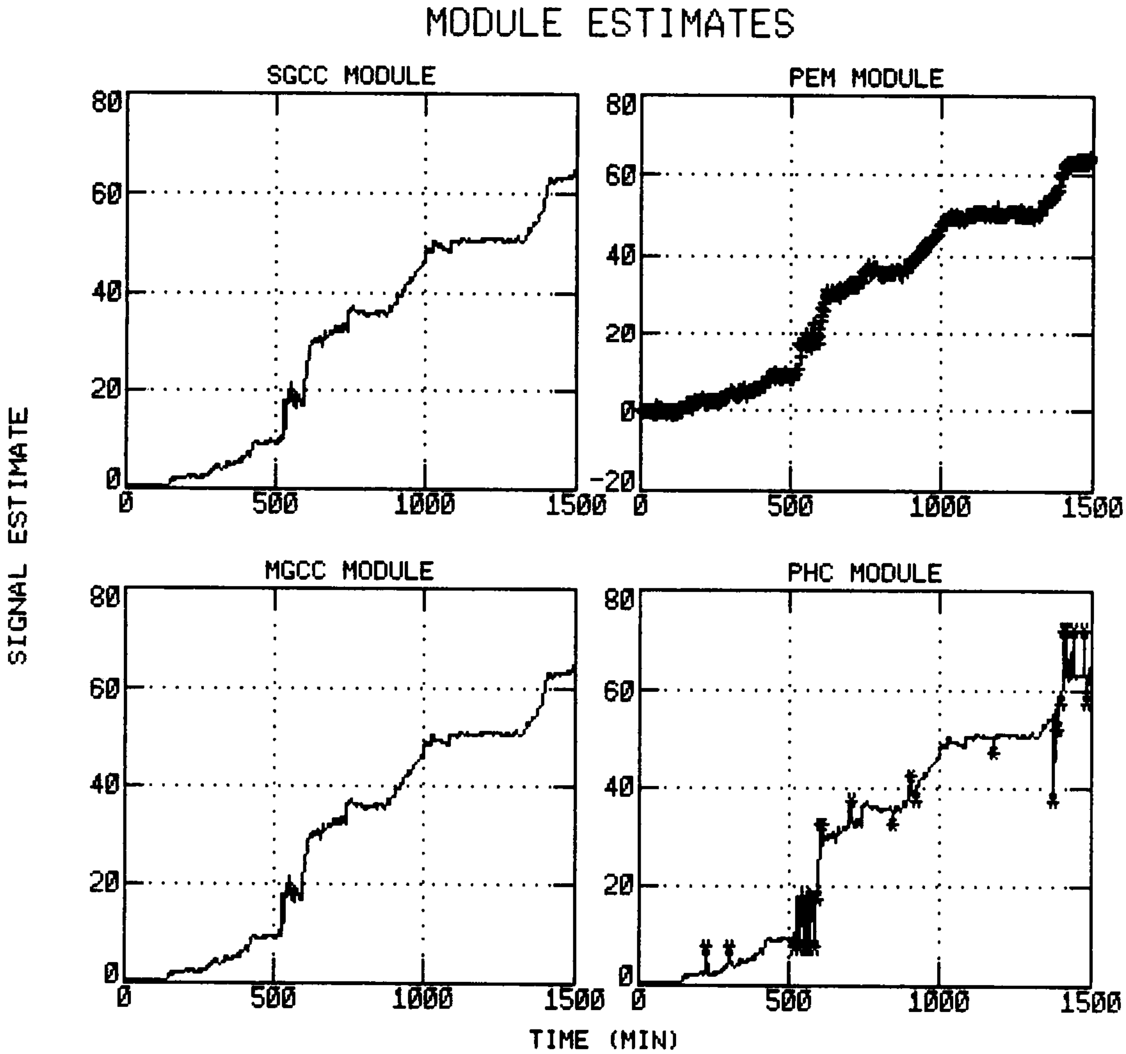

Figure 6.25. PWR Power Estimates.

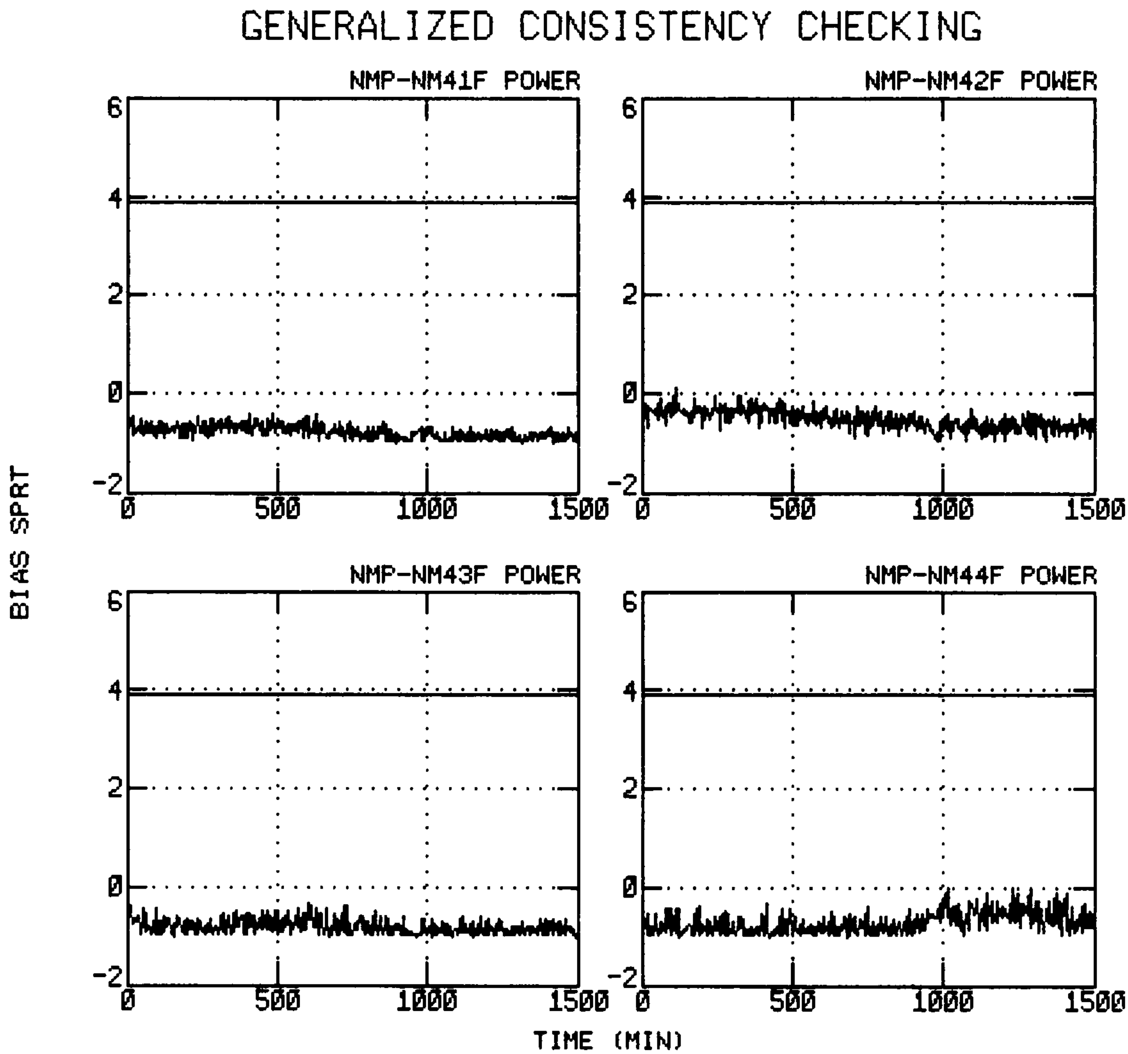

Figure 6.26. SGCC Bias SPRT Results for PWR Power Signals.

any time. The APDF symmetry results from the BND module are not, however, as encouraging as shown in Figure 6.27. The transient behavior of the power signal has resulted in a skewed (non-symmetric) APDF which incorrectly indicates the presence of bias anomaly. In contrast, the APDF for a steady-state steam flow signal is shown in Figure 6.28. The SE conclusions were shown in Figure 6.6.

6.3.3 Biased RCS Flow Signal

Recall the RCS flow signal group presented in the example of Section 6.2.3 and Figure 6.12. One signal was biased with respect to its two redundants. The SGCC bias SPRT results are given in Figure 6.29. The results for the two consistent signals are constantly below the threshold while the biased signal (RCS-F435) always exceeds the threshold. This is the basis for differentiating between the signal level (consistency) versus the bias/drift failure. The level failure is more of a momentary (short-term) nature while the bias/drift failure is observed over a long-term. The SE results were previously given in Figure 6.16.

6.3.4 Loss of Signal

Because the bias detection of the SGCC is a long-term result, an example of the bias SPRT in the loss of signal event is presented. Consider the pressurizer level signals

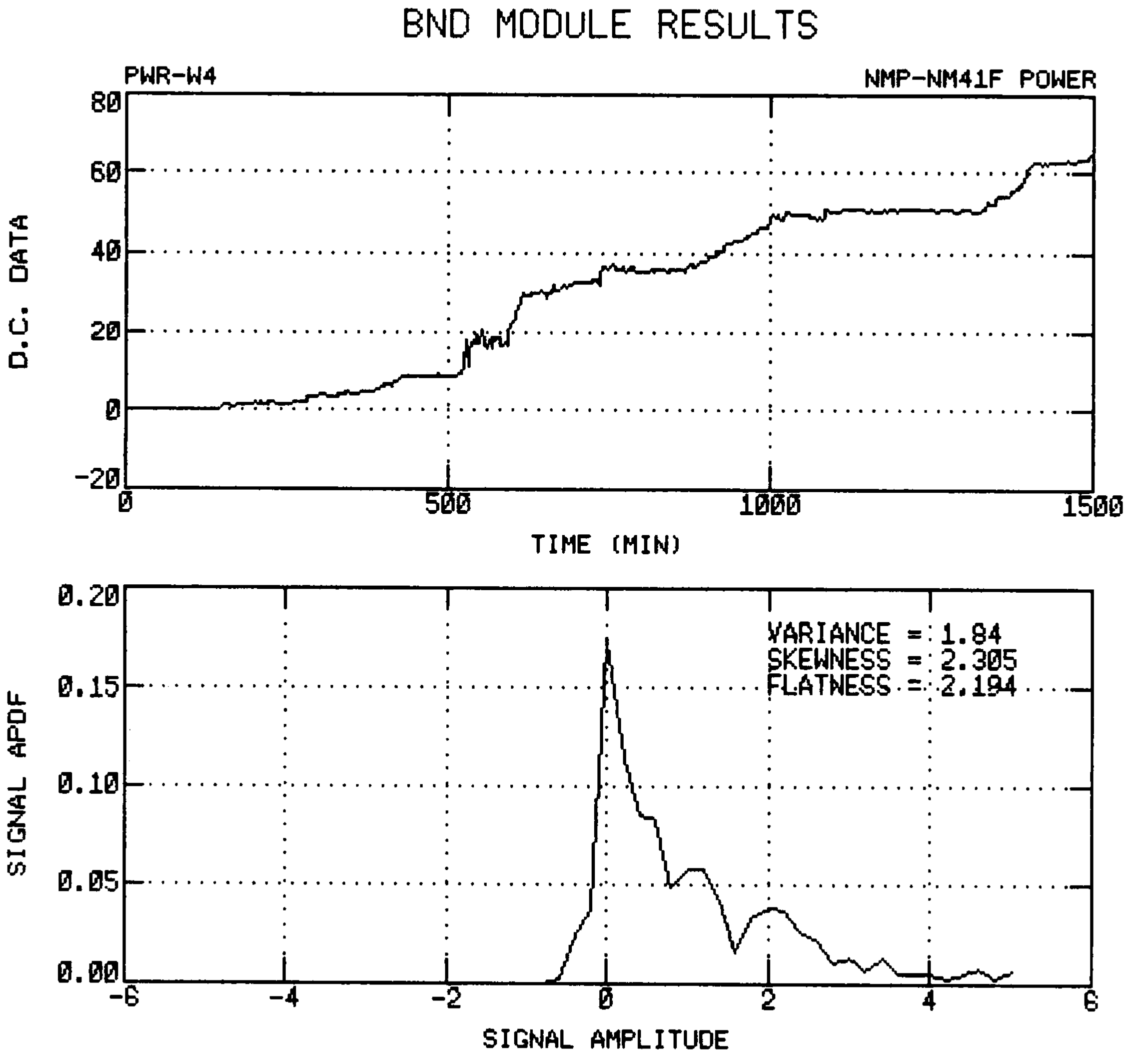

Figure 6.27. BND APDF for a Ramping Power Signal.

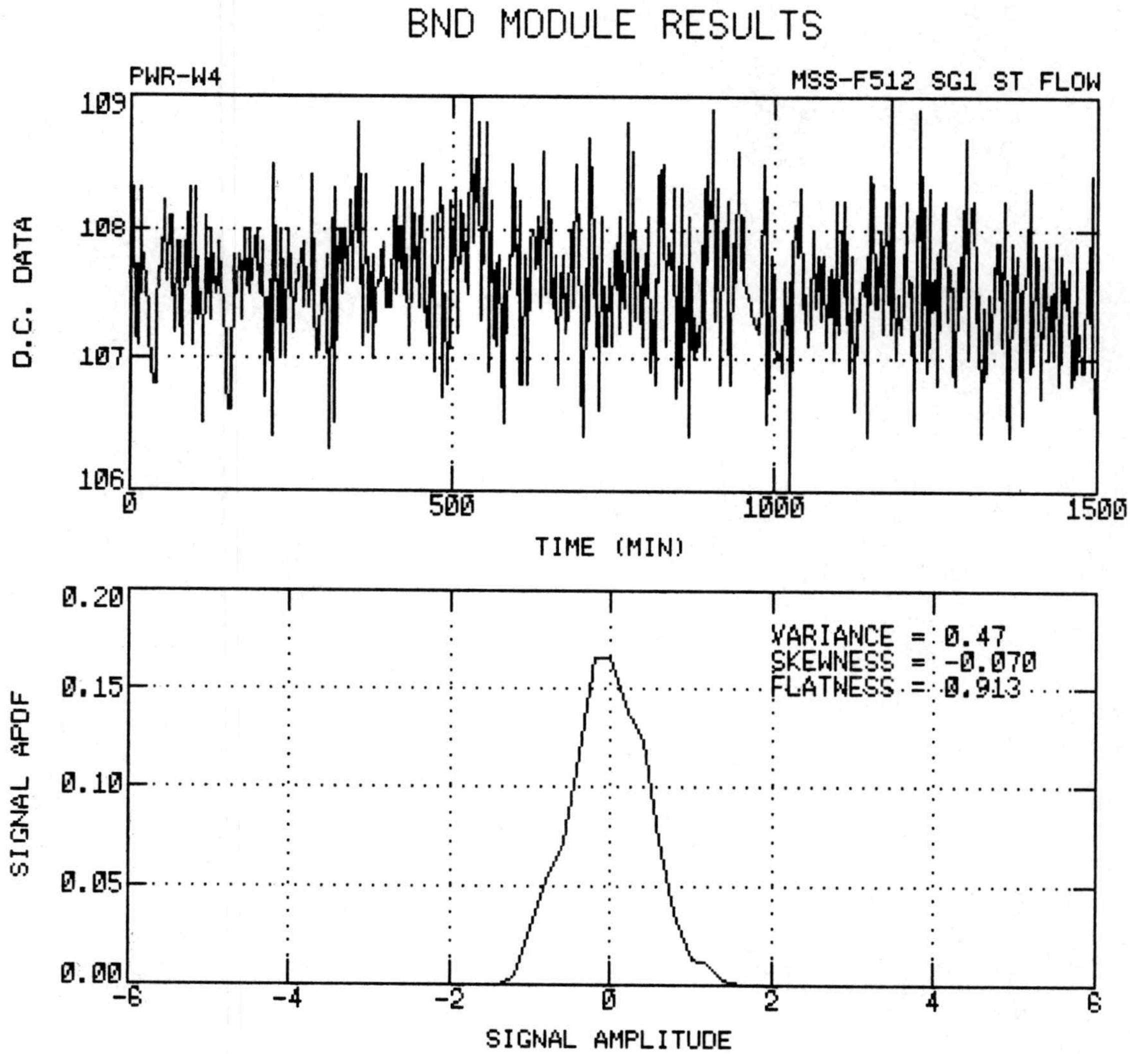

Figure 6.28. BND APDF for a Steady-State Steam Flow Signal.

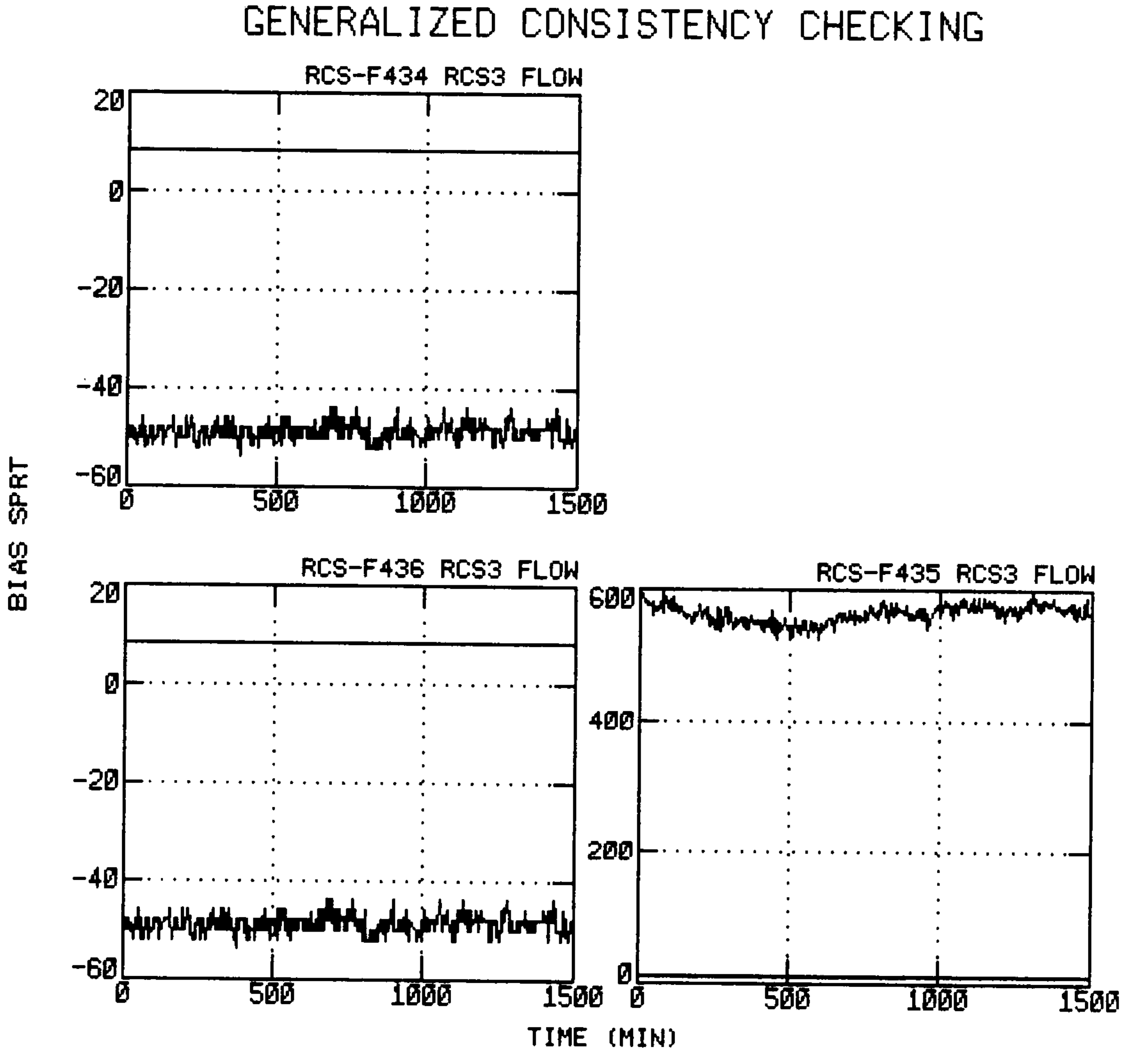

Figure 6.29. SGCC Bias SPRT Results for PWR RCS Flow Signals.

of Section 6.2.4 and Figure 6.17. The MGCC and PEM estimates of Figure 6.21 have already shown their ability to resolve the loss of signal problem correctly. The SGCC bias SPRT results for the pressurizer level signals are given in Figure 6.30. What is interesting to note is that one signal initially appears biased and another is fluctuating about the bias threshold value. However given enough time, the SPRT values drop significantly below the threshold. This demonstrates the need to monitor the signal over a sufficiently long time period before making a declaration of bias failure. The BND APDF results were unacceptable due to the transient nature of the pressurizer level during the data sampling.

6.4 Noise Failure Detection

Noise failure is detectable by the SGCC and BND modules. Acceptable noise levels are quantities which are not generally available. The normal noise values may be learned off-line by observing the process data.

It has been suggested that the pulse and jump detection by the BND module will be sub-optimal in a digital versus analog implementation. While this is probably true for detecting high frequency spikes caused by the electronics, it is shown that the BND can identify spikes found in digital data.

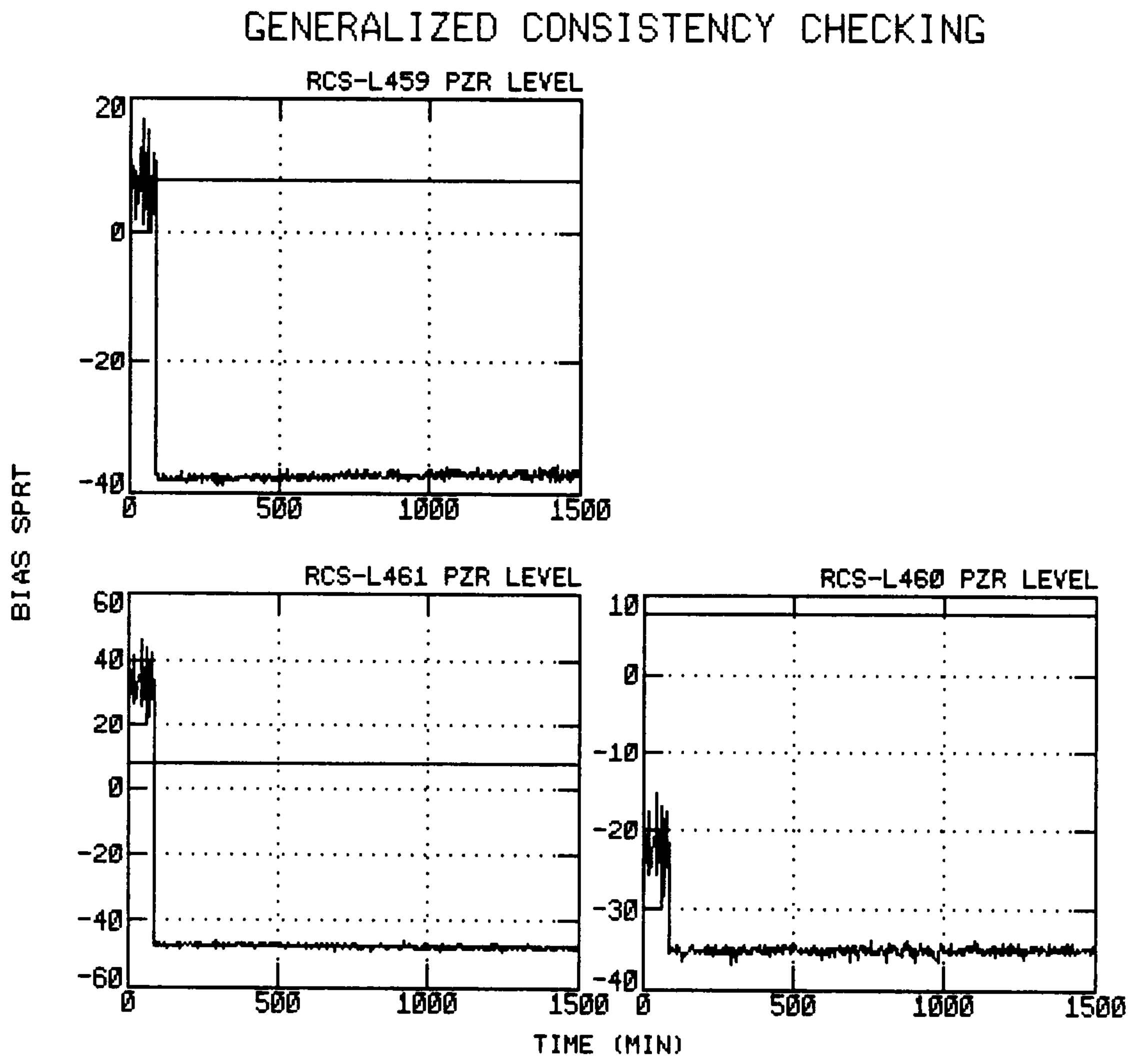

Figure 6.30. SGCC Bias SPRT Results for PWR Pressurizer Level Signals.

6.4.1 Transient Power Signals

The ramping power signals of Figure 6.2 (as any transient signals) have the tendency to produce inaccurate noise analysis results. The SGCC module's noise SPRT results are given in Figure 6.31. For comparison purposes, examples of the SGCC noise SPRT results for steady-state RCS flow signals are shown in Figure 6.32. The points at which the noise SPRT degradation threshold is exceeded may be matched to those time instants when the power signal rises dramatically. The BND module similarly misidentifies the power ramp as a jump anomaly (Figure 6.33) as is expected. Also for example, a BND CUSUM result with no anomaly detection is shown in Figure 6.34 for a steam flow signal. Thus steady-state process conditions are required for acceptable analysis of the signal noise. The final signal status from the SE was shown in Figure 6.6.

6.4.2 Noise Anomaly Detection

Lastly, noise anomaly detection in the cold leg temperature signals is presented. Figure 6.35 shows a cold leg temperature signal with the BND CUSUM results which indicate detection of two pulses in the signal. Figure 6.36 likewise shows another cold leg temperature signal in which both pulses and jumps were identified. The final anomaly indicated in this case is one of pulse anomaly. The SGCC noise SPRT results of Figure 6.37 correctly exceed the

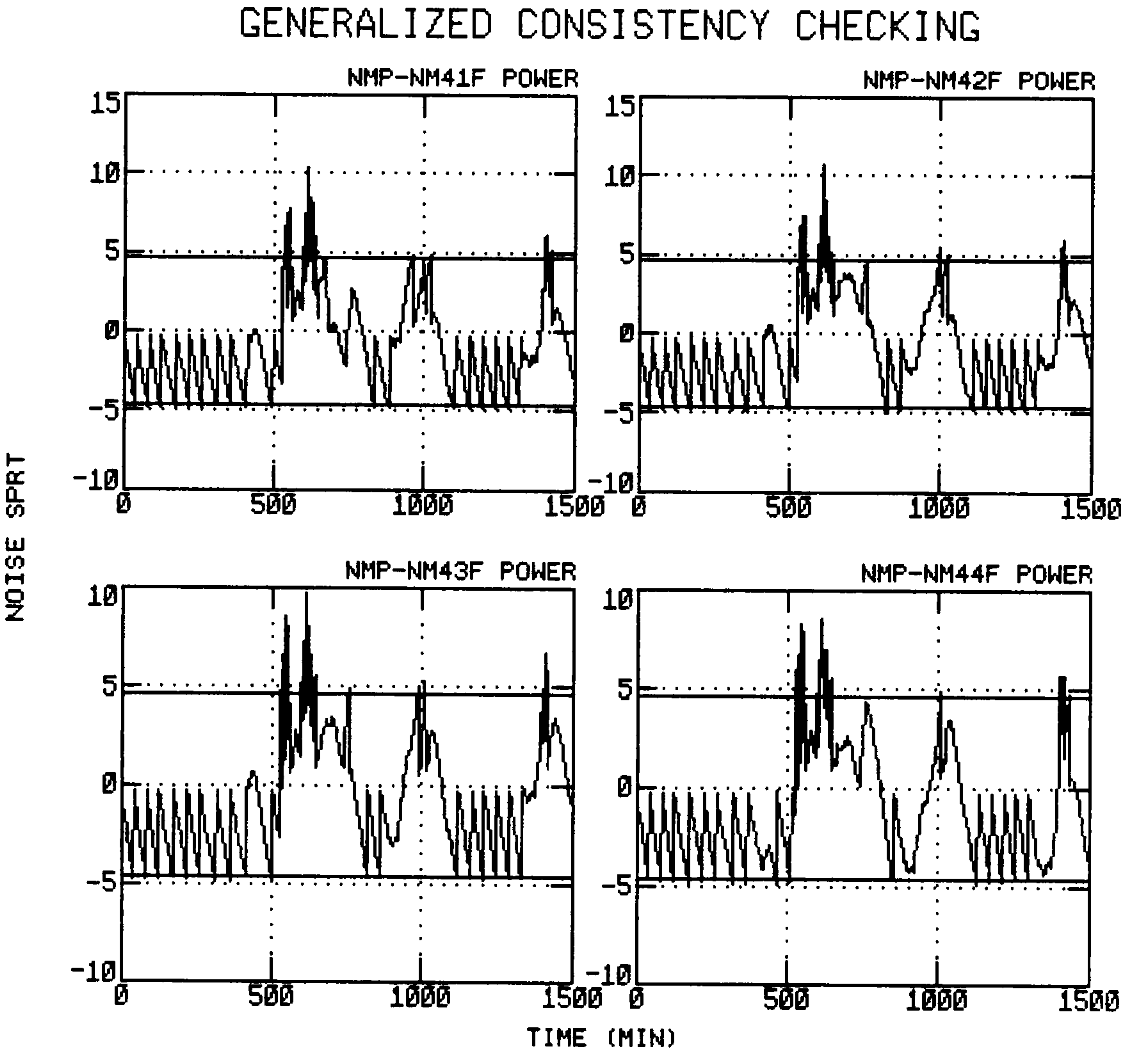

Figure 6.31. SGCC Noise SPRT Results for PWR Power Signals.

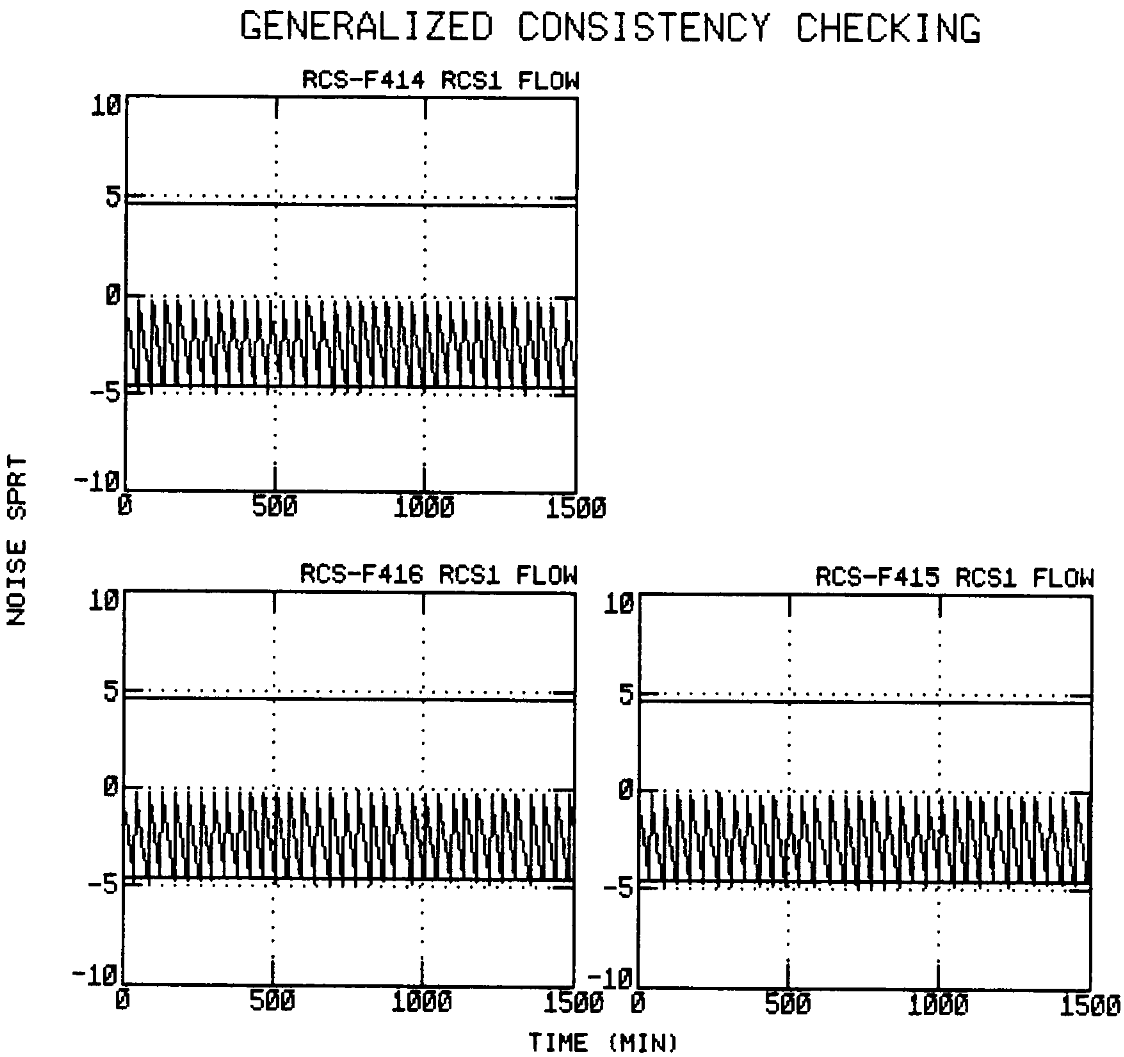

Figure 6.32. SGCC Noise SPRT Results for PWR RCS Flow Signals.

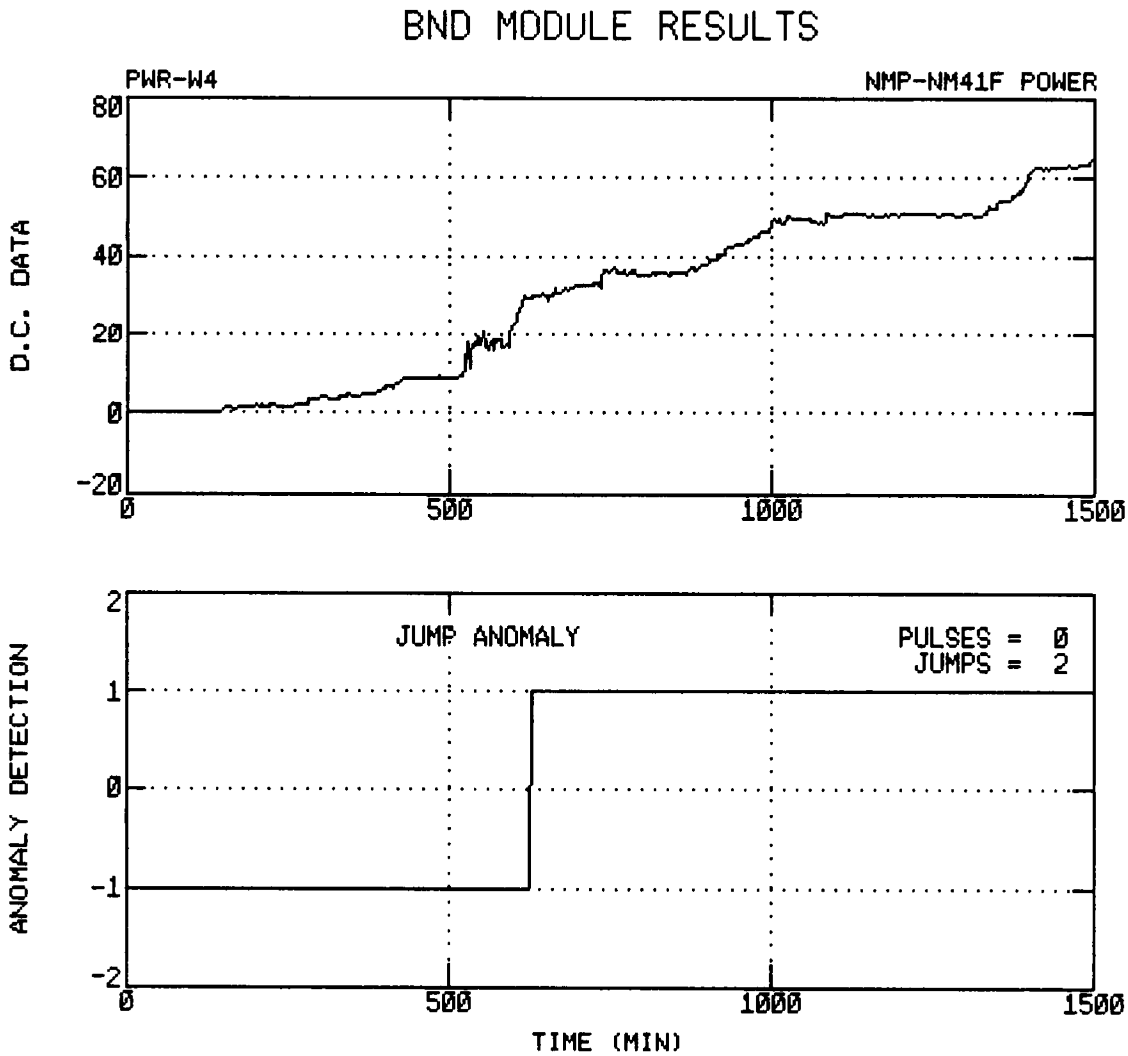

Figure 6.33. Misidentification of Jump Anomaly by BND Module During Transient Power Signal.

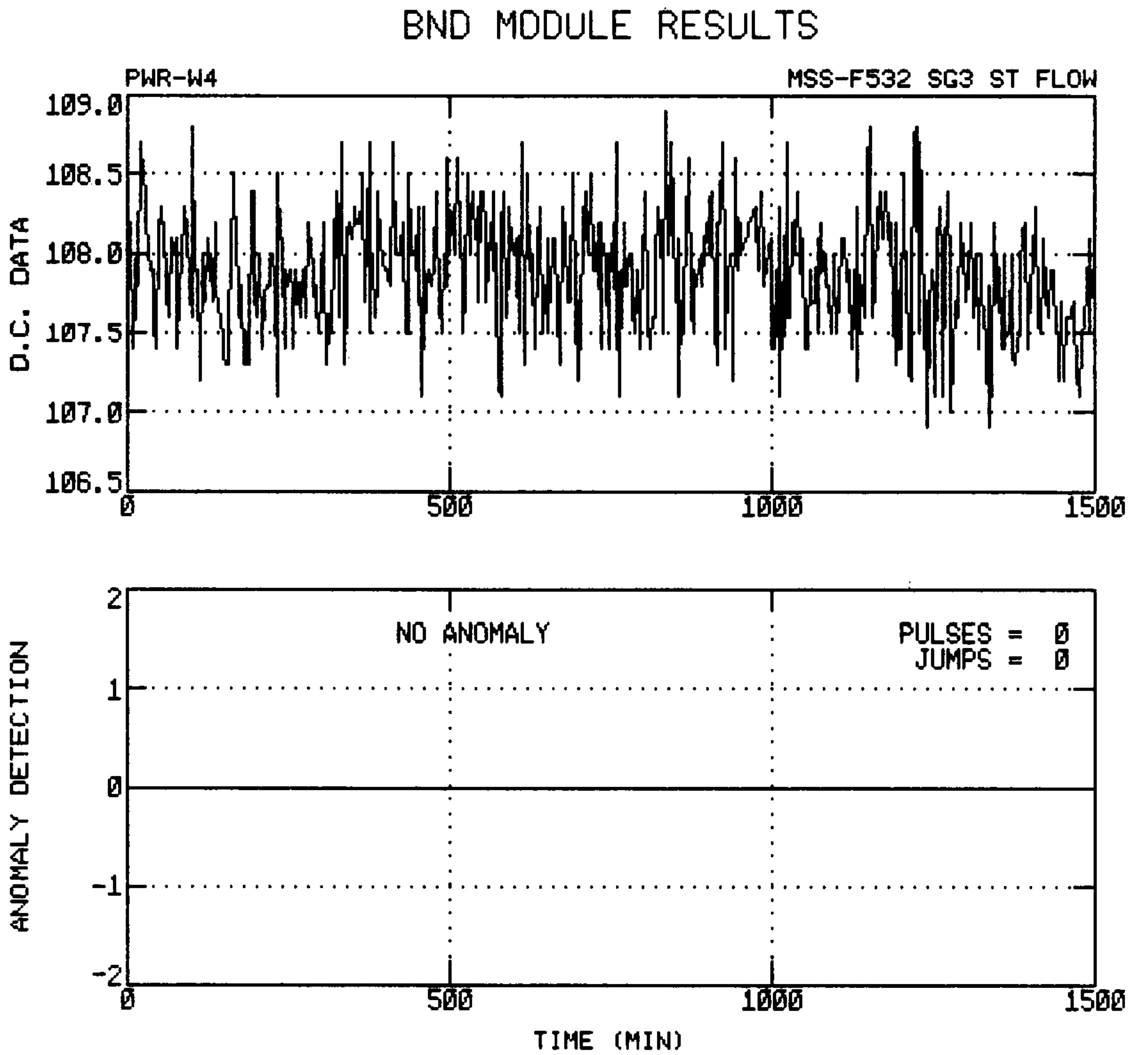

Figure 6.34. BND CUSUM Results for No Anomaly Detected in a PWR Steam Flow Signal.

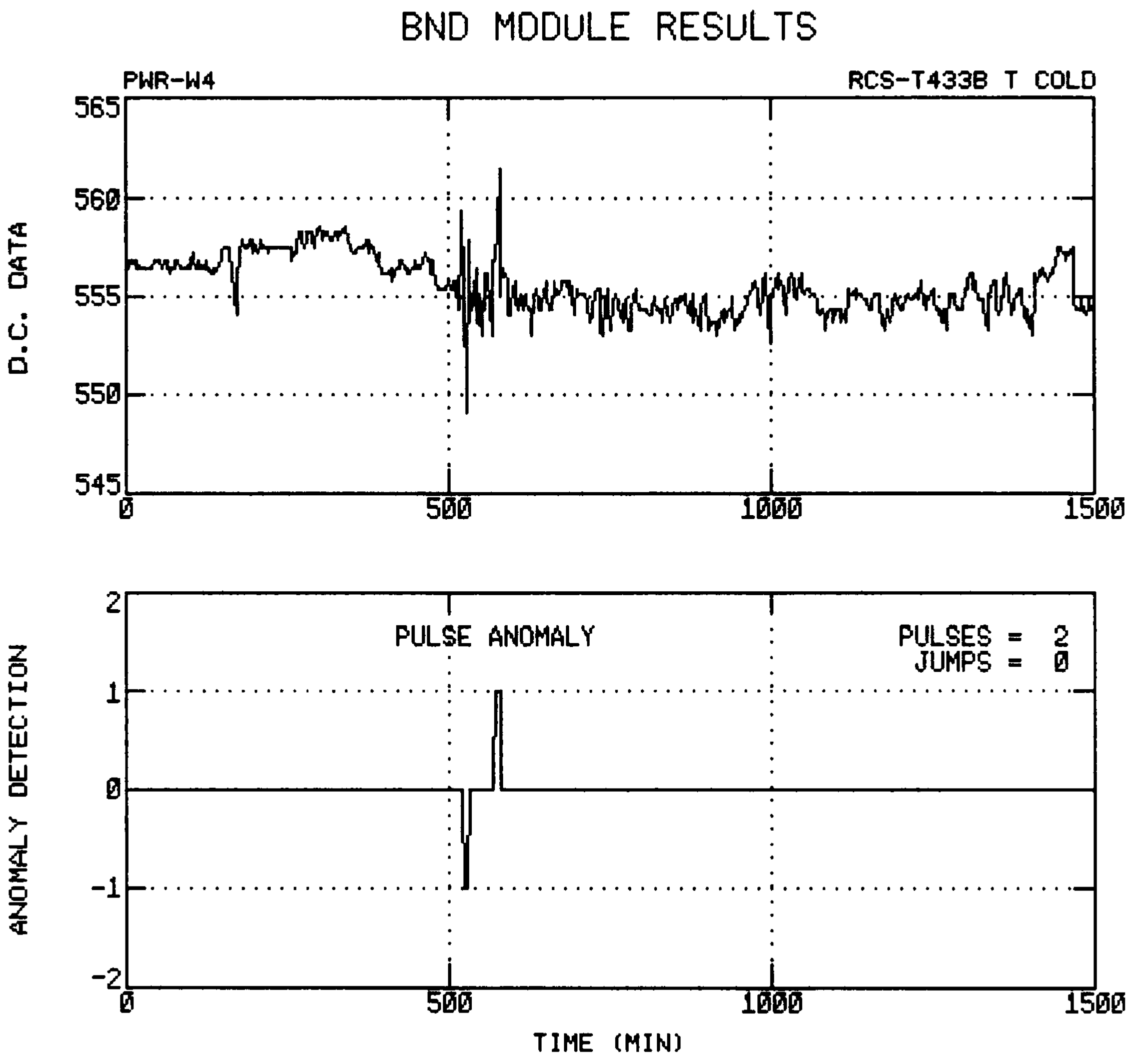

Figure 6.35. Pulse Anomaly Detection by BND CUSUM in a PWR Cold Leg Temperature Signal.

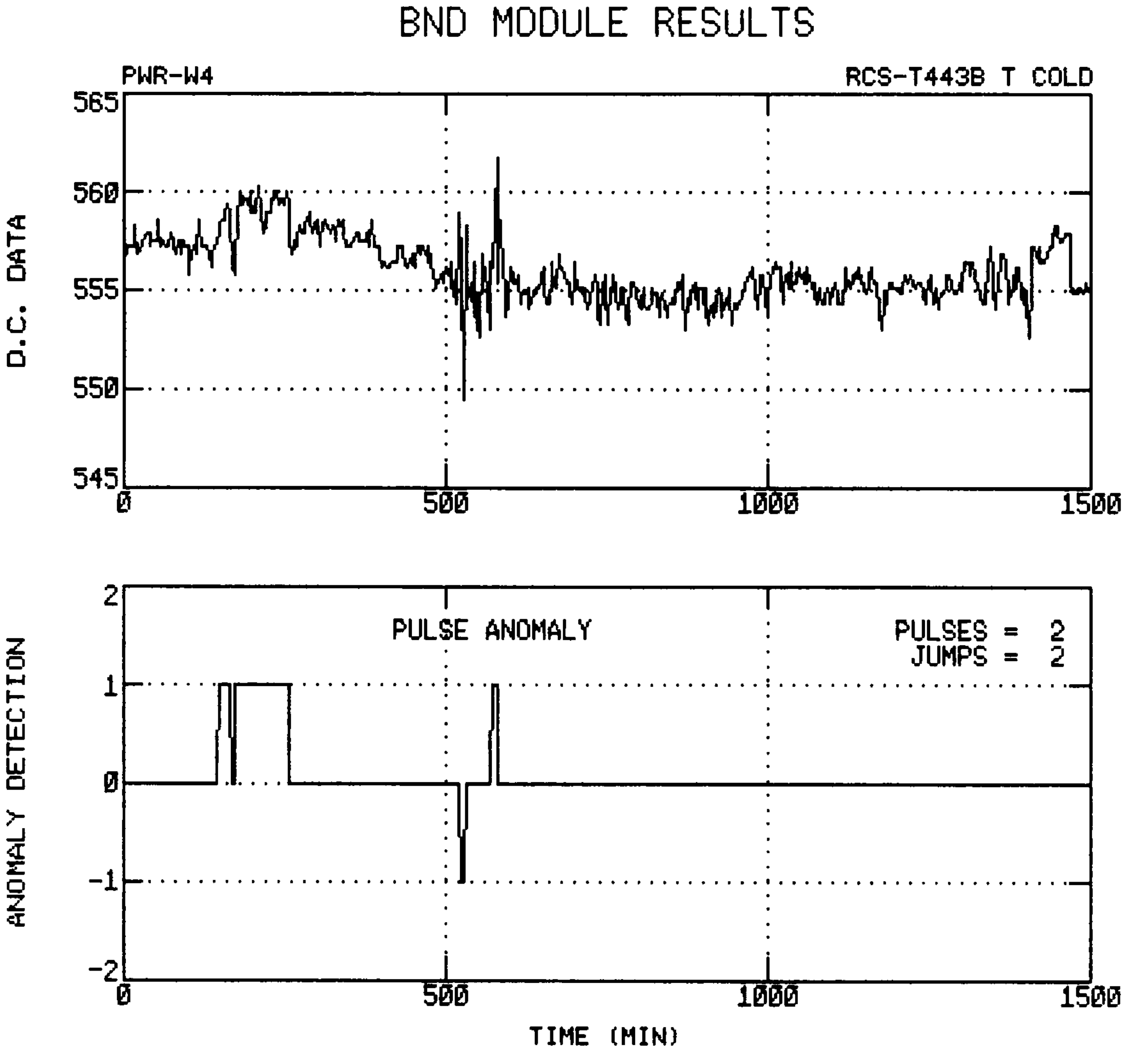

Figure 6.36. Pulse and Jump Anomaly Detection by BND CUSUM in a PWR Cold Leg Temperature Signal.

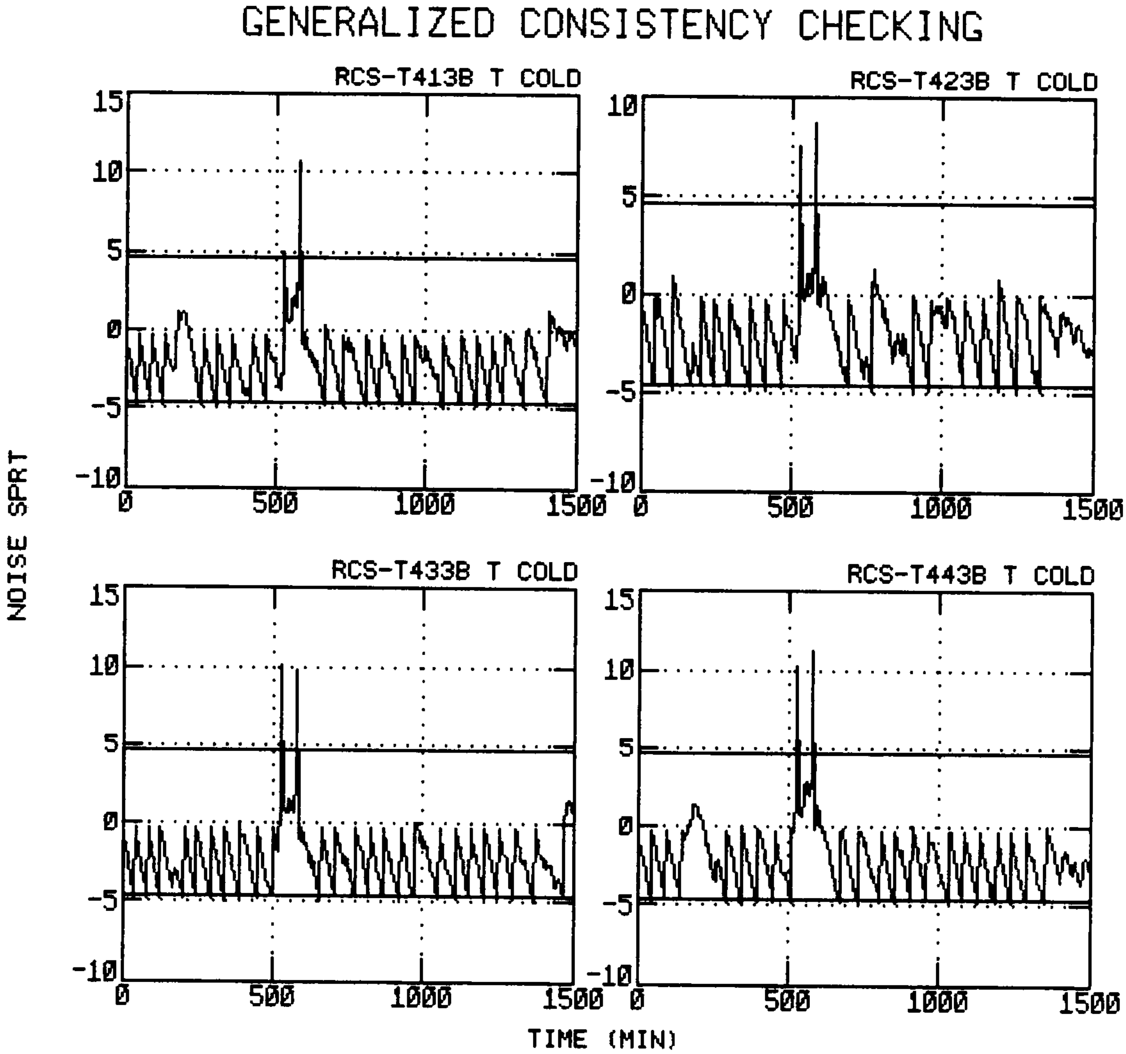

Figure 6.37. SGCC Noise SPRT Results for PWR Cold Leg Temperature Signals.

degradation threshold at these locations of spikes in the data.

6.5 Time Response Failure Detection

Both the UAR and BND modules report on the time response failure mode. Unfortunately both methods require noise data as input and as stated previously, this type of data was not available and had to be artificially generated. More importantly, however, the sampling interval for this data was three minutes (0.0056 Hz) which is much too slow to identify the signal time constants. The time constants for temperature sensors are of the order of 1 to 10 seconds (break frequency: 0.1 to 1 Hz) and less than 1 second for pressure sensors (break frequency: 1 to 10 Hz).

Nonetheless, some results from the UAR module are presented to familiarize the reader with the type of results generated by this module. An example of the UAR computed autocorrelation, and estimation of the power spectral density (PSD) and step response for a RCS flow signal (RCS-F416) is given in Figure 6.38. Note that the frequency range is 10^{-5} to 2.8×10^{-3} Hz which is too low for proper signal analysis. The indicated time constant is 10.8 minutes, well beyond any acceptable (or believable) value. The UAR results for a steam pressure signal are given in Figure 6.39.

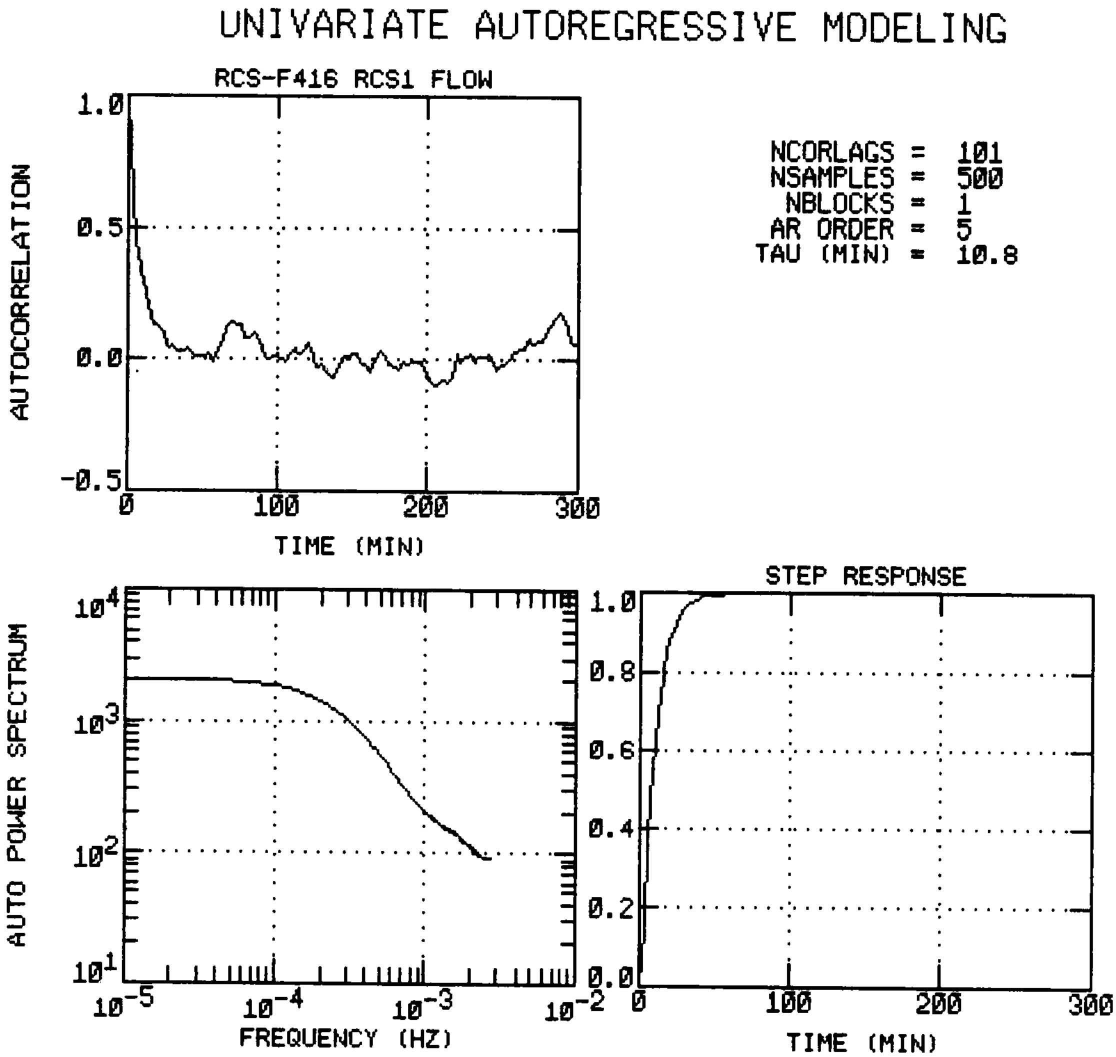

Figure 6.38. UAR Computed Autocorrelation, and Estimation of PSD and Step Response for a RCS Flow Signal.

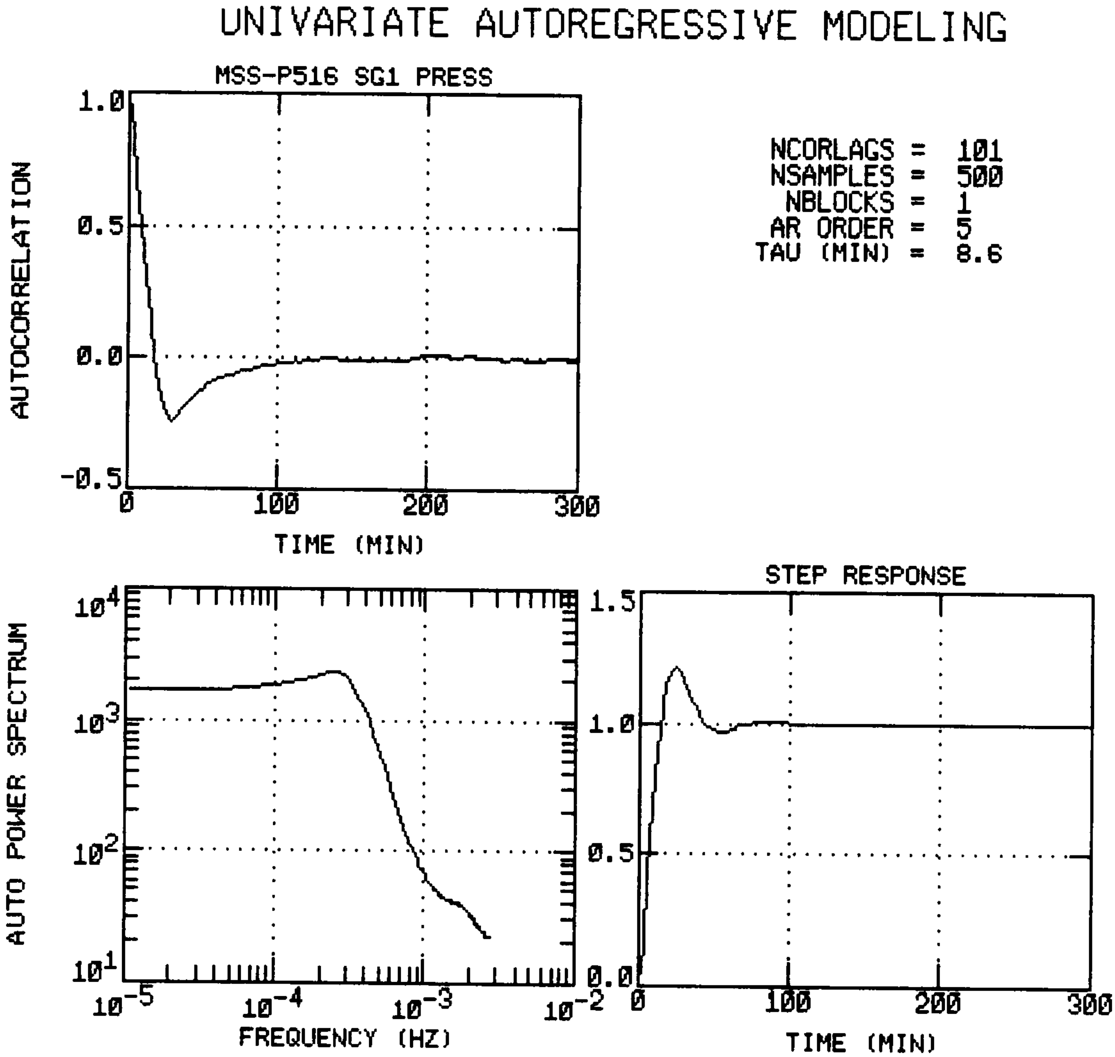

Figure 6.39. UAR Computed Autocorrelation, and Estimation of PSD and Step Response for a Steam Pressure Signal.

The results were presented above to show the available results from the UAR module. But it was demonstrated that the available data were inappropriate. In this case, the UAR (or BND) module could easily compare the sampling rate versus a nominal time constant to identify whether the available data are acceptable or not and return the data analysis error (IERROR) described in Section 5.1.7.

It has been shown that the modules cannot be used to correctly analyze unacceptable data. However, it is argued that these methods, although unable to make a numerical determination of the time constant, can be used to identify relative changes in the time constant. What is suggested is that if the available data does not cover the correct frequency range, that the techniques be used to learn this "normal" time constant. The "normal" (really a biased) value may possibly be used to detect relative changes in the time constant for some signals.

Lastly, the final results from the System Executive for the time response failure mode are presented. Figures 6.6, 6.16 and 6.24 show these results. The SE final decision is that the time response failure is commonality indeterminate. Commonality was detected in the entire plant (which may indicate that the process is the cause). In this case the commonality was actually caused by the slow data sampling rate. This result shows the effectiveness of the commonality search in identifying the possible cause of a false alarm and avoiding such a false alarm.

6.6 PWR Data Analysis Conclusions

One of the advantages of the PWR data over that of the EBR-II data (to be analyzed in the next section) is its characteristic of having several secondary loops. The possibility of different process conditions in the different loops resulted in some of the techniques being re-written in such a manner as to account for this occurrence. For instance, the hypercube methodology checks each secondary loop independently with those process conditions in the primary system, which are common to all secondary loops (e.g. reactor power).

There were several good examples for the consistency failure detection. The bias/drift detection is intended to be conducted over a longer time period, so more data are required. The methodology has been shown to work, but effective demonstration requires a longer data sampling period. The noise data need to be sampled at a faster rate (higher sampling frequency), however the results have shown that the signal processing techniques do work. The noise analysis techniques (modules) tend to operate improperly, as expected, during transient process conditions. The time response failure detection results were also unacceptable due to the sampling interval, however the basic nature of the results was satisfactorily demonstrated.

Of all the modules, the SGCC had the best track record, although there are certainly cases which can fool this methodology. For instance, the case of the wide-range versus narrow-range steam generator level signals. Although correct observation of no signal failure was made, the variable estimate should have actually been made using only the narrow-range indicators. Additional programming could improve the variable estimate possibly based on a weighted estimate proportional to the various signal tolerance limits.

7. EBR-II DATA ANALYSIS

7.1 Introduction

This section presents results of the comprehensive signal validation system (SVS) applied to operational data from the Experimental Breeder Reactor II (EBR-II) plant. A short description and schematic of the plant, and a list of the available signals and their tolerances are given in Appendix B. Results from each module showing examples of both valid and anomalous signals are presented along with the System Executive's (SE) final indication of signal status. Recall that data with signal failure are not routinely available and thus some modules may not detect failure of any type. Also, most of the noise analysis methodologies have suboptimal results since the "noise" data were artificially generated by digitally filtering the d.c. data.

Some of the SVS results for the EBR-II data are similar to those of the PWR data and will not be repeated. There were instances of momentary signal loss, spikes and other phenomena previously observed in the PWR data. This section shows examples of new anomalies.

The advantage of the PWR data was its abundance of redundant signals. Some EBR-II signals are not truly redundant. For example the evaporator (EV) steam outlet temperature signals are actually taken at the outlet of the seven individual evaporators. This type of redundancy is referred to here as "pseudo redundancy." Advantages of the EBR-II data were the greater number of data signals and data samples as well as the faster sampling rate for noise analysis purposes (response time monitoring). Most of the EBR-II signals were temperature measurements whereas the PWR data had a mixture of temperature, pressure, level and flow indicators.

The process (plant) schematic used as the top level display by the System Executive for EBR-II is shown in Figure 7.1. The validated process conditions are displayed on the schematic along with an indication as to the validity of the signal group.

7.2 Consistency Failure Detection

The modules capable of reporting consistency (signal level) failure results include SGCC, MGCC and PHC. The consistency checking algorithms found several cases of signal anomaly. The techniques were shown to work well even in changing process (transient) situations.

The consistency checking algorithms are systematic methods of checking for inconsistencies among redundant measurements of a single process variable. A pairwise comparison of the measurements is made based on the individual signal tolerances, and faulty signals are excluded from a best estimate of the process variable.

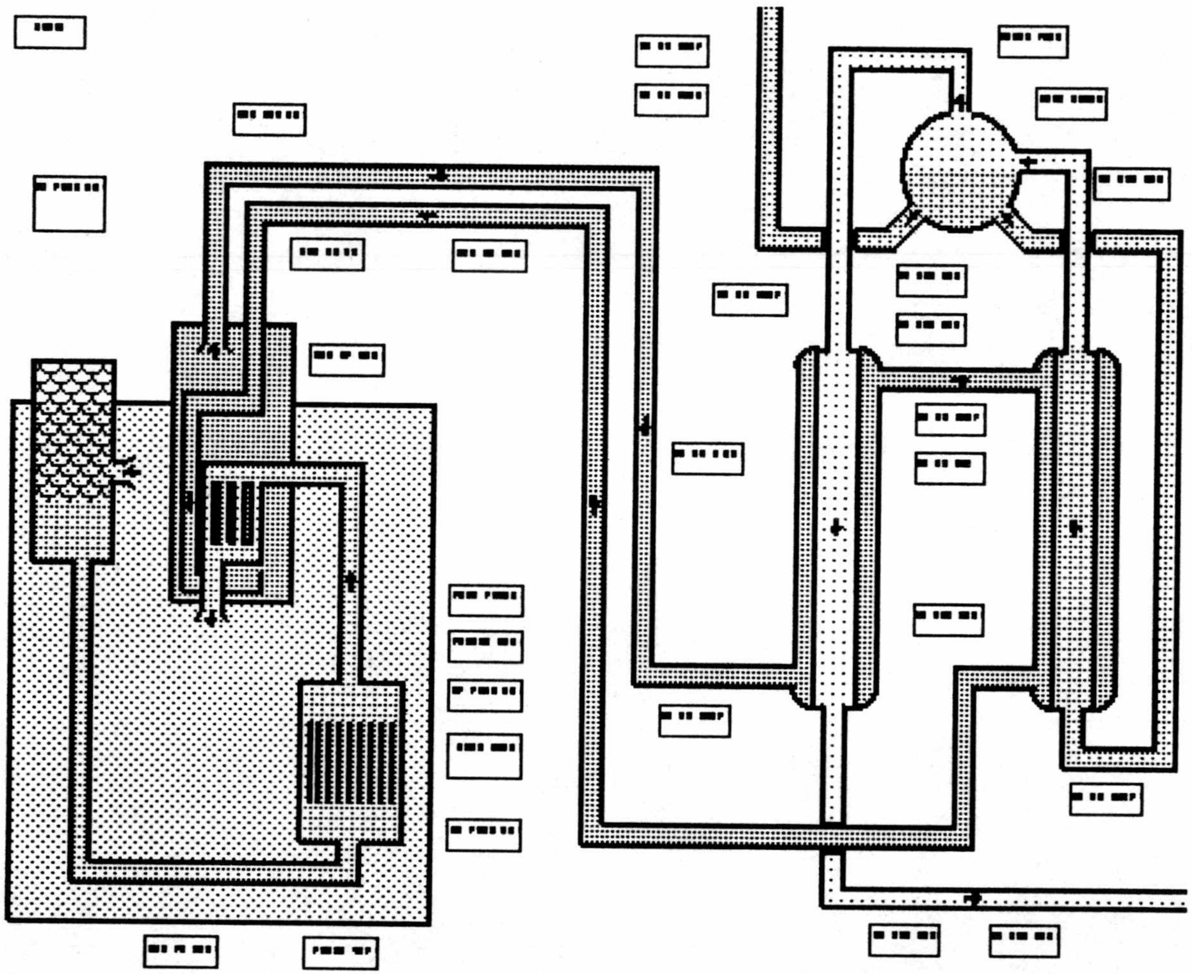

Figure 7.1. Comprehensive Signal Validation System Process Schematic for EBR-II.

7.2.1 Lack of Redundancy

The availability of only two redundant signals for some process variables played havoc with the SGCC algorithm in a couple of cases. Figure 7.2 shows the pair of intermediate heat exchanger (IHX) secondary inlet temperature signals. The top signal (R2-TC-546AR) is at a normal operating value; the bottom signal (R2-RT-533BB) is at a zero level. This second sensor is known to be bad. The inconsistency indices from the SGCC module are given in Figure 7.3. As can be seen, the good (top) signal is always excluded from the SGCC estimate, while the bottom (bad) signal is incorrectly used to compute the variable estimate. The reason for this is that once the SGCC finds the two signals to be inconsistent, a further comparison is made between the two signals and a past estimate. Because the past estimate is initially set to zero, the second signal agrees with the past estimate and is assumed correct. Had the catastrophic failure occurred after any sampling time at all, a correct conclusion would have been reached by the SGCC module. The significance of this example is not the misidentification by the SGCC module but the need for three or more redundant signals to test for inconsistency.

The MGCC inconsistency indices appear in Figure 7.4. The MGCC module correctly identifies the second signal as faulty illustrating the usefulness of the empirical model. The empirical model inputs are evaporator sodium outlet

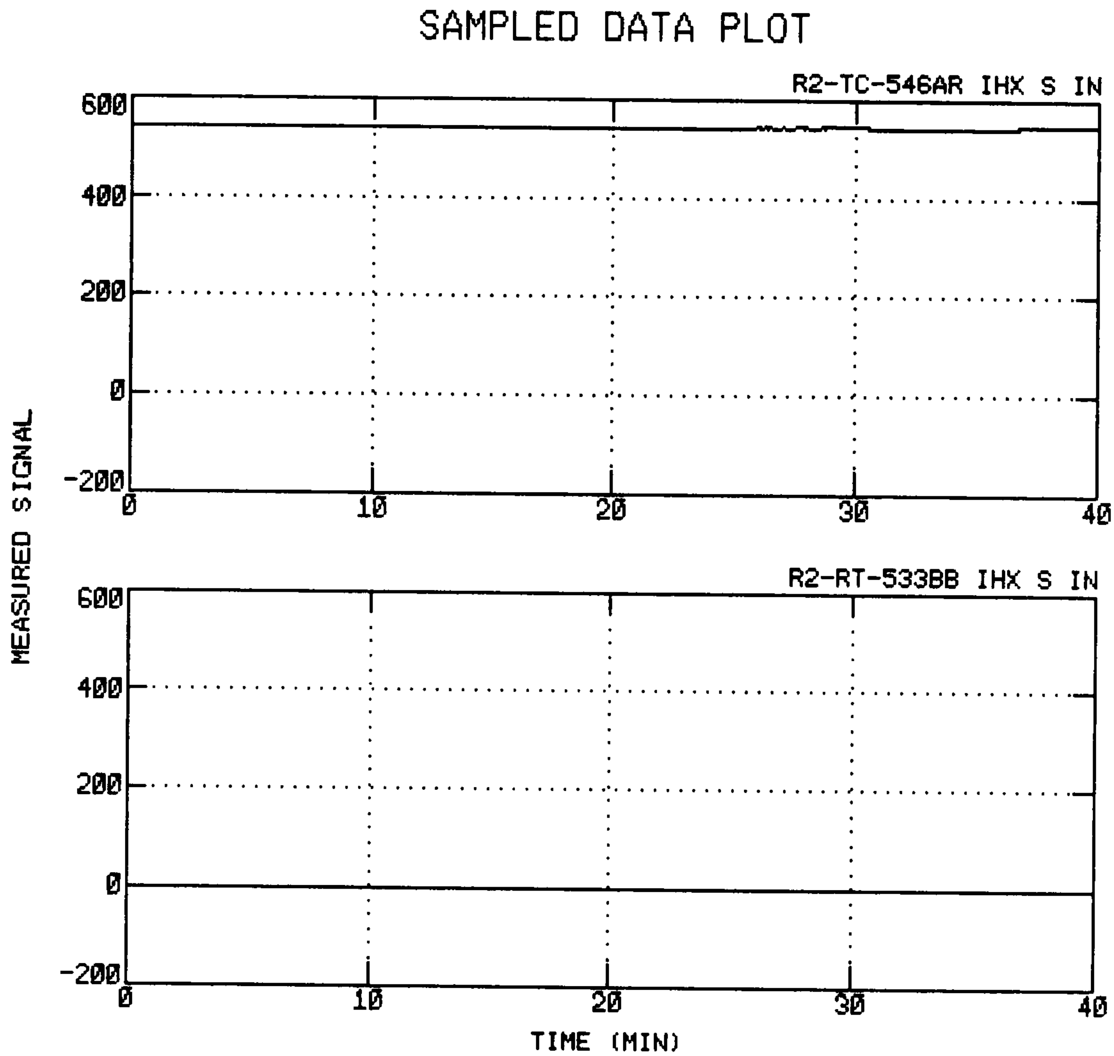

Figure 7.2. Measured Data for the IHX Secondary Inlet Temperature Signals.

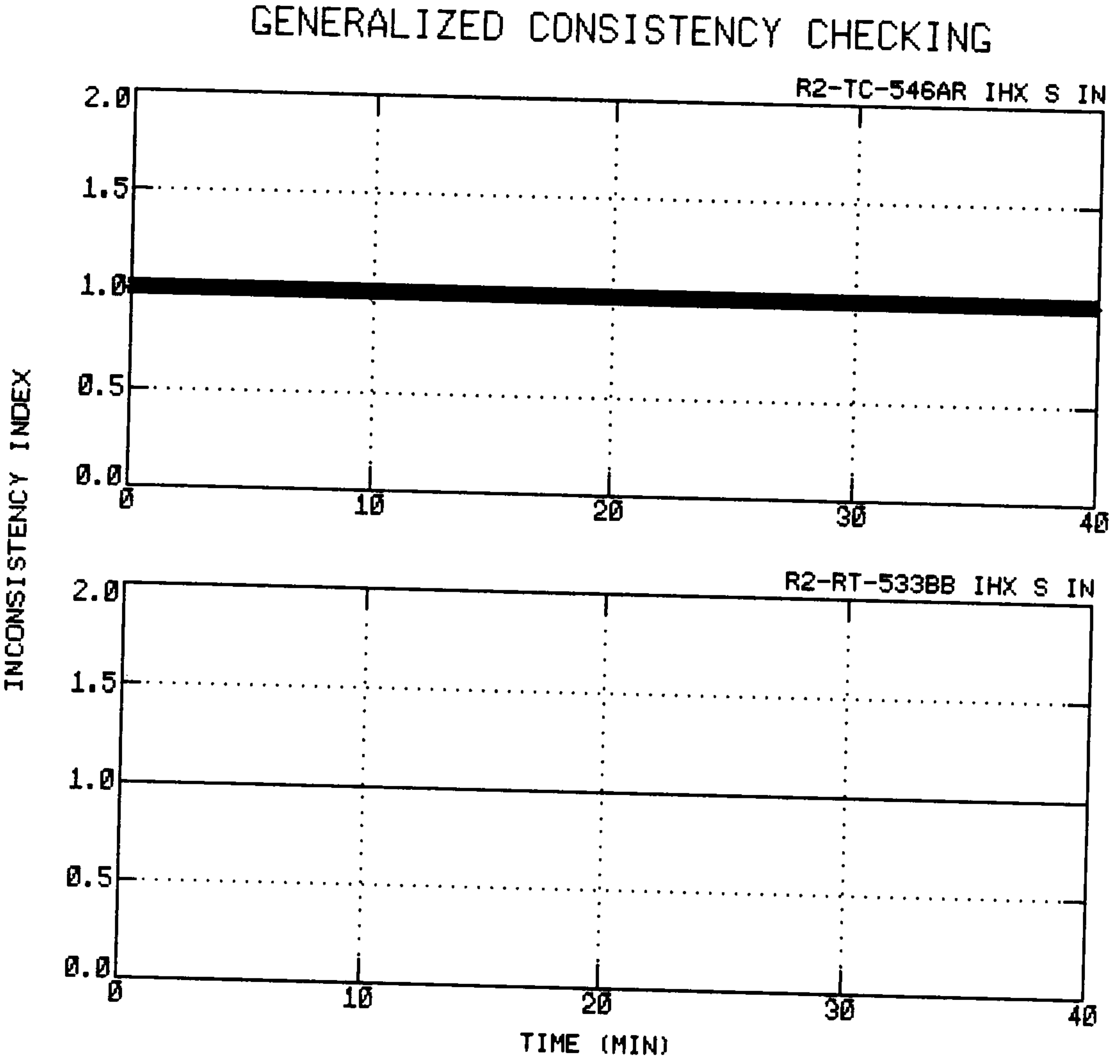

Figure 7.3. SGCC Inconsistency Indices for the IHX Secondary Inlet Temperature Signals.

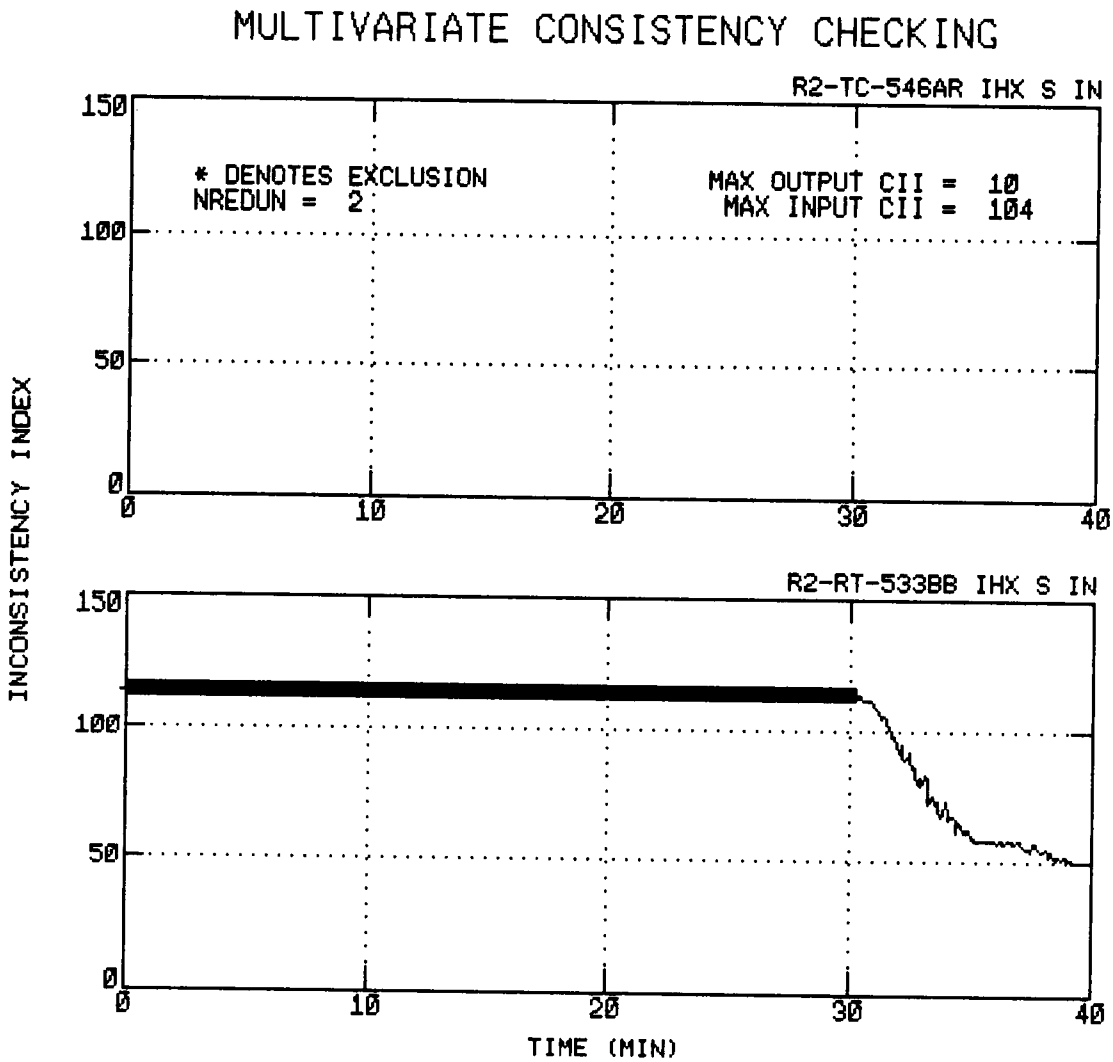

Figure 7.4. MGCC Inconsistency Indices for the IHX Secondary Inlet Temperature Signals.

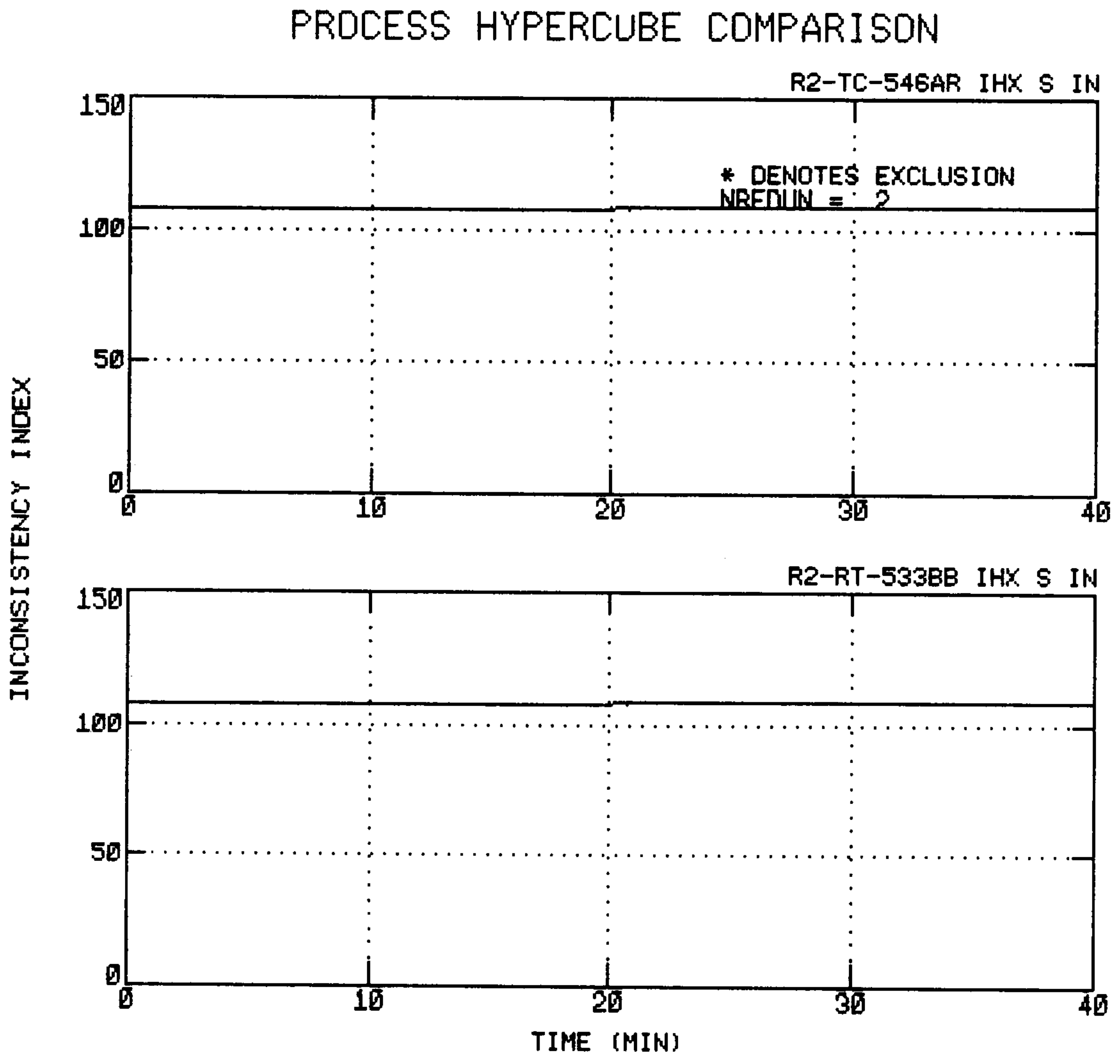

Figure 7.5. PHC Inconsistency Indices for the IHX Secondary Inlet Temperature Signals.

temperature and secondary sodium flow. The PHC inconsistency indices are given in Figure 7.5. The PHC consistency checking scheme is unable to differentiate between the good and bad signal. However, the estimate provided by the PHC is phenomenally better than that of the SGCC module because of the use of the learned process conditions stored in the hypercube. That is, the PHC determined that the variable indication was incorrect (Figure 7.6) and a PHC estimate was subsequently calculated. All the module estimates are shown in Figure 7.7. The SGCC module estimate is incorrect, but the PEM, MGCC and PHC are good.

The final results from the SE are presented in Figure 7.8. The SGCC conclusion is incorrect as discussed above. The MGCC correctly identified the faulty signal. The PHC module results are inconclusive as mentioned above.

7.2.2 Pseudo Redundancy

As mentioned above, one of the drawbacks of the EBR-II data is its lack of redundancy. To compensate for this, "pseudo" redundant signals were combined into a single variable group. For example, there is one evaporator (EV) steam outlet temperature signal located at the exit of each of the seven evaporators. These seven signals were therefore combined into a single "redundant" group. In the event one of the evaporators is isolated, it is entirely probable that faulty indications regarding the signal status

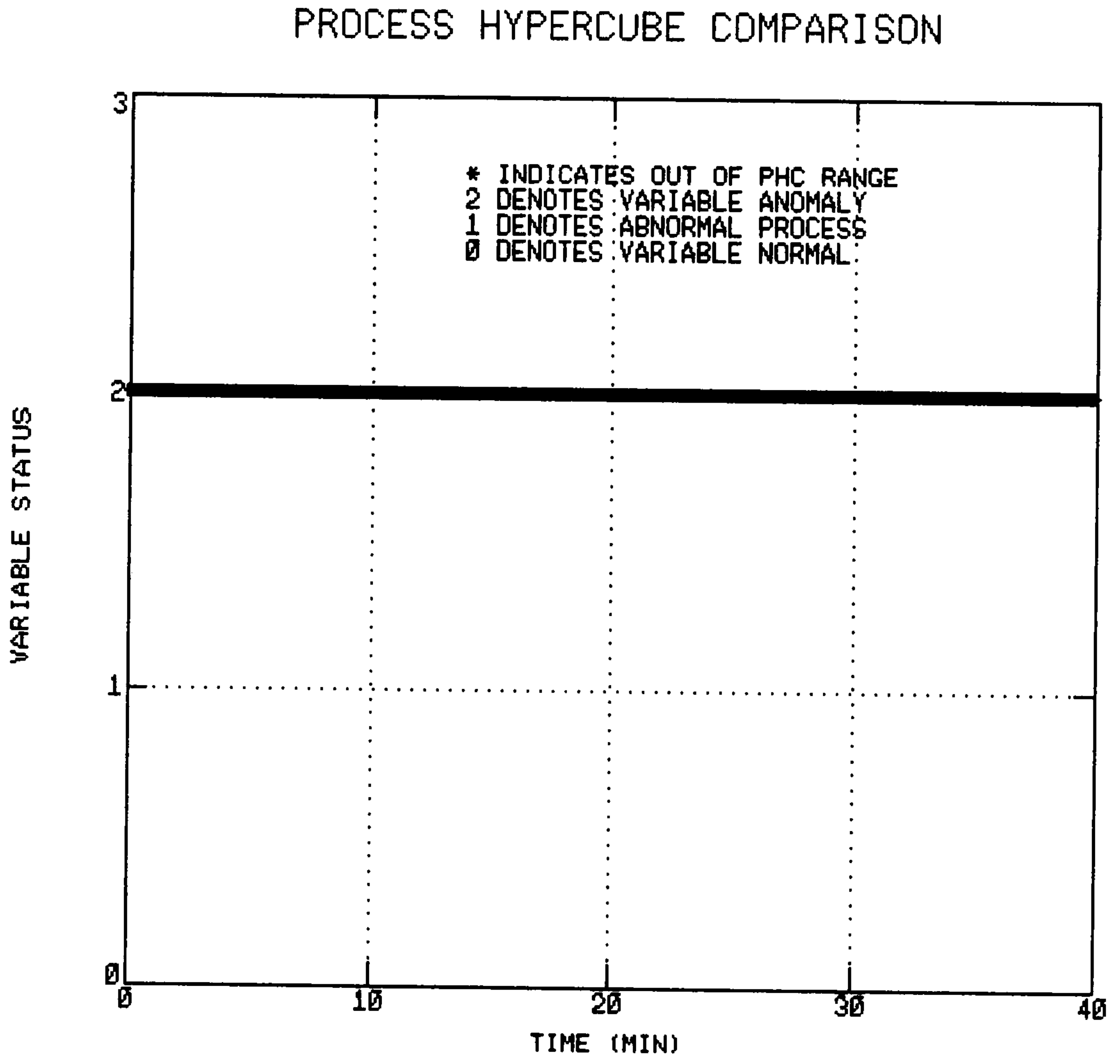

Figure 7.6. PHC Variable Status for the IHX Secondary Inlet Temperature.

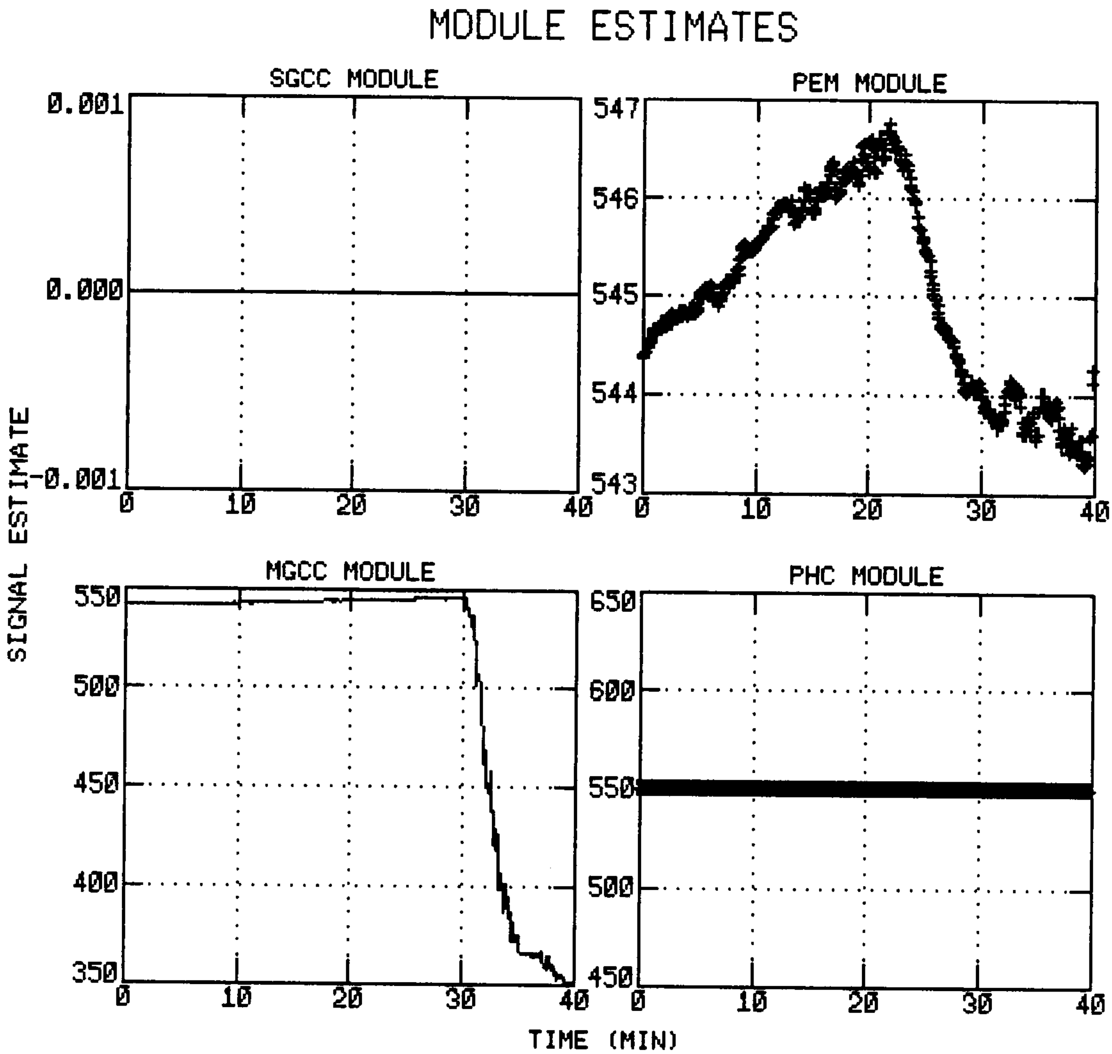

Figure 7.7. IHX Secondary Inlet Temperature Estimates.

```
Results for Sensor R2-TC-546AR IHX S IN, channel # 110.
    Final result indicates signal status is indeterminate.
  Consistency Failure Test indicates signal status is indeterminate.
    SE indicates signal status is indeterminate.
    SGCC indicates signal is ANOMALOUS.
    MGCC indicates signal is valid.
    BND indicates signal is ANOMALOUS.
    PHC indicates signal status is indeterminate.
  Bias/Drift Failure Test indicates signal status is indeterminate.
    SE indicates signal status is indeterminate.
    SGCC indicates signal is ANOMALOUS.
    BND indicates signal is ANOMALOUS.
    PEM indicates signal is valid.
  Response Time Failure Test indicates signal status is COMMONALITY indeterminate.
      Failure commonality has been found in the entire plant (process?).
    SE indicates signal is ANOMALOUS.
    BND indicates signal is ANOMALOUS.
    UAR indicates signal is ANOMALOUS.
  Basic Noise Failure Test indicates signal status is indeterminate.
    SE indicates signal status is indeterminate.
    SGCC indicates signal is valid.
    BND indicates signal is ANOMALOUS.
```

Figure 7.8a. Valid Temperature Signal.

```
Results for Sensor R2-RT-533BB IHX S IN, channel # 111.
    Final result indicates signal status is indeterminate.
  Consistency Failure Test indicates signal status is indeterminate.
    SE indicates signal status is indeterminate.
    SGCC indicates signal is valid.
    MGCC indicates signal is ANOMALOUS.
    BND indicates signal is ANOMALOUS.
    PHC indicates signal status is indeterminate.
  Bias/Drift Failure Test indicates signal status is indeterminate.
    SE indicates signal status is indeterminate.
    SGCC indicates signal is valid.
    BND indicates signal is valid.
    PEM indicates signal is ANOMALOUS.
  Response Time Failure Test indicates signal status is indeterminate.
      Failure commonality has been found in the entire plant (process?).
    SE indicates signal status is indeterminate.
    BND indicates signal is ANOMALOUS.
    UAR indicates signal is valid.
  Basic Noise Failure Test indicates signal is valid.
    SE indicates signal is valid.
    SGCC indicates signal is valid.
    BND indicates signal status is indeterminate.
```

Figure 7.8b. Anomalous Temperature Signal.

Figure 7.8. SE Final Signal Status for IHX Secondary Inlet Temperature Signals.

will be reached by the modules from the inter-signal comparisons.

The measured data for the first and second superheater (SU) sodium inlet temperature signals are shown in Figures 7.9 and 7.10, respectively. The inlet temperatures are at 635°F and 685°F for the two superheaters. The SGCC inconsistency indices for four of the five signals are given in Figure 7.11. Since the temperatures of the superheaters are different, the signals from the first superheater are excluded by the SGCC because they represent a minority (only two of five) redundants in the group. Thus it would be best to separate the superheater signals into two different variable groups in this case, even though the first group will have only two redundant signals in it (there should be a minimum of three signals for each redundant group). The PHC results were similar to the SGCC with the first two signals generally declared faulty. The MGCC model estimates also noted the pattern that the two superheaters should be treated independently.

Another case in which pseudo redundancy did not fare well is for the two superheater (SU) steam inlet temperature signals. The measured data for these two signals are shown in Figure 7.12. In this instance, there is only one signal for each superheater, so that one must use pseudo redundancy or nothing. The SGCC again finds both signals inconsistent and further computes an estimate from the zero valued past

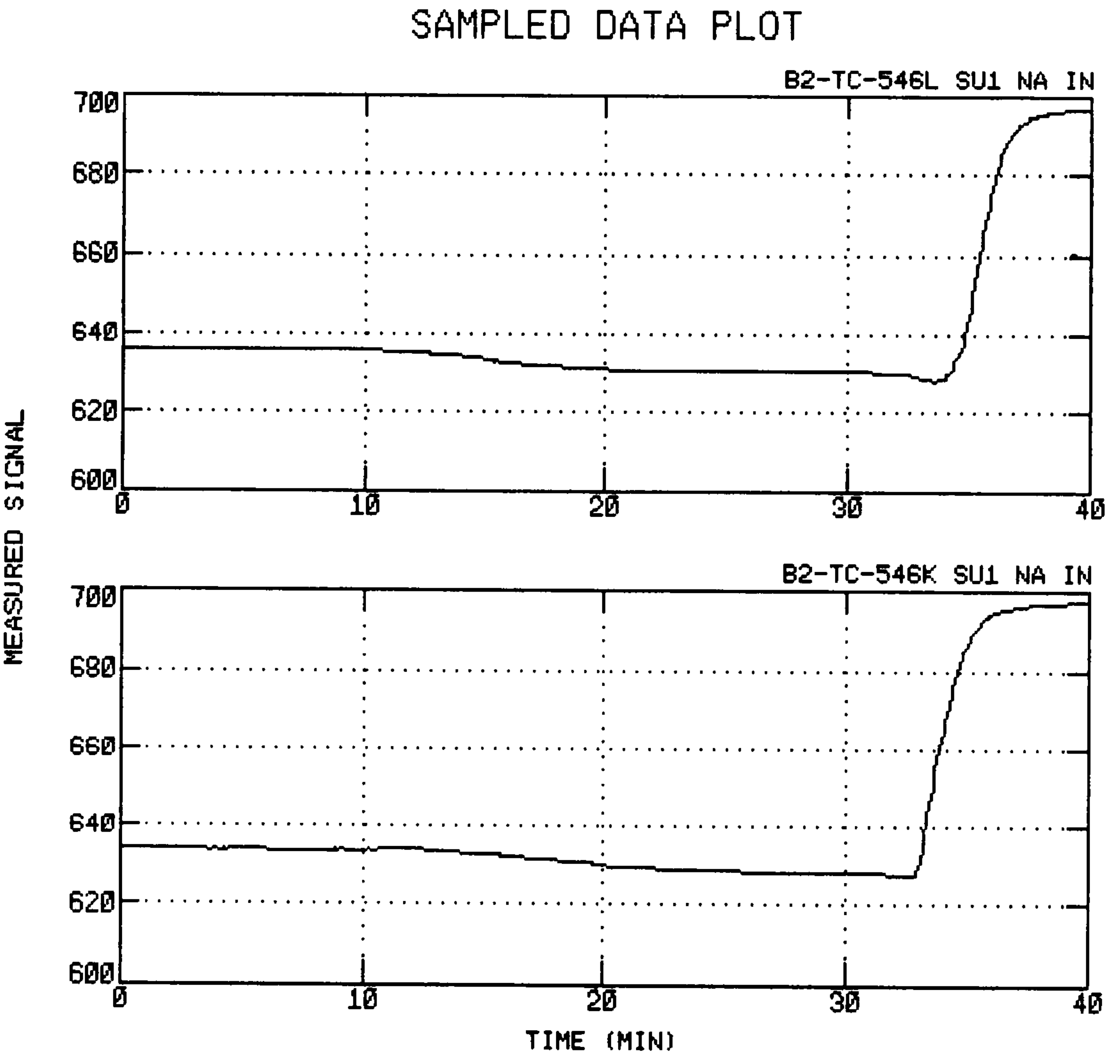

Figure 7.9. Measured Data for the First Superheater Sodium Inlet Temperature Signals.

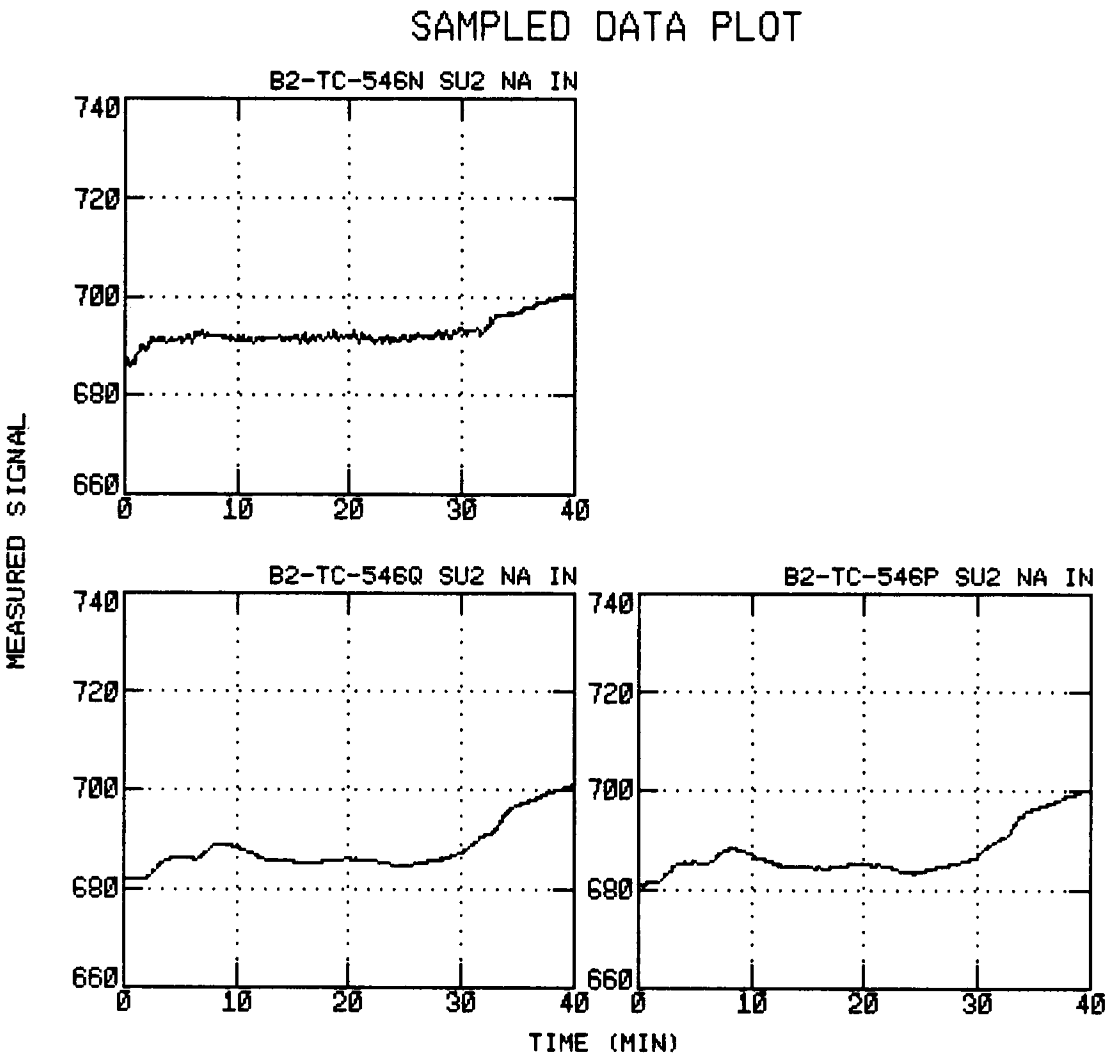

Figure 7.10. Measured Data for the Second Superheater Sodium Inlet Temperature Signals.

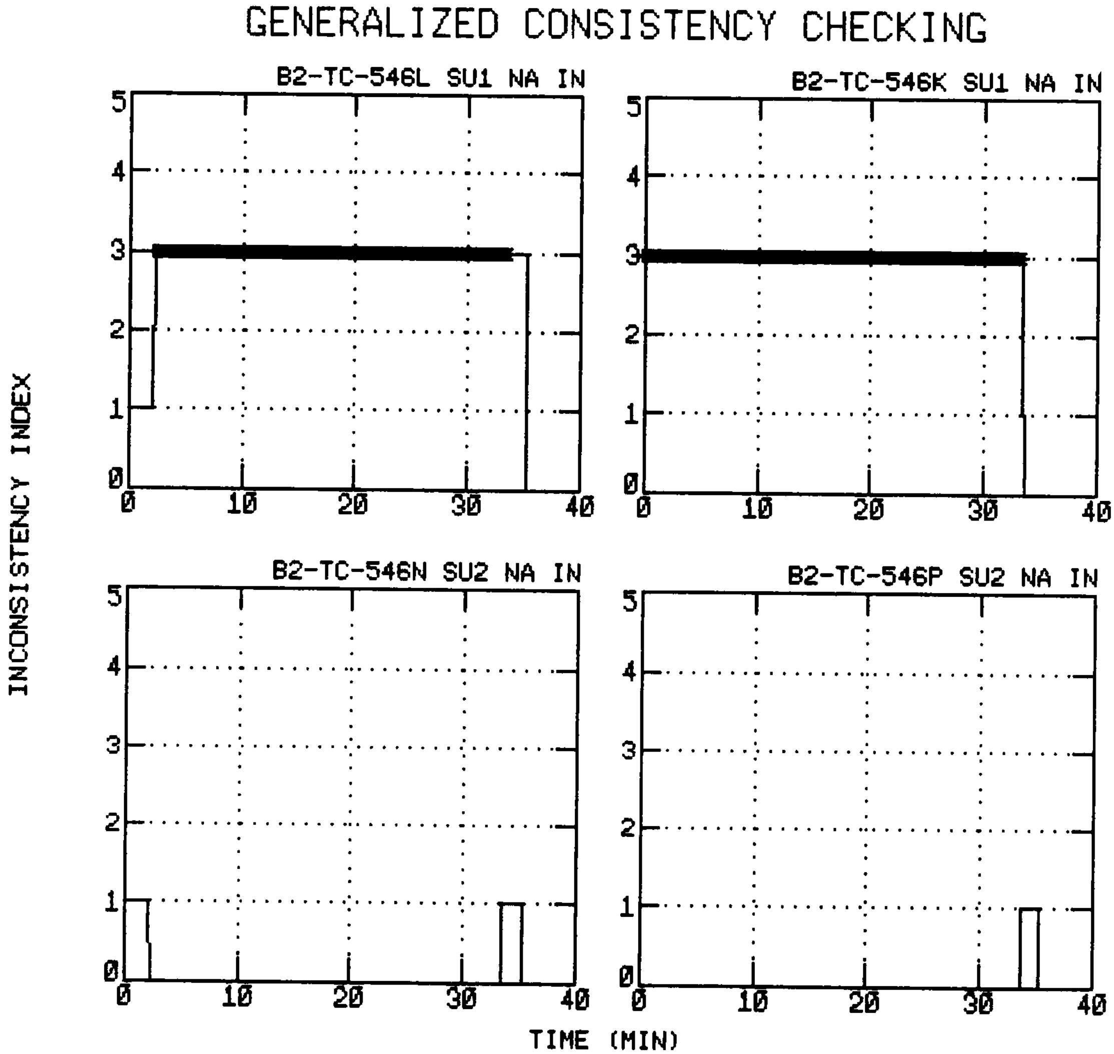

Figure 7.11. SGCC Inconsistency Indices for the Superheater Sodium Inlet Temperature Signals.

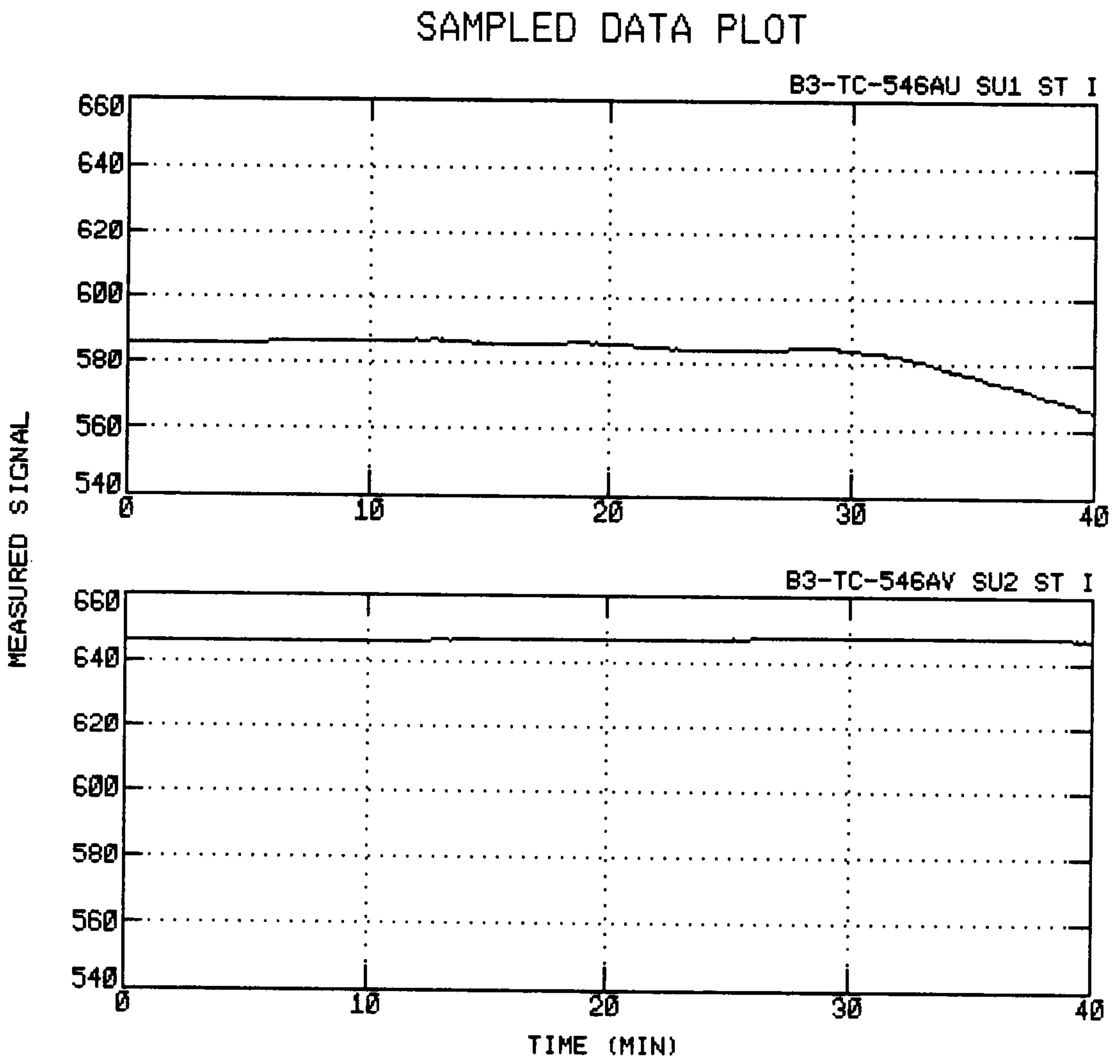

Figure 7.12. Measured Data for the Superheater Steam Inlet Temperature Signals.

estimate. The module estimates are given in Figure 7.13. From the graph the HMS variable estimate computation method is shown to be superior to the SGCC method. The key to this is that the HMS inconsistency indices of Figure 7.14 are equivalent. Thus neither signal is excluded and both are used in computing an estimate. A solution to this SGCC past estimate flaw, which has twice appeared thus far, is to compare the signals against both the upper and lower signal range limits. The upper range value is tested since some signals fail high when the sensor input is removed (turned off).

Incidentally, the above two cases have shown bad results using the "pseudo" redundancy, however on the whole, the use of pseudo redundancy proved to be a good approach.

7.3 Bias/Drift Failure Detection

Bias and drift failure is detectable by the PEM, SGCC, MGCC and BND modules. The SGCC module monitors drift using the sequential probability ratio test (SPRT). The BND module monitors bias using the symmetry of the amplitude probability density function (APDF) as compared to an expected value.

7.3.1 Empirical Modeling

In order to monitor bias or drift failure in the signals with the PEM and MGCC modules, it was first

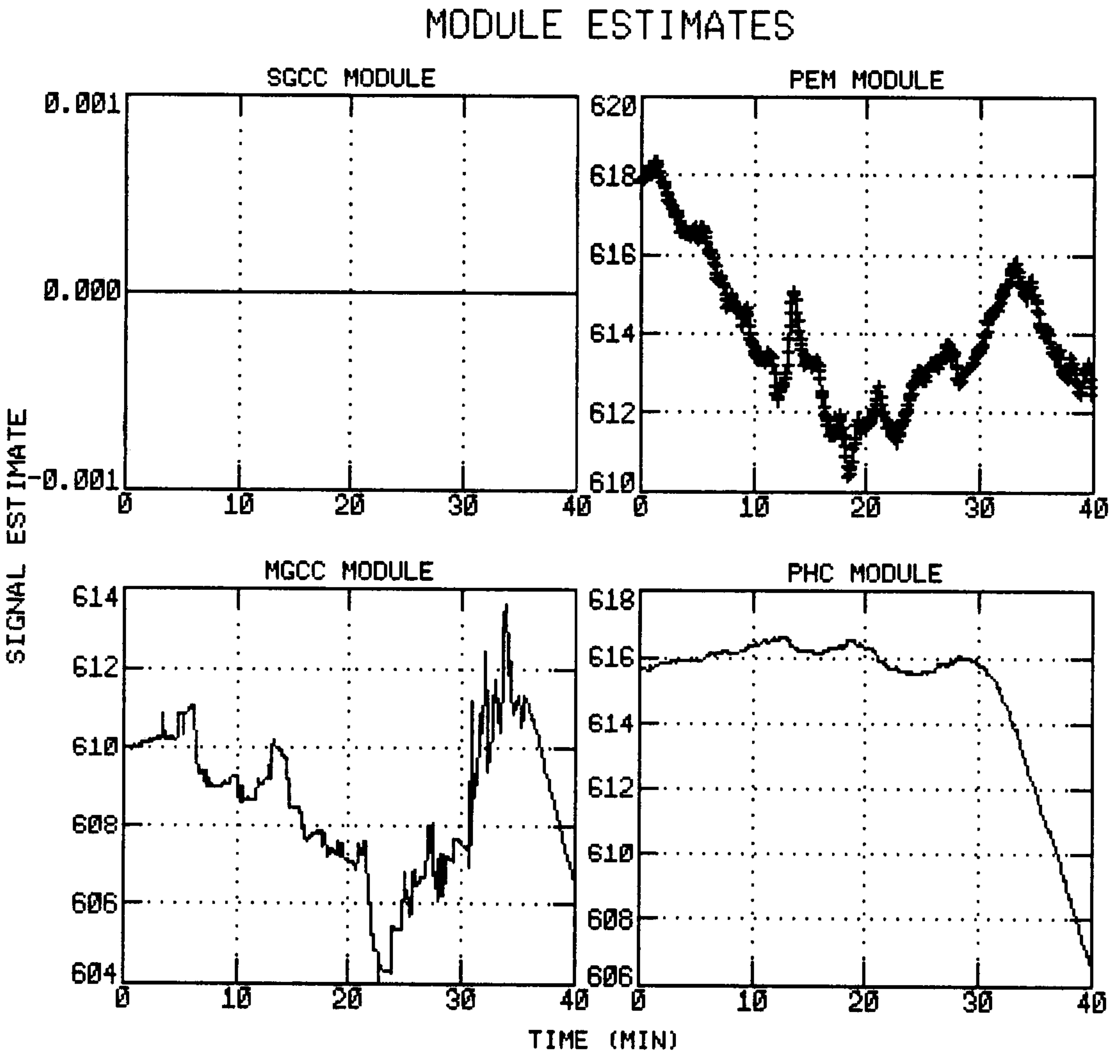

Figure 7.13. Superheater Steam Inlet Temperature Estimates.

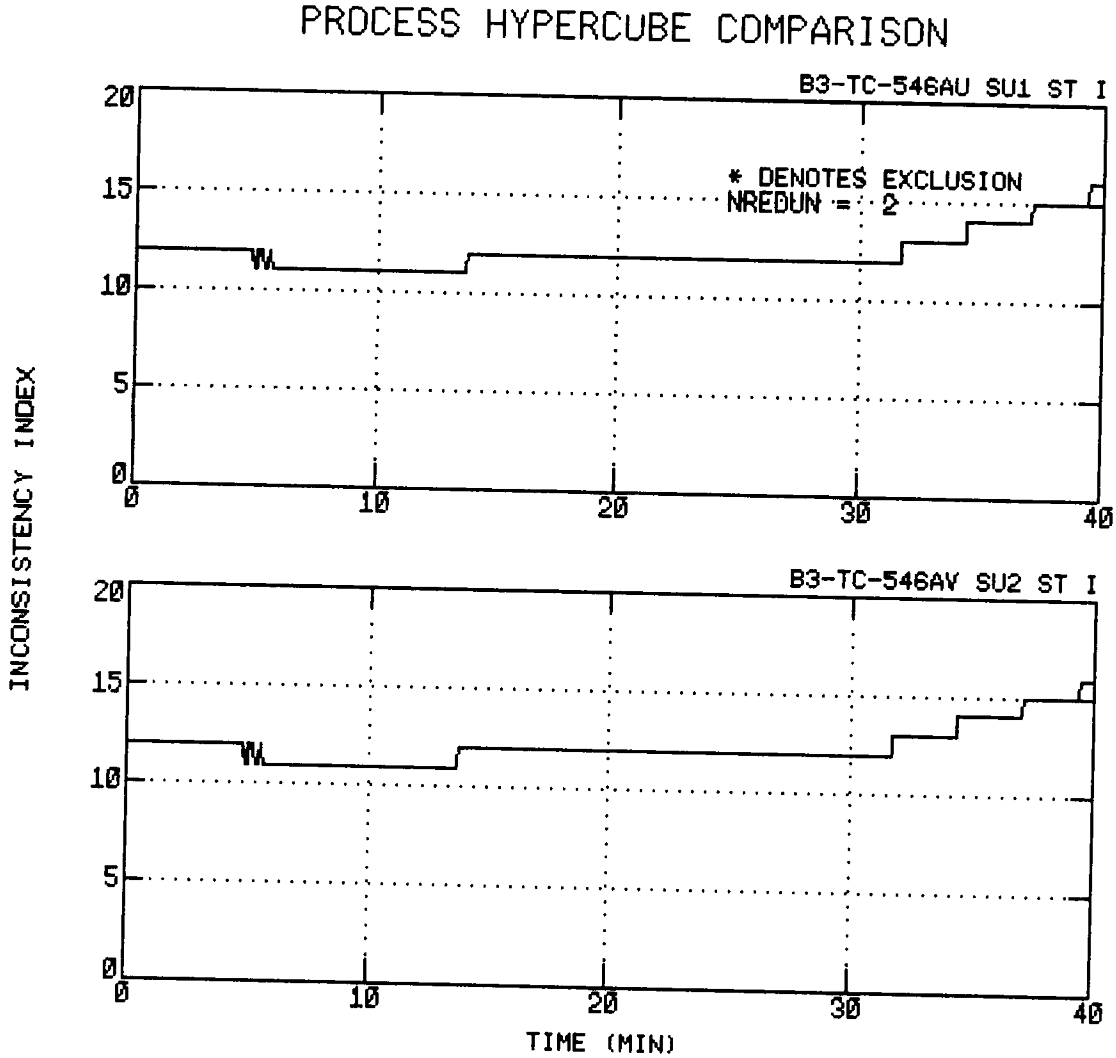

Figure 7.14. PHC Inconsistency Indices for the Superheater Steam Inlet Temperature Signals.

necessary to create empirical models off-line for input to these modules. The modeling effort was a research project in itself. The empirical modeling results for the EBR-II data are given in Appendix F.

The EBR-II empirical modeling showed that a single model can be constructed which accurately describes a given signal over its normal operating range. The start-up type data used is somewhat desirable since many valid operating states are represented by such data; however, there may be transient lags present affecting the results. Two of the modeling results, the steam drum level and blowdown flow, were entirely unacceptable and require more work. The power model was also less than desirable and could stand some more time spent on it.

7.3.2 Biased Signal

The importance of the empirical models has already been seen with the IHX secondary inlet temperature signals of Section 7.2.1. The empirical model estimate essentially provides a third "redundant measurement" for comparison purposes. This "analytical" measurement was used to distinguish between the good and bad temperature signals. The module estimates were shown in Figure 7.7. With the empirical estimates the failed signal was properly identified. The bias SPRT from the SGCC module is shown in Figure 7.15 for these two signals.

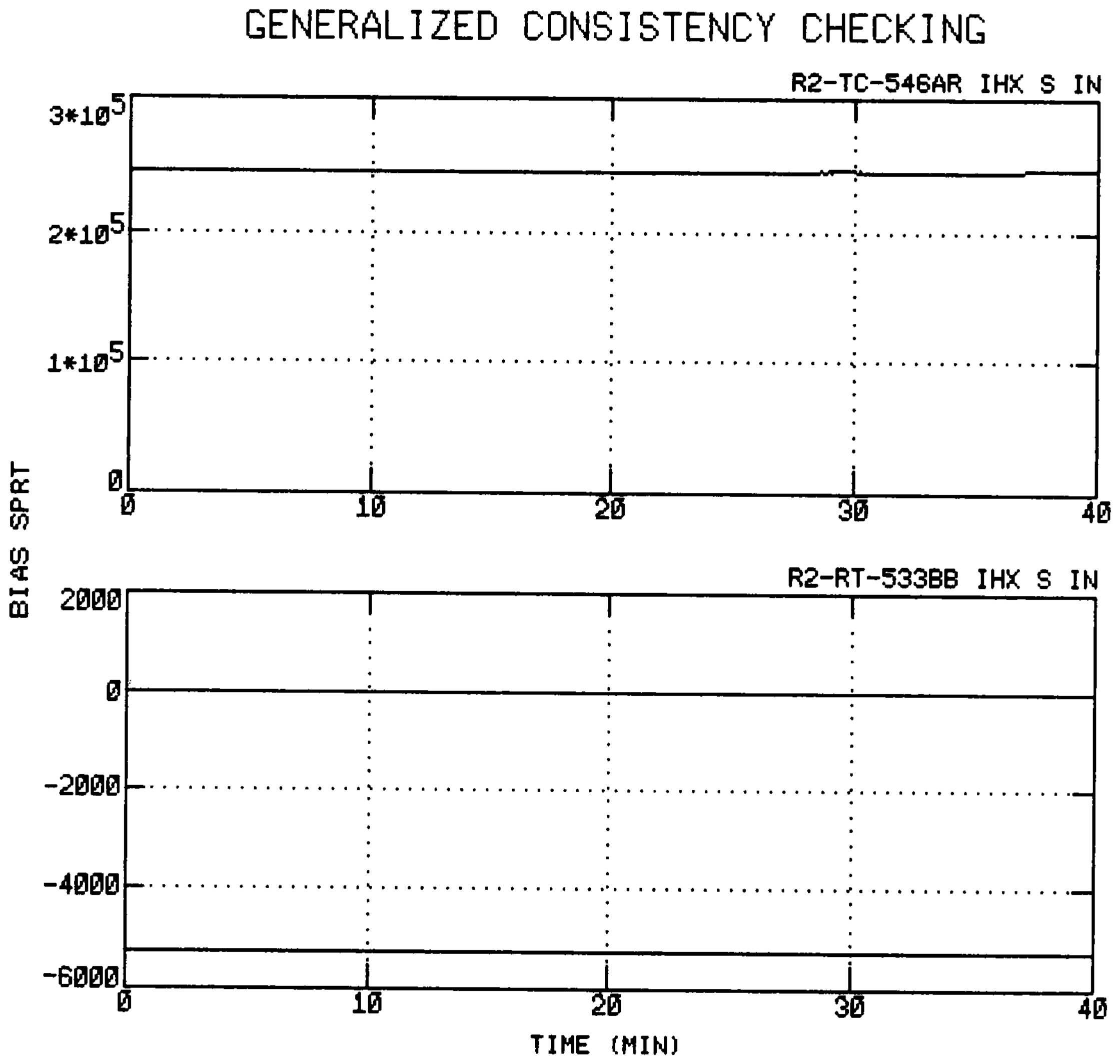

Figure 7.15. SGCC Bias SPRT Results for the IHX Secondary Inlet Temperature Signals.

7.4 Noise Failure Detection

Noise failure is detectable by the SGCC and BND modules. Acceptable noise levels are quantities which are not generally available. The normal noise values may be learned off-line by observing the process data.

Differences in signal noise can sometimes be seen qualitatively from a visual analysis of the signals. An example of a normal and three increasingly noisier signals are shown in Figure 7.16. The noise level may be expressed quantitatively from the RMS noise level computed by the BND module as:

Item	Tag Number	RMS Level
1.	R1-TC-503AA	0.31
2.	R1-TC-503T	0.94
3.	R1-TC-503R	1.57
4.	R1-TC-503W	6.67

These RMS noise levels are compared against both a lower and an upper threshold limit in the BND module. Those signals exceeding the threshold limits are declared anomalous. An extreme example of the lack of noise can be seen in the IHX secondary inlet temperature signal of Figure 7.17. This completely failed signal has no noise fluctuations present and the RMS noise level is thus zero.

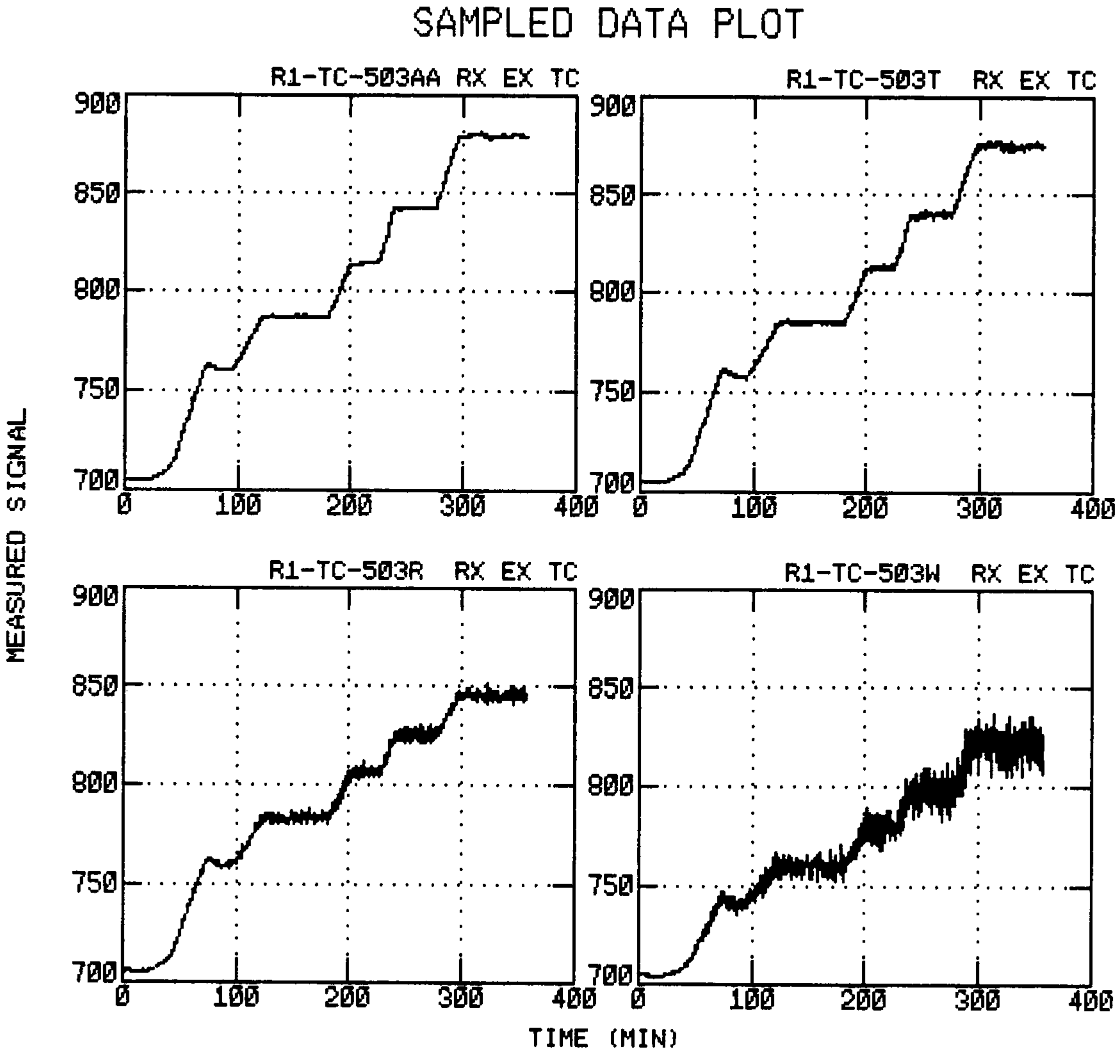

Figure 7.16. Measured Data for Four Core-Exit Temperature Signals Showing Differences in Noise.

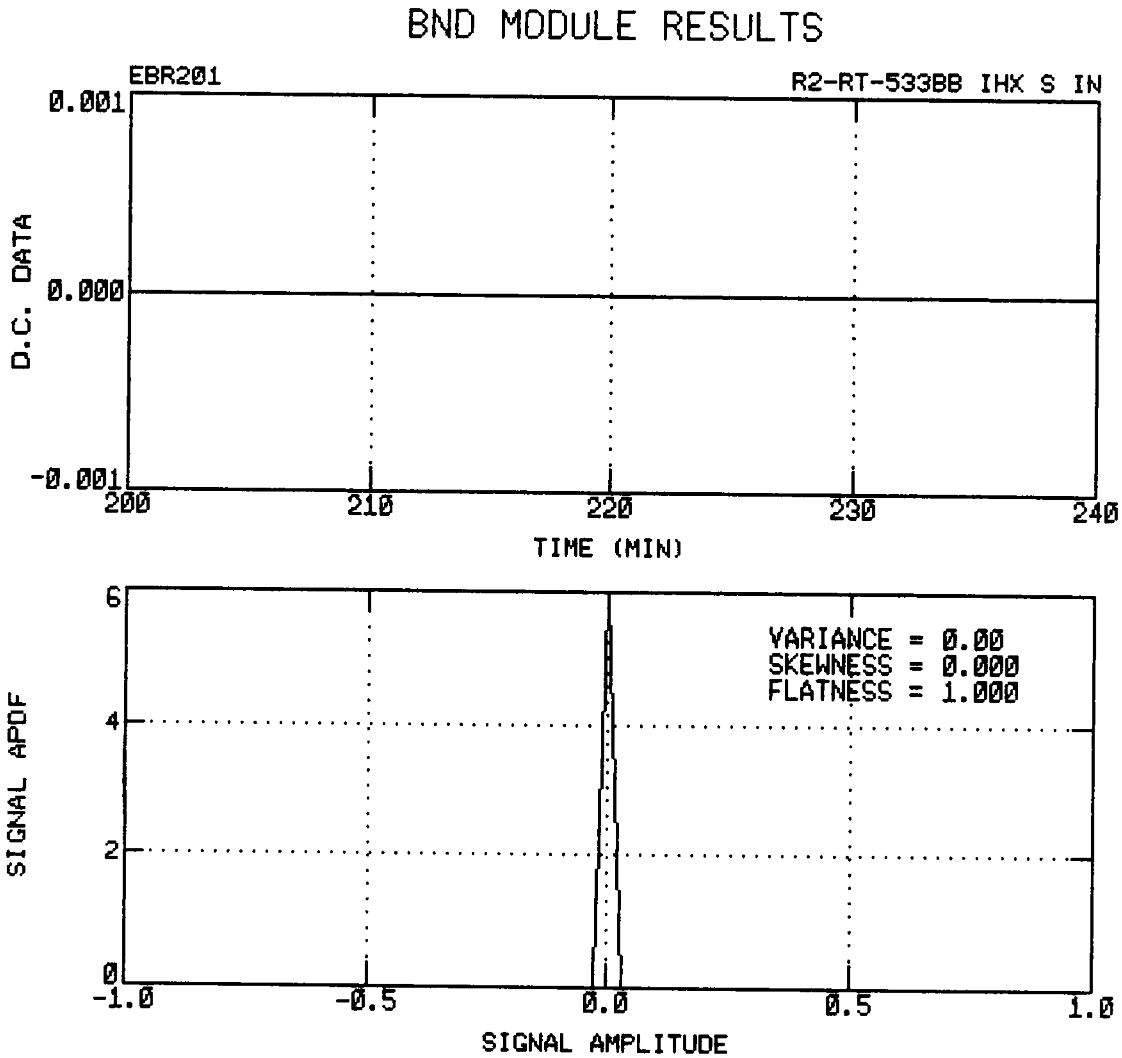

Figure 7.17. BND APDF for a IHX Secondary Inlet Temperature Signal.

7.5 Time Response Failure Detection

Both the UAR and BND modules report on the time response failure mode. Unfortunately both methods require noise data as input and as stated previously, this type of data was not available and had to be artificially generated. More importantly, however, the sampling interval for this data was five seconds (0.2 Hz) which is too slow to identify the signal time constants. The time constants for temperature sensors are of the order of 1 to 10 seconds (break frequency: 0.1 to 1 Hz) and less than 1 second for pressure sensors (break frequency: 1 to 10 Hz).

Nonetheless, results from the UAR module are presented. An example of the UAR computed autocorrelation, and estimation of the power spectral density (PSD) and step response for a bulk sodium pool temperature signal (R1-TC-501M) is given in Figure 7.18. Note that the frequency range is 0.0005 to 0.1 Hz which is too low for proper signal analysis. The indicated time constant is 0.3 minutes, well beyond any acceptable (or believable) value. The UAR results for the blowdown flow signal are given in Figure 7.19.

It was shown that the available data was inappropriate. In this case, the UAR (or BND) module could easily compare the sampling rate versus a nominal time constant to identify whether the available data is acceptable or not and return the data analysis error (IERROR) described in Section 5.1.7.

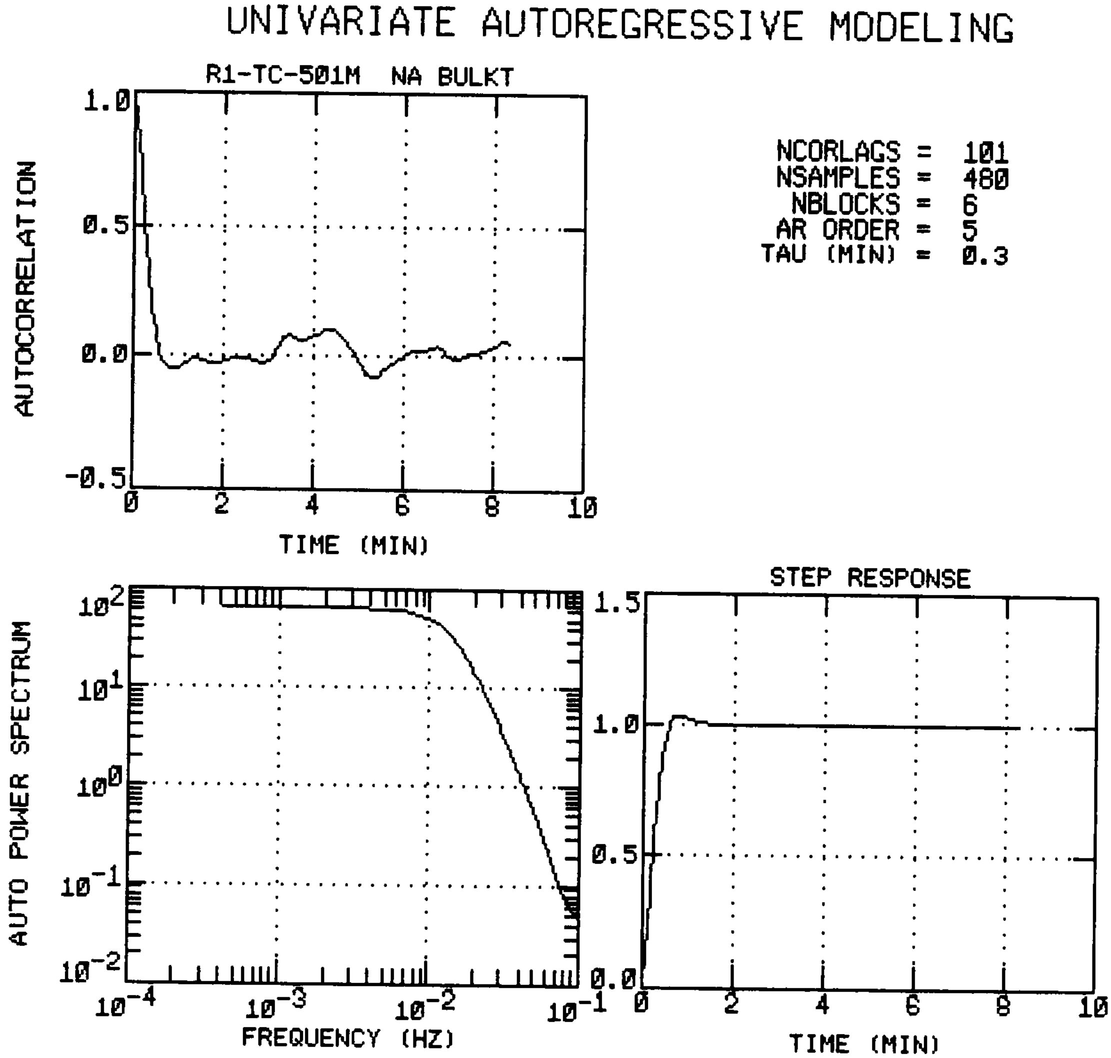

Figure 7.18. UAR Computed Autocorrelation, and Estimation of PSD and Step Response for a Sodium Pool Temperature Signal.

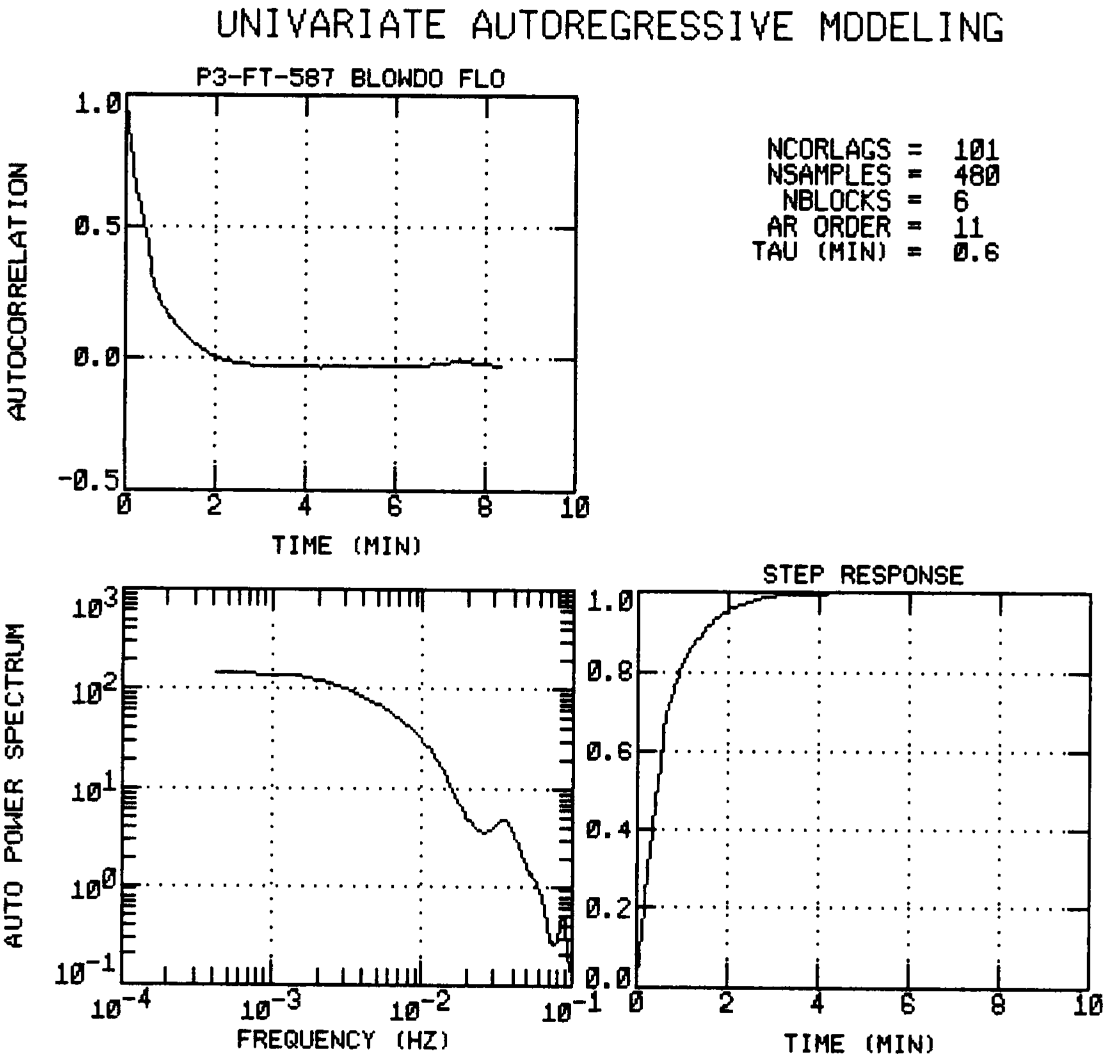

Figure 7.19. UAR Computed Autocorrelation, and Estimation of PSD and Step Response for the Blowdown Flow Signal.

The final results from the System Executive for the time response failure mode are presented. The SE final decision (Figure 7.8) is that the time response failure is commonality indeterminate. Commonality was detected in the entire plant (which may indicate that the process is the cause). In this case the commonality was actually caused by the slow data sampling rate. This result once again shows the effectiveness of the commonality search in identifying and avoiding possible false alarm.

7.6 EBR-II Data Analysis Conclusions

There were several good examples for the consistency failure detection. Of all the modules, the SGCC had the best track record, although there are certainly cases which can fool the methodology as was seen in this section. The bias/drift detection methodology has been shown to work, but effective demonstration requires a longer data sampling period. The noise data need to be sampled at a faster rate (higher sampling frequency), however the results have shown that the signal processing techniques do work. The noise analysis techniques (modules) tend to operate improperly, as expected, during transient process conditions. The time response failure detection results were also unacceptable due to the sampling interval. Overall, the comprehensive signal validation system performed in an acceptable manner.

8. CONCLUSIONS AND RECOMMENDATIONS

8.1 Conclusions

This doctoral research on the development and improvement of signal validation technology has resulted in the following original contributions and innovations:

1. Development of a new technique for performing signal validation. The process hypercube comparison "learns" the valid operating states of a process to which newly observed data points may be compared and faulty signals identified.

2. The consolidation of several fault detection methodologies into a modular comprehensive signal validation system (SVS). This included the development of a decision maker to assess the final signal status based on the results of the diverse signal processing modules. Intra-module results were generated using fuzzy membership functions.

3. Application of the signal validation techniques to operational data from a commercial pressurized water reactor (PWR) and the Experimental Breeder Reactor II (EBR-II).

The performance of the modules themselves has varied. As was seen the single variable consistency checking (SGCC) module fails in instances when there are less than three redundant signals. The noise analysis methodologies require steady-state conditions to be accurate. The empirical models were shown to be highly useful as an independent estimate of the process conditions. The process hypercube comparison (PHC) module has proved to be an excellent technique for performing signal validation based upon a global analysis of the plant process states, but it is not well suited for a microscopic examination of the process signals.

The overall performance of the comprehensive signal validation system was a pleasant surprise. With each of the modules there has been instances in which a particular technique was inadequate to resolve certain types of failure. However, the combination of diverse signal validation methodologies into a comprehensive system was able to avoid such false alarms. The SVS was also able to identify more types of signal anomalies than would be possible using a single fault detection scheme. Although no intricate decision maker (such as an expert system) was utilized, the final positive decision maker (PDM) conclusions were highly accurate. The commonality search implemented also proved to be an effective method of avoiding false alarms. Although a more detailed decision maker could be developed for a given set of modules, it would not be capable of preserving the modular architecture of the system developed here.

8.2 Recommendations

From discussions with some NSSS vendor personnel working on drift detection techniques, it was learned that their emphasis was placed on quantifying the amount of drift. Subsequent to the detection and quantification of drift, the objective was to compensate for the drift either in electronics or software. Economically, it is probably better in most cases to buy a new instrument rather than to perform a detailed analysis followed by the above modifications (and unmodified once the instrument is eventually fixed). Another aspect not yet addressed is NRC approval --- one must also question whether with the compensation fix that the technical specifications are exceeded according to the letter of the law.

Although intricate characterizations of signal anomaly is certainly desirable, it is questionable whether this detailed analysis will be put to use in today's commercial power plants. The nuclear power plant manager is highly concerned with economics, that is, the production of electricity at the lowest possible cost. Retrofitted systems must provide justifiable economic return before purchase, unless of course they are mandated by an organization such as the NRC. For this reason, there will be little concern for identifying small drifts in the signals which do not result in exceeding plant technical operating specifications. What is required is to address the following:

1. Is the signal operating within the required limits?
2. Will the signal fail anytime in the near future?

In answering these two questions, the simplest signal validation techniques will tend to perform the task most efficiently. The basic techniques have been successfully demonstrated in this comprehensive signal validation system. Incipient failure detection may also be applied to other problems such as instrument calibration reduction.

In short, future research should concentrate upon the application of the signal validation methodologies to more operational plant data. This increased experience will provide a greater fundamental trust and acceptance of the module capabilities and provide the necessary insight into making further improvements in the modules as well as the development of new ones.

LIST OF REFERENCES

LIST OF REFERENCES

1. H.P. Polenta et al., "Implementation of a Fault Detection Procedure," Proceeding of the 1986 American Control Conference, Seattle, Washington, pp. 176-181, June 1986.

2. R.N. Clark and B. Campbell, "Instrument Fault Detection in a Pressurized Water Reactor," Nuclear Technology, Vol. 56, pp. 23-32, January 1982.

3. B.R. Upadhyaya et al., "Signal Validation in Nuclear Power Plants," Annual Report prepared for the U.S. Department of Energy by the University of Tennessee, DOE/NE/37959-24, September 1988.

4. O.L. Deutsch, R.S. Ornedo and R.W. Lindsay, "Implementation of Real-Time Signal Validation at EBR-II," Transactions of the American Nuclear Society, Vol. 45, pp. 660-661, 1983.

5. B.J. Benedict, R.I. Lutz and L.P. Smith, "Validation of Critical Signals for the Safety Parameter Display System," EPRI Report NP-5066M, April 1987.

6. J. Mott, R. Young and R. King, "Pattern-Recognition Software For Plant Surveillance," Report prepared for the U.S. Department of Energy, 1987.

7. R. Onken and N. Stuckenburg, "Failure Detection in Signal Processing and Sensing in Flight Control Systems," Proceedings of the 1978 IEEE Conference on Decision and Control, pp. 449-454, 1978.

8. E.Y. Shapiro and H.E. Decarli, "Analytic Redundancy for Flight Control Sensors on the Lockheed L-1011 Aircraft," Proceedings of the 1978 IEEE Conference on Decision and Control, pp. 371-376, 1978.

9. R. C. Montgomery and D. Tabak, "Application of Analytical Redundancy Management to Shuttle Crafts," Proceedings of the 1978 IEEE Conference on Decision and Control, pp. 442-448, 1978.

10. R.D. Fournier et al., "Digital Control and Protection Retrofits in Nuclear Power Plants," Nuclear News, American Nuclear Society, La Grange Park, Illinois, pp. 50-57, November 1988.

11. O.L. Deutsch et al., "Validation and Integration of Critical PWR Signals for Safety Parameter Display Systems," Electric Power Research Institute Report NP-4566, May 1986.

12. O. Glockler, B.R. Upadhyaya and T.W. Kerlin, "Signal Validation Algorithms for Consistency Checking and Sequential Probability Ratio Testing of Redundant Measurements," Topical Report prepared for the U.S. Department of Energy by the University of Tennessee, DOE/NE/37959-6, July 1987.

13. B.R. Upadhyaya and M. Skorska, "Sensor Fault Analysis Using Decision Theory and Data-Driven Modeling of Pressurized Water Reactor Subsystems," Nuclear Technology, Vol. 64, pp. 70-77, 1984.

14. O. Glockler and B.R. Upadhyaya, "Reactor Noise Diagnostics Based on Multivariate Autoregressive Modeling," Fourth Conference on Utility Experiences in Reactor Noise Analysis, Rocky Hill, CT, DOE/NE/37959-5, May 1987.

15. A. Descrochers and S. Mohseni, "On Determining the Structure of a Nonlinear System," International Journal of Control, Vol. 40, No. 5, pp. 923-938, 1984.

16. B.R. Upadhyaya and K.E. Holbert, "Computation of Data-Driven Models with Application to Power Plant Signal Validation," ANS/ENS 1988 International Conference, Washington D.C., November 1988.

17. V.M. Morgenstern, B.R. Upadhyaya and O. Glockler, "Signal Anomaly Detection and Characterization," Topical Report prepared for the U.S. Department of Energy by the University of Tennessee, DOE/NE/37959-18, August 1988.

18. A.L. Qualls, "Signal Validation Using Expert System Technology," M.S. Thesis, University of Tennessee, June 1988.

19. R.A. Frost, Introduction to Knowledge Base Systems, Macmillan Publishing Company, New York, 1986.

20. E.H. Shortliffe and B.G. Buchanan, "A Model of Inexact Reasoning in Medicine," Mathematical Biosciences, Vol. 23, pp. 351-379, 1975.

21. G. Schafer, A Mathematical Theory of Evidence, Princeton University Press, 1976.

22. L.A. Zadeh, "Fuzzy Sets," Information and Control, Vol. 8, pp. 338-353, 1965.

23. N. Rescher, Plausible Reasoning, VanGorcum Amsterdam, 1976.

24. A. Kandel, Fuzzy Techniques in Pattern Recognition, John Wiley & Sons, New York, 1982.

25. A. Kandel, Fuzzy Mathematical Techniques with Applications, Addison-Wesley Publishing Company, 1986.

26. D. Childers and A. Durling, Digital Filtering and Signal Processing, West Publishing Company, 1975.

27. J.A. Thie, Power Reactor Noise, American Nuclear Society, La Grange Park, Illinois, 1981.

28. H.M. Hashemian, T.W. Kerlin and B.R. Upadhyaya, "Apparatus for measuring the degradation of a sensor time constant," United States Patent #4295128, October 1981.

29. B.R. Upadhyaya and T.W. Kerlin, "Estimation of Response Time Characteristics of Platinum Resistance Thermometers by the Noise Analysis Techniques," ISA Transactions, Vol. 17, pp. 21-38, 1978.

30. O. Glockler, B.R. Upadhyaya, V.M. Morgenstern and J. Olvera, "Generalized Consistency Checking of Multivariable Redundant Measurements and Common-mode Failure Detection," Proceedings of the Seventh Power Plant Dynamics, Control & Testing Symposium," Knoxville, Tennessee, May 1989.

APPENDIXES

APPENDIX A

PWR POWER PLANT DATA

The pressurized water reactor (PWR) data were taken from a four-loop Westinghouse commercial nuclear power plant. A schematic of the plant is shown in Figure A.1. The PWR data set from a plant start-up was available for analysis. The data were sampled at three minute intervals. The available process signals are given in Table A.1 and the signal tolerances in Table A.2. Representative plots of the process variables are given in Figure A.2.

The PWR power plant consists of a thermal reactor producing 1150 MW of electric power. The primary system carries heat away from the core in four separate loops to the four steam generators. The steam from the four loops is supplied to a turbine-generator. After passing through the turbine, the steam is sent through a condenser before returning to the steam generators as feedwater.

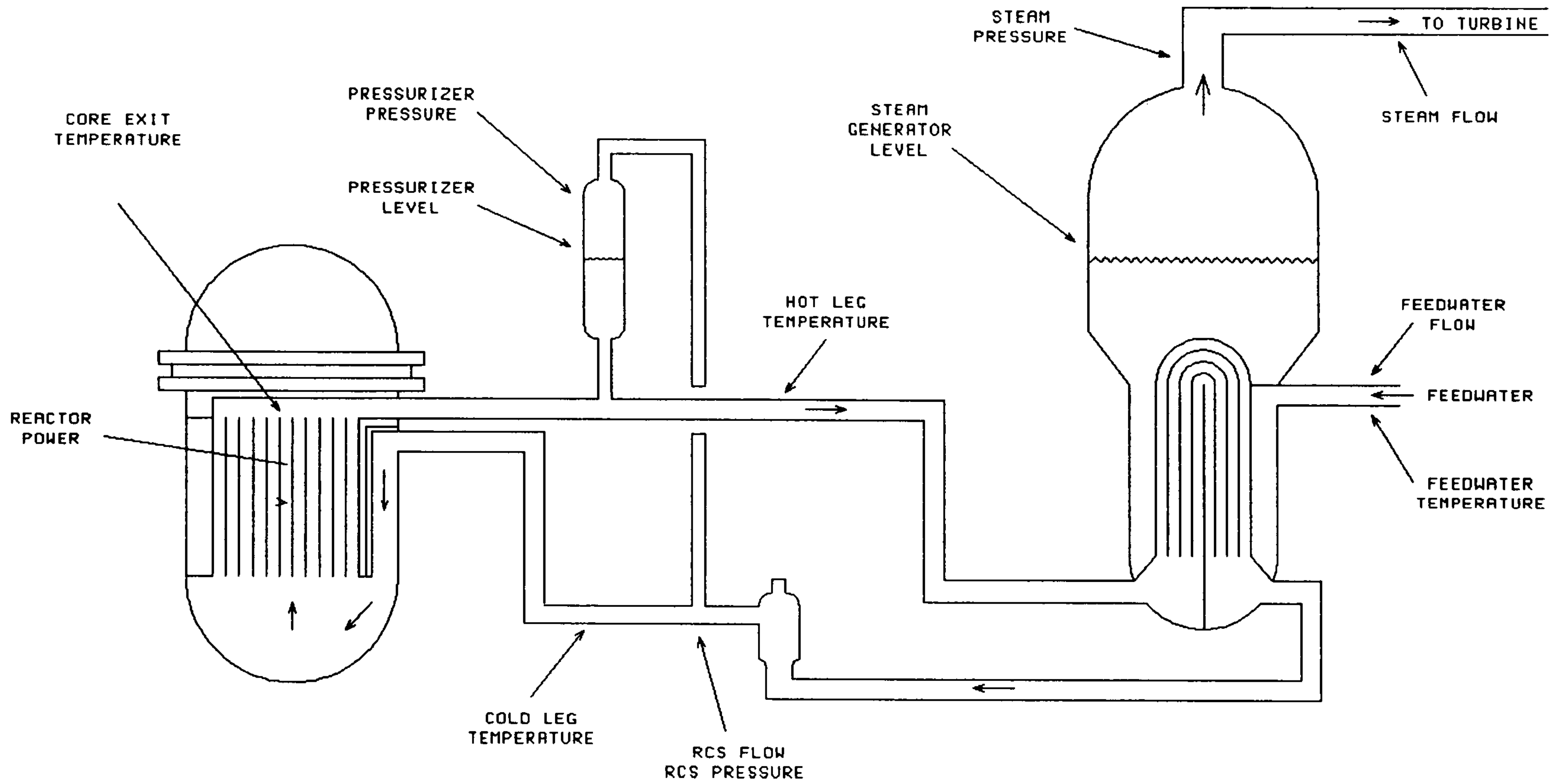

Figure A.1. PWR System Schematic.

TABLE A.1

PWR Process Signals

Signal Number	Sensor Tag Number	Signal Description
1.	NMP-NM41F	Power Range (%)
2.	NMP-NM42F	Power Range (%)
3.	NMP-NM43F	Power Range (%)
4.	NMP-NM44F	Power Range (%)
5.	RCS-L459	Pressurizer Level (%)
6.	RCS-L460	Pressurizer Level (%)
7.	RCS-L461	Pressurizer Level (%)
8.	CVCMBPZR	Pressurizer Pressure (SPDS) (psia)
9.	RCS-P455A*	Pressurizer Pressure (psia)
10.	RCS-P456	Pressurizer Pressure (psia)
11.	RCS-P457	Pressurizer Pressure (psia)
12.	RCS-P458	Pressurizer Pressure (psia)
13.	RCS-T413B	RCS Cold Leg Temperature (WR) (°F)
14.	RCS-T423B	RCS Cold Leg Temperature (WR) (°F)
15.	RCS-T433B	RCS Cold Leg Temperature (WR) (°F)
16.	RCS-T443B	RCS Cold Leg Temperature (WR) (°F)
17.	RCS-T413A	RCS Hot Leg Temperature (WR) (°F)
18.	RCS-T423A	RCS Hot Leg Temperature (WR) (°F)
19.	RCS-T433A	RCS Hot Leg Temperature (WR) (°F)
20.	RCS-T443A	RCS Hot Leg Temperature (WR) (°F)
21.	RCS-P403	RCS Pressure (WR) (psia)
22.	RCS-P405	RCS Pressure (WR) (psia)
23.	FWS-F510	SG 1 Main Feedwater Flow (kpph)
24.	FWS-F511	SG 1 Main Feedwater Flow (kpph)
25.	FWS-F520	SG 2 Main Feedwater Flow (kpph)
26.	FWS-F521	SG 2 Main Feedwater Flow (kpph)
27.	FWS-F530	SG 3 Main Feedwater Flow (kpph)
28.	FWS-F531	SG 3 Main Feedwater Flow (kpph)
29.	FWS-F540	SG 4 Main Feedwater Flow (kpph)
30.	FWS-F541	SG 4 Main Feedwater Flow (kpph)
31.	FWS-L517	Steam Generator 1 Level (NR) (%)
32.	FWS-L518	Steam Generator 1 Level (NR) (%)
33.	FWS-L519	Steam Generator 1 Level (NR) (%)
34.	FWS-L501	Steam Generator 1 Level (WR) (%)
35.	FWS-L527	Steam Generator 2 Level (NR) (%)
36.	FWS-L528	Steam Generator 2 Level (NR) (%)
37.	FWS-L529	Steam Generator 2 Level (NR) (%)
38.	FWS-L502	Steam Generator 2 Level (WR) (%)
39.	FWS-L537	Steam Generator 3 Level (NR) (%)

TABLE A.1 (Continued)

Signal Number	Sensor Tag Number	Signal Description
40.	FWS-L538	Steam Generator 3 Level (NR) (%)
41.	FWS-L539	Steam Generator 3 Level (NR) (%)
42.	FWS-L503	Steam Generator 3 Level (WR) (%)
43.	FWS-L547	Steam Generator 4 Level (NR) (%)
44.	FWS-L548	Steam Generator 4 Level (NR) (%)
45.	FWS-L549	Steam Generator 4 Level (NR) (%)
46.	FWS-L504	Steam Generator 4 Level (WR) (%)
47.	MSS-P514	Steam Generator 1 Pressure (psig)
48.	MSS-P515	Steam Generator 1 Pressure (psig)
49.	MSS-P516	Steam Generator 1 Pressure (psig)
50.	MSS-P524	Steam Generator 2 Pressure (psig)
51.	MSS-P525	Steam Generator 2 Pressure (psig)
52.	MSS-P526	Steam Generator 2 Pressure (psig)
53.	MSS-P534	Steam Generator 3 Pressure (psig)
54.	MSS-P535	Steam Generator 3 Pressure (psig)
55.	MSS-P536	Steam Generator 3 Pressure (psig)
56.	MSS-P544	Steam Generator 4 Pressure (psig)
57.	MSS-P545	Steam Generator 4 Pressure (psig)
58.	MSS-P546	Steam Generator 4 Pressure (psig)
59.	RCS-F414	RCS Flow Loop 1 (%)
60.	RCS-F415	RCS Flow Loop 1 (%)
61.	RCS-F416	RCS Flow Loop 1 (%)
62.	RCS-F424	RCS Flow Loop 2 (%)
63.	RCS-F425	RCS Flow Loop 2 (%)
64.	RCS-F426	RCS Flow Loop 2 (%)
65.	RCS-F434	RCS Flow Loop 3 (%)
66.	RCS-F435	RCS Flow Loop 3 (%)
67.	RCS-F436	RCS Flow Loop 3 (%)
68.	RCS-F444	RCS Flow Loop 4 (%)
69.	RCS-F445	RCS Flow Loop 4 (%)
70.	RCS-F446	RCS Flow Loop 4 (%)
71.	MSS-F512	Steam Generator 1 Steam Flow (kpph)
72.	MSS-F513	Steam Generator 1 Steam Flow (kpph)
73.	MSS-F522	Steam Generator 2 Steam Flow (kpph)
74.	MSS-F523	Steam Generator 2 Steam Flow (kpph)
75.	MSS-F532	Steam Generator 3 Steam Flow (kpph)
76.	MSS-F533	Steam Generator 3 Steam Flow (kpph)
77.	MSS-F542	Steam Generator 4 Steam Flow (kpph)
78.	MSS-F543	Steam Generator 4 Steam Flow (kpph)
79.	FWS-T40A	SG 1 Feedwater Temperature (°F)
80.	FWS-T40B	SG 2 Feedwater Temperature (°F)
81.	FWS-T40C	SG 3 Feedwater Temperature (°F)

TABLE A.1 (Continued)

Signal Number	Sensor Tag Number	Signal Description
82.	FWS-T40D	SG 4 Feedwater Temperature (°F)
83.	CVCTST1	Core Exit Temperature (°F)
84.	CVCTST2	Core Exit Temperature (°F)
85.	CVCTST3	Core Exit Temperature (°F)
86.	CVCTST4	Core Exit Temperature (°F)
87.	CVCTST5	Core Exit Temperature (°F)
88.	CVCTST6	Core Exit Temperature (°F)
89.	CVCTST7	Core Exit Temperature (°F)
90.	CVCTST8	Core Exit Temperature (°F)
91.	CVCTST9	Core Exit Temperature (°F)
92.	CVCTST10	Core Exit Temperature (°F)
93.	CVCTST11	Core Exit Temperature (°F)
94.	CVCTST12	Core Exit Temperature (°F)
95.	CVCTST13	Core Exit Temperature (°F)
96.	CVCTST14	Core Exit Temperature (°F)
97.	CVCTST15	Core Exit Temperature (°F)
98.	CVCTST16	Core Exit Temperature (°F)
99.	CVCTST17	Core Exit Temperature (°F)
100.	CVCTST18	Core Exit Temperature (°F)
101.	CVCTST19	Core Exit Temperature (°F)
102.	CVCTST20	Core Exit Temperature (°F)
103.	CVCTST21	Core Exit Temperature (°F)
104.	CVCTST22	Core Exit Temperature (°F)
105.	CVCTST23	Core Exit Temperature (°F)
106.	CVCTST24	Core Exit Temperature (°F)
107.	CVCTST25	Core Exit Temperature (°F)
108.	CVCTST26	Core Exit Temperature (°F)
109.	CVCTST27	Core Exit Temperature (°F)
110.	CVCTST28	Core Exit Temperature (°F)
111.	CVCTST29	Core Exit Temperature (°F)
112.	CVCTST30	Core Exit Temperature (°F)
113.	CVCTST31	Core Exit Temperature (°F)
114.	CVCTST32	Core Exit Temperature (°F)
115.	CVCTST33	Core Exit Temperature (°F)
116.	CVCTST34	Core Exit Temperature (°F)
117.	CVCTST35	Core Exit Temperature (°F)
118.	CVCTST36	Core Exit Temperature (°F)
119.	CVCTST37	Core Exit Temperature (°F)
120.	CVCTST38	Core Exit Temperature (°F)
121.	CVCTST39	Core Exit Temperature (°F)
122.	CVCTST40	Core Exit Temperature (°F)
123.	CVCTST41	Core Exit Temperature (°F)

TABLE A.1 (Continued)

Signal Number	Sensor Tag Number	Signal Description
124.	CVCTST42	Core Exit Temperature (°F)
125.	CVCTST43	Core Exit Temperature (°F)
126.	CVCTST44	Core Exit Temperature (°F)
127.	CVCTST45	Core Exit Temperature (°F)
128.	CVCTST46	Core Exit Temperature (°F)
129.	CVCTST47	Core Exit Temperature (°F)
130.	CVCTST48	Core Exit Temperature (°F)
131.	CVCTST49	Core Exit Temperature (°F)
132.	CVCTST50	Core Exit Temperature (°F)

Number of Data Channels : 132
Number of Data Samples per Channel : 817
Sampling Interval (seconds) : 180.0

TABLE A.2

PWR Signal Tolerances

Signal	Tolerance	Span
Reactor Power	± 2 %	0 - 120 %
Fission Counter	± 2 %	E-8 - E+2 %
Pressurizer Level	± 10 %	0 - 100 %
Pressurizer Pressure	± 20 psia	1700 - 2500 psia
Cold Leg Temperature (WR)	± 5 °F	0 - 700 °F
Hot Leg Temperature (WR)	± 5 °F	0 - 700 °F
Core-Exit Temperature	± 10 °F	200 - 2300 °F
RCS Flow Rate	± 4 %	0 - 120 %
RCS Pressure (WR)	± 50 psia	0 - 3000 psia
Feedwater Flow	± 185 kpph	0 - 5000 kpph
Feedwater Temperature	± 5 °F	150 - 550 °F
Steam Generator Level (NR)	± 5 %	0 - 100 %
Steam Generator Level (WR)	± 22 %	-100 - 100 %
Steam Generator Pressure	± 20 psig	0 - 1300 psig
Steam Generator Steam Flow	± 185 kpph	0 - 5000 kpph

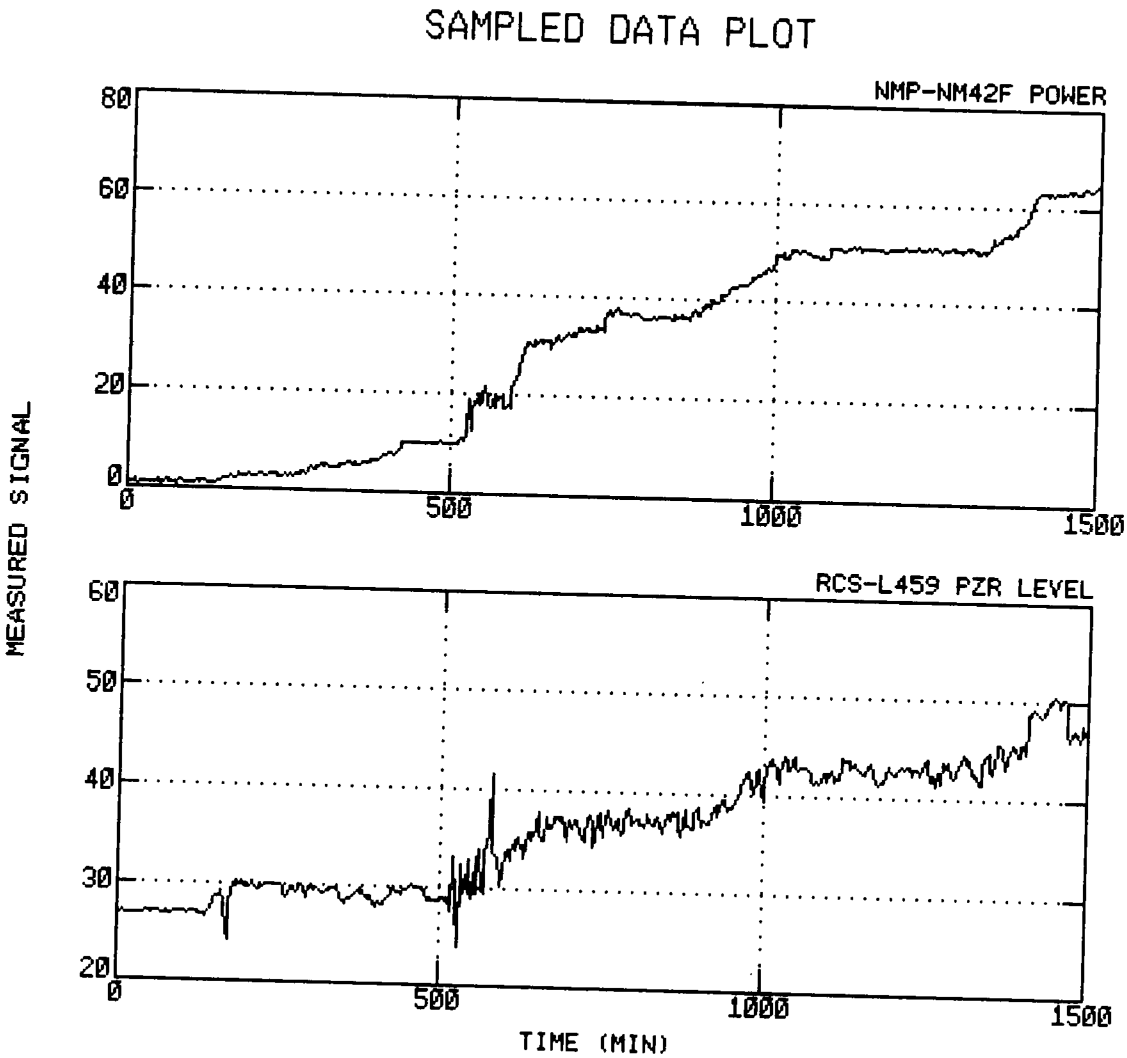

Figure A.2. PWR Process Signals.
Top: Power Signal.
Bottom: Pressurizer Level Signal.

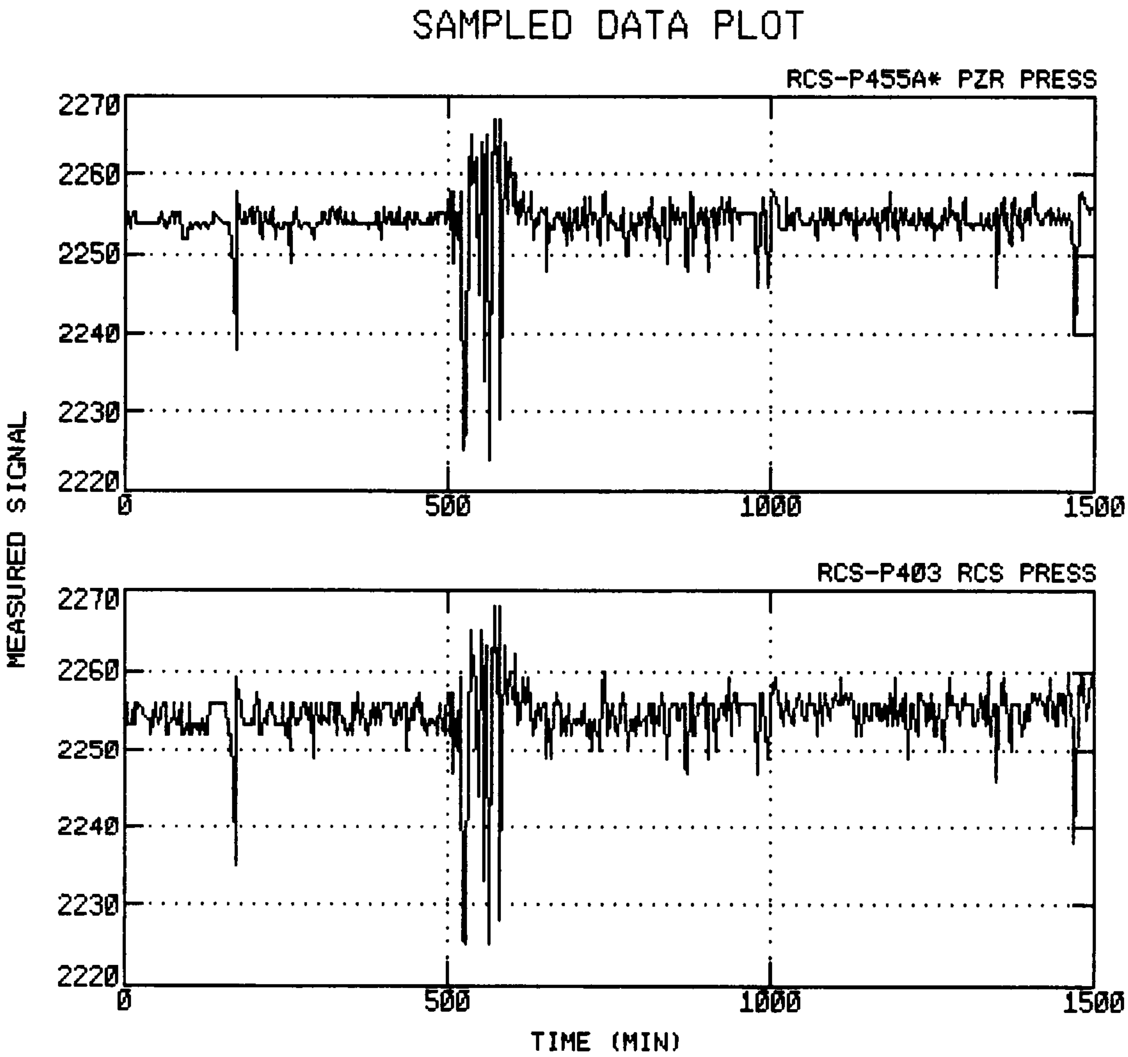

Figure A.2. PWR Process Signals.
Top: Pressurizer Pressure Signal.
Bottom: RCS Pressure Signal.

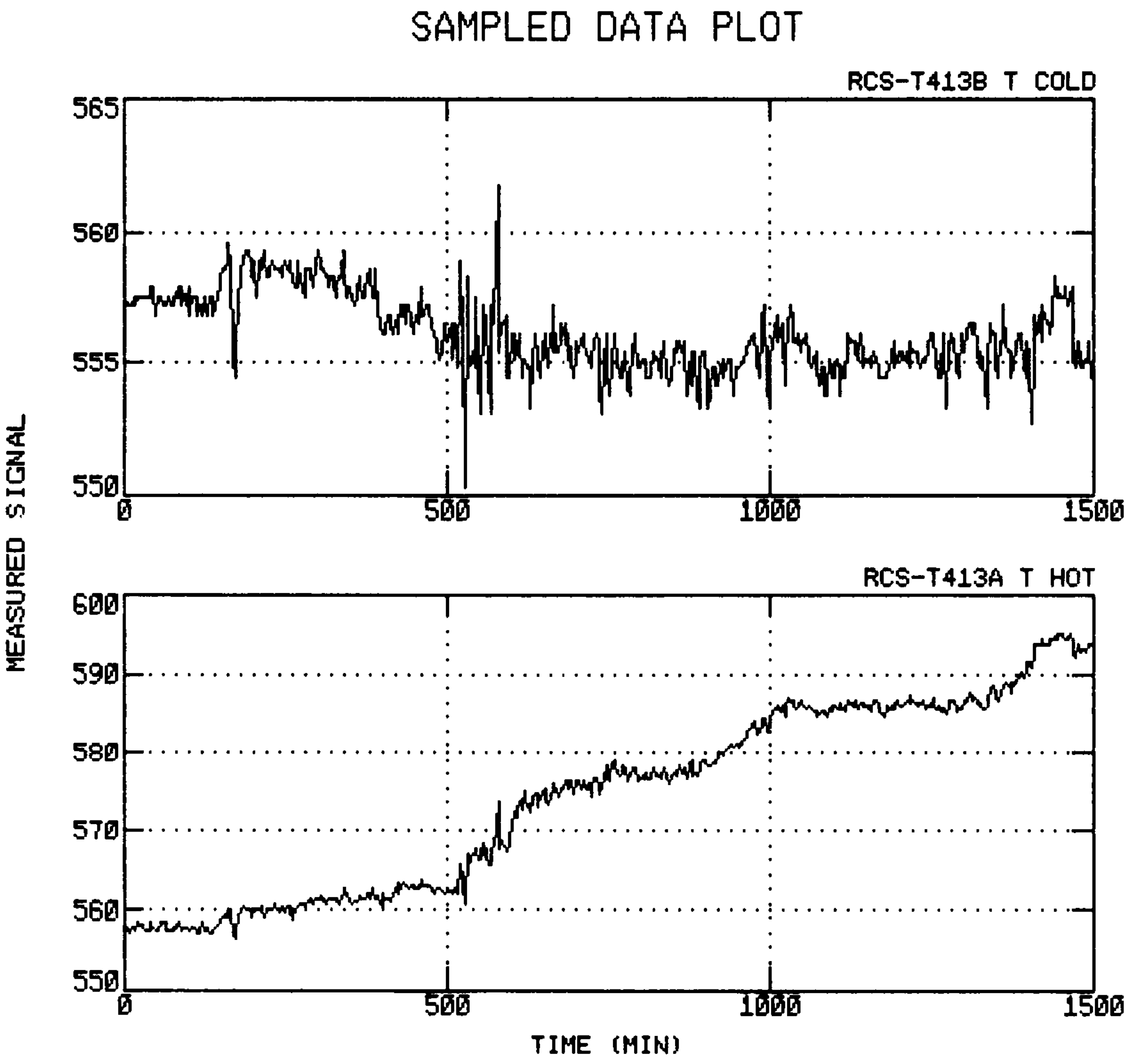

Figure A.2. PWR Process Signals.
Top: Cold Leg Temperature Signal.
Bottom: Hot Leg Temperature Signal.

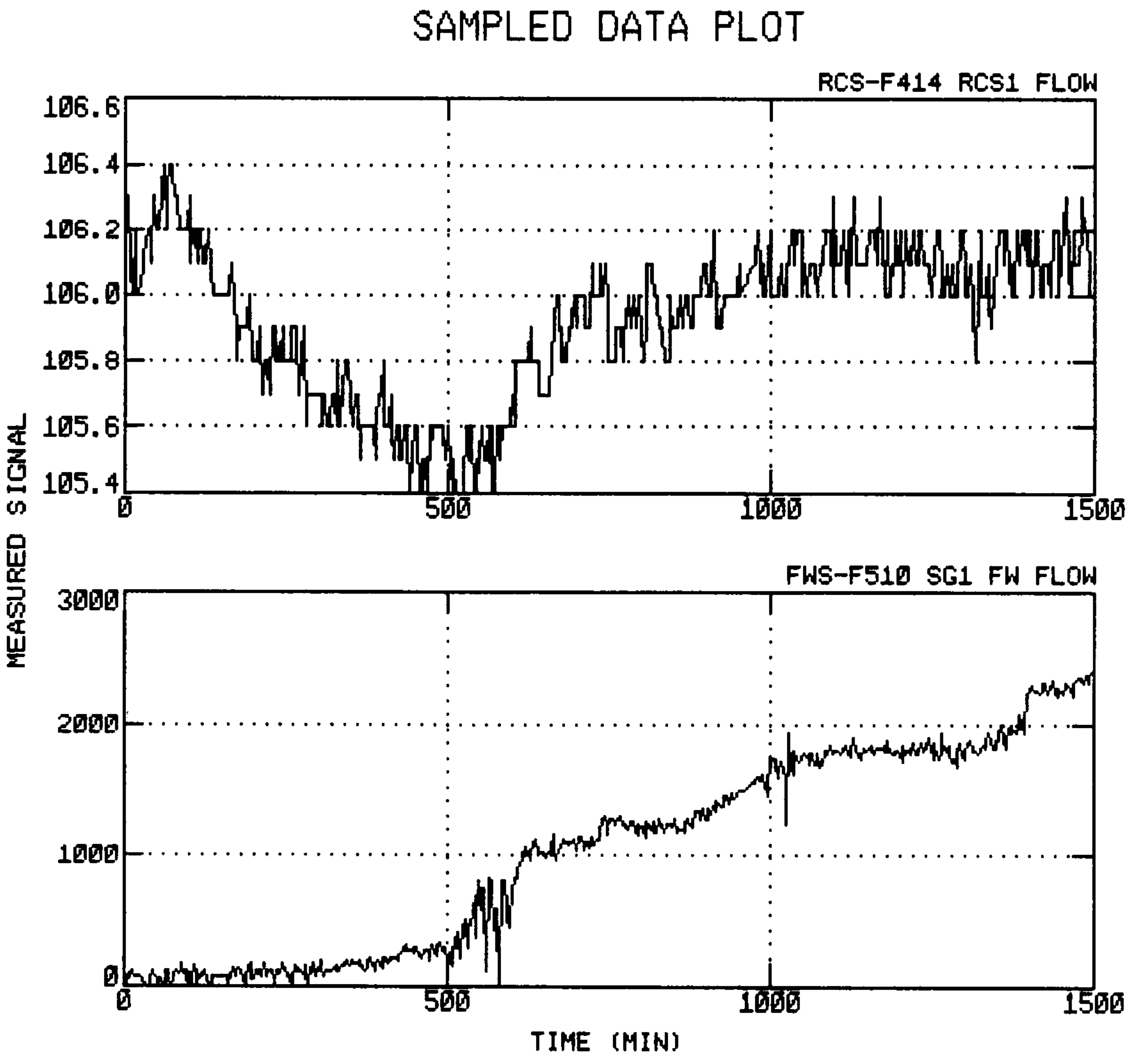

Figure A.2. PWR Process Signals.
Top: RCS Flow Signal.
Bottom: Feedwater Flow Signal.

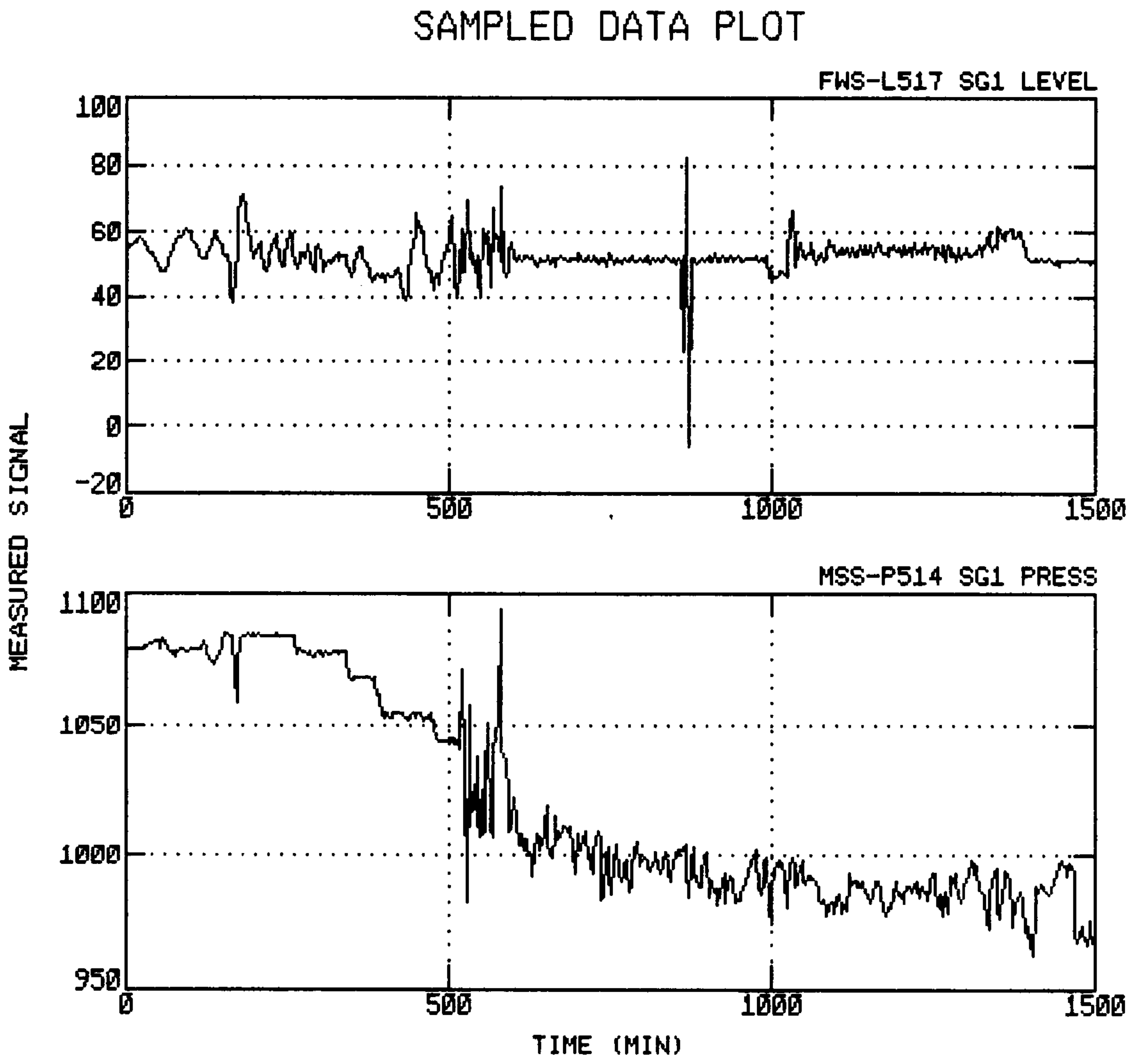

Figure A.2. PWR Process Signals.
Top: Steam Generator Level Signal.
Bottom: Steam Pressure Signal.

APPENDIX B

EBR-II DATA

Operational data were acquired from the Experimental Breeder Reactor II (EBR-II). The EBR-II is a liquid metal, pool-type fast reactor operated by the Argonne National Laboratory (ANL) in Idaho. Figure B.1 shows a schematic of the plant. One data set was taken during a reactor start-up, and was sampled every five seconds for a period of six hours. A second data set was from steady-state full-power operation of the reactor, and was sampled every minute for a period of one week. The available process signals and tolerances are given in Tables B.1 and B.2, respectively. Representative plots of some signals are given in Figure B.2.

The EBR-II plant consists of a primary and a secondary system both using liquid sodium as the coolant, and a conventional steam system. The primary system is completely enclosed in a large double-walled tank. The two primary pumps take their suction directly from the tank for delivery to the reactor. At full power the reactor produces 62.5MWt. An intermediate heat exchanger (IHX) transfers the heat to the secondary sodium. The primary sodium leaving the IHX dumps directly back into the primary tank. The secondary system heat is transferred to a steam system which consists of seven evaporators and two superheaters. The steam is used in a turbine-generator to produce electricity.

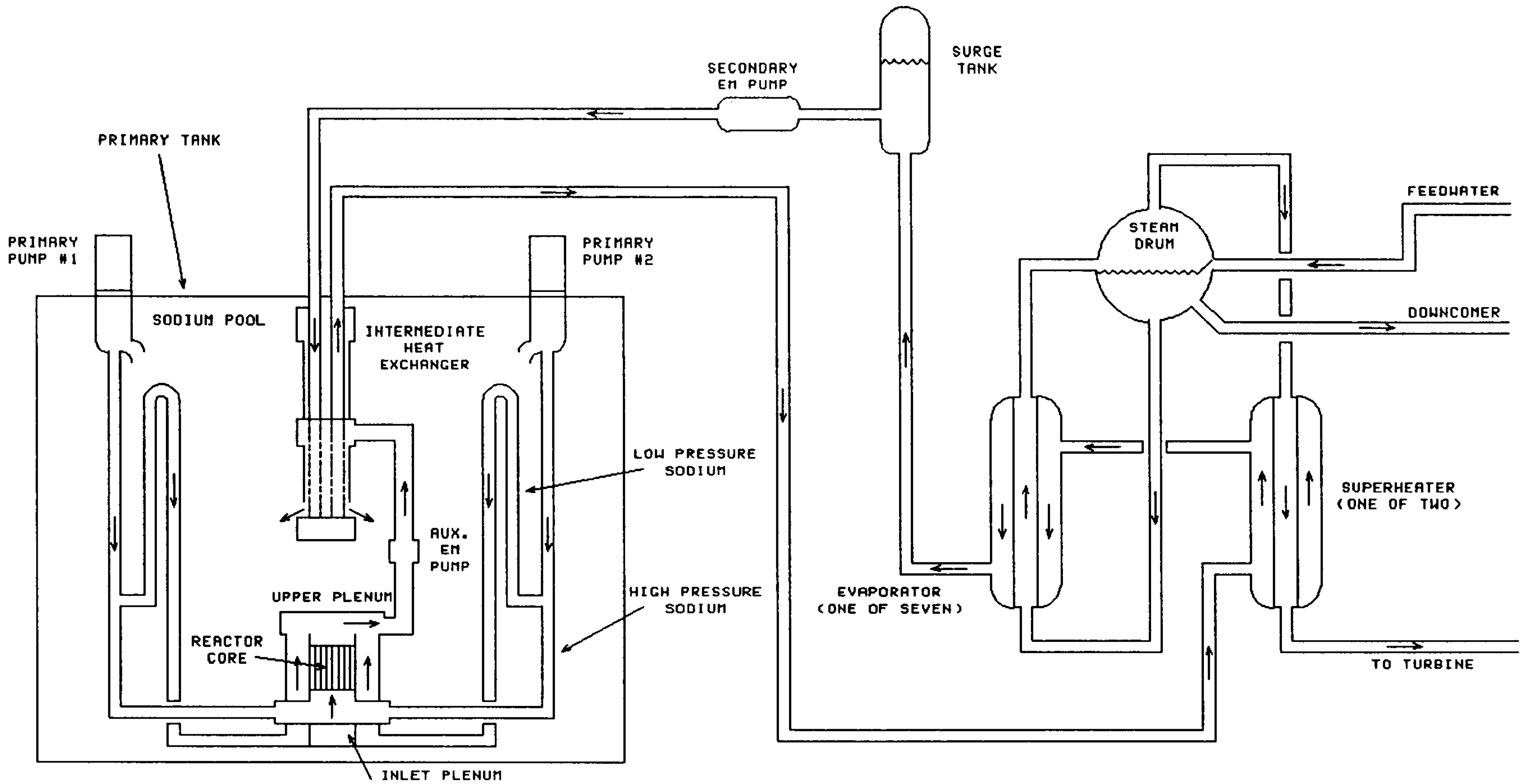

Figure B.1. EBR-II System Schematic.

TABLE B.1

EBR-II Process Signals

Signal Number	Sensor Tag Number	Signal Description
1.	R1-NLC-580	Power Level (%)
2.	P1-NLC-581	Power Level (%)
3.	P1-NLC-582	Power Level (%)
4.	P1-BAM-594A	Control Rod #1 Position (in)
5.	P1-BAM-594C	Control Rod #3 Position (in)
6.	P1-BAM-594D	Control Rod #4 Position (in)
7.	P1-BAM-594E	Control Rod #5 Position (in)
8.	P1-BAM-594G	Control Rod #7 Position (in)
9.	P1-BAM-594K	Control Rod #9 Position (in)
10.	P1-BAM-594L	Control Rod #10 Position (in)
11.	P1-BAM-594M	Control Rod #11 Position (in)
12.	P1-BAM-594N	Control Rod #12 Position (in)
13.	R1-FM-512B	Primary Pump 2 Out Flow (%)
14.	R1-FM-513B	Low Pressure Plenum 2 Flow (%)
15.	R1-FM-541E	Primary Total Flow (%)
16.	R1-DPT-521A	Upper Plenum Flow (%)
17.	R1-DPT-521B	Upper Plenum Flow (%)
18.	R1-DPT-521A	Upper Plenum Pressure (psi)
19.	R1-DPT-521B	Upper Plenum Pressure (psi)
20.	R1-PT-522A	Primary Pump 1 Pressure (psi)
21.	R1-TC-540AR	Lo Pressure Plenum Na Temp (°F)
22.	R1-TC-540AS	Lo Pressure Plenum Na Temp (°F)
23.	R1-TC-540AV	Lo Pressure Plenum Na Temp (°F)
24.	R1-TC-540AT	Hi Pressure Plenum Na Temp (°F)
25.	R1-TC-503AA	Rx Core Exit Temperature (°F)
26.	R1-TC-503H	Rx Core Exit Temperature (°F)
27.	R1-TC-503E	Rx Core Exit Temperature (°F)
28.	R1-TC-503D	Rx Core Exit Temperature (°F)
29.	R1-TC-503P	Rx Core Exit Temperature (°F)
30.	R1-TC-503K	Rx Core Exit Temperature (°F)
31.	R1-TC-503F	Rx Core Exit Temperature (°F)
32.	R1-TC-503C	Rx Core Exit Temperature (°F)
33.	R1-TC-503T	Rx Core Exit Temperature (°F)
34.	R1-TC-503G	Rx Core Exit Temperature (°F)
35.	R1-TC-503AC	Rx Core Exit Temperature (°F)
36.	R1-TC-503Z	Rx Core Exit Temperature (°F)
37.	R1-TC-503V	Rx Core Exit Temperature (°F)
38.	R1-TC-503Q	Rx Core Exit Temperature (°F)
39.	R1-TC-503Y	Rx Core Exit Temperature (°F)

TABLE B.1 (Continued)

Signal Number	Sensor Tag Number	Signal Description
40.	R1-TC-503N	Rx Core Exit Temperature (°F)
41.	R1-TC-503AB	Rx Core Exit Temperature (°F)
42.	R1-TC-503AD	Rx Core Exit Temperature (°F)
43.	R1-TC-503R	Rx Core Exit Temperature (°F)
44.	R1-TC-503X	Rx Core Exit Temperature (°F)
45.	R1-TC-503W	Rx Core Exit Temperature (°F)
46.	R1-TC-521A	Upper Plenum Temperature (°F)
47.	R1-TC-521B	Upper Plenum Temperature (°F)
48.	R1-TC-521C	Upper Plenum Temperature (°F)
49.	R1-TC-521D	Upper Plenum Temperature (°F)
50.	R1-TC-521E	Upper Plenum Temperature (°F)
51.	R1-TC-521F	Upper Plenum Temperature (°F)
52.	R1-TC-521G	Upper Plenum Temperature (°F)
53.	R1-TC-521H	Upper Plenum Temperature (°F)
54.	R1-TC-507CC	IHX Orifice Plate Temp (°F)
55.	R1-TC-507BX	IHX Orifice Plate Temp (°F)
56.	R1-TC-507EF	IHX Orifice Plate Temp (°F)
57.	R1-TC-507CA	IHX Orifice Plate Temp (°F)
58.	R1-TC-507CG	IHX Orifice Plate Temp (°F)
59.	R1-TC-540AC	IHX Primary Outlet Temp (°F)
60.	R1-TC-540AE	IHX Primary Outlet Temp (°F)
61.	R1-TC-540AM	IHX Primary Outlet Temp (°F)
62.	R1-TC-540AP	IHX Primary Outlet Temp (°F)
63.	R1-TC-501T	Bulk Na Pool Temperature (°F)
64.	R1-TC-501X	Bulk Na Pool Temperature (°F)
65.	R1-TC-501AA	Bulk Na Pool Temperature (°F)
66.	R1-TC-501D	Bulk Na Pool Temperature (°F)
67.	R1-TC-501M	Bulk Na Pool Temperature (°F)
68.	R1-TC-501V	Bulk Na Pool Temperature (°F)
69.	R1-TC-501H	Bulk Na Pool Temperature (°F)
70.	R1-TC-501E	Bulk Na Pool Temperature (°F)
71.	R1-TC-501N	Bulk Na Pool Temperature (°F)
72.	R1-TC-501W	Bulk Na Pool Temperature (°F)
73.	R1-TC-501Z	Bulk Na Pool Temperature (°F)
74.	R1-TC-501F	Bulk Na Pool Temperature (°F)
75.	R1-TC-501P	Bulk Na Pool Temperature (°F)
76.	R2-RT-533AA	IHX Secondary Outlet Temp (°F)
77.	R2-TC-546A	IHX Secondary Outlet Temp (°F)
78.	B2-TC-508A	SU Na Inlet Header Temp (°F)
79.	B2-TC-546H	SU Na Inlet Header Temp (°F)
80.	B2-TC-546J	SU Na Inlet Header Temp (°F)
81.	B2-TC-546L	SU 710 Na Inlet Temp (°F)

TABLE B.1 (Continued)

Signal Number	Sensor Tag Number	Signal Description
82.	B2-TC-546K	SU 710 Na Inlet Temp (°F)
83.	B2-TC-546N	SU 712 Na Inlet Temp (°F)
84.	B2-TC-546P	SU 712 Na Inlet Temp (°F)
85.	B2-TC-546Q	SU 712 Na Inlet Temp (°F)
86.	B2-TC-555B	SU 710 Na Outlet Temp (°F)
87.	B2-TC-546S	SU 710 Na Outlet Temp (°F)
88.	B2-TC-546BB	SU 710 Na Outlet Temp (°F)
89.	B2-TC-546U	SU 712 Na Outlet Temp (°F)
90.	B2-TC-546BC	SU 712 Na Outlet Temp (°F)
91.	B2-TC-555D	SU 712 Na Outlet Temp (°F)
92.	B2-TC-546AA	EV 701 Na Inlet Temp (°F)
93.	B2-TC-546AB	EV 702 Na Inlet Temp (°F)
94.	B2-TC-546AC	EV 703 Na Inlet Temp (°F)
95.	B2-TC-546BA	EV 704 Na Inlet Temp (°F)
96.	B2-TC-546AE	EV 705 Na Inlet Temp (°F)
97.	B2-TC-546AK	EV 705 Na Inlet Temp (°F)
98.	B2-TC-546AF	EV 707 Na Inlet Temp (°F)
99.	B2-TC-546AG	EV 708 Na Inlet Temp (°F)
100.	R1-TC-555E	EV 701 Na Outlet Temp (°F)
101.	B2-TC-555F	EV 702 Na Outlet Temp (°F)
102.	B2-TC-546AH	EV 702 Na Outlet Temp (°F)
103.	R1-TC-555G	EV 703 Na Outlet Temp (°F)
104.	B2-TC-555H	EV 704 Na Outlet Temp (°F)
105.	B2-TC-546AD	EV 704 Na Outlet Temp (°F)
106.	R1-TC-555K	EV 705 Na Outlet Temp (°F)
107.	R1-TC-546AJ	EV 705 Na Outlet Temp (°F)
108.	R1-TC-555N	EV 707 Na Outlet Temp (°F)
109.	B2-TC-555P	EV 708 Na Outlet Temp (°F)
110.	R2-TC-546AR	IHX Secondary Inlet Temp (°F)
111.	R2-RT-533BB	IHX Secondary Inlet Temp (°F)
112.	B2-FM-539	SU 710 Na Outlet Flow (Volt)
113.	B2-FM-539	SU 712 Na Outlet Flow (Volt)
114.	B2-FM-538	EV 704 Na Inlet Flow (Volt)
115.	B2-FM-538	EV 705 Na Inlet Flow (Volt)
116.	S2-FM-516	Secondary Pump Inlet Flow (%)
117.	B2-PT-527	SU Na Inlet Pressure (psi)
118.	P3-PT-501A	Turbine Inlet Pressure (psi)
119.	P3-FT-587	Blowdown Flow (lbm/hr)
120.	S5-LT-596	Steam Drum Level (in)
121.	B3-PT-505	Steam Drum Pressure (psig)
122.	P3-FT-590	Steam Drum Feedwater Flow (lbm/hr)
123.	B5-FT-594	Steam Drum Feedwater Flow (lbm/hr)

TABLE B.1 (Continued)

Signal Number	Sensor Tag Number	Signal Description
124.	B5-PR-503	Steam Drum Feedwater Press (psi)
125.	P5-TC-552	Steam Drum Feedwater Temp (°F)
126.	B5-RTT-1600	Steam Drum Feedwater Temp (°F)
127.	B5-TC-555S	EV 701 Feedwater Temp (°F)
128.	B5-TC-555T	EV 702 Feedwater Temp (°F)
129.	R1-TC-555V	EV 703 Feedwater Temp (°F)
130.	B5-TC-555W	EV 704 Feedwater Temp (°F)
131.	B3-TC-546AZ	EV 704 Feedwater Temp (°F)
132.	R1-TC-555X	EV 705 Feedwater Temp (°F)
133.	R1-TC-546AS	EV 705 Feedwater Temp (°F)
134.	B3-TC-546AT	EV 705 Feedwater Temp (°F)
135.	R1-TC-555Z	EV 707 Feedwater Temp (°F)
136.	B5-TC-555AA	EV 708 Feedwater Temp (°F)
137.	B3-TC-555AB	EV 701 Steam Outlet Temp (°F)
138.	B3-TC-555AC	EV 702 Steam Outlet Temp (°F)
139.	B3-TC-555AD	EV 703 Steam Outlet Temp (°F)
140.	B3-TC-555AE	EV 704 Steam Outlet Temp (°F)
141.	B3-TC-555AF	EV 705 Steam Outlet Temp (°F)
142.	B3-TC-555AH	EV 707 Steam Outlet Temp (°F)
143.	B3-TC-555AK	EV 708 Steam Outlet Temp (°F)
144.	B3-TC-546AU	SU 710 Steam Inlet Temp (°F)
145.	B3-TC-546AV	SU 712 Steam Inlet Temp (°F)
146.	B3-TC-546AW	SU 710 Steam Outlet Temp (°F)
147.	B3-TC-555AN	SU 710 Steam Outlet Temp (°F)
148.	B3-TC-546AX	SU 712 Steam Outlet Temp (°F)
149.	B3-TC-555AQ	SU 712 Steam Outlet Temp (°F)
150.	B3-PT-520	SU Outlet Pressure (psig)
151.	P5-FT-580	SU Outlet Flow (lbm/hr)
152.	P3-FT-588	Turbine Inlet Steam Flow (lbm/hr)
153.	P3-PT-501B	Turbine Inlet Steam Press (psig)
154.	P3-TC-545	Turbine Inlet Steam Temp (°F)

Number of Data Channels : 154
Number of Data Samples per Channel : 4300
Sampling Interval (seconds) : 5.0

TABLE B.2

EBR-II Signal Tolerances

Signal	Tolerance	Span
Reactor Power	± 2 %	n/a
Control Rod Position	± 0.1 in	0 - 14 in
Primary Flows	± 1.05 %	0 - 105 %
Primary Low Pressures	± 0.075 psi	0 - 10 psi
Primary High Pressures	± 1 psi	0 - 100 psi
Inlet Plenum Na Temperature	± 23 °F	0 - 2300 °F
Core-Exit Na Temperature	± 23 °F	0 - 2300 °F
Upper Plenum Na Temperature	± 23 °F	0 - 2300 °F
IHX Orifice Plate Temperature	± 23 °F	0 - 2300 °F
IHX Primary Outlet Temperature	± 23 °F	0 - 2300 °F
Bulk Na Pool Temperature	± 23 °F	0 - 2300 °F
IHX Secondary Outlet Temperature	± 23 °F	0 - 2300 °F
IHX Secondary Inlet Temperature	± 23 °F	0 - 2300 °F
SU Na Inlet Temperature	± 23 °F	0 - 2300 °F
SU Na Outlet Temperature	± 23 °F	0 - 2300 °F
SU Na Outlet Flow	± 0.1 V	0 - 10 V
EV Na Inlet Temperature	± 23 °F	0 - 2300 °F
EV Na Outlet Temperature	± 23 °F	0 - 2300 °F
EV Na Inlet Flow	± 0.1 V	0 - 10 V
Secondary Pump Inlet Flow	± 1 %	0 - 100 %
SU Na Inlet Pressure	± 1 psi	0 - 50 psi
Turbine Inlet Pressure	± 37.5 psi	0 - 2500 psi
Blowdown Flow	± 200 pph	0 - 20000 pph
Steam Drum Level	± 0.36 in	0 - 36 in
Steam Drum Steam Pressure	± 25 psi	0 - 2500 psi
Steam Drum Feedwater Flow	± 3000 pph	0 - 300000 pph
Steam Drum Feedwater Pressure	± 25 psi	0 - 2500 psi
Steam Drum Feedwater Temp #125	± 23 °F	0 - 2300 °F
Steam Drum Feedwater Temp #126	± 10 °F	0 - 1000 °F
EV Feedwater Temperature	± 23 °F	0 - 2300 °F
EV Steam Outlet Temperature	± 23 °F	0 - 2300 °F
SU Steam Inlet Temperature	± 23 °F	0 - 2300 °F
SU Steam Outlet Temperature	± 23 °F	0 - 2300 °F
SU Outlet Pressure	± 50 psi	0 - 2500 psi
SU Outlet Flow	± 3000 pph	0 - 300000 pph
Turbine Inlet Steam Flow	± 2500 pph	0 - 250000 pph
Turbine Inlet Steam Pressure	± 25 psi	0 - 2500 psi
Turbine Inlet Steam Temperature	± 10 °F	0 - 1000 °F

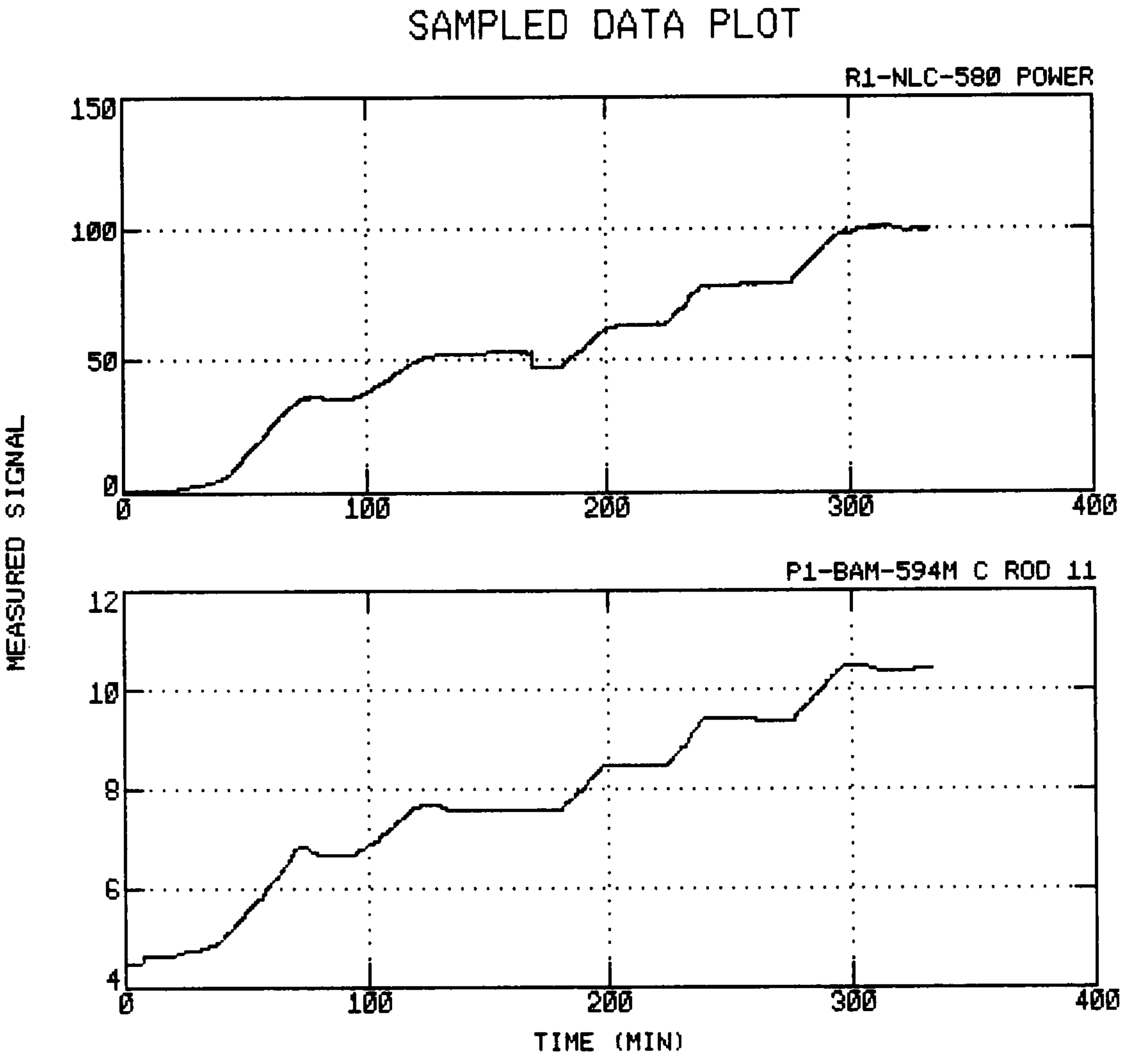

Figure B.2. EBR-II Process Signals.
Top: Power Signal.
Bottom: Control Rod Position.

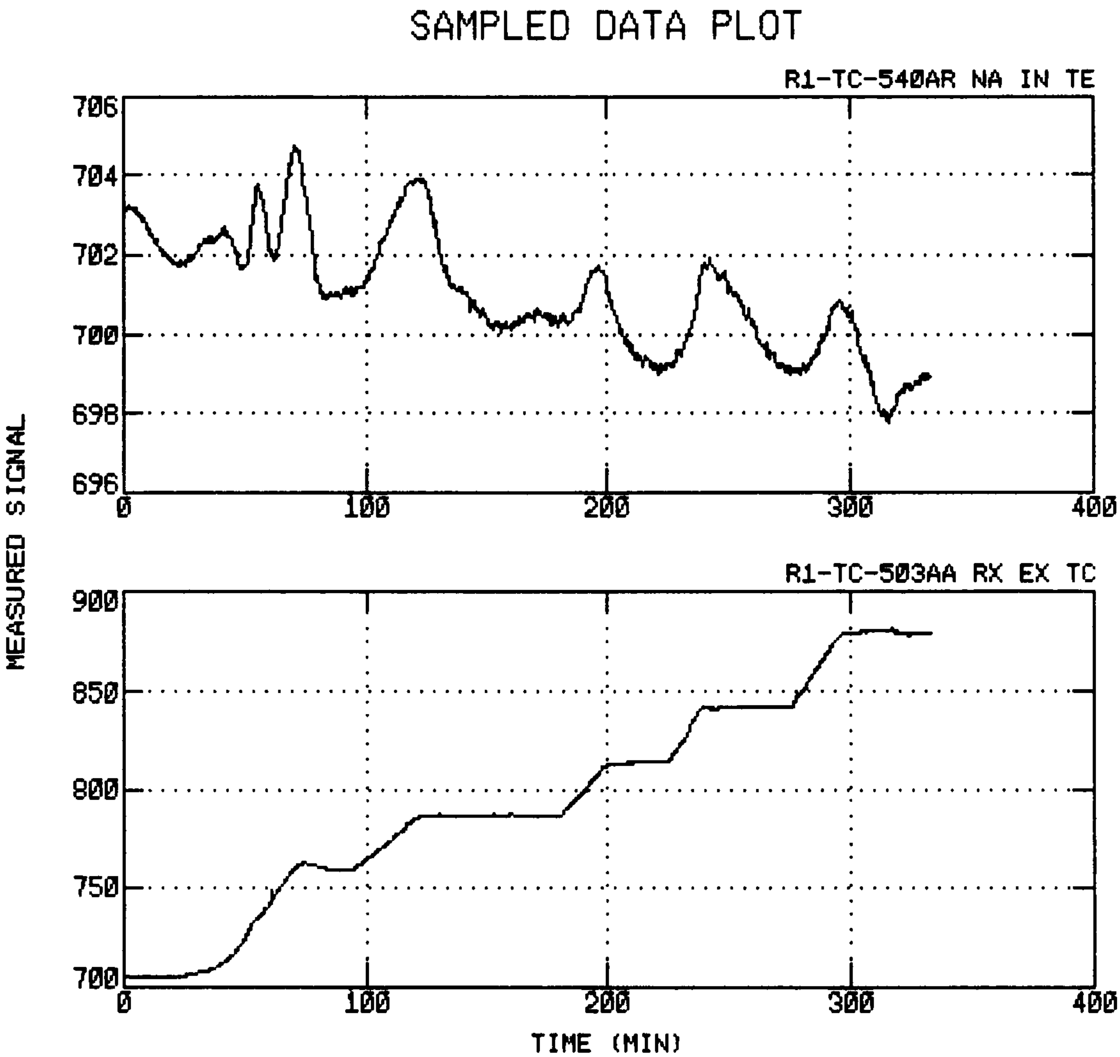

Figure B.2. EBR-II Process Signals.
Top: Inlet Plenum Sodium Temperature Signal.
Bottom: Core-Exit Temperature Signal.

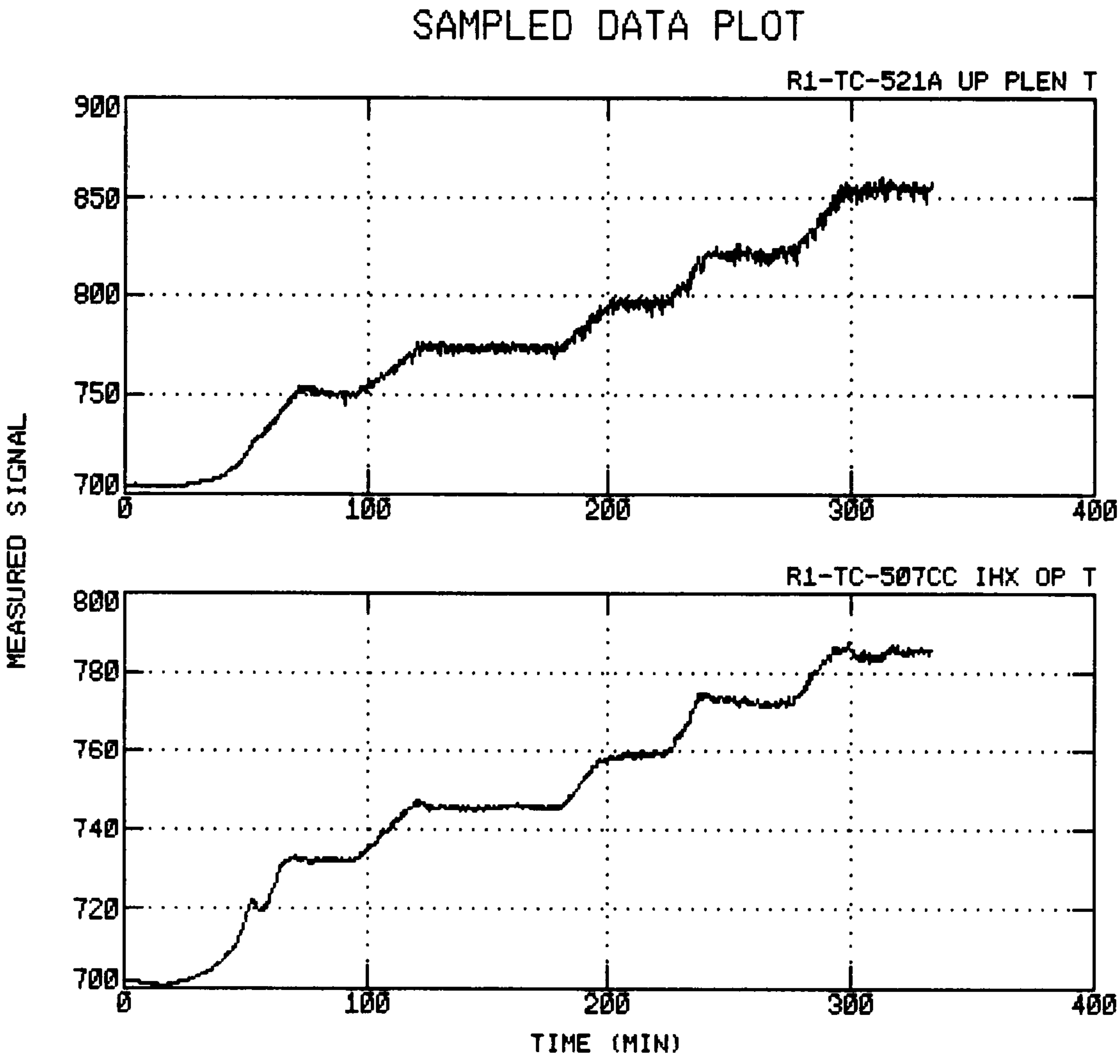

Figure B.2. EBR-II Process Signals.
Top: Upper Plenum Temperature Signal.
Bottom: IHX Orifice Plate Temperature Signal.

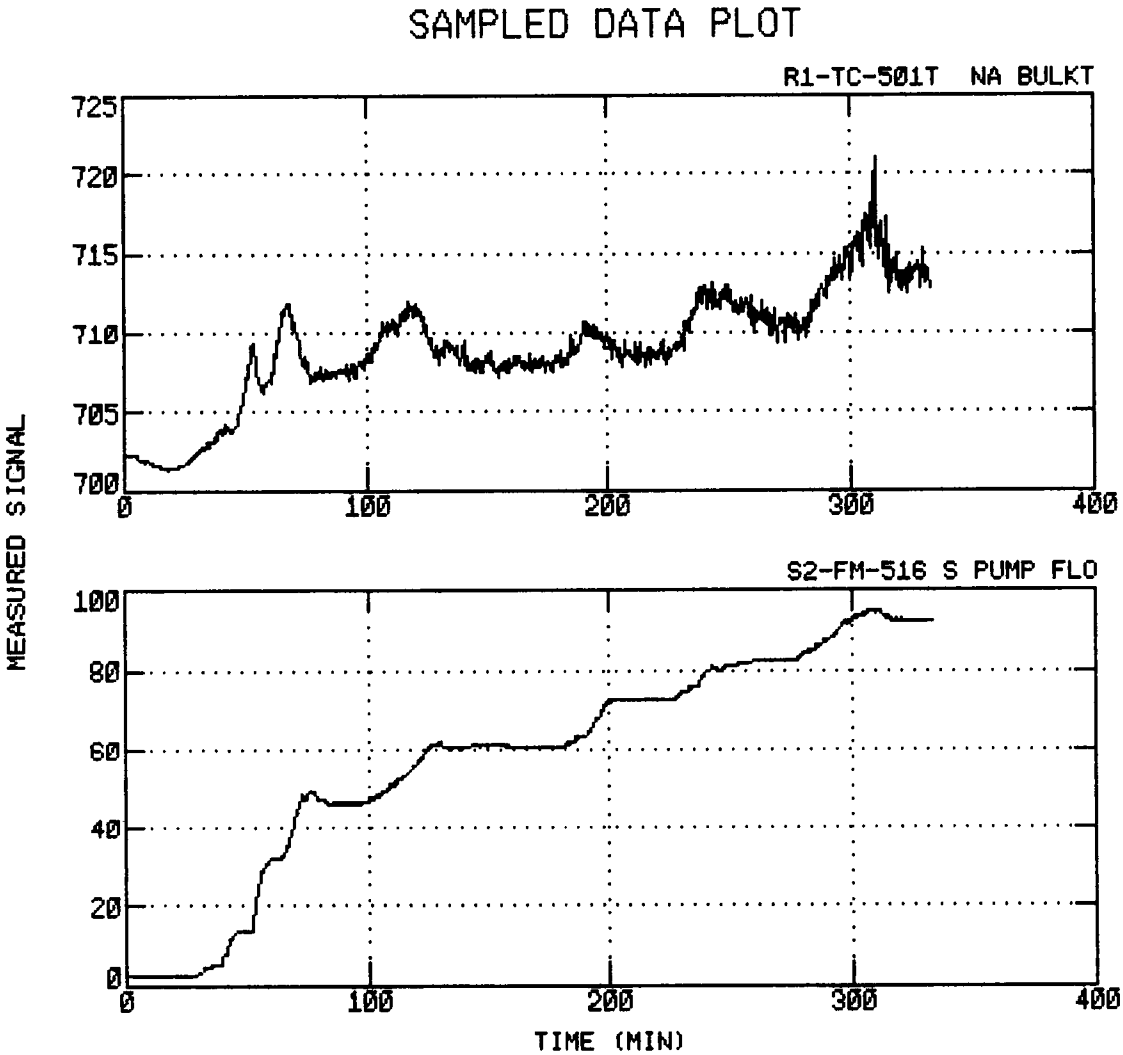

Figure B.2. EBR-II Process Signals.
Top: Bulk Sodium Pool Temperature Signal.
Bottom: Secondary Sodium Flow Signal.

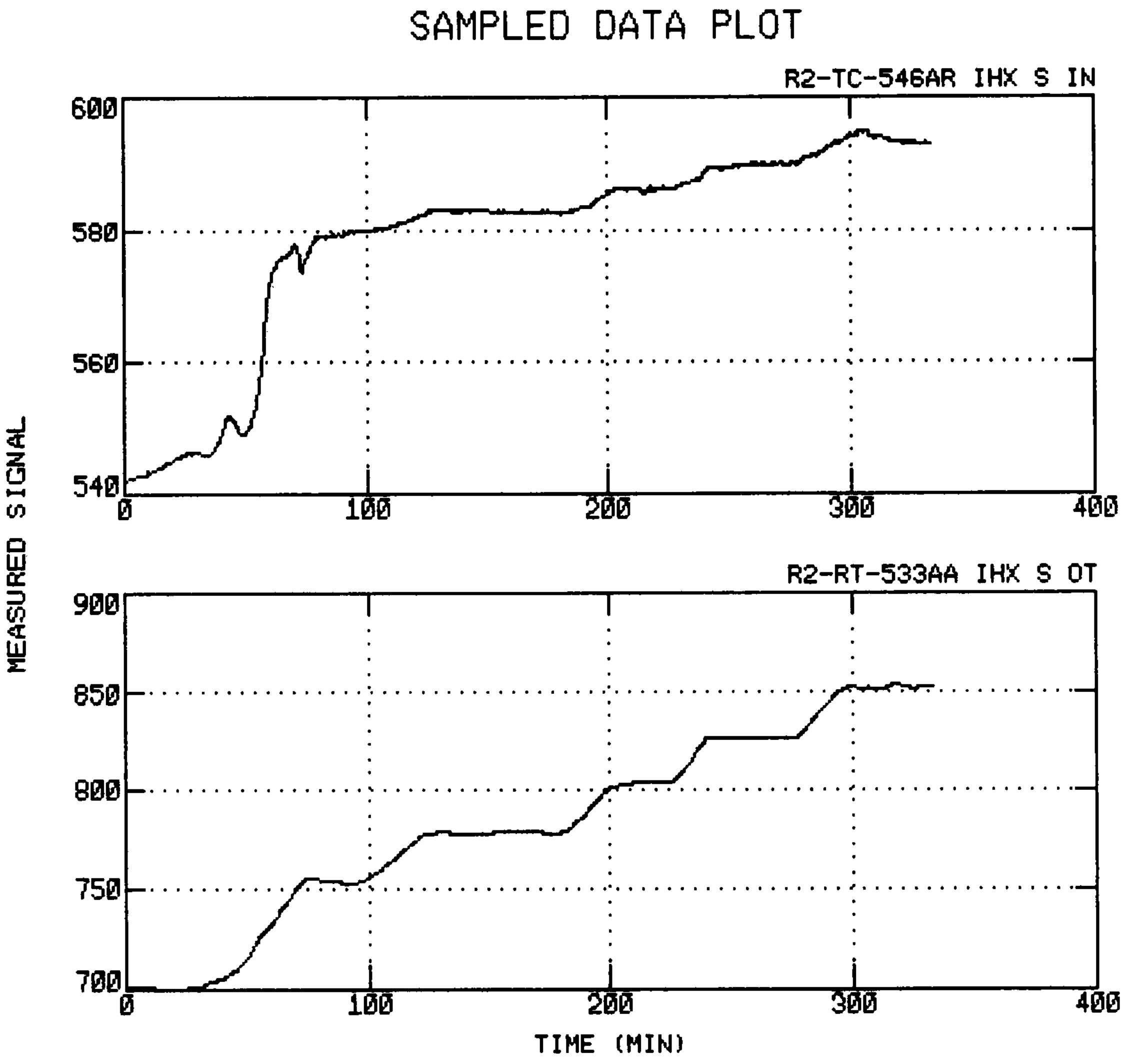

Figure B.2. EBR-II Process Signals.
Top: IHX Secondary Inlet Temperature Signal.
Bottom: IHX Secondary Outlet Temperature Signal.

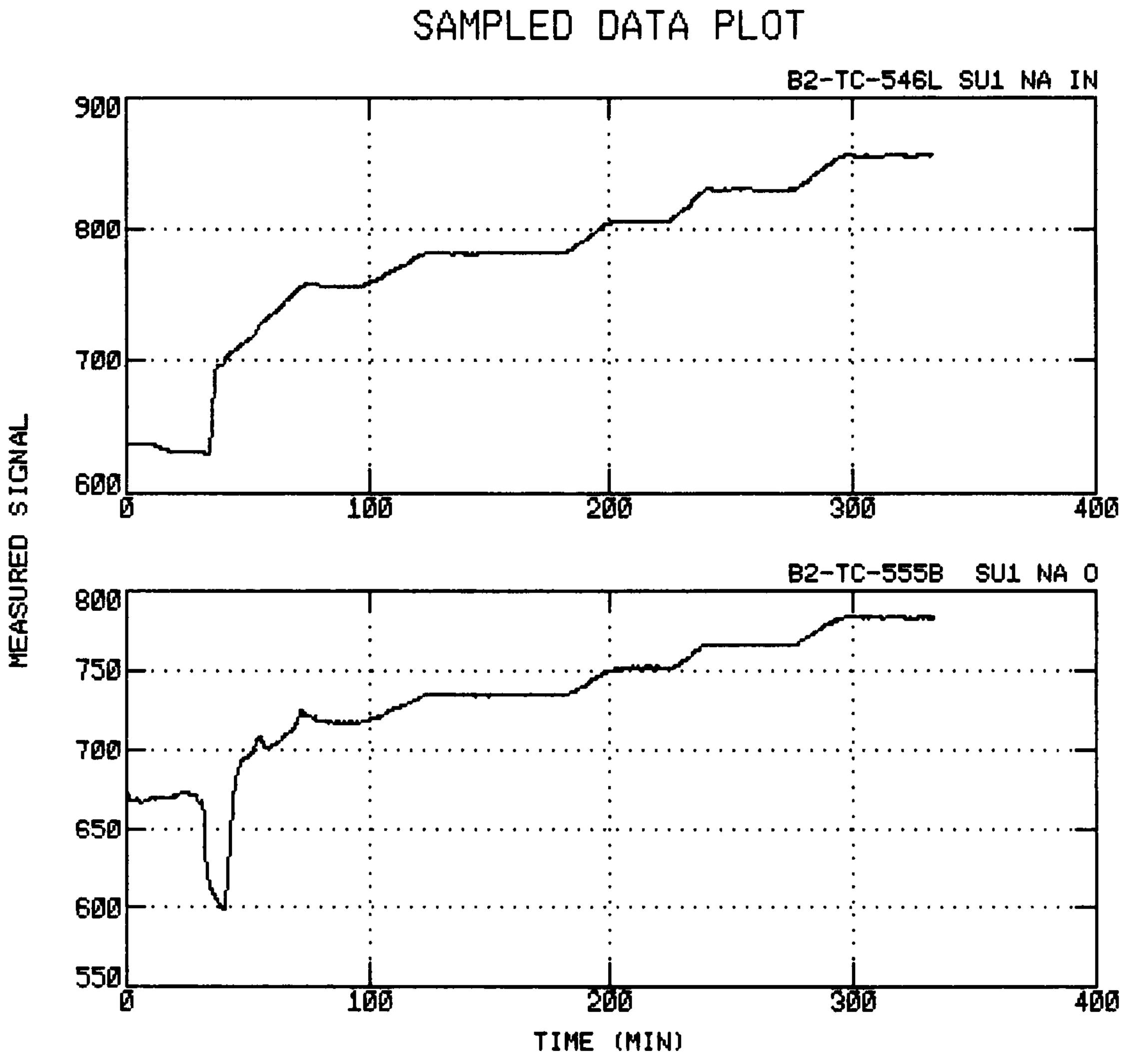

Figure B.2. EBR-II Process Signals.
Top: Superheater Sodium Inlet Temperature.
Bottom: Superheater Sodium Outlet Temperature.

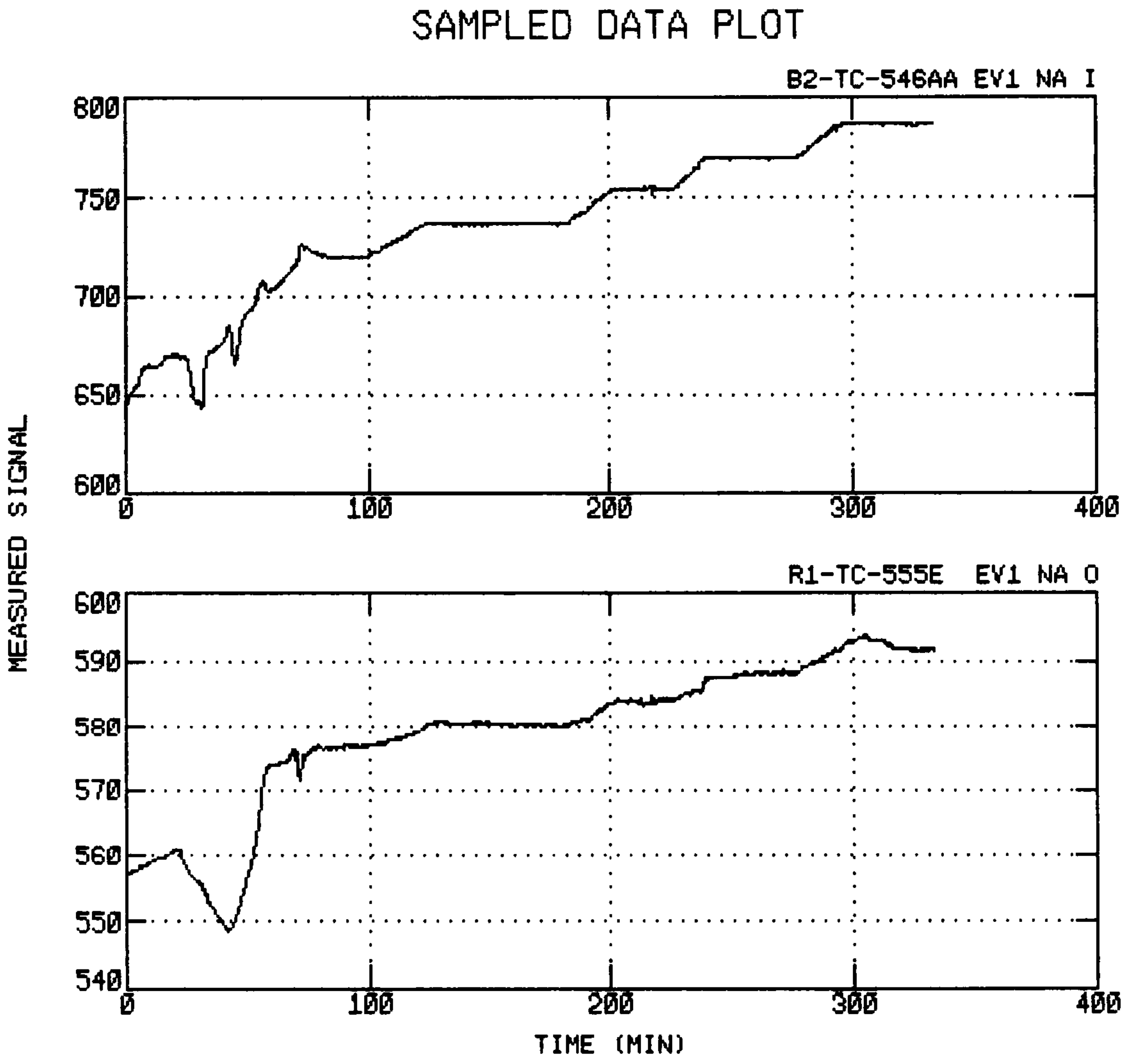

Figure B.2. EBR-II Process Signals.
Top: Evaporator Sodium Inlet Temperature.
Bottom: Evaporator Sodium Outlet Temperature.

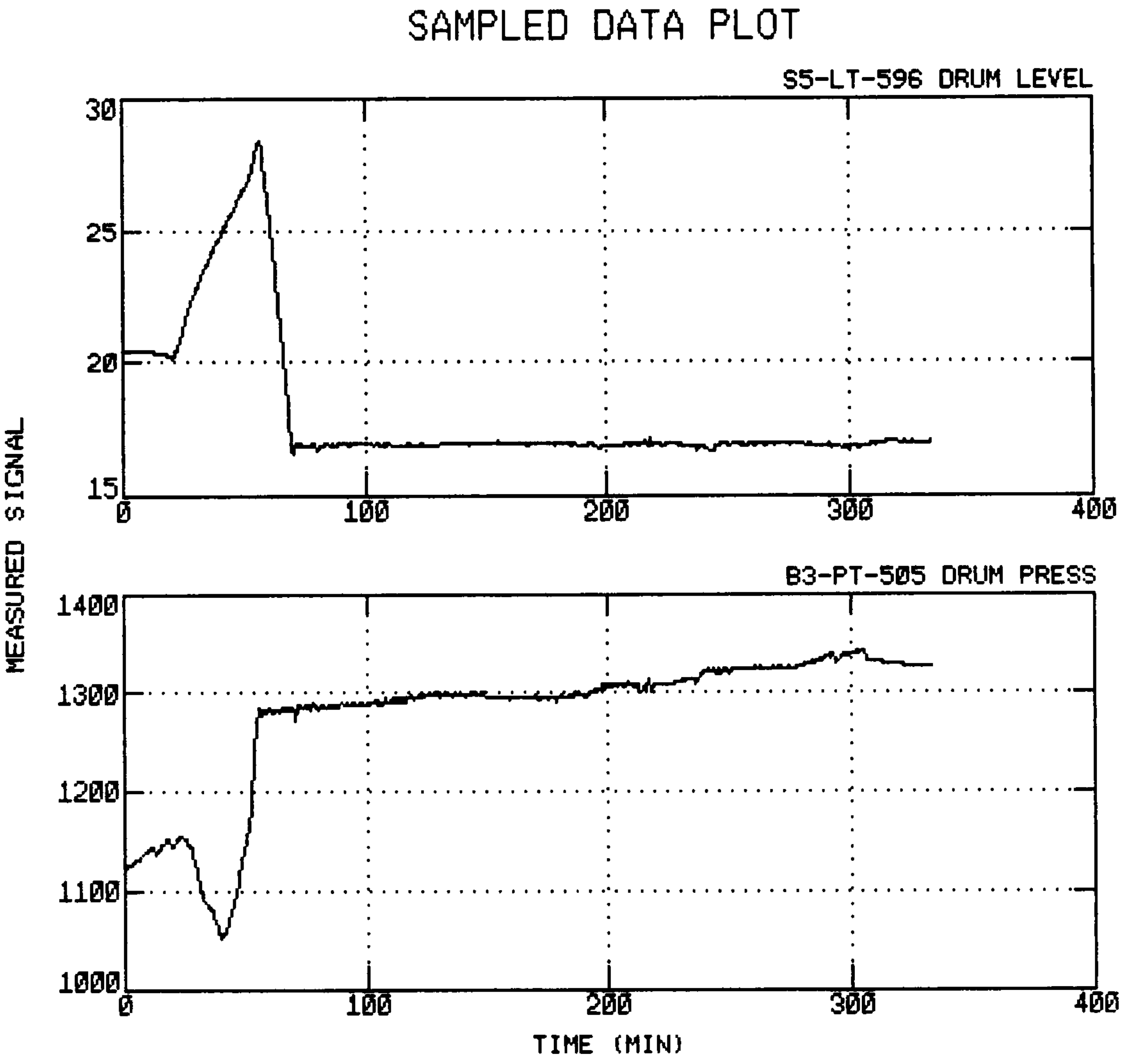

Figure B.2. EBR-II Process Signals.
Top: Steam Drum Level Signal.
Bottom: Steam Drum Steam Pressure Signal.

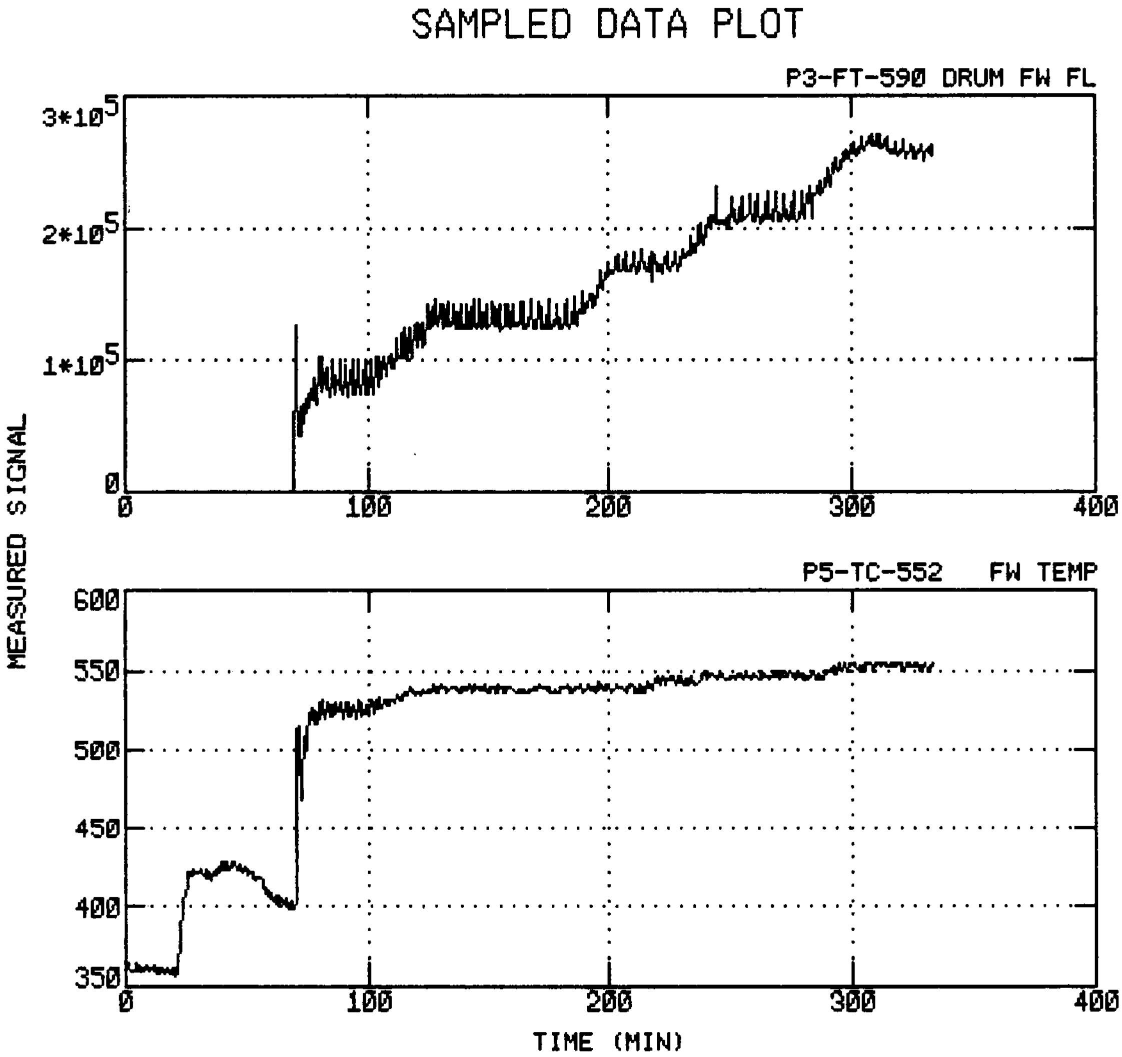

Figure B.2. EBR-II Process Signals.
Top: Steam Drum Feedwater Flow Signal.
Bottom: Feedwater Temperature Signal.

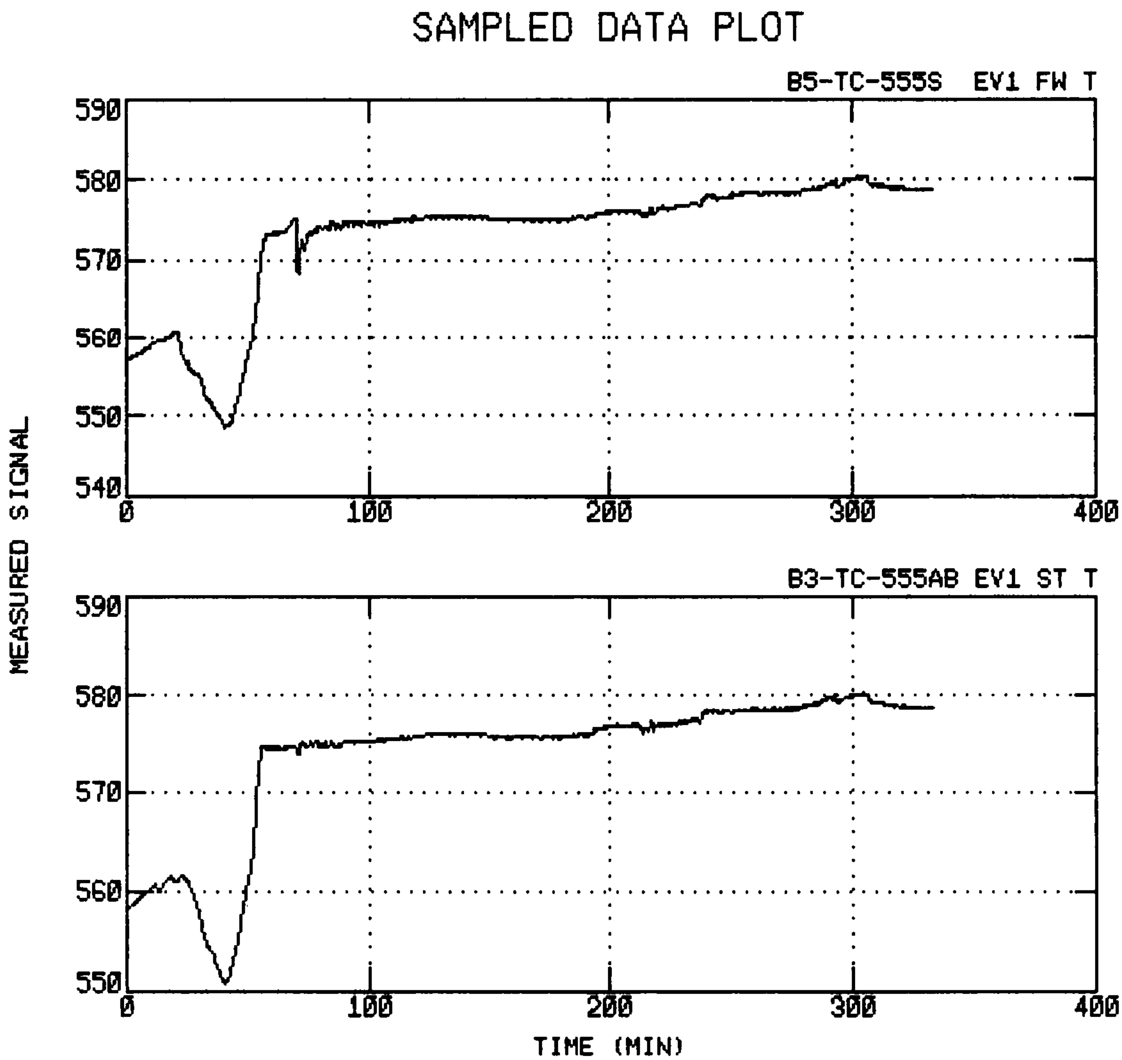

Figure B.2. EBR-II Process Signals.
Top: Evaporator Feedwater Temperature Signal.
Bottom: Evaporator Steam Temperature Signal.

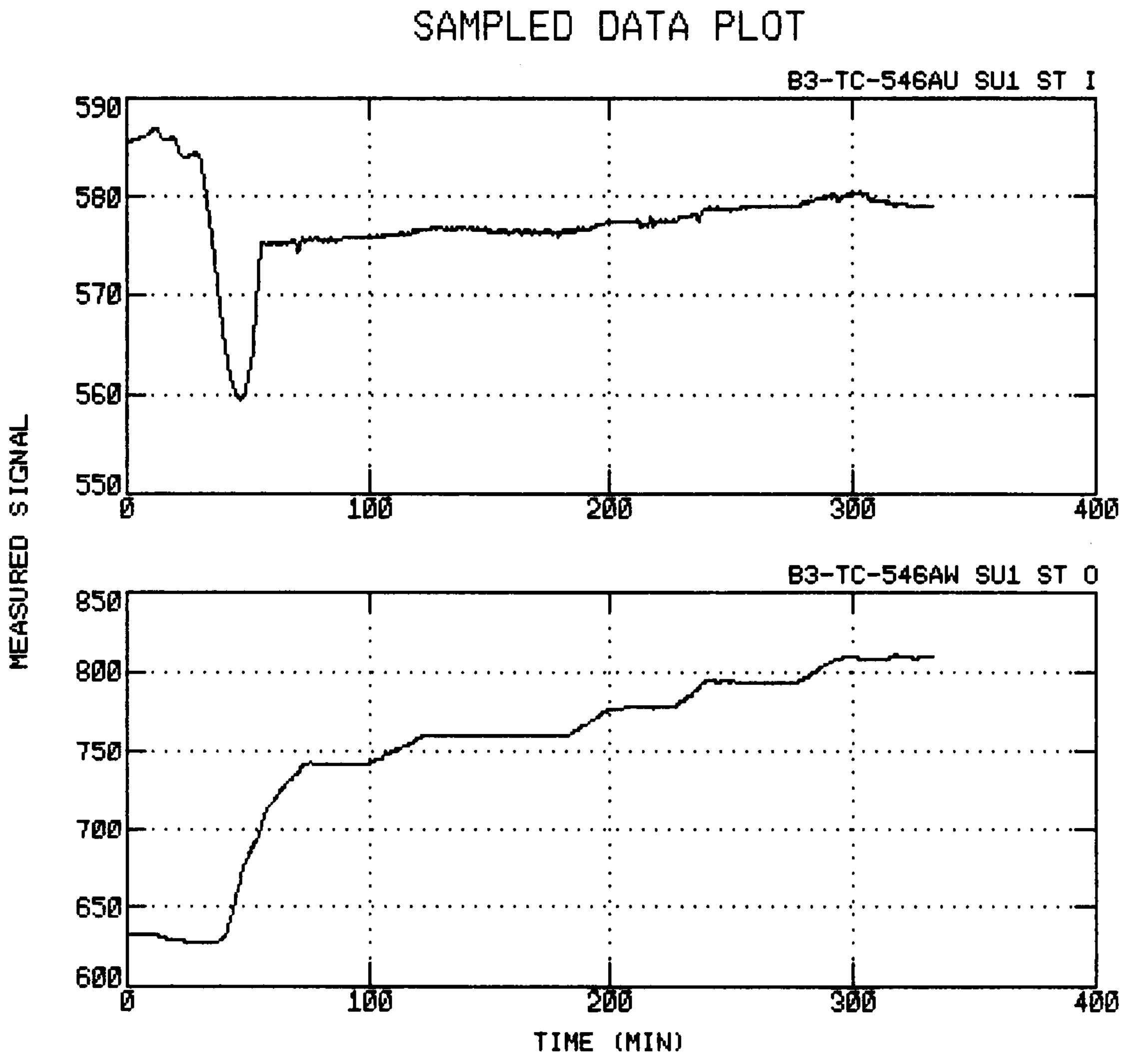

Figure B.2. EBR-II Process Signals.
Top: Superheater Steam Inlet Temperature.
Bottom: Superheater Steam Outlet Temperature.

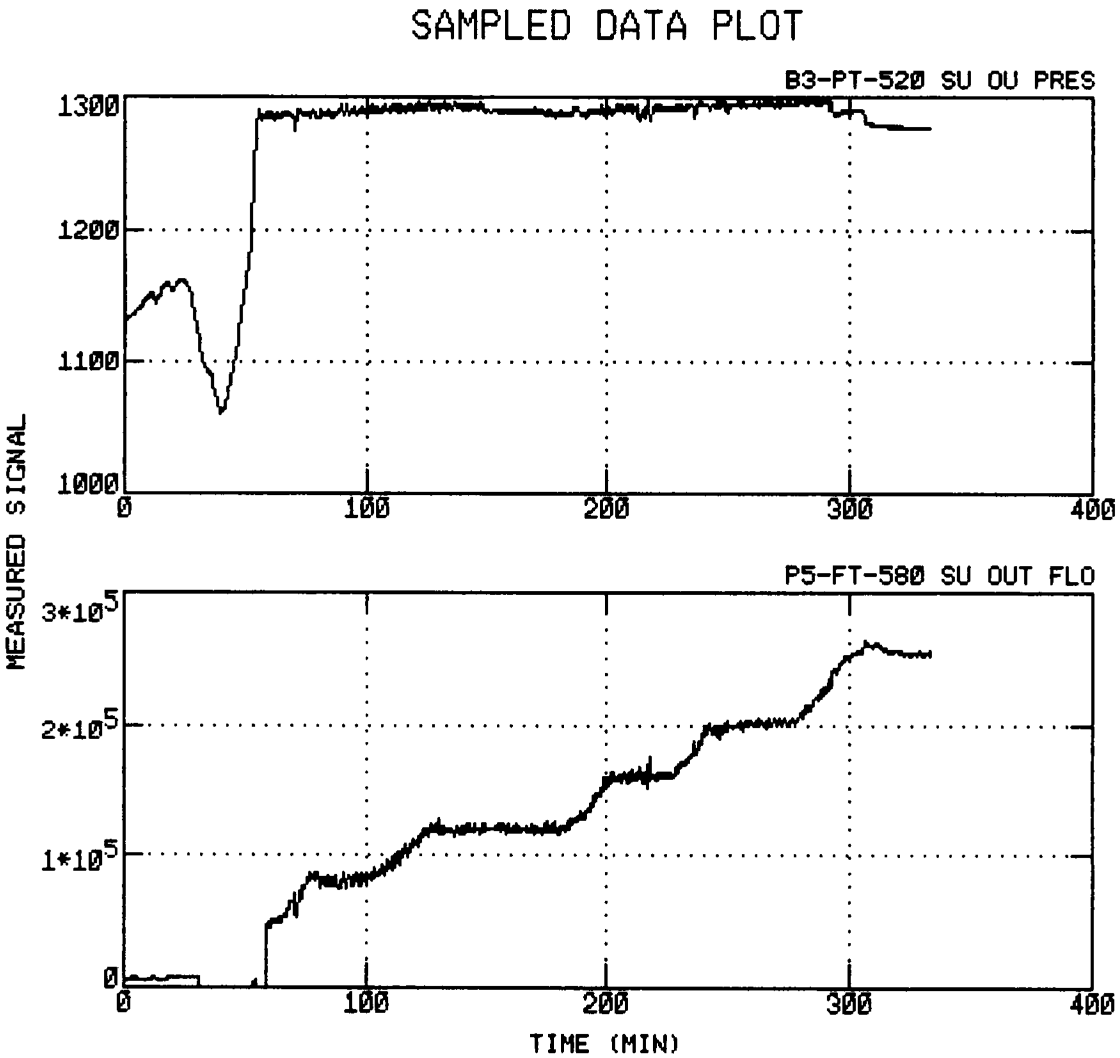

Figure B.2. EBR-II Process Signals.
Top: Superheater Steam Outlet Pressure Signal.
Bottom: Superheater Steam Outlet Flow Signal.

APPENDIX C

DATA FILE STRUCTURE

There are three files containing all the necessary information about the sampled data. The first is the sampling parameter file which contains information such as the number of data channels, number of data samples per channel and the data sampling interval. The second file contains the actual data. Process noise data, when available, are placed in the third file. All files are essentially binary files, and allow the most efficient use of disk space and shortest access time.

C.1 Sampling Parameter File

The sampling parameter file is a direct access file with record length of 20 bytes each and a total number of records equal to NCHANNEL+1. The internal file structure is shown in Figure C.1. The full filename is {filename}.SAM. The sampling parameter file contains the number of data samples and signals, the data sampling interval, and the identification numbers of the individual signals.

C.2 Data File

The raw data file is also a direct access file with a record length of 4 bytes each. There are a total of NCHANNEL*NSAMPLE records in each data file. The data are

Record #1

Number of Data Channels NCHANNEL	Number of Samples/ Channel NSAMPLE	Sampling Interval (seconds) DELTAT	Reserved for Future Use (4 bytes)	Reserved for Future Use (4 bytes)

Record #2

Sensor (Signal) Tag Number or Identification Number and Abbreviated Description for the first signal in the data TAGNO(1)

Record #3

Sensor (Signal) Tag Number or Identification Number and Abbreviated Description for the second signal in the data TAGNO(2)

Record #4

Sensor (Signal) Tag Number or Identification Number and Abbreviated Description for the third signal in the data TAGNO(3)

.
.
.

Record #NCHANNEL+1

Sensor (Signal) Tag Number or Identification Number and Abbreviated Description for the last signal in the data TAGNO(NCHANNEL)

Figure C.1. Sampling File Structure.

addressed as X(I,J) where I is the channel (signal) number and J is the data sample number. The internal file structure is shown in Figure C.2. The full filename is {filename}.DAT. The data are stored as floating-point values.

C.3 Noise Data File

The noise data file is constructed identically to the raw data file, except that the filename should be {filename}.NOS. In the event there is no noise data available, the noise data file is not created.

Record #1

Signal #1 Sample #1 X(1,1)	Signal #2 Sample #1 X(2,1)	Signal #3 Sample #1 X(3,1)	....	Last Signal # Sample #1 X(NCHANNEL,1)

Record #2

Signal #1 Sample #2 X(1,2)	Signal #2 Sample #2 X(2,2)	Signal #3 Sample #2 X(3,2)	....	Last Signal # Sample #2 X(NCHANNEL,2)

Record #3

Signal #1 Sample #3 X(1,3)	Signal #2 Sample #3 X(2,3)	Signal #3 Sample #3 X(3,3)	....	Last Signal # Sample #3 X(NCHANNEL,3)

.
.
.

Record #NSAMPLE

Signal #1 Last Samp X(1,NSAMP)	Signal #2 Last Samp X(2,NSAMP)	Signal #3 Last Samp X(3,NSAMP)	....	Last Signal # Last Sample # X(NCHAN,NSAMP)

Figure C.2. Raw Data and Noise Data File Structure.

APPENDIX D

SIGNAL VALIDATION SYSTEM USER'S MANUAL

This manual is intended to guide a potential user through the steps required to setup and analyze data with the comprehensive signal validation system (SVS). It is assumed that the user is familiar with the theory behind the SVS and the individual modules. This manual first addresses the System Executive (SE) setup followed by that required for each module currently installed. Finally, the procedure for data processing is described. It is important to realize that the user may send any text or graphics (plots) to the printer at any time using the VAX workstation print screen option.

First some nomenclature is established. NSAMPLE is the total number of data samples per signal in the data file, while NPTS is the number of arbitrarily selected data samples analyzed together in any given data block. NBLOCK designates the number of data blocks to analyze. DELTAT is the data sampling interval in seconds. NSKIP (≥0) is the number of data samples skipped at the beginning of a data set. ISKIP (≥1) is the number of data samples alternately skipped in the data, that is the sampling interval is effectively changed to DELTAT*ISKIP. The following relationship must hold NSKIP+NPTS*ISKIP*NBLOCK ≤ NSAMPLE.

D.1 System Executive Setup

D.1.1 Module Activation/Deactivation

The modules may be turned on or off at will by the user. To activate (turn on) a given module, the module definition variable in the SE.H include file is set to a non-zero number. Deactivation of the module is achieved by making the value zero. The SE.C program is then compiled and linked to complete this task using the SE.COM command file.

D.1.2 Process Schematic

The information required to draw the process (plant) schematic is stored in the SYSEXE.DRAWRX file. The commands necessary to draw lines, arcs, boxes, paint, etc... are placed in this file according to the format required by the VAX workstation software. In those cases where new data from a similar plant are analyzed, the file can be re-used.

The drawing format is based on the structure given below. An ASCII file is created which contains pairs of input lines. The first line contains a command and an attribute with which to use the specific command. The commands are

-1 - to end the drawing,
 0 - for a comment line for file readability,
 1 - for writing text on the screen,
 2 - for two parallel lines (filled if attribute > 3),
 3 - for an arc (filled in attribute > 3),

4 - for a single straight line,
5 - for a single dashed line,
6 - for filling in a polygon shaped area,
7 - for filling in an arc shaped area.

The attribute is used for shading or coloring based on the workstation graphics setup. The second line of each pair contains the coordinates at which to make the requested drawing primitive.

D.1.3 Plant Data Base

The information which will generally change from one data set to another is placed in the SYSEXE.PLANT file. This file is structured according to the example given in Figure D.1. This file contains all the information related to the data analysis as well as the plant and data specific information.

D.1.4 Utility Programs

There are several utility programs of interest.

1. MDATPLT.EXE - this program is used to plot d.c. data in a selected data file. After the user enters the filename, the total number of available signals, the total number of data samples and the sampling interval is displayed. The user may then enter NSAMPLE, NSKIP and ISKIP to select a region of data to plot. A single data signal is selected to plot.

```
{FNAME   - Data Filename}
{NSAMPLE - Number of Data Samples per Block}
{NSKIP   - Initial Number of Data Samples to Skip}
{ISKIP   - Integral Data Skipping Factor}
{NBLOCK  - Number of Data Blocks}
{NVARIAB - Number of Variables}
{NLOCATE - Number of Locations in Plant}

{IDLOC(I)      - Location Reference Number,
 TXTLOC(I)     - Text Description of Location}        Repeat for
{NUPSTR(I)     - Number of Locations Upstream,        Each Location
 IUPSTR(I,J)   - List of Locations Upstream}          (I=1,NLOCATE)
{NDWNSTR(I)    - Number of Locations Downstream,
 IDWNSTR(I,J)  - List of Locations Downstream}

{NGROUP(I) - Number of Groups for I-th Variable,
 X(I),Y(I) - Screen Location to Place Text,
 TXTVAR(I) - Text Description of this Variable}
                                                                          Repeat for
{NREDUN(I,J) - Number of Redundant Signals in Group,                      Each Variable
 LOCATION(I,J) - Location of Signal Group in Plant,      Repeat for       (I=1,NVARIAB)
 X(I,J),Y(I,J) - Screen Location to Place Estimate,      Each Loop
 TXTGROUP(I,J) - Text Description of this Group}}        (J=1,NGROUP(I))
{MCHAN(I,J,K);K=1,NREDUN(I,J) - List of Redundant
                                Signals in this Group}
```

Figure D.1. SYSEXE.PLANT File Structure.

2. SHOWPARAM.EXE - each of the modules relies on a parameter file. By entering the module name and the number of parameters that a given module maintains, this program will produce a tabular listing of all the current parameters stored for each signal. This table is placed in an ASCII file designated PARAMETER.TXT.

3. SVSPLOT.EXE - this program basically provides all the results viewing (plotting) capabilities of the SVS in a stand-alone program. The previously computed results from the SVS may be read in for plotting. This program is very useful for producing report quality output. This program also provides the unique feature of multiple plots on a single screen.

4. LEARN.EXE - this program may be used to "learn" the nominal noise variance and zero-crossing rate for a selected signal since they are not routinely available.

D.2 Module Setup

Almost all the modules are setup by running a unique program into which the threshold values (parameters) for each signal are entered. The exception is in the cases where an empirical model must be computed or a hypercube created. The parameter input programs have been structured in such a manner that the parameters in a file for one signal may be changed without altering or requiring the re-input of the parameters for those signals left unchanged. The parameter file generating programs request the signal (channel) number to describe after which the user enters the module specific parameter values.

D.2.1 <u>Single Variable Generalized Consistency Checking</u>

The SGCC module requires that the following information be entered for each signal to create the parameter file named PARAMETER.SGCC:

1. Signal error bounds in measured (real) units.
2. Maximum acceptable bias magnitude in real units.
3. Normal noise standard deviation in real units.
4. Maximum acceptable noise standard deviation.

The program SGCCPARAM.EXE may be used to automatically enter these numbers.

D.2.2 <u>Process Empirical Modeling</u>

The program PEMPARAM.EXE is used to enter the sole parameter for each signal. The requested parameter is the signal tolerance in measured units which is placed in the file PARAMETER.PEM.

The PEM module requires that empirical models be fitted off-line before the SVS is executed. The PEMMODEL.EXE program is used to create these models. The inputs include the data filename, number of data samples to fit (≤100), NSKIP, ISKIP, the output signal channel number, the number of input signals (≤5) and a list of the input signal channel numbers. Both a binary (PEMMODEL) and an ASCII (PEMRESULT) file are produced by the modeling program. Only the binary file is required by the SVS. The internal contents of the binary file are given in Table D.1. The ASCII file may be

TABLE D.1

PEM Model File Contents

Variable	Variable Description
NOI	Number of inputs signals in the model
NTERM	Number of terms in the model
ERROR	Modeling error in percent
NORDER	Nonlinear model order
NSAMPLE	Number of data samples used in model fit
IDOUT	Output signal number (verifies filename)
MCHAN(NOI)	List of the input signals (channels)
SCALE(0)	Scaling factor for the output variable
SCALE(NOI)	Scaling factors for the input variables
COEFF(0)	Constant term
COEFF(NTERM)	Coefficients of the various terms
NPOWER(NOI,NTERM)	Integer powers of inputs for each term

printed or deleted, if desired. It is suggested that the modeling program be run overnight in a VAX batch job.

The PEM binary model file is described below. The disk filename identifies the following information:

1. The source of the model (PEM).
2. The output signal number.
3. The model number (there can be more than one model composed of different input signals for each output signal).

The disk filename is of the following syntax:

PEMMODEL.###L

where,

= the output signal number,

L = the model number (A=1, B=2, C=3,...).

Two utility programs are used in conjunction with the modeling program. PEMCOMPARE.EXE is used to produce plots to compare the raw data and the empirical model prediction. The inputs to this program are the data filename, number of data samples, NSKIP, ISKIP and the output signal. The last PEM model created (if there is more than one) is used for the prediction. This visual comparison between the measured and predicted values is invaluable. The PEMDUMP.EXE program may be used to dump the binary models for a particular output signal into an ASCII file (named PEMDUMP.TXT) for examination.

D.2.3 Multivariate Generalized Consistency Checking

The MGCC module also requires the input of empirical models for the data signals. The SGCC module is used to create a temporary data file containing the variable estimates. The PEMMODEL program then uses this data set as input for the fitting of a single model for each redundant signal group (variable). The same variable identification numbers as designated by the SE should be used here. The PEMDUMP.EXE program is used to dump the modeling results to ASCII files which are concatenated together to form the PARAMETER.MGCC file. This parameter file is then edited to add some additional information concerning which original data signals belong to each redundant signal group. See Figure D.2 for the format of the required information.

D.2.4 Bias and Noise Detection

The BND parameter file (PARAMETER.BND) requires several values to be entered for each signal. These include:

1. Percent tolerance for the mean value.
2. Nominal noise standard deviation in real units.
3. Upper limit factor for standard deviation.
4. Lower limit factor for standard deviation.
5. Nominal time constant (zero-crossing rate).
6. Minimum duration (sec) for a jump type anomaly.

The program BNDPARAM.EXE may be used to enter these thresholds.

```
{NGROUPS - Number of Signal Groups}

{NREDUN(I)  - Number of Redundant Signals in I-th Group}          Repeat for Each
{MCHAN(I,J);J=1,NREDUN(I) - List of Redundant Signal Numbers}      Signal Group
{TOLER(I,J);J=1,NREDUN(I) - List of Tolerances for Signal}        (I=1,NGROUPS)

{NOFMOD - Number of Empirical Models}

{IDOUT(I)  - Output Variable Number for I-th Model}
{ACCUR(I)  - Empirical Model Accuracy in Percent}
{NOFINP(I) - Number of Input Variables}
{INPUT(I,J);J=1,NOFINP(I) - List of Input Variables}
{NTERM(I)  - Number of Terms in the Model}                           Repeat for
                                                                     Each Model
  [Repeat following input line for each Term; K=1,NTERM(I)]        (I=1,NOFMOD)
{COEFF(I,K),NPOWER(I,K,J) - Term Coefficients and Integer
                            Power to Raise Each Variable to}

{CONST(I) - Constant Coefficient}
```

Figure D.2. PARAMETER.MGCC File Structure.

D.2.5 Process Hypercube Comparison

The main hypercube program (HYPER.EXE) is used to create (learn) the process hypercube. HYPER.EXE may also be used as a stand-alone signal validation program. Data from more than one data set may be added to the hypercube. Once the hypercube has been created, infrequently appearing cells may be removed (cleaned-up). The two files FREQUENCY.PHC and KEYINDEX.PHC are created from this overall learning procedure.

Before creation of the hypercube however, two files must be created by the user to inform the HYPER.EXE program as to the contents of the input data file (or file on which signal validation is to performed). The first ASCII file is INTERVALS.PHC which contains the number of variables on the first line. This is followed by an input line for each variable containing the variable lower and upper limit, and the number of intervals between these two limits.

The last input file (SIGNALS.PHC) contains the information describing the actual signal arrangements according to the following format:

```
{NGROUPS - Number of signal groups}
{NVAR    - Number of variables not in a loop (e.g. Power)}
{NONVAR  - Number of variable in a loop (e.g. RCS Flow)}

 [Repeat the following for each signal group (I=1,NGROUPS)]

{IDGROUP(I) - Group identification number,
 NREDUN(I)  - Number of redundant signals in this group,
 TOLER(I)   - Signal tolerance for each group}
{MCHAN(I,J);J=1,NREDUN(I) - List of signals in the group}
```

The group ID number above should correspond to the same number designated by the SVS.

D.2.6 Univariate Autoregressive Modeling

The UAR module requires that only the nominal time constant (in seconds) for each signal be entered into its data base (PARAMETER.UAR). This of course is done using the program UARPARAM.EXE.

D.3 Data Processing

The data processing is initiated by executing the SE program from the directory in which the data and parameter files exist. Note that the results files will be placed in this directory. Data processing stops at the end of each data block to allow the user the opportunity to view the results of that block. Signal validation is then continued through each block in succession. Data processing may be completely stopped at any time, confirmation is requested before the program is halted.

At any time during the signal validation the left mouse button may be pressed, the data processing will be suspended and the results thus far computed may be viewed or other action taken. This feature must be used with care, since a casual user may be unable to distinguish between the results of the previous block and those of the current block.

D.3.1 <u>Utility Functions</u>

Certain basic utility functions are provided at the top level of the SE menu system. These options include:

1. Signal d.c. data plotting.
2. Signal noise data plotting.
3. Alteration of the results view level.
4. Display of the entire plant data base.
5. List redundant sensors in a group.
6. List sensors at a given location.
7. List all locations in the plant.
8. List locations upstream and downstream.
9. Stop the data processing.

D.3.2 <u>System Executive Results</u>

Normally the validated signals are displayed on the screen using a schematic of the process (plant). A validated value for each process signal is displayed. In the case of four steam generators, four levels are displayed. A faulty signal is indicated by sounding a bell and altering the signal estimate display.

The results from the system executive decision making are examined at five levels:

1. The top level contains the estimates displayed on the process (plant) schematic.

2. The next level displays the final status results for each sensor in a selected redundant group.

3. The detailed results status for a sensor group may also be shown which includes results for each failure mode.

4. The brief results for a single sensor includes an output similar to #3 above.

5. The last level is detailed results for a selected signal including results from each failure mode as well as the final results from each module.

D.3.3 Module Results

Windows are used to access the results of the individual modules. Deeper level menus are used to select the specific results of the individual modules. In the view results mode, each module has its own format to show the results since each has varying information available. A useful data analysis sheet is included in Figure D.3.

During data processing, intermediate computational results from the individual modules are displayed in a separate window. The amount of intermediate results shown by each module may be controlled. One of four levels may be selected.

1. No results.

2. Minimal results - which displays only the resultant confidence factors for each signal.

3. Detailed results - which provides intermediate computational results. The exact results shown depend on the specific module.

4. Debug level - which is basically used in debugging when new modules are added for viewing all the steps of the data processing.

The results view level can be altered at any time during data processing.

Comprehensive Signal Validation System Results Worksheet	Redundant Group # ___				
	Sig#___	Sig#___	Sig#___	Sig#___	Sig#___
D.C. Data					
Noise Data					
SGCC Estimate					
SGCC Bias SPRT					
SGCC Noise SPRT					
SGCC Inconsistency Index					
BND APDF					
BND CUSUM					
PEM Estimate					
MGCC Inconsistency Index					
MGCC Estimate					
PHC Inconsistency Index					
PHC Estimate					
PHC Variable Status					
UAR Autocorrelation					
UAR PSD					
UAR Step Response					
SE Final Results					

Figure D.3. SVS Analysis Data Sheet.

APPENDIX E

PWR EMPIRICAL MODELING

A systematic effort was undertaken to create empirical models for a pressurized water reactor (PWR). This study involved modeling of twelve different process variables available from a Westinghouse four-loop PWR. The objectives of the modeling were

1. To determine whether a single model can be developed which will properly describe a signal over the complete normal operating range of the signal.

2. To assess whether or not a single generalized functional form can be used to fit given data.

3. To develop models for input into both the Process Empirical Modeling (PEM) module and the Multivariate Generalized Consistency Checking (MGCC) module of the Signal Validation System (SVS).

E.1 Empirical Modeling Technique

The empirical modeling method used creates an optimal nonlinear multiple-input single-output (MISO) model from the given data. The modeling was set to have a maximum nonlinearity of order three (note that a linear model is also possible). The model may have from zero (a constant only) to eight terms. The form of the model is

$$y = C_0 + \sum_{i=1}^{n} C_i \, \Phi_i(\underline{x}) \tag{E.1}$$

where,

y = output signal of interest,

$\underline{x}$ = vector of input signals,

n = number of terms in the model,

Φ_i = nonlinear combination of input signals,

C_i = constant coefficient.

The modeling program varies both the model order and the number of terms. The optimal model is selected from the model with the minimum error between the predicted output and the measured output.

E.2 Empirical Modeling Results

A total of nine variables (91 signals) from a PWR were modeled. A representative plot of each variable is found in Appendix A. A summary of the modeling results is presented in Table E.1. Note that more than one model for each output signal was generated by using different combinations of the input signals. That is, with redundant signals more than one model may be created. Output signals from a given primary/secondary loop were modeled using only those input signals from the same loop. The results for each of the process variables will be discussed below.

TABLE E.1

PWR Empirical Modeling Summary

Process Signal	No. of Signals	No. Models Per Signal	Total No. of Models
Power	4	16	64
Cold Leg Temperature	4	16	64
Hot Leg Temperature	4	16	64
Core Exit Temperature	50	16	800
RCS Flow	12	8	96
RCS Pressure	2	24	48
Pressurizer Level	3	16	48
Pressurizer Pressure	4	24	96
Feedwater Flow	8	12	96
	91		1376

One-hundred data measurements were fit to generate each empirical model. The data used in the modeling was taken over two days during a plant start-up procedure. Each data signal was carefully examined. Approximately three weeks of around-the-clock computer time was required on a VAX station II computer to complete the modeling.

The empirical models created for input to the MGCC module differed somewhat from those constructed for the PEM module. For the MGCC models a temporary data set was created from the original data set using the single variable generalized consistency checking (SGCC) routine to reduce each redundant group of signals to a single best estimate at each data point. This data set of best estimates was used as input to the empirical modeling program after which the temporary data set was discarded. Thus a single empirical model was created for each process variable (redundant group) for entry into the MGCC module rather than the multiple models for each signal as for the PEM module.

Original Data Set	->	SGCC Module	->	Temporary Data Set	->	Empirical Modeling	->	MGCC Module

The modeling results for each output variable will be presented below. The functional forms exhibited by the modeling for the PEM module and those for the MGCC module will be compared. The models produced from the individual signals (versus the SGCC estimates) are presented in the tables. Coefficients will be given from the MGCC models, since they are more representative. The results for the individual signals are referred to as PEM models while the results from SGCC variable estimates are designated MGCC models.

E.2.1 Power Empirical Models

Four power signals were available for modeling. Logically, the cold leg temperature, hot leg temperature and reactor coolant system (RCS) flow rate should provide an excellent input set. Preliminary results using the above three signals showed that the RCS flow rate was routinely omitted from the model. Further analysis showed this to be caused by a nearly constant flow rate. For this reason the RCS flow rate was omitted from the modeling effort. The functional form for the power (%) signal was thus:

$$\text{Power} = f(\text{Cold Leg Temperature, Hot Leg Temperature}) \qquad (E.2)$$

The PEM modeling results for power are given in Table E.2. Six different functional forms were found from the various signal combinations. The similarities between the six forms are evident. In fact using the MGCC form:

$$\text{Power} = c_0 + c_1\, y^2 + c_2\, x + c_3\, x^2 + c_4\, y \qquad (E.3)$$

where,

TABLE E.2

Empirical Models For Power

Functional Form	No. of Models	Percentage of Total
$y^2 + x + x^2$	21	33
$y^2 + x + x^2 + y$	29	45
$y^2 + x + x^2 + y + xy$	1	2
$y^3 + x + x^2$	6	9
$y^3 + x + x^2 + x^3 + y$	3	5
$y^3 + x + x^2 + x^3 + y + x^2y$	4	6
	64	

x = Cold Leg Temperature
y = Hot Leg Temperature

x = Cold leg temperature (°F)

y = Hot leg temperature (°F)

c_0 = 18178.246

c_1 = 0.0025441560

c_2 = -64.497696

c_3 = 0.056761283

c_4 = -1.1794285

a total of 78% of the PEM results are included. The PEM modeling error ranged from 1.2% to 2.0% with an average of 1.7%. The MGCC modeling error was 1.0%. A comparison of a measured and predicted power signal is shown in Figure E.1. The prediction lies directly on the measured values --- a visual proof of the goodness of the fit.

E.2.2 Cold Leg Temperature Empirical Models

Four cold leg temperature signals were modeled using the same combination as used for power with a final input-output combination as given below:

$$\text{Cold Leg Temperature} = f(\text{Power, Hot Leg Temperature}) \quad (E.4)$$

The results from modeling the cold leg temperature are given in Table E.3. There are again six generalized functional forms describing the data. If the following MGCC form were used a total of 39% of the PEM forms would be encompassed.

$$\text{T-Cold} = c_0 + c_1\, y + c_2\, y^2 + c_3\, x^2 + c_4\, x + c_5\, x^3 \quad (E.5)$$

where,

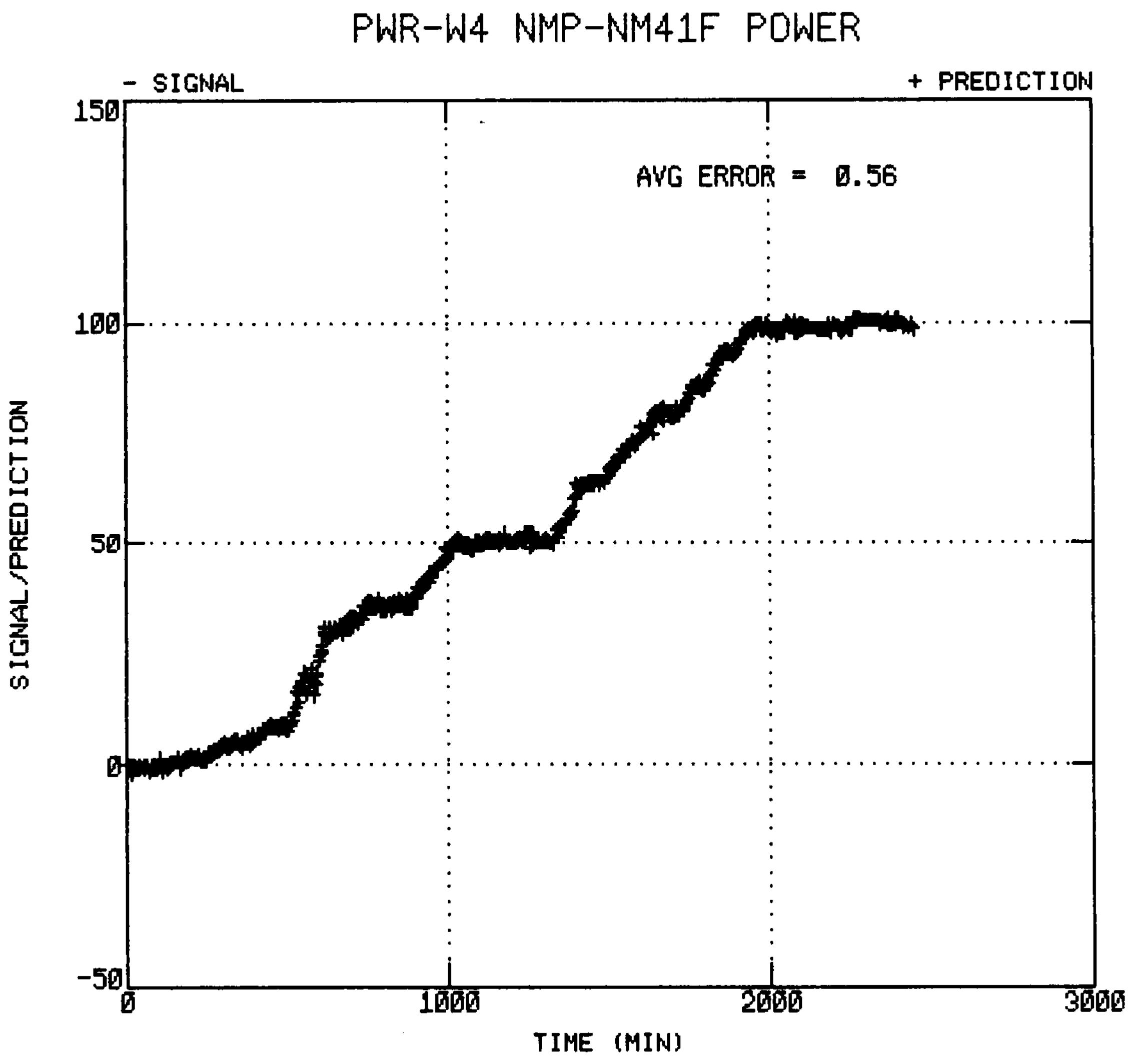

Figure E.1. Comparison of Measured and Predicted Power Signal.

TABLE E.3

Empirical Models For
Cold Leg Temperature

Functional Form	No. of Models	Percentage of Total
$y + y^2 + x^2 + x$	2	3
$y + y^2 + x^2 + x + xy$	3	5
$y + y^2 + x^2 + x + x^3$	23	36
$y + y^2 + x^2 + x + x^3 + xy^2$	18	28
$y + y^2 + x^2 + x + x^3 + xy^2 + x^2y$	12	19
$y + y^2 + x^2 + x + x^3 + xy^2 + x^2y + y^2$	6	9
	64	

x = Power
y = Hot Leg Temperature

x = Power (%)

y = Hot leg temperature (°F)

c_0 = 1719.4670

c_1 = -5.0331573

c_2 = 0.0052820551

c_3 = -0.00089699362

c_4 = -0.55271053

c_5 = -0.00000042823697

The PEM modeling error ranged from 0.07% to 0.12% with an average of 0.11%. The MGCC modeling error was 0.06%. A comparison of a measured and predicted cold leg temperature signal is shown in Figure E.2.

E.2.3 Hot Leg Temperature Empirical Models

With four hot leg temperature signals available for modeling a total of 64 PEM models were created. The functional relationship is given by:

$$\text{Hot Leg Temperature} = f(\text{Power, Cold Leg Temperature}) \quad \text{(E.6)}$$

The PEM modeling results appear in Table E.4 with only four different functional forms having been found. On close examination of the results, only two different models were identified. The difference between the models comes only as a result of the order in which the modeling algorithm selects the strongest terms. In fact 86% of the models have the exact form of the MGCC model:

$$\text{T-Hot} = c_0 + c_1\, y + c_2\, y^2 + c_3\, x^2 + c_4\, x + c_5\, x^3 \quad \text{(E.7)}$$

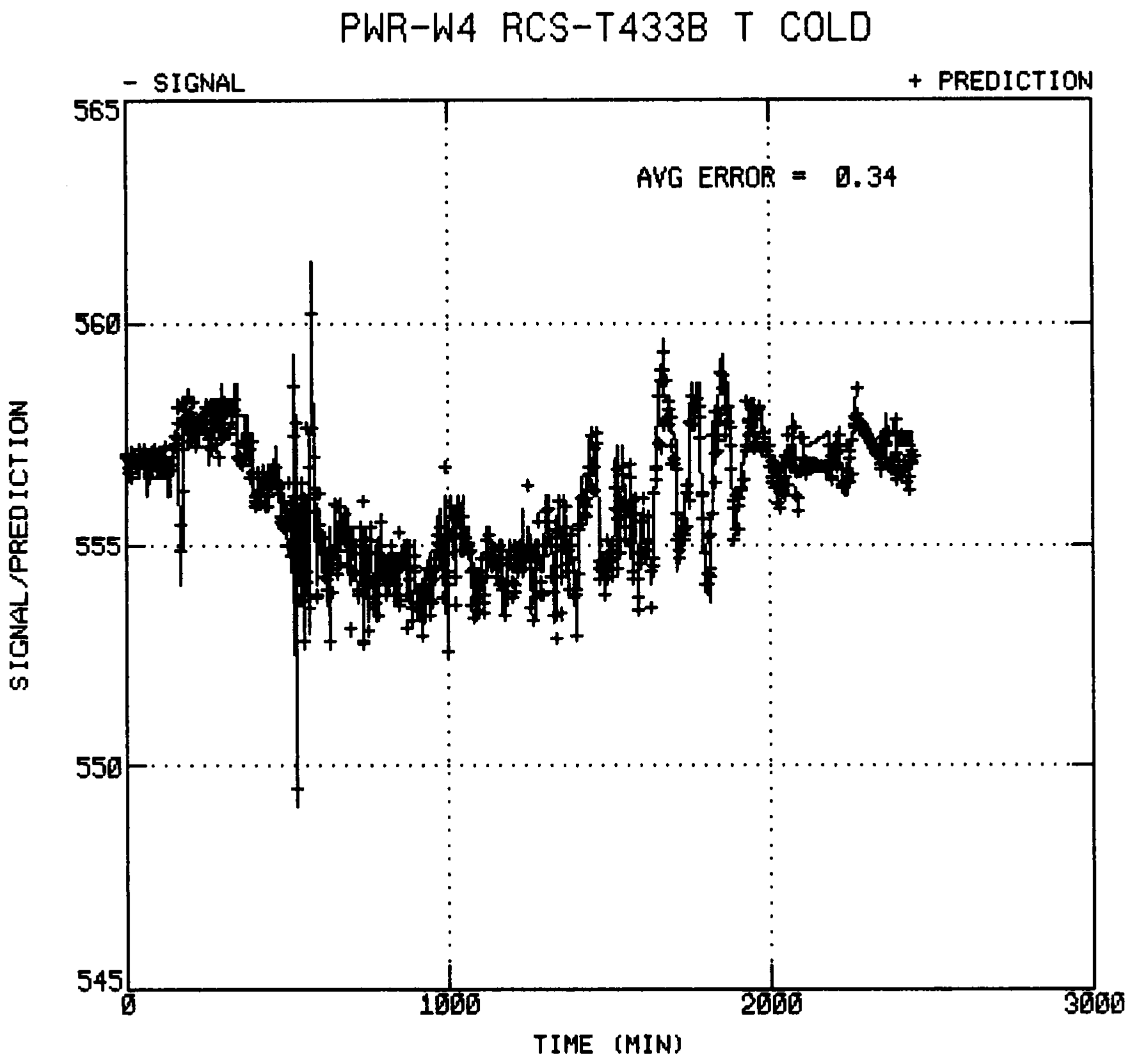

Figure E.2. Comparison of Measured and Predicted Cold Leg Temperature Signal.

TABLE E.4

Empirical Models For Hot Leg Temperature

Functional Form	No. of Models		Percentage of Total
$y^2 + x + x^2 + x^3 + y$	14	A	22
$y + y^2 + x^2 + x + x^3$	41	A	64
$y + y^2 + x^2 + x$	7	B	11
$y^2 + x + x^2 + y$	2	B	3
	64		

x = Power
y = Cold Leg Temperature

where,

x = Power (%)

y = Cold leg temperature (°F)

c_0 = -12154.215

c_1 = 45.013397

c_2 = -0.039834477

c_3 = -0.000013430063

c_4 = 0.58095384

c_5 = -0.0000026944554

The PEM modeling error ranged from 0.06% to 0.10% with an average of 0.09%. The MGCC modeling error was 0.05%.

E.2.4 Core-Exit Temperature Empirical Models

The core-exit temperature provided the greatest number of signals (50) and total number of different models (800). The core-exit temperature was modeled using the same input-output combination as the hot leg temperature, namely:

$$\text{Core-Exit Temp} = f(\text{Power, Cold Leg Temperature}) \qquad (E.8)$$

The core-exit temperature modeling results are shown in Table E.5. With the large number of models created, there was a greater number of functional forms (14). Also, the core-exit temperature is not uniform across the core, thus resulting in the possibility of a greater number of functional forms. Interesting, however, is the fact that 93% of the functional forms are included in the following:

$$\text{Core-Exit Temp} = y + y^2 + x^2 + x + x^3 + xy^2 \qquad (E.9)$$

TABLE E.5

Empirical Models For
Core-Exit Temperature

Functional Form	No. of Models		Percentage of Total
$y + y^2 + x^2 + x^3 + x + y^3 + xy + xy^2$	3		<1
$y + y^2 + x^2 + x^3 + x + y^3 + xy$	15		2
$y + y^2 + x^2 + x^3 + x + y^3$	4		<1
$y + y^2 + x^2 + x^3 + x$	26	A	3
$y + y^2 + x^2 + x + x^3$	310	A	39
$y^2 + x + x^2 + x^3 + y$	132	A	17
$y^2 + x + x^2 + x^3 + y + xy$	4		<1
$y^2 + x + x^2 + x^3$	21		3
$y^2 + x + x^2 + y + xy$	10	C	1
$y + y^2 + x^2 + x + xy$	16	C	2
$y^2 + x + x^2 + y$	11	B	1
$y + y^2 + x^2 + x$	24	B	3
$y + y^2 + x^2 + x + x^3 + xy^2 + x^2y$	1		<1
$y + y^2 + x^2 + x + x^3 + xy^2$	223		28
	800		

x = Power
y = Cold Leg Temperature

where

x = Power (%)

y = Cold leg temperature (°F)

The modeling error ranged from 0.3% to 33.0%. This latter value was a result of a huge spike in the measured data of three signals (some type of instrument anomaly). Omitting these three channels, the error ranged from 0.28% to 0.45% with an average of 0.33%. There was no MGCC modeling performed since the various core-exit temperature signals are not redundant to each other and thus a single MGCC model is undesirable based on the logic of the MGCC algorithm.

E.2.5 RCS Flow Empirical Models

The reactor coolant system (RCS) flow rate (%) was not entirely suitable for modeling since its value was nearly constant as mentioned above. Modeling of this signal was, however, performed to satisfy any curiosity. The functional relationship selected was

$$\text{RCS Flow} = f(\text{Power, RCS Pressure}) \tag{E.10}$$

The PEM results of modeling the twelve flow signals is given in Table E.6. There was one MGCC model created for each of the four primary loops. Three of the four MGCC results exhibited the following functional form:

TABLE E.6

Empirical Models For RCS Flow

Functional Form	No. of Models	Percentage of Total
$y + y^2 + x^2 + x + xy$	1	1
$y + y^2 + x^2 + x + x^3$	24	25
$y + y^2 + x^2 + x + x^3 + xy^2$	64	67
$y + y^2 + x^2 + x + x^3 + xy^2 + x^2y$	4	4
$y + y^2 + x^2 + x + x^3 + xy^2 + x^2y + y^3$	3	3
	96	

x = Power
y = RCS Pressure

$$\text{RCS Flow} = c_0 + c_1\, y + c_2\, y^2 + c_3\, x^2 + c_4\, x + c_5\, x^3 + c_6\, xy^2 \qquad \text{(E.11)}$$

where,

x = Power (%)

y = RCS pressure (psia)

The fourth MGCC form was identical to the above except for the addition of another term, $c_7 \cdot x^2 y$. This encompasses a total of 92% of the five functional forms found in the PEM results. The coefficients are given in Table E.7. The PEM modeling error ranged from 0.07% to 0.24% with an average of 0.14%. The MGCC modeling error ranged from 0.06% to 0.13% with an average of 0.10%.

E.2.6 RCS Pressure Empirical Models

The reactor coolant system (RCS) pressure also remains nearly constant at all normal operating conditions, but was modeled in the interest of completeness. The RCS flow rate was initially included in the model created, but was removed after it was excluded by the modeling algorithm. The final selected functional relationship was

$$\text{RCS Pressure} = f(\text{Power, PRZR Level, PRZR Pressure}) \qquad \text{(E.12)}$$

The results for RCS pressure shown in Table E.8 show a fair amount of scatter. It must be noted that only two RCS pressure signals were available which provided 48 models,

TABLE E.7

RCS Flow Coefficients

Term	RCS Flow Loop #1	#2	#3	#4
c_0	-2522.5955	-1145.6392	-1535.3096	52.356640
c_1	2.3486288	1.1215415	1.4671211	0.030849492
c_2	-5.24579e-4	-2.50708e-4	-3.27964e-4	-7.923975e-6
c_3	1.570846e-4	9.144785e-3	2.49452e-4	2.319459e-4
c_4	-0.11121079	-0.36160031	-0.11801821	-0.15393820
c_5	-1.747110e-6	-1.26820e-6	-1.76813e-6	-1.038627e-6
c_6	2.374422e-8	7.25482e-8	2.25114e-8	2.922255e-8
c_7		-4.02502e-6		

TABLE E.8

Empirical Models For RCS Pressure

Functional Form	No. of Models	Percentage of Total
$z + z^2 + x^2 + y + y^2$	3	6
$z + z^2 + x^2 + y + y^2 + xz$	16	33
$z + z^2 + x^2 + y + y^2 + xz + y^3$	3	6
$z + z^2 + x^2 + y + y^2 + xz + y^3 + x$	3	6
$z + z^2 + x^2 + y + y^2z$	2	4
$z + z^2 + x^2 + y + y^2z + xz$	9	19
$z + z^2 + x^2 + yz + y + xz$	5	10
$z + z^2 + x^2 + yz + y + x$	2	4
$z + z^2 + x^2 + yz + y + x + xz$	1	2
$z + z^2 + x^2 + yz + y + x + xz + y^2$	1 A	2
$z + z^2 + x^2 + yz + y + xz + x + y^2$	3 A	6
	48	

x = Power
y = Pressurizer Level
z = Pressurizer Pressure

the lowest amount for any signal modeled here. Using the MGCC model found:

$$\text{RCS Pressure} = c_0 + c_1\, z + c_2\, z^2 + c_3\, x^2 + c_4\, y + c_5\, y^2 + c_6\, xz \qquad \text{(E.13)}$$

where,

x = Power (%)

y = Pressurizer pressure (psia)

c_0 = -17773.281

c_1 = 16.907852

c_2 = -0.0035610560

c_3 = 0.00029141182

c_4 = 0.42043442

c_5 = -0.00032162403

c_6 = -0.000027140883

a total of 40% of the PEM functional forms are included. The PEM error ranged from 0.07% to 0.17% with an average of 0.09%. The MGCC modeling error was 0.06%.

E.2.7 Pressurizer Level Empirical Models

The greatest number of input signals (4) was used in the modeling of the pressurizer level. The input-output relationship chosen was

$$\text{Pressurizer Level} = f(\text{Power, Pressurizer Pressure, Cold Leg Temp, Hot Leg Temp}) \qquad \text{(E.14)}$$

The pressurizer level with only three available signals also tied for the lowest number of total models created. The results of modeling given in Table E.9 show not only the sole linear model found but also the only case in which a single functional form was found. The PEM and MGCC functional form is

$$\text{PRZR Level} = c_0 + c_1\, z + c_2\, w + c_3\, x + c_4\, y \qquad \text{(E.15)}$$

where,

w = Power (%)
x = Pressurizer pressure (psia)
y = Cold leg temperature (°F)
z = Hot leg temperature (°F)
c_0 = -722.97754
c_1 = 0.73653889
c_2 = -0.068457201
c_3 = -0.0086162146
c_4 = 0.64008898

The PEM modeling error ranged from 1.0% to 1.6% with an average of 1.3%. The MGCC modeling error was 1.0%. A comparison of a measured and predicted pressurizer level signal is shown in Figure E.3. The flows that can possibly affect the pressurizer level, such as charging pump, let-down flow and spray flow are not included in the modeling. These signals were not available in the data base and are assumed constant.

E.2.8 Pressurizer Pressure Empirical Models

The pressurizer pressure with four signals was modeled using the following form:

TABLE E.9

Empirical Model For Pressurizer Level

Functional Form	No. of Models	Percentage of Total
z + w + x + y	48	100
	48	

w = Power
x = Pressurizer Pressure
y = Cold Leg Temperature
z = Hot Leg Temperature

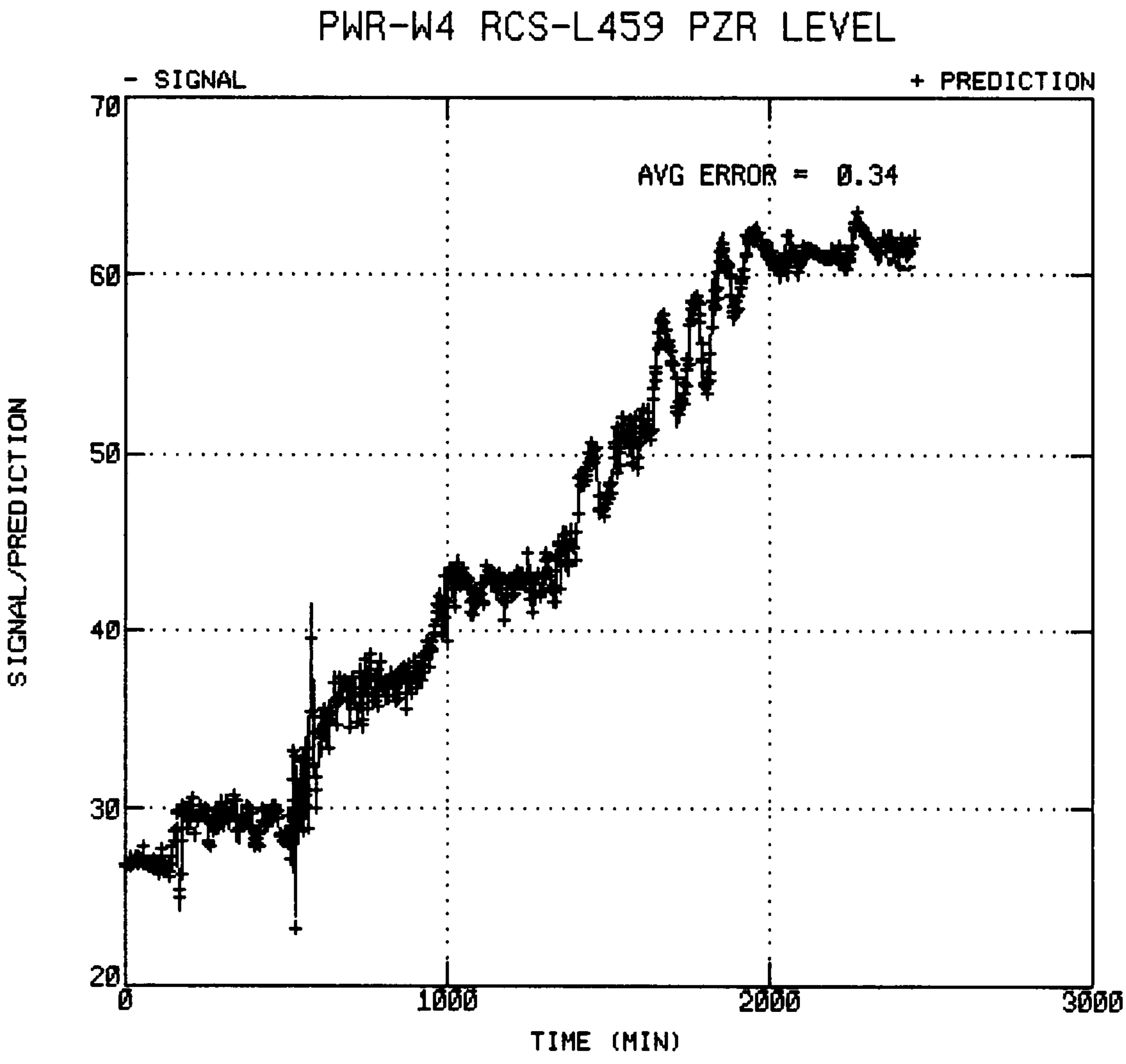

Figure E.3. Comparison of Measured and Predicted Pressurizer Level Signal.

$$\text{PRZR Pressure} = f(\text{Power, PRZR Level, RCS Pressure}) \tag{E.16}$$

The PEM modeling results appear in Table E.10. The results are again scattered. In this case two generalized PEM functional forms seem to be appropriate. The first PEM form is

$$\text{PRZR Pressure} = z + z^2 + x^2 + y + y^2 + xz + y^3 + x \tag{E.17}$$

And the second form appearing in many of the PEM results is

$$\text{PRZR Pressure} = z + z^2 + x^2 + y + y^2 z + xz + y^2 \tag{E.18}$$

Even with the difference in the two models, the first four terms of each remain the same. The PEM models encompass 65% and 23% of all the models created, respectively for a total of 88%. The MGCC form was

$$\begin{aligned}\text{PRZR Pressure} = c_0 + c_1\, z + c_2\, z^2 + c_3\, x^2 +& \\ c_4\, y + c_5\, y^2 + c_6\, xz&\end{aligned} \tag{E.19}$$

where,

x = Power (%)
y = Pressurizer level (%)
z = RCS pressure (psia)
c_0 = -54826.855
c_1 = 50.90942
c_2 = -0.010987222
c_3 = -0.00038292413
c_4 = -0.30182481
c_5 = 0.0016712024
c_6 = 0.000030928699

TABLE E.10

Empirical Models For Pressurizer Pressure

Functional Form	No. of Models		Percentage of Total
$z + z^2 + x^2 + y + y^2$	3		3
$z + z^2 + x^2 + y + y^2 + xz$	18		19
$z + z^2 + x^2 + y + y^2 + xz + y^3$	32		33
$z + z^2 + x^2 + y + y^2 + xz + y^3 + x$	9		9
$z + z^2 + x^2 + y + y^2 + xz + y^3 + x^3$	1		1
$z + z^2 + x^2 + y + y^2 + xz + y^2z + x^3$	4		4
$z + z^2 + x^2 + y + y^2 + x + y^3 + x^3$	3		3
$z + z^2 + x^2 + y + y^2 + x + y^2z + x^3$	1	A	1
$z + z^2 + x^2 + y + y^2z + x + y^2 + x^3$	1	A	1
$z + z^2 + x^2 + y + y^2z$	2		2
$z + z^2 + x^2 + y + y^2z + xz$	17		18
$z + z^2 + x^2 + y + y^2z + xz + y^2$	3		3
$z + z^2 + x^2 + y + x + y^3 + x^3$	1		1
$z + z^2 + x^2 + yz + y + x + xz + y^2$	1		1
	96		

x = Power
y = Pressurizer Level
z = RCS Pressure

Note that this MGCC form for pressurizer pressure is the same as that for RCS pressure, as might be expected. The PEM modeling error ranged from 0.06% to 2.9% with this latter value being caused by a spike in one of the data channels. Omitting this signal, the error ranges from 0.06% to 0.07%. The MGCC modeling error was 0.06%.

E.2.9 Feedwater Flow Empirical Models

Eight different feedwater flow signals were modeled. The modeling originally included the steam generator level and steam flow but both variables were removed by the modeling algorithm. The functional relationship is

$$\text{Feedwater Flow} = f(\text{Power, Steam Pressure}) \qquad \text{(E.20)}$$

The results are given in Table E.11. More different functional forms were created for the feedwater flow than for any other variable. A marginal model encompassing 41% of the PEM functional forms is given below in the MGCC model:

$$\text{FW Flow} = c_0 + c_1\, x + c_2\, x^2 + c_3\, xy^2 + c_4\, x^3 \qquad \text{(E.21)}$$

where,

x = Power (%)

y = Steam pressure (psia)

TABLE E.11

**Empirical Models For
Feedwater Flow**

Functional Form	No. of Models		Percentage of Total
$x + x^2 + x^3 + y^3 + y + y^2 + xy^2$	4		4
$x + x^2 + x^3 + y^3 + y + xy + x^2y + y^2$	1		1
$x + x^2 + x^3 + y^3 + y + xy + x^2y$	1	B	1
$x + x^2 + x^3 + y + y^3 + xy + x^2y$	1	B	1
$x + x^2 + y^3 + x^3 + y + xy + x^2y$	1	B	1
$x + x^2 + y^3 + x^3 + y$	2		2
$x + x^2 + y^3 + x^3 + y^2$	1		1
$x + x^2 + y^3 + x^3 + y + xy + y^2$	3		3
$x + x^2 + y^3 + x^3 + y + xy$	3	C	3
$x + x^2 + x^3 + y + y^3 + xy$	2	C	2
$x + x^2 + x^3 + y^3 + y^2 + xy$	1		1
$x + x^2 + x^3 + y^3 + xy + xy^2$	1		1
$x + x^2 + x^3 + xy^2 + y + xy + x^2y$	1		1
$x + x^2 + x^3 + xy^2 + y^2 + xy + y^3$	1		1
$x + x^2 + x^3 + xy^2$	2	A	2
$x + x^2 + xy^2 + x^3$	37	A	39
$x + x^2 + xy^2 + x^3 + xy + y$	1		1
$x + x^2 + xy^2 + x^3 + xy$	1		1
$x + x^2 + xy^2 + x^3 + y$	6	D	6

TABLE E.11 (Continued)

Functional Form	No. of Models		Percentage of Total
$x + x^2 + xy^2 + y + x^3$	5	D	5
$x + x^2 + xy^2 + y + x^3 + y^2$	1		1
$x + x^2 + xy^2 + y + x^3 + y^3$	1		1
$x + x^2 + xy^2 + y + y^2 + xy^2$	2		2
$x + xy + y^2 + x^2$	1	E	1
$x + x^2 + y^2 + xy$	2	E	2
$x + x^2 + y^2 + y$	2		2
$x + x^2 + y^2 + y + xy$	1	F	1
$x + x^2 + xy + y^2 + y$	9	F	9
$x + xy^2 + y^3 + x^3$	1		1
$x + xy^2 + y^3 + x^3 + y$	1		1
	96		

x = Power
y = Steam Pressure

The coefficients are given in Table E.12 for the four MGCC models created. The PEM modeling errors ranged from 3.3% to 4.4% with an average of 3.9%. The MGCC modeling error ranged from 3.4% to 3.8% with an average of 3.6%. A comparison of a measured and predicted feedwater flow signal is shown in Figure E.4.

E.3 PWR Empirical Modeling Conclusions

The PWR empirical modeling has shown that indeed a single model may be constructed which can accurately describe a given signal over its normal operating range. Many of the signals have shown that a single functional form may be used to fit the data. The advantage of a single functional form is that the computational resources required for the modeling will be much less than that needed for complete model optimization. Data which do not fit well to the model may also be readily identified as unsatisfactory. In those cases where a single functional form is not well defined, a trade-off between a single functional form and the model accuracy may be feasible. It is anticipated that these functional forms will change for different plants.

The fitting errors have shown average prediction accuracies from 0.09% to 3.9% which will provide reliable process variable estimates using the PEM and MGCC signal validation modules. Table E.13 compares the signal tolerances versus the modeling errors. Any model with a

TABLE E.12

Feedwater Flow Coefficients

Term	Steam Generator #1	#2	#3	#4
c_0	-1.6716485	-14.505486	21.819035	30.709864
c_1	42.866653	51.296566	47.301949	46.985939
c_2	0.14256939	0.12077165	0.16249624	0.19922687
c_3	-1.368509e-5	-2.153076e-5	-1.874636e-5	-2.016646e-5
c_4	-6.140419e-4	-5.740621e-4	-7.627459e-4	-1.017504e-3

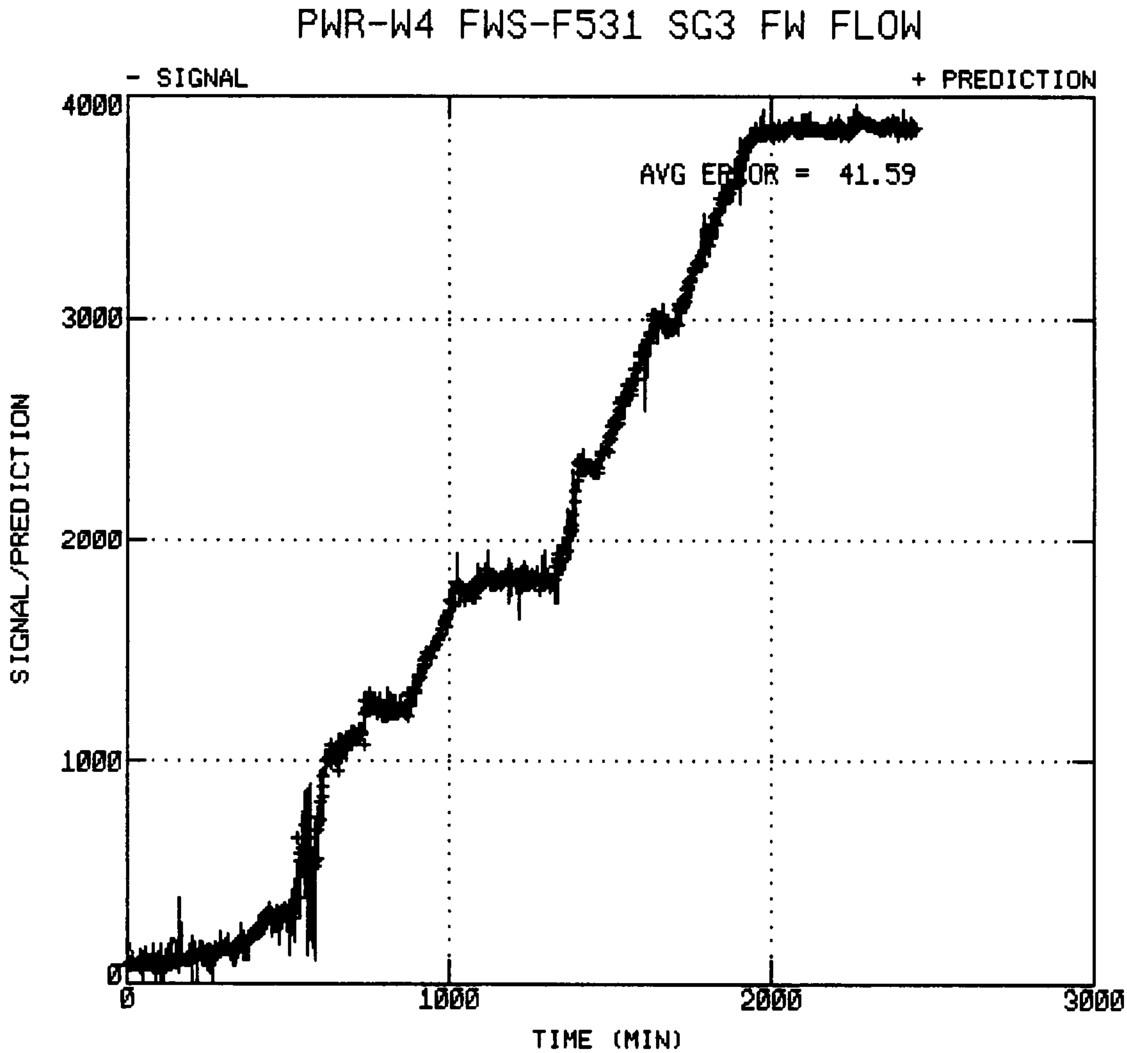

Figure E.4. Comparison of Measured and Predicted Feedwater Flow Signal.

TABLE E.13

PWR Empirical Modeling Errors

Process Signal	Signal Tolerance	Average Error PEM	Average Error MGCC
Power	2 %	1.7 %	1.0 %
Cold Leg Temperature	1 %	0.11 %	0.06 %
Hot Leg Temperature	1 %	0.09 %	0.05 %
Core Exit Temperature	2 %	0.33 %	n/a
RCS Flow	4 %	0.14 %	0.10 %
RCS Pressure	2 %	0.09 %	0.06 %
Pressurizer Level	10 %	1.3 %	1.0 %
Pressurizer Pressure	1 %	0.8 %	0.06 %
Feedwater Flow	5 %	3.9 %	3.6 %

fitting error greater than (or approximately equal to) the signal tolerance is certainly unacceptable. The data used as input to the modeling algorithm must be carefully studied. The start-up type data used is somewhat desirable since many valid operating states are represented by such data; however, there may be transient lags present affecting the results.

With redundant signals available in a nuclear power plant, more than one model may easily be generated for each process signal. It should be pointed out that signal substitutions may also be made. For example, instead of using power as an input for modeling certain parameters on the secondary side, the combination of cold leg and hot leg temperature could just as easily have been used. This is important in situations when certain measurements are not available. Some questions still remain unanswered. For instance, will the models change over time (e.g. a core-exit temperature model over a given fuel cycle).

In the future it is suggested that some type of data clustering algorithm be used to exclude any infrequently appearing data points from the modeling program. This would avoid such problems as spikes appearing in the various data signals such as core-exit temperature, pressurizer pressure, and steam generator level.

APPENDIX F

EBR-II EMPIRICAL MODELING

Empirical modeling of various EBR-II process signals was performed similar to those computed for the PWR in the previous appendix. One advantage of the EBR-II data versus that of the PWR data was that more signals were available. The reader is referred to Section 5.5 and Appendix E for details on the empirical modeling methodology. The EBR-II plant and process signals are described in Appendix B.

F.1 Empirical Modeling Results

A total of nineteen variables (114 signals) from the EBR-II were modeled. A representative plot of each variable is given in Appendix B. A summary of the modeling results is presented in Table F.1. Redundant signals provided for the generation of more than one output signal based upon using different combinations of the input signals. The results for each of the process variables will be discussed below.

One-hundred data measurements were fit to generate each empirical model. The data used in the modeling was sampled over six hours during a plant start-up procedure. Similar to the PWR modeling, two sets of models were created. One set for input into the PEM module and the other for entry into the MGCC module.

TABLE F.1

EBR-II Empirical Modeling Summary

Process Signal	No. of Signals	No. Models Per Signal	Total No. of Models
Power	3	25	75
Upper Plenum Temperature	8	12	96
Core-Exit Temperature	21	12	252
IHX Orifice Plate Temp.	5	8	40
IHX Primary Outlet Temp.	4	16	64
Bulk Na Pool Temperature	13	16	208
IHX Secondary Inlet Temp.	1	10	10
IHX Secondary Outlet Temp.	2	16	32
SU Na Inlet Header Temp.	3	2	6
SU Na Inlet Temperature	5	3	15
SU Na Outlet Temperature	6	≈5	30
EV Na Inlet Temperature	8	9	72
EV Na Outlet Temperature	10	≈2	22
Steam Drum Level	1	2	2
Blowdown Flow Rate	1	2	2
EV Feedwater Temperature	10	24	240
EV Steam Outlet Temp.	7	≈3	22
SU Steam Inlet Temp.	2	7	14
SU Steam Outlet Temp.	4	≈7	30
	114		1232

The modeling results for each output variable will be presented below. The functional forms exhibited by the modeling for the PEM module and those for the MGCC module will be compared. The PEM models produced from the individual signals (versus the SGCC estimates) are presented in the tables. Coefficients will be given from the MGCC models, since they are more representative.

F.1.1 Power Empirical Models

Three power signals were available for modeling. Based upon heat balance considerations, the power (%) signal was modeled using the following three inputs:

$$\text{Power} = f(\text{Inlet Plenum Temp, Upper Plenum Temp, Secondary Na Flow}) \qquad (F.1)$$

The secondary sodium flow is used as an input since it is used to control the power level. The primary sodium flow was initially used as an input, but was routinely omitted by the modeling algorithm due to the nearly constant primary flow rate. The PEM results appear in Table F.2. The resulting MGCC functional form was

$$\text{Power} = c_0 + c_1\, z + c_2\, x + c_3\, y \qquad (F.2)$$

where,

x = Inlet plenum temperature (°F)

y = Upper plenum temperature (°F)

z = Secondary Na flow (%)

c_0 = -297.81720

c_1 = 0.18492852

TABLE F.2

Empirical Models For Power

Functional Form	No. of Models	Percentage of Total
$z + x + y$	56	78
$yz + x + x^2 + y$	9	13
$yz + x + x^2 + y + xy + z^2 + xz$	1	1
$yz + z^2 + x^2 + x + xy$	2	3
$y^2z + x + x^2 + y^3 + y$	4	6
	72	

x = Inlet Plenum Temperature
y = Upper Plenum Temperature
z = Secondary Na Flow Rate

$c_2 = -0.081697963$
$c_3 = \ 0.50669384$

A total of 78% of the PEM functional forms were identical to that found in the MGCC model. The PEM modeling error ranged from 1.7% to 2.9% with an average of 2.4%. The MGCC modeling error was 2.2%. A comparison of a measured and predicted power signal is shown in Figure F.1.

As an added experiment, the reactor power was also modeled using the single control rod which was moved during start-up.

$$\text{Power} = f(\text{Control Rod Position}) \qquad (F.3)$$

The three PEM results and the MGCC each possessed the following functional form:

$$\text{Power} = c_0 + c_1\, x^3 + c_2\, x^2 + c_3\, x \qquad (F.4)$$

where,

x = Control rod #11 position (inches)
$c_0 = -114.90222$
$c_1 = \ 0.12661622$
$c_2 = -2.6642342$
$c_3 = \ 34.5961$

This control rod was the only one moved during the reactor start-up procedure. The MGCC modeling error was 2.7%. A measured versus predicted power signal from the control rod position is shown in Figure F.2. Note that this single input model is nearly able to describe the power as well as the model of Equation F.2.

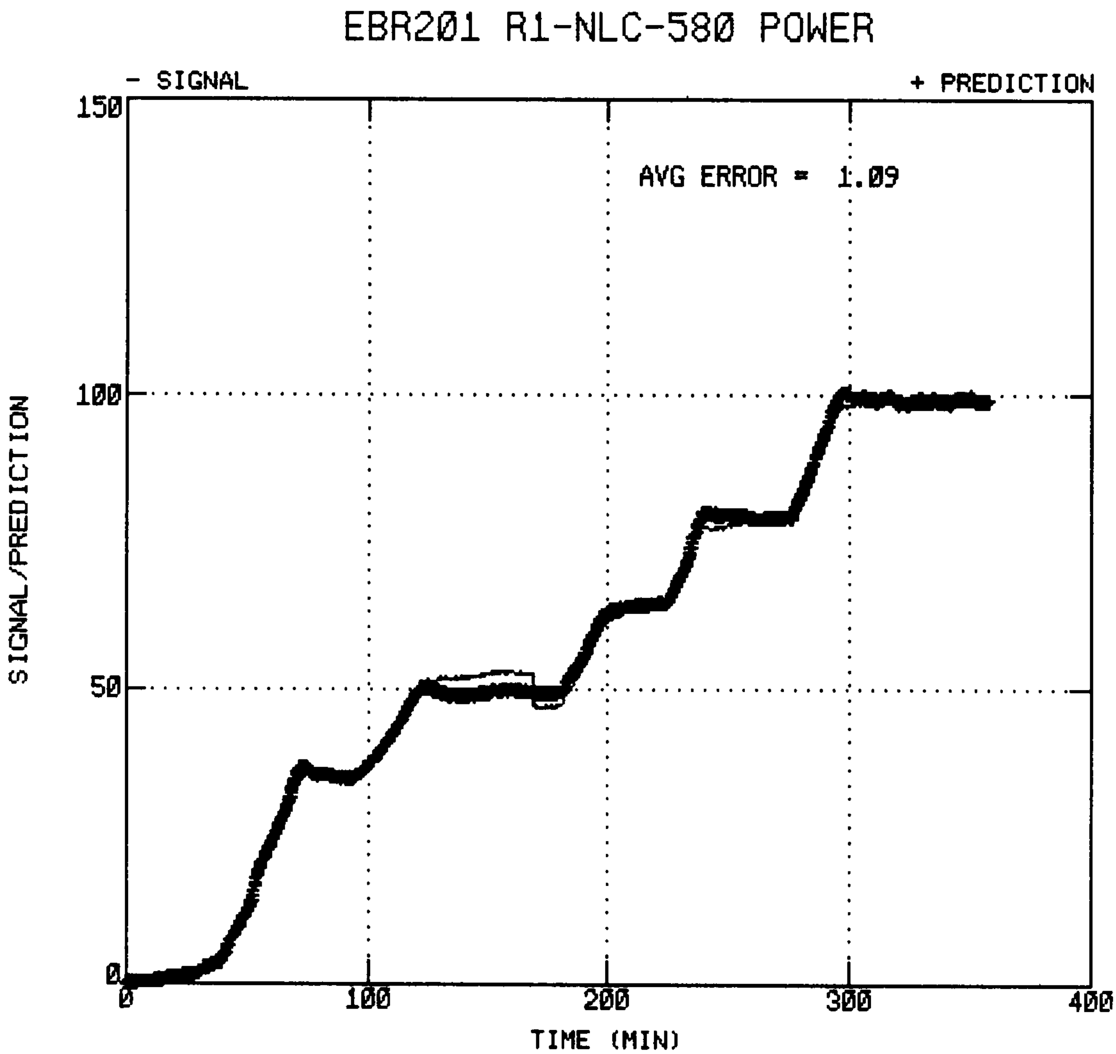

Figure F.1. Comparison of Measured and Predicted Power Signal.

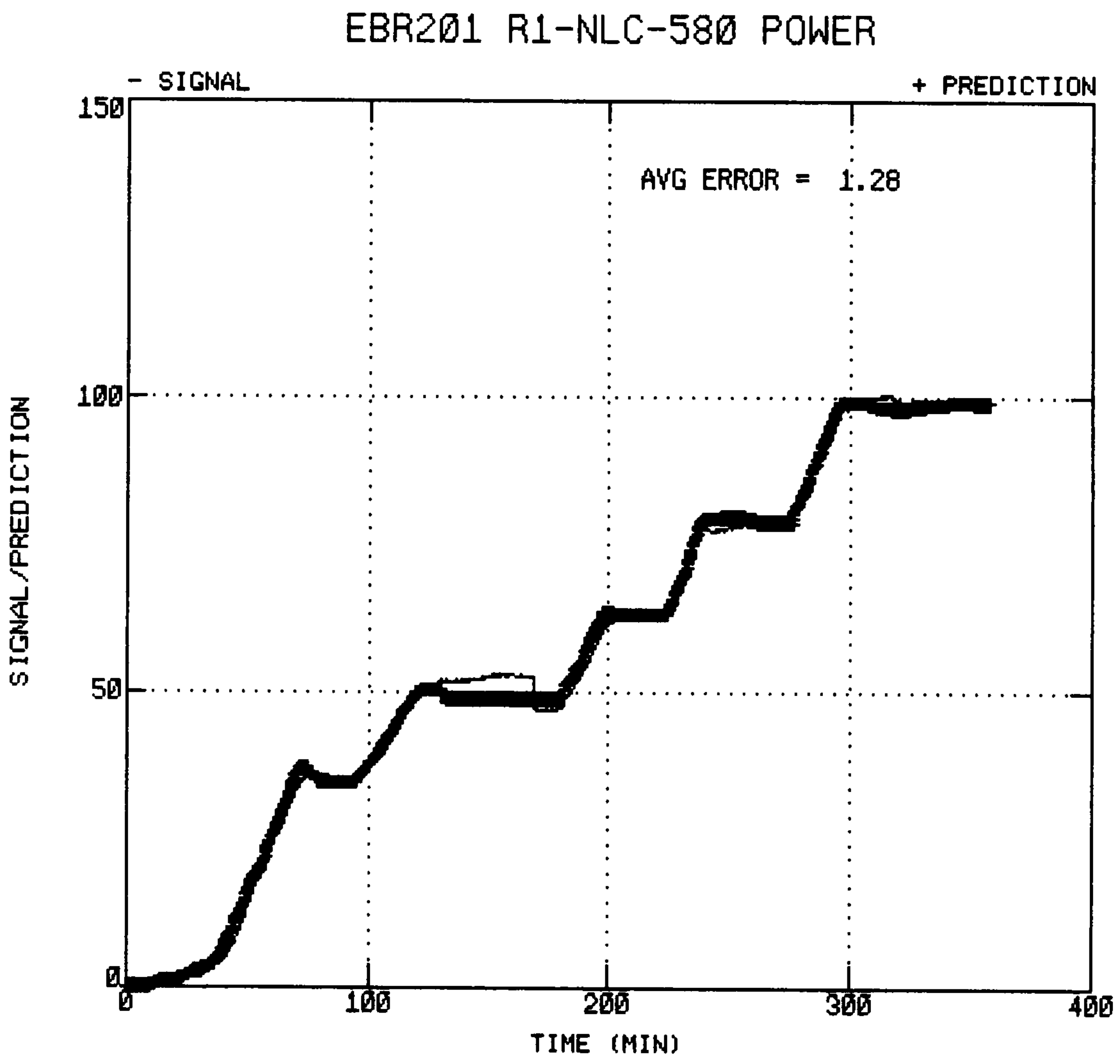

Figure F.2. Comparison of Measured and Predicted Power Signal from Control Rod Position.

F.1.2 Upper Plenum Temperature Empirical Models

The eight upper plenum temperature signals were modeled using the power and inlet plenum temperature.

$$\text{Upper Plenum Temp} = f(\text{Power, Inlet Plenum Temp}) \qquad \text{(F.5)}$$

The constant primary sodium flow rate was once again omitted from the empirical model. The PEM results appear in Table F.3. The functional form found from the MGCC fitting was

$$\text{Upper Plenum Temp} = c_0 + c_1\, y + c_2\, x + c_3\, y^2 + c_4\, x^3 + c_5\, x^2 y \qquad \text{(F.6)}$$

where,

x = Power (%)

y = Inlet plenum temperature (°F)

c_0 = 1991.1262

c_1 = -3.1840515

c_2 = 1.1501837

c_3 = 0.0019199266

c_4 = -0.000051762094

c_5 = 0.000014061327

The MGCC form contains 71% of the PEM results. The PEM modeling error ranged from 0.22% to 0.52% with an average of 0.35%. The MGCC modeling error was 0.32%.

F.1.3 Core-Exit Temperature Empirical Models

The input signal combination used to model the upper plenum temperature was also used to fit the core-exit temperature. Primary flow was included, then omitted.

TABLE F.3

Empirical Models For Upper Plenum Temperature

Functional Form	No. of Models	Percentage of Total
$y + x$	18	19
$y + x + y^2 + x^2$	11 A	11
$y + y^2 + x^2 + x$	15 A	16
$y + y^2 + x^2 + x + xy$	1	1
$y + x + y^2 + x^3$	14	15
$y + x + y^2 + x^3 + x^2y$	36	38
$y + x + y^2 + x^3 + x^2y + y^3$	1	1
	96	

x = Power
y = Inlet Plenum Temperature

$$\text{Core-Exit Temp} = f(\text{Power, Inlet Plenum Temp}) \tag{F.7}$$

The PEM results appear in Table F.4. Two functional forms were exhibited from the MGCC modeling. The first MGCC functional form, with a fitting error of 0.31%, is

$$\text{Core-Exit Temp} = c_0 + c_1\, y + c_2\, x + c_3\, y^2 + c_4\, x^2 \tag{F.8}$$

where,

x = Power (%)

y = Inlet plenum temperature (°F)

c_0 = -42896.633

c_1 = 124.18116

c_2 = 1.4557229

c_3 = -0.088428624

c_4 = 0.0017555681

The second MGCC form, with a fitting error of 0.42%, is

$$\text{Core-Exit Temp} = c_0 + c_1\, y + c_2\, x + c_3\, y^2 + c_4\, x^3 \tag{F.9}$$

where,

c_0 = -47105.012

c_1 = 134.79559

c_2 = 1.7127849

c_3 = -0.095008098

c_4 = 0.000012474708

The deviation in the two forms is due to the difference in location. A total of 56% and 35% (with an overlap of 25%) of the PEM results are given in the first and second MGCC forms, respectively. The PEM modeling error ranged from 0.2% to 2.6% with an average of 0.6%. The average MGCC modeling error was 0.37%.

TABLE F.4

Empirical Models For Core-Exit Temperature

Functional Form	No. of Models	Percentage of Total
$y + x$	63	25
$y + y^2 + x^2 + x$	45 A	18
$y + x + y^2 + x^2$	32 A	13
$y + x + y^2 + x^2 + xy$	2	<1
$y + x + y^2 + x^3$	26	10
$y + x + y^2 + x^3 + x^2y$	77	31
$y + x + y^2 + x^3 + x^2y + y^3$	5	2
$y + x + y^2 + x^3 + x^2y + y^3 + x^2$	1	<1
$y + x + y^2 + x^3 + x^2y + y^3 + xy^2$	1	<1
	252	

x = Power
y = Inlet Plenum Temperature

F.1.4 IHX Orifice Plate Temperature Empirical Models

The intermediate heat exchanger (IHX) orifice plate temperature is located in the IHX in a region where heat transfer between the primary and secondary sodium takes place. The selected input set was therefore:

$$\text{IHX Orifice Plate Temp} = f(\text{Upper Plenum Temp}, \text{IHX Secondary Inlet Temp}) \quad (F.10)$$

The PEM results are given in Table F.5. The functional form found from the MGCC fit includes 55% of the PEM models:

$$\text{IHX Orifice Plate Temp} = c_0 + c_1\, y^2 + c_2\, x + c_3\, x^2 + c_4\, y \quad (F.11)$$

where,

x = Upper plenum temperature (°F)

y = IHX secondary inlet temperature (°F)

c_0 = 739.83435

c_1 = 0.0074856626

c_2 = 5.9074225

c_3 = -0.0032731963

c_4 = -8.8033419

The PEM modeling error ranged from 0.05% to 0.28% with an average of 0.15%. The MGCC modeling error was 0.28%. The measured and predicted values of Figure F.3 are indistingui able.

TABLE F.5

Empirical Models For IHX Orifice Plate Temperature

Functional Form	No. of Models		Percentage of Total
$x + y + x^3$	1		3
$x + y^2 + x^3 + y$	1		3
$x + y^2 + x^3 + x^2y$	1		3
$x + y + y^2 + x^2$	6	B	15
$x + y + y^2 + x^2 + xy$	1	C	3
$x + x^2y + x^2$	2		5
$x + x^2y + x^3$	2		5
$x + xy + x^2 + y$	2	A	5
$x + x^2 + xy + y$	2	A	5
$y + x + y^2 + x^2$	10	B	25
$y + x + y^2 + x^2 + xy$	1	C	3
$y + x + y^2 + x^2y$	5		13
$y^2 + x + x^2$	6		15
	40		

x = Upper Plenum Temperature
y = IHX Secondary Inlet Temperature

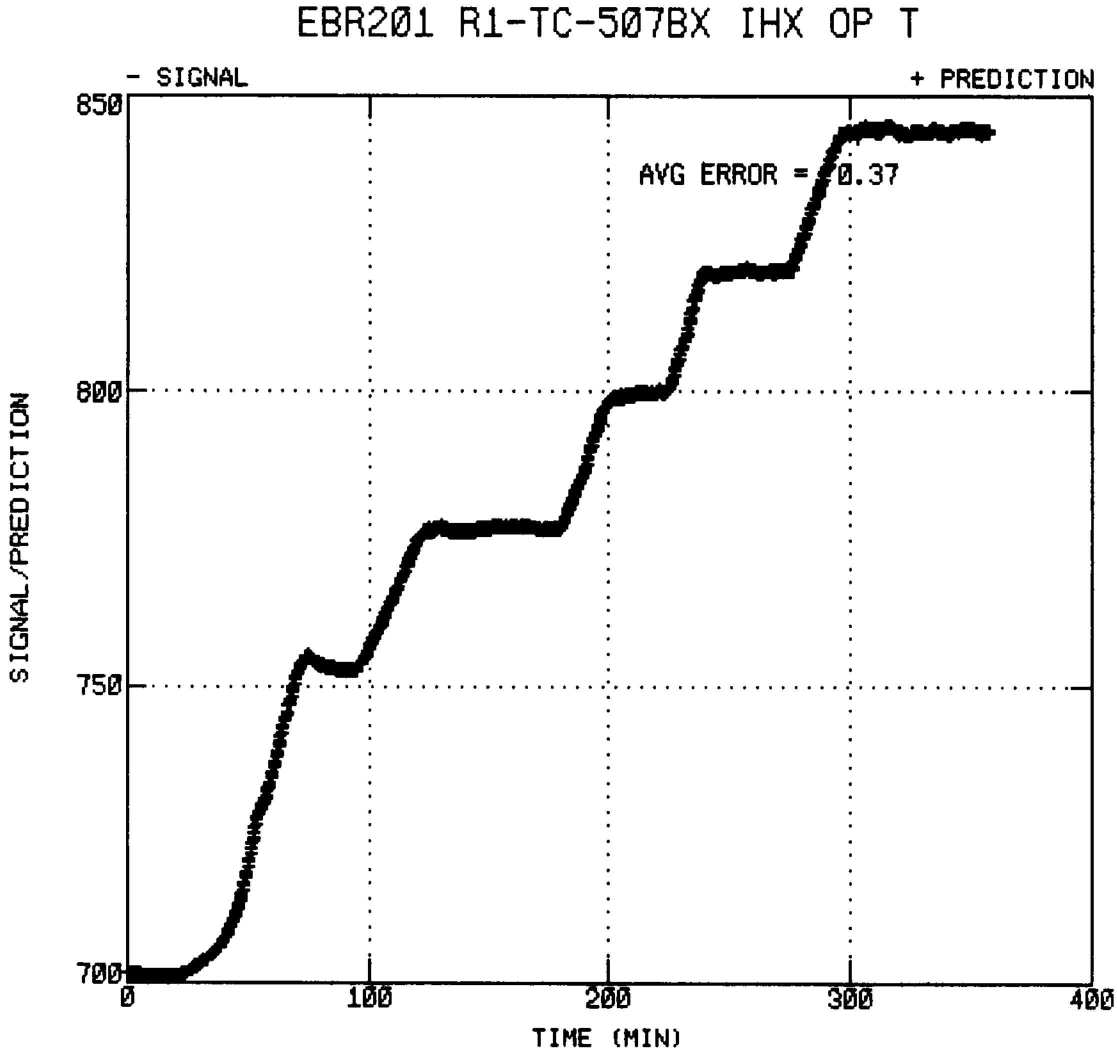

Figure F.3. Comparison of Measured and Predicted IHX Orifice Plate Temperature Signal.

F.1.5 IHX Primary Outlet Temperature Empirical Models

Four IHX primary outlet temperature signals were available for modeling. The selected input signals were based upon a simple heat balance on the IHX.

$$\text{IHX Primary Outlet Temp} = f(\text{Upper Plenum Temp}, \text{IHX Secondary Outlet Temp}, \text{IHX Secondary Inlet Temp}, \text{Secondary Na Flow Rate}) \quad (F.12)$$

The PEM results are given in Table F.6. The MGCC result was

$$\text{IHX Primary Outlet Temp} = c_0 + c_1\, y + c_2\, w + c_3\, w^2 + c_4\, wx + c_5\, wy + c_6\, x^2 + c_7\, z^2 + c_8\, xy \quad (F.13)$$

where,

w = Upper plenum temperature (°F)

x = IHX secondary outlet temperature (°F)

y = IHX secondary inlet temperature (°F)

z = Secondary Na flow (%)

c_0 = 1355.3479

c_1 = -2.0513110

c_2 = -0.47910854

c_3 = -0.00079276116

c_4 = 0.00012994665

c_5 = 0.0032942260

c_6 = 0.000083634215

c_7 = -0.0051503056

c_8 = -0.00045117782

and includes 69% of the PEM functional forms found. The PEM modeling error ranged from 0.11% to 0.16% with an average of 0.12%. The MGCC modeling error was 0.10%.

TABLE F.6

Empirical Models For
IHX Primary Outlet Temperature

Functional Form	No. of Models	Percentage of Total
$y + w + x + z$	2	3
$y + w + x + w^2y + w^2x$	10	16
$y + w + x + w^2y + w^2x + wx$	5	8
$y + w + x + w^2y + w^2x + wx + wx^2$	1	2
$y + w + x + wx + w^2 + x^2 + wy + xy$	2	3
$y + w + w^2 + wx + wy + x^2 + z^2$	31	48
$y + w + w^2 + wx + wy + x^2 + z^2 + xy$	13	20
	64	

w = Upper Plenum Temperature
x = IHX Secondary Outlet Temperature
y = IHX Secondary Inlet Temperature
z = Secondary Na Flow Rate

F.1.6 Bulk Sodium Pool Temperature Empirical Models

There were thirteen primary Na pool temperature signals available.

$$\text{Bulk Na Pool Temp} = f(\text{IHX Primary Outlet Temp, Inlet Plenum Temp}) \quad (F.14)$$

Table F.7 contains the large number of scattered PEM modeling results. The MGCC models are subdivided into three groups representing the three different elevations where measurements are made in the primary tank (pool). The first MGCC form, with an error of 0.58%, was exhibited by one of the three MGCC models:

$$\text{Bulk Na Pool Temp} = c_0 + c_1\, x + c_2\, y^3 + c_3\, x^2 + c_4\, y \quad (F.15)$$

where,

x = IHX primary outlet temperature (°F)

y = Inlet plenum temperature (°F)

The second MGCC form was exhibited in two of the three MGCC models, both with a fitting error of 0.18%:

$$\text{Bulk Na Pool Temp} = c_0 + c_1\, y^2 + c_2\, x + c_3\, x^2 + c_4\, y \quad (F.16)$$

The PEM modeling error ranged from 0.1% to 1.1% with an average of 0.4%. The average MGCC modeling error was 0.31%. The two MGCC functional forms encompass half of the PEM models found. The MGCC coefficients are given in Table F.8 for the three models. The first model is for the temperature measured at a height of 36 inches and the second

TABLE F.7

Empirical Models For Bulk Sodium Pool Temperature

Functional Form	No. of Models	Percentage of Total
$y + x + xy + x^2 + y^2$	5 A	2
$y + x + xy + x^2y + x^2 + y^2$	1 G	<1
$y + x + xy + x^2y + x^2 + y^2 + xy^2$	2 H	<1
$y + x + y^2$	15	7
$y + x + y^2 + xy$	12	6
$y + x + y^2 + xy + x^2$	4 A	2
$y + x + y^2 + x^2y$	17	8
$y + x + y^2 + x^2y + x^2$	2 E	<1
$y + x + y^2 + x^2y + x^2 + xy$	2 G	<1
$y + x + y^2 + x^2y + x^2 + xy + xy^2$	6 H	3
$y + x + y^2 + xy + x^2$	5 A	2
$y + y^2 + x^2 + x$	8 B	4
$y^2 + x + x^2$	4 C	2
$y^2 + x + x^2 + y$	5 B	2
$y^2 + x + x^2 + y + x^2y$	4 E	2
$y^2 + x + x^2 + y + x^2y + xy$	2 G	<1
$y^2 + x + x^2 + y + x^2y + xy + xy^2$	1 H	<1
$xy + x^2 + x^3 + y + y^3 + y^2 + x^2y$	1	<1
$x + y$	2	<1

TABLE F.7 (Continued)

Functional Form	No. of Models		Percentage of Total
$x + x^2 + xy + y + y^2$	1	A	<1
$x^2 + x$	7		3
$x^2 + x + xy$	11		5
$x^2 + x + y$	31		15
$x^2 + x + y + xy$	3		1
$x^2 + x + y + x^3 + y^3$	1	F	<1
$x^2 + x + y + y^2 + xy$	5	A	2
$x^2 + x + y + y^3$	2	D	<1
$x^2 + x + y + y^3 + x^3$	1	F	<1
$x^2 + x + y^2$	28	C	13
$x^2 + x + y^2 + x + x^3$	1		<1
$x^2 + x + y^3 + y$	2	D	<1
$x^2 + x + y^3 + xy$	1		<1
$x^2 + x + xy^2$	3		1
$x^2 + x + x^2y$	4		2
$x^2 + x + x^2y + y$	2		<1
$x^2 + x + x^2y + y^3$	2		<1
$x^2 + x + xy + y^2$	2		<1
$x^2 + x + xy + y^2 + y$	1	A	<1
$x^2 + x + xy + y + y^3 + y^2 + x^2y$	1		<1
$x^2 + x + y^2 + y + y^3$	1		<1
	208		

x = Primary Outlet Temperature
y = Inlet Plenum Temperature

TABLE F.8

Bulk Sodium Pool Temperature Model Coefficients

Term	Model #1	Model #2	Model #3
c_0	222251.38	-7195.2866	-20555.248
c_1	379.90924	-0.23353009	-0.25610247
c_2	0.00050991063	-307.68716	-301.43207
c_3	-0.26760530	0.21735148	0.21301356
c_4	-758.94012	330.29416	361.96057

and third models are for signals at a height of 222 and 276 inches, respectively.

F.1.7 IHX Secondary Inlet Temperature Empirical Models

Only a single IHX secondary inlet temperature signal was suitable for modeling.

$$\text{IHX Secondary Inlet Temp} = f(\text{EV Na Outlet Temperature, Secondary Na Flow Rate}) \quad (F.17)$$

The PEM results are given in Table F.9. The MGCC result is shown below:

$$\text{IHX Secondary Inlet Temp} = c_0 + c_1\, x + c_2\, y + c_3\, x^2 + c_4\, xy \quad (F.18)$$

where,

x = EV Na outlet temperature (°F)

y = Secondary Na flow (%)

c_0 = 23313.613

c_1 = -82.140793

c_2 = 19.176495

c_3 = 0.074071512

c_4 = -0.033186026

and is identical to 70% of the PEM forms found. The PEM modeling error ranged from 0.17% to 0.29% with an average of 0.24%. The MGCC modeling error was 0.25%.

F.1.8 IHX Secondary Outlet Temperature Empirical Models

Two IHX secondary outlet temperature signals were modeled. The following inputs were utilized.

TABLE F.9

Empirical Models For
IHX Secondary Inlet Temperature

Functional Form	No. of Models	Percentage of Total
$x + y + x^2 + xy$	6 A	60
$x^2 + x + xy + y$	1 A	10
$x^2 + x + y^2 + y$	3	30
	10	

x = EV Na Outlet Temperature
y = Secondary Na Flow Rate

IHX Secondary Outlet Temp = f(Upper Plenum Temp, IHX Primary Outlet Temp, IHX Secondary Inlet Temp, Secondary Na Flow Rate) (F.19)

The PEM results are shown in Table F.10. The MGCC functional form is

$$\text{IHX Secondary Outlet Temp} = c_0 + c_1\, wx + c_2\, w + c_3\, w^2 + c_4\, x \qquad \text{(F.20)}$$

where,

w = Upper plenum temperature (°F)

x = IHX primary outlet temperature (°F)

y = IHX secondary inlet temperature (°F)

z = Secondary Na flow (%)

c_0 = 4978.0459

c_1 = 0.0099775465

c_2 = -4.1882887

c_3 = -0.0012010777

c_4 = -8.0649767

Note that the last two input variables (y and z) were omitted from the final MGCC model, thus making comparison to the PEM results is complicated. The PEM modeling error ranged from 0.06% to 0.26% with an average of 0.15%. The MGCC modeling error was 0.11%. Comparison of a measured and predicted IHX secondary outlet temperature signal is shown in Figure F.4.

F.1.9 SU Na Inlet Header Temperature Empirical Models

The superheater (SU) receives its sodium flow directly from the IHX. Thus the following input signal set:

TABLE F.10

Empirical Models For IHX Secondary Outlet Temperature

Functional Form	No. of Models	Percentage of Total
$w + z + x + y$	4	13
$w + z^3 + x^2y + w^2 + x$	2	6
$w + y^2 + x^2z + w^3 + w^2x$	3	9
$w + y^2 + x^2z + w^3 + w^2x + wx$	1	3
$wx + wx^2 + w^2$	1	3
$wx + w + w^2 + x$	7	22
$wx + w + w^2 + wy$	6	19
$wx + w + w^2 + wy + w^2y + x$	3	9
$wx + w + w^2 + wy + w^2y + x + w^3$	2	6
$wx + w + w^2 + x + x^2 + z + xy$	2	6
$wx^2 + w + w^2$	1	3
	32	

w = Upper Plenum Temperature
x = IHX Primary Outlet Temperature
y = IHX Secondary Inlet Temperature
z = Secondary Na Flow Rate

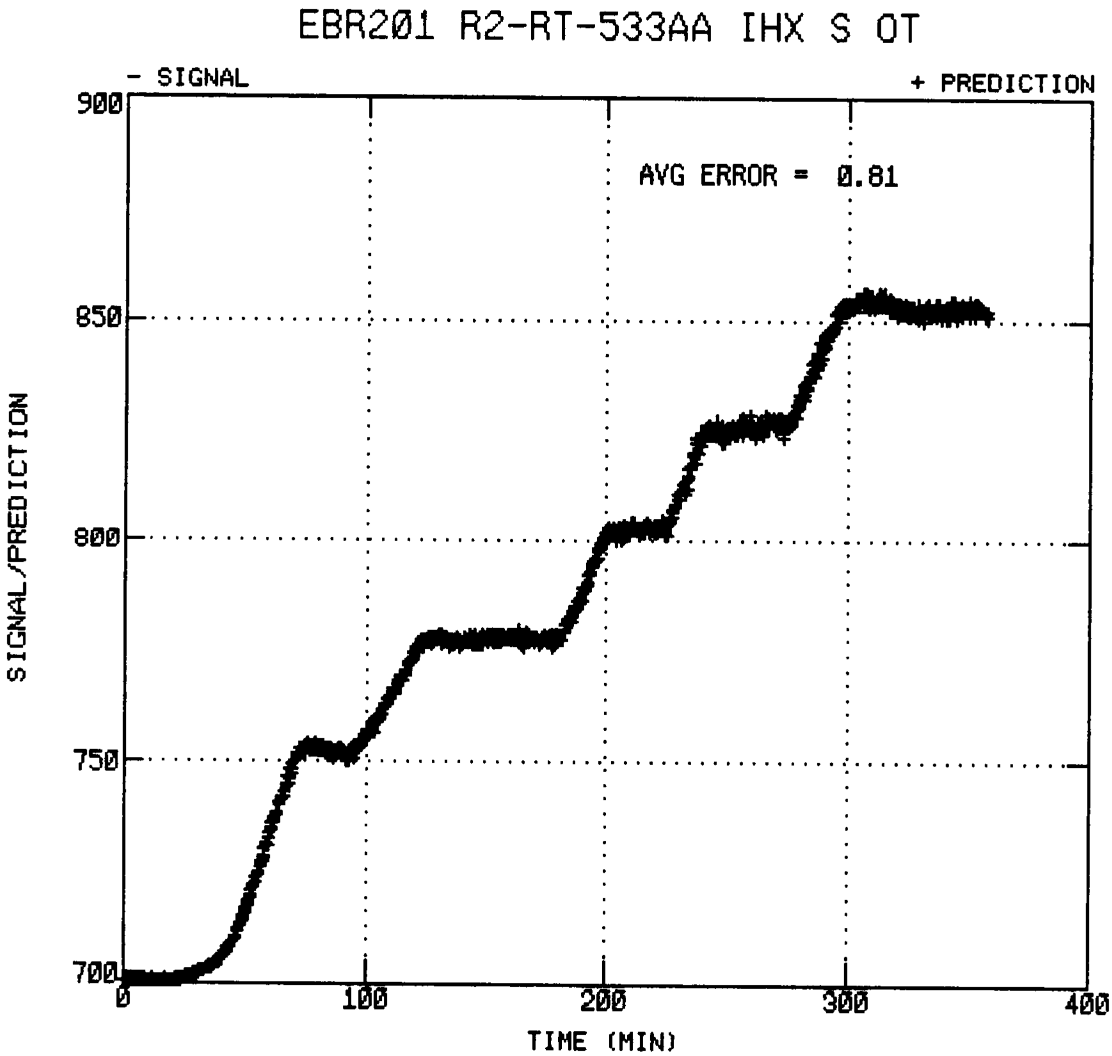

Figure F.4. Comparison of Measured and Predicted IHX Secondary Outlet Temperature Signal.

SU Na Inlet Header Temp = f(IHX Secondary Outlet Temp, Secondary Na Flow Rate) (F.21)

The PEM fitting results appear in Table F.11. The MGCC functional form includes half the PEM results, and is

$$\text{SU Na Inlet Header Temp} = c_0 + c_1\, x + c_2\, y + c_3\, y^3 + c_4\, x^3 + c_5\, y^2 \qquad (F.22)$$

where,

x = IHX secondary outlet temperature (°F)

y = Secondary Na flow (%)

c_0 = 172.30467

c_1 = 0.66918039

c_2 = 0.29345182

c_3 = 0.00000072886775

c_4 = 0.00000015895652

c_5 = -0.0017548926

The PEM modeling error ranged from 0.04% to 0.17% with an average of 0.09%. The MGCC modeling error was 0.07%.

F.1.10 <u>SU Na Inlet Temperature Empirical Models</u>

The input signals for the two individual superheater inlet temperatures are

SU Na Inlet Temp = f(SU Na Inlet Header Temp, Secondary Na Flow Rate) (F.23)

Note that the IHX secondary outlet temperature could have just as easily been used instead of the superheater sodium inlet header temperature. The PEM functional forms are given in Table F.12, and the MGCC result was

TABLE F.11

Empirical Models For SU Sodium Inlet Header Temperature

Functional Form	No. of Models	Percentage of Total
$x + y + x^2$	2	33
$x + y + y^2 + x^2$	1	17
$x + y + y^3 + x^3 + y^2$	3	50
	6	

x = IHX Secondary Outlet Temperature
y = Secondary Na Flow Rate

TABLE F.12

Empirical Models For SU Sodium Inlet Temperature

Functional Form	No. of Models	Percentage of Total
$x + y + x^2$	2	13
$x + y + x^2 + xy$	1	7
$x + y + y^3 + x^3 + y^2$	12	80
	15	

x = SU Na Inlet Header Temperature
y = Secondary Na Flow Rate

$$\text{SU Na Inlet Temp} = c_0 + c_1\, x + c_2\, y + c_3\, y^3 + c_4\, x^3 + c_5\, y^2 \quad \text{(F.24)}$$

where,

x = SU Na inlet header temperature (°F)

y = Secondary Na flow (%)

c_0 = -1040.8524

c_1 = 2.9400499

c_2 = 0.073489383

c_3 = 0.00011715262

c_4 = -0.00000095004776

c_5 = -0.014599155

Of the PEM forms, 80% are contained within the MGCC result. The PEM modeling error ranged from 0.1% to 1.1% with an average of 0.5%. The MGCC modeling error was 0.14%.

F.1.11 SU Na Outlet Temperature Empirical Models

Six superheater (SU) sodium outlet temperature signals were available for modeling.

$$\text{SU Na Outlet Temp} = f(\text{SU Na Inlet Temp, Secondary Flow Rate, SU Steam Inlet Temp, SU Steam Outlet Temp, SU Steam Outlet Flow}) \quad \text{(F.25)}$$

Table F.13 contains the PEM results. The MGCC result was

$$\text{SU Na Outlet Temp} = c_0 + c_1\, vx + c_2\, v + c_3\, v^2 + c_4\, w + c_5\, z^2 \quad \text{(F.26)}$$

where,

v = SU Na inlet temperature (°F)

w = Secondary Na flow (%)

x = SU steam inlet temperature (°F)

y = SU steam outlet temperature (°F)

TABLE F.13

Empirical Models For SU Sodium Outlet Temperature

Functional Form	No. of Models	Percentage of Total
$xy + v + v^2 + w + w^2$	2	7
$xy + y + v + vw + wy + w^2$	2	7
$xy + y + v + vw + wy + w^2 + z$	1	3
$xy + y + v + vw + wy + w^2 + z + x^2$	1	3
$xy + y + v + w + vw + vy$	1	3
$xy + y + v + w + vw + vy + wy$	1	3
$xy + y + x^2 + v^2x + v^2w + wx$	1	3
$xy + y + x^2 + vw + wy + w^2 + z$	2	7
$xy + y + x^2 + w + vw + wy + z + v^2$	1	3
$x^2y + xy + v^2 + vx^2$	1	3
$x^2y + xy + v^2 + vx^2 + v^2y$	1	3
$v + z + w + x + y$	6 A	20
$v + w + z + x + y$	10 A	33
	30	

v = SU Na Inlet Temperature
w = Secondary Na Flow Rate
x = SU Steam Inlet Temperature
y = SU Steam Outlet Temperature
z = SU Steam Outlet Flow

z = SU steam outlet flow (lbm/hr)

$c_0 = 775.74139$

$c_1 = -0.00019916463$

$c_2 = -0.66259664$

$c_3 = 0.00093149499$

$c_4 = 0.062630430$

$c_5 = -0.15399319\text{x}10^{-09}$

Input variable y, the superheater steam outlet temperature, was excluded from the final MGCC model. Because of this omission, it is difficult to compare the PEM and MGCC results. The PEM modeling error ranged from 0.15% to 0.73% with an average of 0.33%. The MGCC modeling error was 0.37%.

F.1.12 EV Na Inlet Temperature Empirical Models

The secondary sodium leaving the two superheaters moves directly to the seven evaporator (EV) sodium inlets, hence the following input quantities:

$$\text{EV Na Inlet Temp} = f(\text{SU 710 Na Outlet Temp}, \text{SU 712 Na Outlet Temp}) \quad \text{(F.27)}$$

The PEM functional forms found appear in Table F.14 while the MGCC form was

$$\text{EV Na Inlet Temp} = c_0 + c_1\, y + c_2\, x + c_3\, xy + c_4\, x^2 \quad \text{(F.28)}$$

where,

x = SU 710 Na outlet temperature (°F)

y = SU 712 Na outlet temperature (°F)

$c_0 = -1075.3777$

TABLE F.14

Empirical Models For EV Sodium Inlet Temperature

Functional Form	No. of Models	Percentage of Total
$y + x + xy$	18	25
$y + x + xy + x^2$	28	39
$y + x + xy + x^2 + y^2$	17	24
$y + x + xy + x^2y$	4	6
$y + x + xy + x^2y + x^2$	4	6
$y + x + xy + x^2y + x^2 + x^3 + xy^2 + y^2$	1	1
	72	

x = SU710 Na Outlet Temperature
y = SU712 Na Outlet Temperature

$c_1 = 3.2178626$

$c_2 = 0.61109310$

$c_3 = -0.0030703724$

$c_4 = 0.0012092605$

The MGCC form includes 64% of the PEM forms. The PEM modeling error ranged from 0.17% to 0.58% with an average of 0.37%. The MGCC modeling error was 0.25%.

F.1.13 EV Na Outlet Temperature Empirical Models

Ten evaporator sodium outlet temperature signals were available for modeling.

$$\text{EV Na Outlet Temp} = f(\text{EV Na Inlet Temp, Secondary Na Flow, EV FW Inlet Temp, EV Steam Outlet Temp, SU Steam Outlet Flow}) \quad \text{(F.29)}$$

The PEM results are given in Table F.15. The MGCC result is

$$\text{EV Na Outlet Temp} = c_0 + c_1\,x + c_2\,v + c_3\,y + c_4\,vx + c_5\,vw + c_6\,w^2 + c_7\,v^2 \quad \text{(F.30)}$$

where,

v = EV Na inlet temperature (°F)

w = Secondary Na flow (%)

x = EV feedwater inlet temperature (°F)

y = EV steam outlet temperature (°F)

z = SU steam outlet flow (lbm/hr)

$c_0 = 1440.8019$

$c_1 = -2.0145378$

$c_2 = -1.7194023$

$c_3 = 0.0045851436$

$c_4 = 0.0043542725$

$c_5 = -0.00011063858$

TABLE F.15

Empirical Models For
EV Sodium Outlet Temperature

Functional Form	No. of Models	Percentage of Total
$x + y + w + z + v$	4 A	18
$x + v + w + z + y$	13 A	59
$x + v + y + vx + vw + w^2$	2	9
$x + v + y + v^2x + v^2w + w$	1	5
$x + v + y + v^2y + v^2w + wy + w^2$	2	9
	22	

v = EV Na Inlet Temperature
w = Secondary Na Flow Rate
x = EV Feedwater Inlet Temperature
y = EV Steam Outlet Temperature
z = SU Steam Outlet Flow

$c_6 = \ \ 0.0016658873$
$c_7 = -0.00052596285$

The last variable, the SU steam outlet flow, was omitted from the final MGCC model. This omission makes comparison of the PEM and MGCC forms difficult. The PEM modeling error ranged from 0.04% to 0.24% with an average of 0.09%. The MGCC modeling error was 0.06%. A comparison of the measured versus predicted EV sodium outlet temperature signal is given in Figure F.5 for the first evaporator.

F.1.14 Steam Drum Level Empirical Models

Only a single steam drum level signal was available for modeling. The selected input signal set was

$$\text{Steam Drum Level} = f(\text{Blowdown Flow, Steam Drum FW Flow,} \\ \text{Drum Pressure, SU Steam Outlet Flow}) \qquad (F.31)$$

The PEM results are shown in Table F.16. The MGCC result is

$$\text{Drum Level} = c_0 + c_1\, y + c_2\, y^2 + c_3\, w^2 + c_4\, w + \\ c_5\, x + c_6\, wx + c_7\, xy + c_8\, z^2 \qquad (F.32)$$

where,

w = Blowdown flow (lbm/hr)
x = Steam drum feedwater flow (lbm/hr)
y = Steam drum steam pressure (psi)
z = SU steam outlet flow (lbm/hr)
$c_0 = \ \ 336.24908$
$c_1 = -0.53418785$
$c_2 = \ \ 0.00022693140$
$c_3 = -0.41618772\text{x}10^{-07}$
$c_4 = \ \ 0.97886143\text{x}10^{-04}$

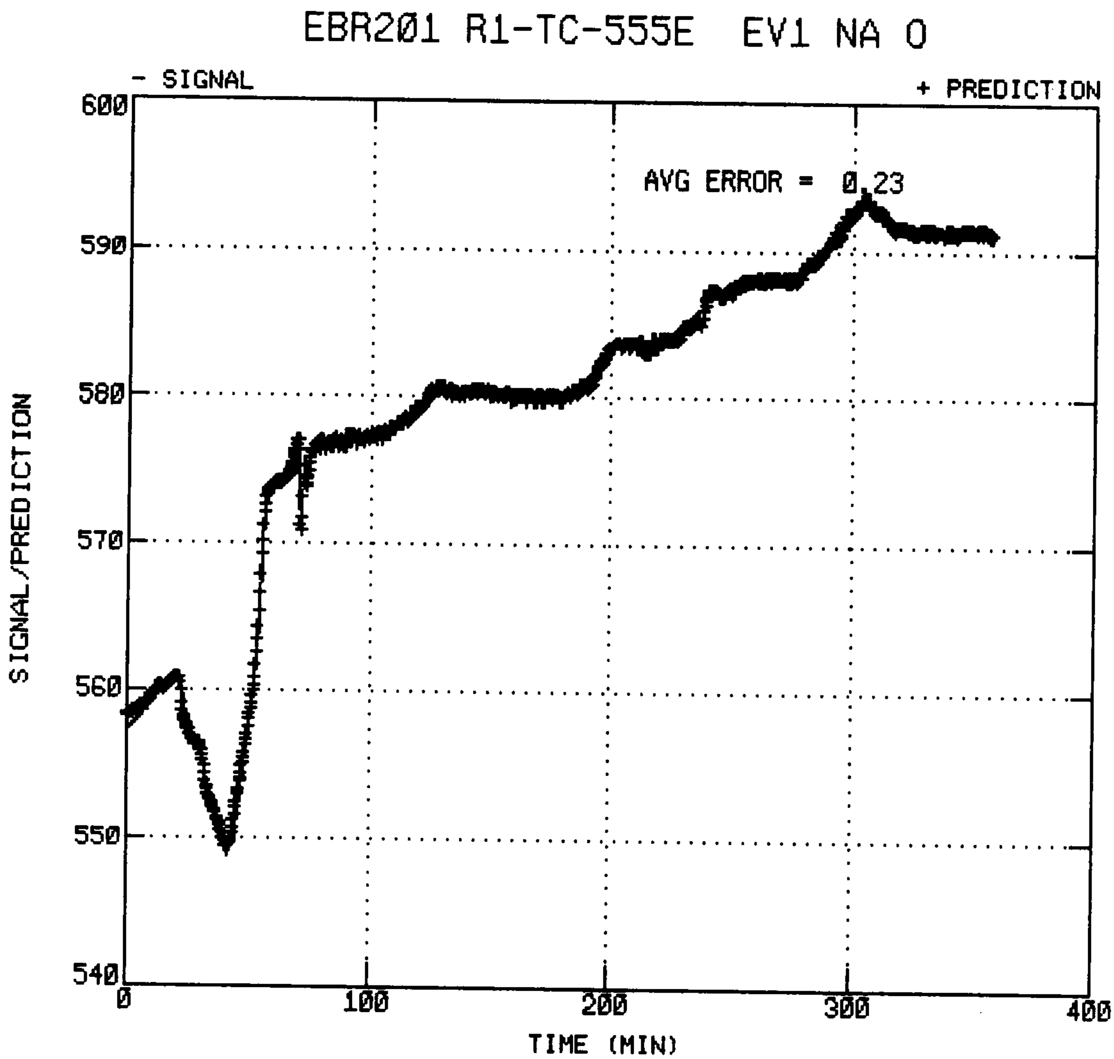

Figure F.5. Comparison of Measured and Predicted EV Sodium Outlet Temperature Signal.

TABLE F.16

Empirical Models For Steam Drum Level

Functional Form	No. of Models	Percentage of Total
$y + y^2 + w^2 + w + x + wx + x^2 + z^2$	1	50
$y + y^2 + w^2 + w + x + wx + xy + z^2$	1	50
	2	

w = Blowdown Flow Rate
x = Steam Drum Feedwater Flow Rate
y = Steam Drum Pressure
z = SU Steam Outlet Flow

c_5 = 0.00040163568
c_6 = $0.99550732 \times 10^{-08}$
c_7 = $-0.43000097 \times 10^{-06}$
c_8 = $0.22543757 \times 10^{-10}$

Only two PEM models were formed with an error of 6.6% and 7.0% (average of 6.8%). The MGCC modeling error was 6.7%.

F.1.15 Blowdown Flow Empirical Models

The blowdown flow also provided just one signal for modeling. The following signals were used as input:

$$\text{Blowdown Flow} = f(\text{Steam Drum Level, Steam Drum FW Flow, SU Steam Outlet Flow}) \quad (F.33)$$

The PEM results are given in Table F.17. The MGCC functional form found was

$$\text{Blowdown Flow} = c_0 + c_1\, y + c_2\, xy + c_3\, x^2 y + c_4\, x + c_5\, y^2 z + c_6\, x^2 + c_7\, x^3 + c_8\, xy^2 \quad (F.34)$$

where,
x = Steam drum level (inches)
y = Steam drum feedwater flow (lbm/hr)
z = SU steam outlet flow (lbm/hr)
c_0 = -633501.81
c_1 = -1.7029917
c_2 = 0.25845814
c_3 = -0.0080805533
c_4 = 82740.031
c_5 = $0.17852700 \times 10^{-11}$
c_6 = -3592.3779
c_7 = 51.960709
c_8 = $-0.85140293 \times 10^{-07}$

TABLE F.17

Empirical Models For Blowdown Flow Rate

Functional Form	No. of Models	Percentage of Total
$y + xy + x + z^2 + y^2 + xz + yz + x^2$	2	100
	2	

x = Steam Drum Level
y = Steam Drum Feedwater Flow Rate
z = SU Steam Outlet Flow Rate

The single PEM functional form did not match the MGCC form above. The PEM modeling error ranged from 9.0% to 9.5% with an average of 9.2%. The MGCC modeling error was 8.7%.

F.1.16 EV Feedwater Temperature Empirical Models

Ten evaporator feedwater (FW) temperature signals were available for modeling purposes.

$$\text{EV FW Temp} = f(\text{Drum Feedwater Flow, Drum Feedwater Temp, EV Steam Outlet Temp, SU Steam Inlet Temp, SU Steam Outlet Flow}) \quad (F.35)$$

The large number of PEM functional results are given in Table F.18. The MGCC result is

$$\text{EV FW Temp} = c_0 + c_1 x + c_2 x^2 + c_3 v^2 + c_4 w^2 + c_5 w + c_6 v + c_7 vx + c_8 vw \quad (F.36)$$

where,

v = Steam drum feedwater flow (lbm/hr)

w = Steam drum feedwater temperature (°F)

x = EV steam outlet temperature (°F)

y = SU steam inlet temperature (°F)

z = SU steam outlet flow (lbm/hr)

c_0 = 2775.5017

c_1 = -8.8012609

c_2 = 0.0088074841

c_3 = 0.85670351×10^{-11}

c_4 = 0.00028903136

c_5 = -0.24854456

c_6 = 0.00036134620

c_7 = $-0.99306521\times10^{-06}$

c_8 = 0.34906972×10^{-06}

TABLE F.18

Empirical Models For
EV Feedwater Temperature

Functional Form	No. of Models	Percentage of Total
$x + y + w + v + z$	43	18
$x + xy + v^2 + w^2 + vz + y^2$	2	<1
$x + xy + v^2 + w^2 + vz + y^2 + vy$	2	<1
$x + xy + v^2 + w^2 + vz + y^2 + vx$	14	6
$x + xy + v^2 + w^2 + vz + y^2 + vx + v$	10	4
$x + xy + v^2 + w^2 + vz + x^2$	5	2
$x + xy + v^2 + w^2 + vz + x^2 + vy$	16	7
$x + xy + v^2 + w^2 + vz + x^2 + vy + v$	1	<1
$x + xy + v^2 + w^2 + vz + x^2 + vx$	14 A	6
$x + xy + v^2 + w^2 + vz + x^2 + vx + v$	6	3
$x + xy + v^2 + w^2y + w$	20	8
$x + xy + v^2 + w^2y + w + wy$	1	<1
$x + xy + v^2 + w^2y + w + wy + vwz$	1	<1
$x + xy + v^2 + w^2y + w + wy^2 + vwz$	5	2
$x + xy + v^2 + w^2y + w + wy^2 + vwz + vw$	10	4
$x + xy + v^2 + wx^2 + w + wy^2 + vwz$	3	1
$x + xy + v^2 + wx^2 + w + wy^2 + vwz + vw$	6	3
$x + x^2 + v^2 + w^2 + w$	7	3
$x + x^2 + v^2 + w^2 + w + v$	17	7

TABLE F.18 (Continued)

Functional Form	No. of Models	Percentage of Total
$x + x^2 + v^2 + w^2 + w + v + vy$	13	5
$x + x^2 + v^2 + w^2 + w + v + vy + vw$	7	3
$x + x^2 + v^2 + w^2 + vz + xy + vx$	8 A	3
$x + x^2 + v^2 + wx^2 + w$	3	1
$x + x^2 + v^2 + wx + w$	4	2
$x + x^2 + v^2 + wx + w + y$	1	<1
$x + x^2 + v^2 + wx + w + y^3$	5	2
$x + x^2 + v^2 + wx + w + y^3 + vw^2$	6	3
$x + x^2 + v^2 + wx + w + y^3 + vw^2 + vw$	10	4
	240	

v = Steam Drum Feedwater Flow
w = Steam Drum Feedwater Temperature
x = EV Steam Outlet Temperature
y = SU Steam Inlet Temperature
z = SU Steam Outlet Flow

The last two variables (y and z) were omitted from the final MGCC model. Thus the MGCC and PEM results are not directly compared. The PEM modeling error ranged from 0.05% to 0.30% with an average of 0.13%. The MGCC modeling error was 0.11%. Comparison of a measured and predicted evaporator feedwater temperature signal is shown in Figure F.6.

F.1.17 EV Steam Outlet Temperature Empirical Models

One steam outlet temperature signal was available for each of the seven evaporators.

$$\text{EV Steam Outlet Temp} = f(\text{EV Na Inlet Temp, EV Na Outlet Temp, Secondary Na Flow Rate, EV FW Inlet Temp, SU Steam Outlet Flow}) \qquad (F.37)$$

The PEM results are shown in Table F.19. The functional form found from the MGCC modeling was

$$\text{EV Steam Outlet Temp} = c_0 + c_1\, y + c_2\, w + c_3\, z + c_4\, x + c_5\, v \qquad (F.38)$$

where,

v = EV Na inlet temperature (°F)
w = EV Na outlet temperature (°F)
x = Secondary Na flow (%)
y = EV feedwater inlet temperature (°F)
z = SU steam outlet flow (lbm/hr)
c_0 = 30.612364
c_1 = 0.54015023
c_2 = 0.31737170
c_3 = -0.000040013427
c_4 = -0.012090875
c_5 = 0.077161543

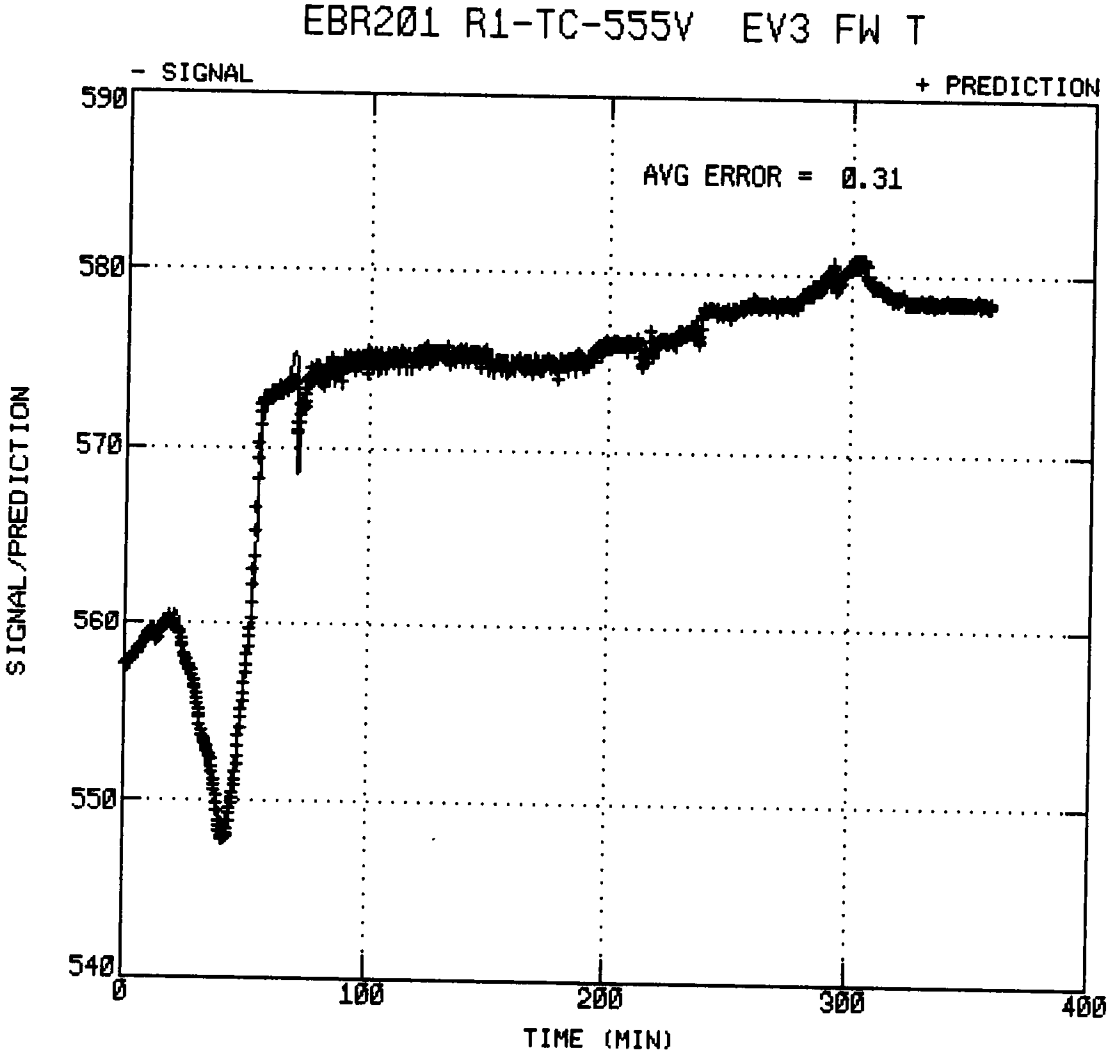

Figure F.6. Comparison of Measured and Predicted EV Feedwater Temperature Signal.

TABLE F.19

Empirical Models For
EV Steam Outlet Temperature

Functional Form	No. of Models	Percentage of Total
$y + v + w + x + z$	1 A	5
$y + w + z + v + x$	5 A	23
$y + w + z + x + v$	7 A	32
$y + w + v + vw + vy + w^2$	1	5
$y + w + v + vw + vy + w^2 + x$	2	9
$y + w + v + vw + vy + w^2 + x + z$	5	23
$y + w + v + v^2w + v^2 + v^3 + v^2x + y^2$	1	5
	22	

v = EV Na Inlet Temperature
w = EV Na Outlet Temperature
x = Secondary Na Flow Rate
y = EV Feedwater Inlet Temperature
z = SU Steam Outlet Flow

A total of 59% of the PEM forms are duplicated in the MGCC result. The PEM modeling error ranged from 0.08% to 0.13% with an average of 0.11%. The MGCC modeling error is 0.11%.

F.1.18 SU Steam Inlet Temperature Empirical Models

A steam inlet temperature signal was available from both of the superheaters.

SU Steam Inlet Temp = f(Steam Drum Level, Steam Pressure, EV Steam Outlet Temp) (F.39)

The functional forms found in the PEM modeling appear in Table F.20. The MGCC result was

$$\text{SU Steam Inlet Temp} = c_0 + c_1 z + c_2 x + c_3 x^2 + c_4 xz + c_5 yz + c_6 y^2 + c_7 y \qquad (F.40)$$

where,

x = Steam drum level (inches)
y = Drum steam pressure (psi)
z = EV steam outlet temperature (°F)
c_0 = -677.90454
c_1 = 7.0724163
c_2 = -189.46523
c_3 = -0.27844810
c_4 = 0.35423824
c_5 = -0.017678294
c_6 = 0.0024175255
c_7 = 4.7449141

Only 43% of the PEM results are contained within the MGCC functional form. The PEM modeling error ranged from 0.22%

TABLE F.20

Empirical Models For SU Steam Inlet Temperature

Functional Form	No. of Models	Percentage of Total
$z + x + x^2 + xz + yz + y^2$	3	21
$z + x + x^2 + xz + yz + y^2 + y$	3	21
$z + x + x^2 + xz + y + x^2y$	1	7
$z + z^2 + x^2 + xz + xz^2 + y + x^2z$	2	14
$z + z^2 + x^2 + xz + xz^2 + y + x^2z + xy$	3	21
$z + z^2 + x^2 + xz + xy + x + y^2$	1	7
$z + z^2 + x^2 + xz + xy + x + y^2 + y$	1	7
	14	

x = Steam Drum Level
y = Steam Pressure
z = EV Steam Outlet Temperature

to 0.77% with an average of 0.51%. The MGCC modeling error was 0.43%.

F.1.19 <u>SU Steam Outlet Temperature Empirical Models</u>

A total of four superheater steam outlet temperature signals were available for modeling.

$$\text{SU Steam Outlet Temp} = f(\text{SU Na Inlet Temp}, \text{SU Na Outlet Temp}, \text{Secondary Na Flow Rate}, \text{SU Steam Inlet Temp}, \text{SU Steam Outlet Flow}) \quad \text{(F.41)}$$

The PEM modeling results are shown in Table F.21 and the MGCC result is

$$\text{SU Steam Outlet Temp} = c_0 + c_1\, v + c_2\, vy + c_3\, v^2 + c_4\, z + c_5\, vx + c_6\, yz \quad \text{(F.42)}$$

where,

v = SU Na inlet temperature (°F)
w = SU Na outlet temperature (°F)
x = Secondary Na flow (%)
y = SU steam inlet temperature (°F)
z = SU steam outlet flow (lbm/hr)
c_0 = 660.45313
c_1 = 0.73321670
c_2 = -0.0023328057
c_3 = 0.00093157811
c_4 = -0.012443575
c_5 = 0.0014506135
c_6 = 0.000020791693

Variable w, the superheater sodium outlet temperature, was omitted from the final MGCC model. Thus the PEM and MGCC

TABLE F.21

Empirical Models For
SU Steam Outlet Temperature

Functional Form	No. of Models	Percentage of Total
$v + y + w + x + z$	2	7
$v + vy + v^2 + x^2 + vx$	1	3
$v + vy + v^2 + x^2 + vx + z$	3	10
$v + vy + v^2 + x^2 + vx + z + wx$	1	3
$v + vy + v^2 + x^2 + vx + z + wx + vw$	1	3
$v + vy + v^2 + vz + vx + x^2$	4	13
$v + vy + v^2 + vz + vx + x^2 + wx$	1	3
$v + vy + v^2 + vz + vx + x^2 + wx + z^2$	1	3
$v + vy + v^2 + vz + vx + x^2 + wx + vw$	3	10
$v + w + wy + y + v^2$	2	7
$v + w + wy + y + v^2 + v^2w$	1	3
$v + w + wy + y + vx + v^2 + wx + xy$	2	7
$v + w + v^2 + vw + vx + wy$	1	3
$vy + v + v^2 + w + vw$	1	3
$vy + v + v^2 + w + vw + x^2 + x$	2	7
$vy + v + v^2 + w + vw + x^2 + x + z^2$	3	10
$w^2 + v + v^2 + w + vw + x^2 + x + z^2$	1	3
	30	

v = SU Na Inlet Temperature
w = SU Na Outlet Temperature
x = Secondary Na Flow Rate
y = SU Steam Inlet Temperature
z = SU Steam Outlet Flow

results are difficult to compare. The PEM modeling error ranged from 0.16% to 0.75% with an average of 0.43%. The MGCC modeling error was 0.46%.

F.2 EBR-II Empirical Modeling Conclusions

The EBR-II empirical modeling has shown that a single model may be constructed which can accurately describe a given signal over its normal operating range. Some of the signals have shown that a unique functional form may be used to fit the data. In some cases, it may be desirable to make signal substitutions. This is important in situations where certain measurements are not available.

Table F.22 compares the average fitting error from both the PEM and MGCC modeling to the signal tolerance of each process variable. Any model with a fitting error greater than (or approximately equal to) the signal tolerance is certainly unacceptable. As can be seen, two variables do not perform well at all, namely the steam drum level and blowdown flow rate. The power fit is also just outside of its tolerance value. As noted with the PWR modeling, the MGCC models almost always have smaller fitting errors, as might be expected.

Besides the three signals previously mentioned, the fitting errors have shown average prediction accuracies from 0.06% to 0.6% which will provide reliable process variable estimates using the PEM and MGCC signal validation modules.

TABLE F.22

EBR-II Empirical Modeling Errors

Process Signal	Signal Tolerance	Average Error PEM	Average Error MGCC
Power	2 %	2.4 %	2.2 %
Upper Plenum Temperature	1 %	0.35 %	0.32 %
Core-Exit Temperature	1 %	0.6 %	0.37 %
IHX Orifice Plate Temp.	1 %	0.15 %	0.28 %
IHX Primary Outlet Temp.	1 %	0.12 %	0.10 %
Bulk Na Pool Temperature	1 %	0.4 %	0.31 %
IHX Secondary Inlet Temp.	1 %	0.24 %	0.25 %
IHX Secondary Outlet Temp.	1 %	0.15 %	0.11 %
SU Na Inlet Header Temp.	1 %	0.09 %	0.07 %
SU Na Inlet Temperature	1 %	0.5 %	0.14 %
SU Na Outlet Temperature	1 %	0.33 %	0.37 %
EV Na Inlet Temperature	1 %	0.37 %	0.25 %
EV Na Outlet Temperature	1 %	0.09 %	0.06 %
Steam Drum Level	1 %	6.8 %	6.7 %
Blowdown Flow Rate	1 %	9.2 %	8.7 %
EV Feedwater Temperature	1 %	0.13 %	0.11 %
EV Steam Outlet Temp.	1 %	0.11 %	0.11 %
SU Steam Inlet Temp.	1 %	0.51 %	0.43 %
SU Steam Outlet Temp.	1 %	0.43 %	0.46 %

VITA

Keith Edwin Holbert was born in Knoxville, Tennessee on June 14, 1962. His parents are William T. and Marjorie M. Holbert. Keith is married to the former Miss Elizabeth Kay Patterson and they have a daughter Kara Elizabeth Holbert.

In September 1980, Keith entered the University of Tennessee to obtain a Bachelor of Science degree in Nuclear Engineering. This degree was obtained in June 1984. In September of the same year, Keith entered the graduate Nuclear Engineering program at the University of Tennessee. An intermediate goal of a Master of Science degree was attained in March 1986 before the conference of this Doctor of Philosophy degree. Keith plans to continue his pursuit of knowledge by teaching at a university and has thus accepted a faculty position at Arizona State University.